Characterization of the human tryptophan hydroxylase isoforms

Tidemand, Kasper Damgaard

Publication date:
2017

Document Version
Publisher's PDF, also known as Version of record

Characterization of the *human* tryptophan hydroxylase isoforms

Kasper Damgaard Tidemand

PhD Dissertation

Department of Chemistry

Technical University of Denmark

2017

Characterization of the *human* tryptophan hydroxylase isoforms

Kasper Damgaard Tidemand

Supervisors:
Associate Professor Günther H. Peters
Associate Professor Hans E. M. Christensen
Associate Professor Pernille Harris

PhD Dissertation

DTU Chemistry
Technical University of Denmark
Kgs. Lyngby

August 2017

Preface and acknowledgements

The present dissertation is submitted to the Technical University of Denmark and is in partial fulfillment of the requirements for the PhD degree. The dissertation is based on work carried out at the Department of Chemistry, from September 2014 to September 2017 under supervision of Associate Professor Günther H. Peters, Associate Professor Hans E. M. Christensen, and Associate Professor Pernille Harris. The project was funded by the Academic Excellence Scholarship granted by DTU Chemistry.

The aim of this project was to characterize the intriguing enzyme tryptophan hydroxylase by shedding some light on its complex structure-function relationship. After 77 purifications of tryptophan hydroxylase variants and among other experiments 1658 steady-state kinetic measurements and 102 analytical gel filtrations, tryptophan hydroxylase has been brought a bit further out of the darkness.

During the project, I have been thoroughly supported by my supervisors. I would therefore first of all like to thank Associate Professor Günther H. Peters and Associate Professor Hans E. M. Christensen for their help and guidance throughout the project and for supporting and believing in all the projects I have committed to. I would also like to thank my co-supervisor Associate Professor Pernille Harris for support, guidance, and scientific discussions.

I owe special thanks to Laboratory Technicians Martin H. Pedersen and David F. Nielsen for technical assistance, preparative work, and for teaching me how to operate some of the experimental equipment. I would also like to thank the B.Sc. and M.Sc. students, I have co-supervised, and who have been involved in the project and contributed to the experimental work; Eva Stensgaard, Kathrine K. Øgendahl, Ida M. Vedel, Laura A. Andersen, Lisette P. Henriksen, Niklas Kristiansen, Beatrice F. Schultz, Camilla A. Jakobsen, Katja Lund-Rasmussen, Shu Li, and Line M. Aastrup.

Thanks to the talented PhD students and Postdocs with whom I have shared office in building 206, room 204 for pleasant company and scientific discussions; Line A. Ryberg, Tine M. Frederiksen, Sindrila D. Banik, and Sowmya Indrakumar. Additionally, thanks to Line for organizing cake-meetings to celebrate special occasions. Thanks to the rest of the students on the 2nd floor of building 206 and the PIPPI students for creating a nice work environment.

From University of Copenhagen, I would like to thank Postdoc Jerzy J. Dorosz, PhD student Sarah E. Jones, and Postdoc Simon Foster from the Department of Drug Design and Pharmacology for letting me borrow equipment and helping me with the differential scanning fluorimetry experiments. Furthermore, thanks to Professor Emeritus Kaj Frank Jensen from Department of Biological Chemistry for inspiring discussions and help with analyzing the steady-state kinetic data.

I am grateful to Professor Edward I. Solomon for hosting me as a visiting scholar at the Department of Chemistry, Stanford University. I am thankful that the entire Solomon laboratory, and especially graduate student Shyam R. Iyer, made my research stay a pleasant and rewarding experience. I acknowledge the Kaj and Hermilla, Otto Mønsted, and Idella foundations for granting me financial support to cover the research stay.

Last, but not least, thanks to my friends and family, and especially my girlfriend Stine Weibel, for patience, love, and support.

Kasper D. Tidemand
Kgs. Lyngby, August 31st, 2017

Abstract

Tryptophan hydroxylase (TPH) catalyzes the hydroxylation of tryptophan to L-5-hydroxytryptophan, which is the first and rate-limiting step in the biosynthesis of 5-hydroxytryptamine (serotonin). Serotonin acts as a hormone and neurotransmitter in a variety of tissues and is involved in a wide range of physiological functions. Dysregulation of the level of serotonin is associated with a variety of physiological and psychiatric disorders. TPH exists in two homologous isoforms; TPH1 and TPH2. Isoform 1 is primarily expressed in the peripheral tissues, while isoform 2 is mainly found in the central nervous system. As the rate-limiting enzymes in the synthesis of serotonin, TPH1 and TPH2 play vital roles in the serotonergic systems of the peripheral tissues and central nervous system, respectively.

The active form of TPH contains iron(II) and catalyzes tryptophan hydroxylation utilizing 6*R*-L-erythro-5,6,7,8-tetrahydrobiopterin (BH_4) and molecular oxygen. The TPH isoforms are members of an enzyme subfamily of iron(II)-containing mono-oxygenases, referred to as the aromatic amino acid hydroxylases. The family also includes phenylalanine hydroxylase and tyrosine hydroxylase. These homologous enzymes all form homotetramers, in which each subunit comprises an N-terminal regulatory domain, a highly conserved catalytic domain, and a C-terminal tetramerization domain.

In this dissertation, both *human* TPH isoforms were under investigation. Of the isoforms, TPH2 is less characterized in literature due to low purification quantities caused by its inherent instability and tendency to aggregate. To overcome this challenge, three variants of *human* TPH2 with deletion mutations of entire or parts of domains were expressed, purified, and examined. Removal of the C-terminal tetramerization domain resulted in TPH variants which could be purified in quantities sufficient for enzymatic characterization. However, this variant suffered from a high inactivation rate. Upon further removal of the N-terminal regulatory domain, a significant decrease in rate of inactivation was observed. This observation renders the regulatory domain the main source of instability. To overcome the inherent instability of the regulatory domain, differential scanning fluorimetry was used to identify stabilizing ligands. In absence of ligands the unfolding was continuous and polyphasic. However, in presence of tryptophan or phenylalanine the unfolding shifted to apparent two-state, indicative of increased thermostability and monodispersity. The shift in unfolding behavior was accompanied by a ligand concentration-dependant increase in transition temperature. This thermostabilizing effect was confirmed by a significant decrease in inactivation rate. Analytical gel filtration revealed that in the presence of the regulatory domain, the TPH2 variant resides in a monomer-dimer equilibrium. With the addition of phenylalanine a significantly shift towards dimer was observed explaining the ligand-induced increase in thermostability. These results led to the addition of phenyalanine in the purification buffer solutions which significantly increased the purification yields.

Very little is known about the catalytic mechanism of TPH and most of the knowledge in literature stem from extrapolations of results obtained for the other members of the enzyme subfamily. In this dissertation, results are presented that demonstrate that the steady-state kinetic mechanism of the catalytic domain of *human* TPH1 follows a hybrid Ping Pong-ordered mechanism. In this mechanism, the reaction can either occur through a Ping Pong or a sequential mechanism depending on the concentration of tryptophan, and substrate inhibition occurs via competitive inhibition of BH_4 binding. The kinetic study also revealed that the isoforms display very different kinetic properties despite their high sequence identity. One of the major differences is that TPH1 is substrate inhibited, while TPH2 is not. By scrutinizing the crystal structures of the isoforms, it was found that differences reside in the orientation of a loop lining the active site. Point mutations were conducted within this loop, and significant changes in the kinetic parameters of the mutant TPH1 variants were observed. Molecular dynamics simulations revealed that the substrate inhibition mechanism occurs through a closure of the BH_4 binding pocket upon tryptophan binding, and that the active site loop is involved in this mechanism by propagating structural changes from the tryptophan binding site to the BH_4 binding pocket.

Dansk resumé

Tryptophanhydroxylase (TPH) katalyserer hydroxylering af tryptophan, hvorved L-5-hydroxytryptophan dannes. Dette er det første og hastighedsbestemmende trin i biosyntesen af 5-hydroxytryptamin (serotonin). Serotonin agerer som hormon og neurotransmitter i forskelligt væv og er involveret i en lang række fysiologiske funktioner. Forstyrrelser i serotoninbalancen er associeret med flere fysiske og psykiske sygdomme. TPH eksisterer som to isoformer; TPH1 og TPH2. Isoform 1 bliver primært udtrykt i det perifere væv, imens isoform 2 hovedsageligt udtrykkes i centralnervesystemet. Som de hastighedsbestemmende enzymer i syntesen af serotonin, spiller TPH1 og TPH2 vigtige roller i de serotonergiske systemer i henholdsvis det perifere væv og centralnervesystemet.

Den aktive form af TPH indeholder jern(II) og katalyserer hydroxylering af tryptophan ved hjælp af 6*R*-L-erythro-5,6,7,8-tetrahydrobiopterin (BH_4) og molekylært ilt. TPH isoformerne er medlemmer af enzym underfamilien kaldet de aromatiske aminosyre hydroxylaser. Denne familie inkluderer også fenylalaninhydroxylase og tyrosinhydroxylase. Medlemmerne i denne familie er nært beslægtede og danner alle homotetramerer. Hver underenhed i tetrameren består af et N-terminalt regulatorisk domæne, et konserveret katalytisk domæne og et C-terminalt tetrameriseringsdomæne.

I denne afhandling er begge humane TPH isoformer blevet undersøgt. Af de to isoformer er specielt TPH2 en udfordring at oprense i mænger, der muliggør karakterisering. Der forefindes derfor færre undersøgelser af TPH2 i litteraturen. For at overkomme denne udfordring, blev tre TPH2 varianter med trunkeringer af hele eller dele af domæner udtrykt, oprenset og undersøgt. Trunkering af det C-terminale tetrameriserings-domæne resulterede i en TPH2 variant, der kunne oprenses i mængder, der muliggjorde karakterisering af denne variant. Denne variant havde dog en meget høj inaktiveringshastighed. Inaktiveringshastigheden kunne sænkes markant ved yderligere at trunkere det N-terminale regulatoriske domæne. Dette viser, at det regulatoriske domæne er hovedoversagen til den ringe stabilitet. For at finde en løsning på dette problem, blev differential scanning fluorimetry benyttet til at identificere stabiliserende ligander. Uden ligander viste resultaterne, at proteinudfoldningen var kontinuerlig. Udfoldningen ændres dog til tilsyneladende to-stadie ved at tilsætte fenylalanin eller tryptophan. Dette indikerer øget termostabilitet og monodispersitet. Skiftet i udfoldning var ledsaget af en koncentrations-afhængig forøgelse af smeltetemperaturen. Denne termostabiliserende effekt blev bekræftet ved at iagttage, at inaktiveringshastigheden også blev sænket. Analytisk gelfiltrering viste sidenhen, at tilstedeværelsen af det regulatoriske domæne gør, at TPH varianten forefindes i en monomer-dimer ligevægt. Disse resultater viste også, at tilsætning af fenylalanin skifter denne ligevægt betragteligt mod dimer, hvilket kan forklare den observerede forøgelse af termostabiliteten. Disse resultater førte til, at fenylalanin blev tilsat i oprensningsopløsningen, hvilket resulterede i højere oprensningsudbytter.

Man ved meget lidt om TPH's katalytiske mekanisme. Den bliver derfor beskrevet med udgangspunkt i de resultater, man har opnået for de andre medlemmer af AAAH familien. I denne afhandling præsenteres resultater, der peger på, at det katalytiske domæne af TPH1 følger en Ping Pong-ordnet steady-state mekanisme. I denne mekanisme kan reaktionen enten forløbe via en Ping Pong eller sekventiel mekanisme afhængig af koncentrationen af tryptophan. Substratinhibering forekommer ved kompetitiv hæmning af BH_4 binding. Den kinetiske undersøgelse viste også, at isoformerne udviser meget forskellige kinetiske parametre på trods af deres høje sekvensidentitet. Én af de største forskelle er, at kun TPH1 udviser substratinhibering. Ved minutiøs gennemgang af isoformernes krystalstrukturer blev der fundet forskelle i et loop der ligger over det aktive site. Der blev foretaget punktmutationer i dette loop, og det viste sig at resultere i ændringer af de kinetiske parametre for TPH1. Molekylærdynamiske simuleringer afslørede, at inhiberingsmekanismen fungerer ved, at BH_4 bindingslommen blokeres efter binding af tryptophan. Loopet er involveret i denne mekanisme ved at forlænge de strukturelle ændringer fra tryptophan's bindingslomme til BH_4's bindingslomme.

Abbreviation list

3CP	Human rhinovirus 3C protease
3D	Three-dimensional
4a-hydroxy-BH_4	4a-carbinolamine tetrahydrobiopterin
5-HT	5-hydroxytryptamin
5-HTP	5-hydroxytryptophan
6-MePH_4	6-methyl-5,6,7,8-tetrahydropterin
AA	Amino acid
AAAH	Aromatic amino acid hydroxylases
AADC	Aromatic amino acid decarboxylase
ACT	Aspartate kinase, chorismate mutase, and TyrA
ANS	8-anilino 1-naphthalenesulfonic acid
AUC	Area under the curve
BH_2	7,8-dihydrobiopterin
BH_4	5,6,7,8-tetrahydrobiopterin
BLAST	Basic Local Alignment Search Tool
CaMKII	Ca2+/calmodulin-dependent protein kinase II
CNS	Central nervous system
DF	Dilution factor/degrees of freedom
$DMPH_4$	6,7-Dimethyl-5,6,7,8-tetrahydropterine
DMSO	Dimethyl sulfoxide
DNA	Deoxyribonucleic acid
DOPA	3,4-dihydroxyphenylalanine
DSF	Differential scanning fluorimetry
DTT	Dithiothreitol
GTP	Guanosine triphosphate
HEPES	4-(2-hydroxyethyl)-1-piperazineethanesulfonic acid
HPLC	High-performance liquid chromatography
ITC	Isothermal titration calorimetry
MBP	Maltose binding protein
MD	Molecular dynamics
NAD(P)H	Nicotinamide adenine dinucleotide phosphate
NMR	Nuclear Magnetic Resonance
OPLS	Optimized Potentials for Liquid Simulations
PAH	Phenylalanine hydroxylase
PDB	Protein Data Bank
PKA	Protein kinase A
PPW	Protein Preparation Wizard
qBH_2	Quinonoid dihydrobiopterin
qPCR	Quantitative polymerase chain reaction
RESPA	Reversible reference system propagator algorithms
RMSD	Root-mean-square deviation
SAXS	Small-angle X-ray scattering
SDS-PAGE	Sodium dodecyl sulfate polyacrylamide gel electrophoresis
SEC-SAXS	Size exclusion chromatography small-angle X-ray scattering
TEV	Tobacco Etch Virus
TH	Tyrosine hydroxylase
TIP3P	Transferable intermolecular potential 3 point
TPH	Tryptophan hydroxylase
TRIS	Tris(hydroxymethyl)aminomethane
UV-Vis	Ultraviolet–visible

List of content

Dissertation introduction

This dissertation concerns characterization of the enzyme tryptophan hydroxylase (TPH) which catalyzes the first and rate-limiting step in the biosynthesis of the neurotransmitter and hormone serotonin.[1,2] This step is catalyzed by two distinct tryptophan hydroxylase isoforms in the brain and peripheral tissues, respectively.[2-4] The existence of two isoforms introduces the possibility of selectively targeting the serotonergic systems of the brain and peripheral tissues by e.g. isoform-specific modulators of activity.[5] This, however, requires thorough characterization of both isoforms on a molecular level.

The overall aim of this project was to characterize the TPH isoforms to improve the current understanding of their structure-function relationships. So far, proper characterization of the isoforms has been hampered by insufficient purification yields caused by their notorious instability and tendency to aggregate.[6] This challenge has to be overcome to fully understand the intriguing functions of the TPH isoforms. The Metalloprotein Chemistry and Engineering Group at DTU has paved the way for TPH characterization by advancing the purification strategies of a variety of TPH variants.[7-9] Despite great efforts, TPH isoform 2 variants comprising the regulatory domain still pose a challenge to purify. In this dissertation, special emphasis is on overcoming this challenge.

Although the isoforms are expressed in different tissues, they are highly homologous. The isoforms share a high sequence identity, they both form complex homotetrameric structures, and are believed to follow the same reaction mechanism.[10-12] Despite these observations, it was discovered by former members of the Metalloprotein Chemistry and Engineering Group that the isoforms display very different kinetic parameters.[13] This is puzzling and the underlying mechanism of this observation is not understood. It was, therefore, set forth to thoroughly study the kinetic mechanism of TPH and to identify the structural origin of the different kinetic properties of the isoforms.

To shed light on the characteristics of the TPH isoforms, an interdisciplinary approach has been conducted in which an array of experimental methods has been utilized in conjugation with computational techniques. As full-length TPH isoform 2 proves challenging to purify, an ensemble of variants with deletion mutations of either entire or parts of domains has been studied throughout this dissertation. In addition, variants with point mutations were also analyzed to identify the significance of single residues. The results presented in this dissertation improve the understanding of fragments of the complicated function of the TPH isoforms.

Outline of dissertation

This dissertation is divided into eight chapters concerning different aspects of the structure and function of tryptophan hydroxylase. The first chapter provides a fundamental introduction to the enzyme and how it is involved in the synthesis of one of the most important hormone and neurotransmitters in human beings. Each of the following chapters concerns individual areas of tryptophan hydroxylase research and within each chapter a comprehensive introduction to the current TPH research area will be found.

Chapters 2 through 4 concern the identification of ligands which influence the oligomeric state of TPH resulting in increased thermostabiliy. Results from these chapters have been pulished in *FEBS Open Bio* (Appendix A.1). Chapter 5 presents results obtrained from experiements conducted at Stanford University during a 3 month research stay. In chaptes 6 through 8, the steady-state and substrate inhibition mechanisms are investigated. Based on the results presented in these chapters a manuscript has been prepared and submitted (Appendix A.2).

Throughout the dissertation, the chapters will gradually delve into the complicated molecular mechanisms exerted by tryptophan hydroxylase. The content of the chapters and how they narrow down from isolation of the full-length enzyme to studying specific residues of an active site loop is outlined in the following figure.

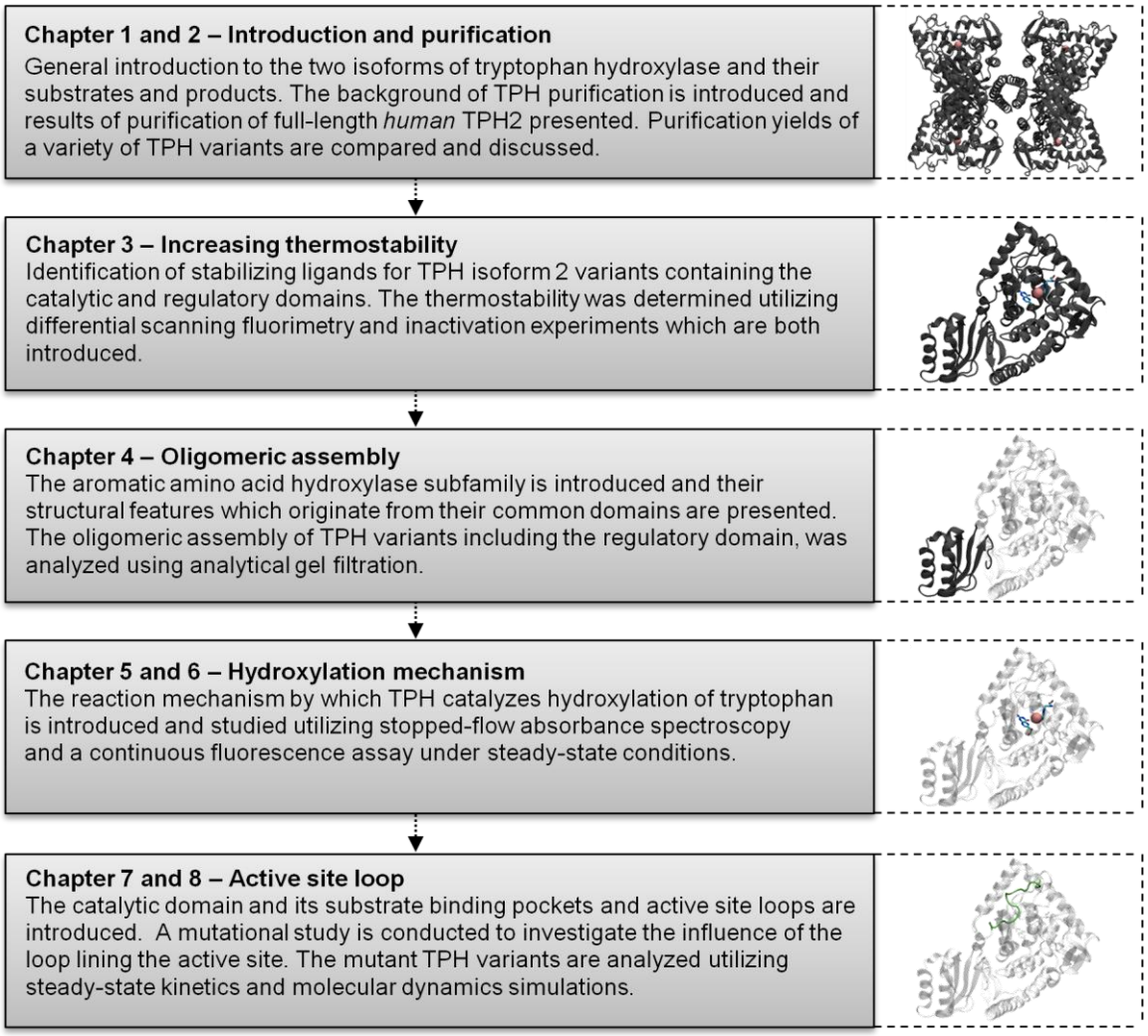

References

[1] Boadle-Biber, M.C., 1993, Regulation of serotonin synthesis, *Prog. Biophys. Molec. Biol. 60*, 1-15.

[2] Lovenberg, W., Jequier, E., and Sjoerdsma, A., 1967, Tryptophan hydroxylation: measurement in pineal gland, brainstem, and carcinoid tumor, *Science 155*, 217-219.

[3] Walther, D. J., Peter, J.-U., Bashammakh, S., Hörtnagl, H., Voits, M., Fink, H., and Bader, M., 2003, Synthesis of serotonin by a second tryptophan hydroxylase isoform, *Science 299*, 76.

[4] Amireault, P., Sibon, D., and Cote, F., 2013, Life without peripheral serotonin: insights from tryptophan hydroxylase 1 knockout mice reveal the existence of paracrine/autocrine serotonergic networks, *Chem. Neurosci. 4(1)*, 64–71.

[5] Matthes, S., Mosienko, V., Bashammakh, S., Alenina, N., and Bader, M., 2010, Tryptophan hydroxylase as novel target for the treatment of depressive disorders, *Pharmacology 85(2)*, 95-109.

[6] McKinney, J., Knappskog, P. M., Pereira, J., Ekern, T., Toska, K., Kuitert, B. B., Levine, D., Gronenborn, A. M., Martinez, A., and Haavik, J., 2004, Expression and purification of human tryptophan hydroxylase from Escherichia coli and Pichia pastoris, *Protein Expr. Purif. 33(2)*, 185-194.

[7] Boesen, J., 2010, Cloning, expression, purification and characterization of tryptophan hydroxylase variants, Ph.D. thesis, Department of Chemistry, Technical University of Denmark, Kgs. Lyngby.

[8] Haahr, L.T., 2012, Purification and Characterization of Tryptophan Hydroxylase, Ph.D. thesis, Department of Chemistry, Technical University of Denmark, Kgs. Lyngby.

[9] Nielsen, M. S., 2007, Expression, purification and characterization of tryptophan hydroxylase, Ph.D. thesis, Department of Chemistry, Technical University of Denmark, Kgs. Lyngby.

[10] Mockus S. M., Kumer S. C., and Vrana K. E., 1997, Carboxyl terminal deletion analysis of tryptophan hydroxylase, *Biochim. Biophys. Acta 1342*, 132-140.

[11] Carkaci-Salli, N., Flanagan, J. M., Martz, M. K., Salli, U., Walther, D. J., Bader. M., and Vrana, K. E., 2006, Functional Domains of Human Tryptophan Hydroxylase 2 (hTPH2), *J. Biol. Chem. 281(38)*, 28105-28112.

[12] Fitzpatrick, P. F., 2003, Mechanism of Aromatic Amino Acid Hydroxylation, *Biochemistry 42(48)*, 14083–14091.

[13] Windahl, M. S., Boesen, J., Karlsen, P. E., and Christensen H. E. M., 2009, Expression, Purification and Enzymatic Characterization of the Catalytic Domains of Human Tryptophan Hydroxylase Isoforms, *Protein J. 28*, 400–406.

Chapter 1

Introduction to tryptophan hydroxylase

In this chapter, the importance of tryptophan hydroxylase (TPH) will be described and some key concepts about TPH will be introduced. This chapter will serve as brief introduction to some of the fundamental concepts, while more thorough introductions to the individual branches of the TPH theory are found in the relevant chapters.

Outline

1.1 The aromatic amino acid hydroxylases

Tryptophan hydroxylase (TPH) is a member of an enzyme subfamily of iron(II)-containing mono-oxygenases, referred to as the aromatic amino acid hydroxylases (AAAHs). Together with TPH, the family also comprise phenylalanine hydroxylase (PAH) and tyrosine hydroxylase (TH), which all originate from a common protein.[14] While PAH only exists in one form, TPH exists in two isoforms, and TH in four isoforms. In TH, the four isoforms only differ in the length of the N-terminus, which originates from alternative splicing of a single gene.[15] The isoforms of TPH are less conserved and are encoded by two different genes.[16]

Common for the AAAHs, is that they catalyze the hydroxylation of their respective amino acid substrate utilizing iron(II), 6*R*-L-erythro-5,6,7,8-tetrahydrobiopterin (BH_4), and molecular oxygen.[17] All AAAHs are only active with ferrous iron in the active site.[18-20] Iron is bound in the active site by a common structural motif consisting of three endogenous protein ligands, referred to as the 2-His-1-carboxylate facial triad.[21] In the absence of amino acid substrate, the iron atom will also coordinate three water molecules, Figure 1.1 A. In the presence of substrate and co-substrate a rearrangement occurs in the AAAHs which results in dissociation of two water molecules from the iron, and the glutamic acid residue changes from a monodentate to bidentate ligand, Figure 1.1 B.[22-24]

The homologous AAAHs all form homotetramers, in which each subunit comprise an N-terminal regulatory domain, a highly conserved catalytic domain, and a C-terminal tetramerization domain, Figure 1.1 C.[25] The sequence identity, structure, and function of the domains will be further discussed in chapter 4, 6, and 7.

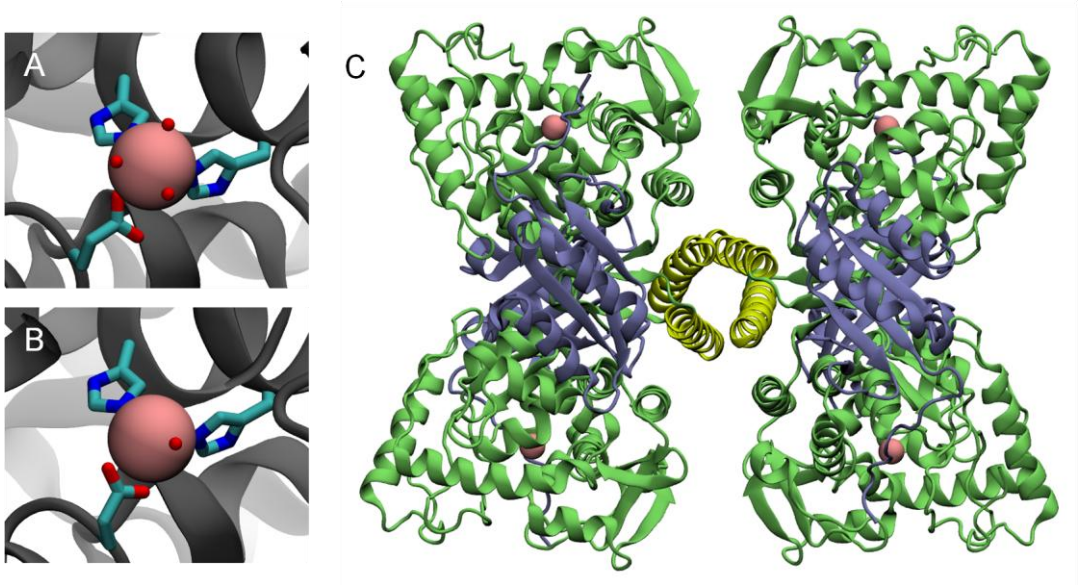

Figure 1.1. Representation of the coordination of iron and the quaternary structure of the AAAHs. (A) Octahedral coordination of iron by the 2-His-1-carboxylate facial triad and three water molecules in the absence of substrates (PDB entry: 1PAH). (B) Trigonal bipyramidal coordination of iron in the presence of substrate and co-substrate (PDB entry: 1KW0). Iron is shown in pink and water molecules are represented as red spheres. (C) Cartoon illustration of the tetrameric structure of full-length *rat* phenylalanine hydroxylase (PDB entry: 5FGJ). Regulatory domains are colored blue, catalytic domains are colored green, and tetramerization domains are colored yellow.

1.1.1 AAAH catalyzed reactions

TPH catalyzes the hydroxylation of tryptophan to L-5-hydroxytryptophan (5-HTP), which is the first step in the synthesis of 5-hydroxytryptamine (5-HT, serotonin), Figure 1.2.[26] Dysregulation of serotonin is associated with a variety of disorders, as discussed in a following section. PAH is a liver enzyme and catalyses the conversion of L-phenylalanine to L-tyrosine in the rate limiting step in phenylalanine catabolism.[27,28] Loss of PAH activity impairs catabolism of phenylalanine resulting in phenylketonuria which leads to intellectual disability and mental disorders.[29] TH is mainly expressed in the brain and catalyzes the hydroxylation of tyrosine to L-3,4-dihydroxyphenylalanine (L-dopa).[30] This is the rate limiting step in the synthesis of catecholamines such as dopamine, epinephrine, and norepinephrine, which are important neurotransmitters and hormones.[31]

Because the AAAHs are very homologous and their substrates are similar, the enzymes are not fully specific towards their respective substrates. This is evident from studies of the catalytic domain of *human* and *rabbit* TPH1, where comparable V_{max}/K_m-values for phenylalanine and tryptophan as substrates have been found.[20,32] However, compared to tryptophan, hydroxylation of tyrosine is at least three orders of magnitude slower.[20] Similarly, TH is able to hydroxylate phenylalanine and tryptophan with V_{max}/K_m-values one and two order of magnitude lower than with tyrosine, respectively.[33,34] Compared to TPH and TH, PAH displays a higher degree of substrate specificity, as V_{max}/K_m-value for phenylalanine is three orders of magnitude greater than that for tryptophan, and tyrosine is not hydroxylated.[35]

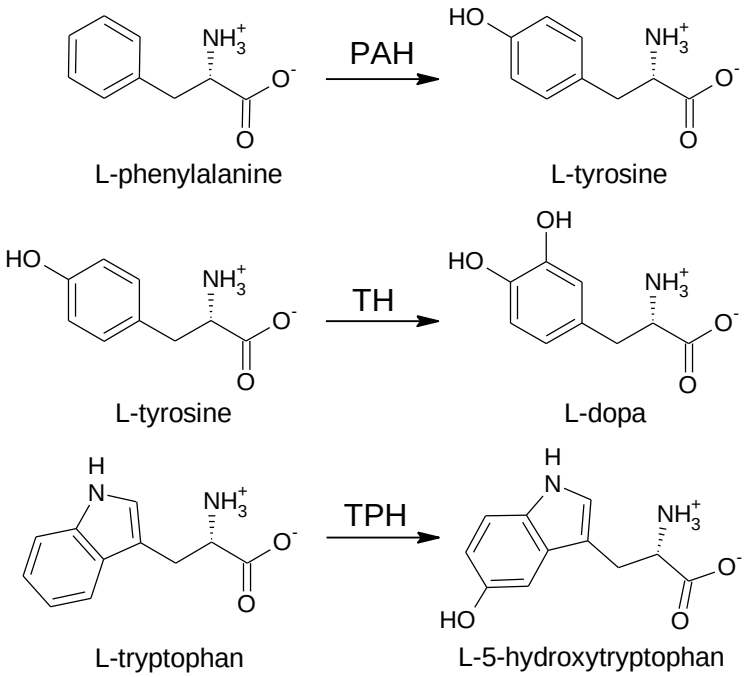

Figure 1.2. The enzymatic reactions catalyzed by the AAAHs. PAH converts L-phenylalanine to L-tyrosine, TH converts L-tyrosine to L-3,4-dihydroxyphenylalanine (L-dopa), and TPH converts L-tryptophan to L-5-hydroxytryptophan (5-HTP).

1.2 The TPH isoforms

Tryptophan hydroxylase exists in two homologous isoforms; TPH1 and TPH2 which consist of 444 and 490 amino acid residues, respectively (Figure 1.3).[16] Isoform 1 is primarily expressed in the peripheral tissues, such as in enterochromaffin cells of the gastrointestinal tract and in the adrenal glands, while isoform 2 primarily is found in serotonergic neurons in the central nervous system (CNS).[36,37]

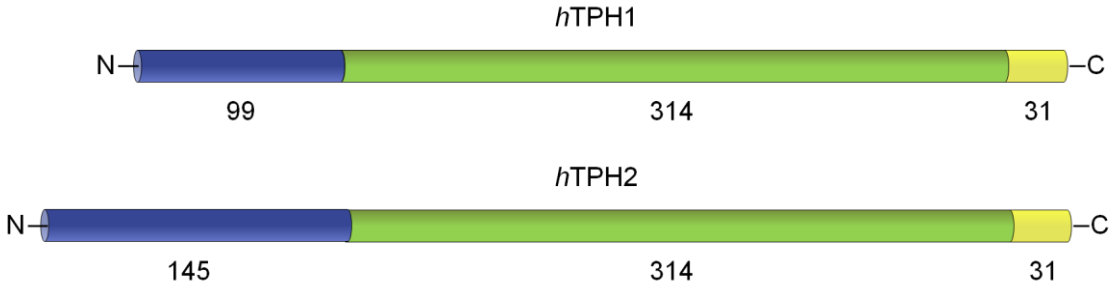

Figure 1.3. Number of amino acid residues in the regulatory (blue), catalytic (green), and tetramerization (yellow) domains of TPH1 and TPH2.

The main differences between the two isoforms are found in the regulatory domain, where TPH2 have additional 46 residues in the N-terminus.[16] The extended N-terminus of TPH2 has been found to reduce expression level [38], decrease enzymatic activity [39], and posses an additional phosphorylation site [40].

1.2.1 TPH phosphorylation

The isoforms have a common phosphorylation site at Ser58(TPH1)/Ser104(TPH2) which is phosphorylated by protein kinase A (PKA).[41,42] An additional phosphorylation site, Ser19, resides in the extended N-terminus of TPH2. Ser19 has been found to be phophorylated by PKA and Ca2+/calmodulin dependent

protein kinase II (CaMKII).[38,43] Phosphorylation of TPH2 results in a modest increase in activity. Of the two phosphorylation sites in TPH2, Ser19 is the main site responsible for increased activity.[41]

Besides increasing the activity, phosphorylation of Ser19 also acts as a 14-3-3 protein binding site.[41] 14-3-3 proteins represent a family of proteins which are present in the majority of eukaryotic organisms, where they bind to a wide variety of phosphorylated proteins.[44] The binding of a 14-3-3 protein increase the activity and stability of phosphorylated TPH2.[41,45] In addition, binding of a 14-3-3 protein inhibits phosphatase-catalyzed dephosphorylation resulting in prolonged activation.

1.3 Serotonin and related disorders

Serotonin (5-hydroxytryptamine, 5-HT) acts as hormone and neurotransmitter in a variety of tissues and is involved in a wide range of physiological functions.[37,46,47] Serotonin is synthesized from L-tryptophan in two steps, Figure 1.4. The first step is the TPH catalyzed hydroxylation of L-tryptophan to L-5-hydroxytryptophan (5-HTP).[17] The second step is decarboxylation of 5-HTP to serotonin catalyzed by aromatic amino acid decarboxylase (AADC).[48]. A detailed review of the reaction mechanism is presented in chapter 5.

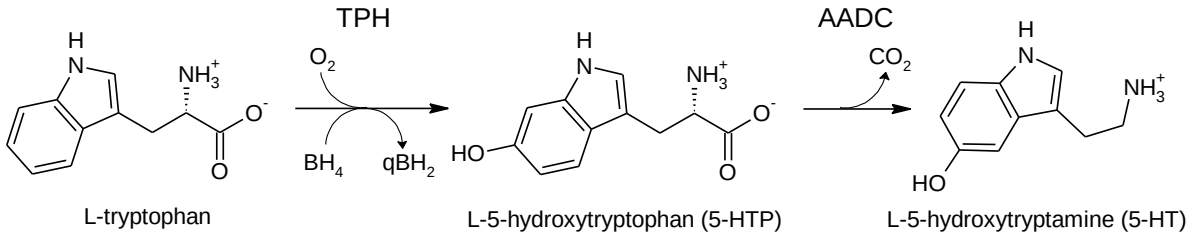

Figure 1.4. The biosynthesis of serotonin from L-tryptophan. The conversion of L-tryptophan to 5-HTP is catalyzed by TPH and requires molecular oxygen and BH_4 as co-substrates. The conversion of 5-HTP to serotonin is catalyzed by AADC.

Serotonin exerts its function by acting on 15 different 5-HT receptors which are distributed throughout the entire human body.[49] In the peripheral tissues, the rate-limiting reaction in the synthesis of serotonin is mainly catalyzed by TPH1.[37] Here serotonin acts as a hormone to constrict large blood vessels and regulates platelet adhesion.[50,51] Serotonin is also found in the intestines where it is involved in e.g. gastrointestinal motility and homeostasis.[52,53] Dysregulation of peripheral serotonin level is involved in several conditions e.g. functional gastrointestinal disorders, lung fibrosis, carcinoid syndrome, and osteoporosis.[54-57]

In the central nervous system, the rate-limiting step in the serotonin synthesis is primarily catalyzed by TPH2.[36] The synthesis is mainly in the dorsal raphe nuclei of the brain stem where it acts as a neurotransmitter.[58] Here, serotonin is involved in regulating centers of the brain that involve e.g. wakefulness, temperature regulation, blood-pressure regulation, aggressive and sexual behavior.[59,60] Several disorders have been reported to be related to dysfunction of the serotonin system in the CNS, such as depression, schizophrenia, autism, and ADHD.[61]

As TPH is the rate-limiting step in the synthesis of serotonin, it is a potential target in treatments of the serotonin associated disorders.[52,62] The neurological disorders are associated with decreased levels of neuronal serotonin and the gastrointestinal disorders are associated with increased levels of serotonin.[63-65] As the groups of disorders are oppositely influenced by serotonin, a TPH isoform-specific modulator is desirable to independently regulate the two isoforms.[66] This is evident from the substrate analogue p-chlorophenylalanine, which has been used as a TPH1 inhibitor in treatment of carcinoid syndrome.[67,68] As p-chlorophenylalanine also inhibits TPH2, serotonin is depleted in the CNS resulting in severe side-effects

such as depression.[69-72] More recent inhibitors for TPH1 have been identified.[73,74] These inhibitors are not isoform-specific, as they also inhibit TPH2, but they do not cross the blood-brain barrier, and therefore only deplete 5-HT in the gastrointestinal tract.[63] Very recently compounds that selectively inhibit TPH1 over TPH2 have been identified.[75] These compounds bind in an inhibitory site that is located in the catalytic domain but is separated from the active site.

With improved knowledge about the TPH isoforms, potential drugs which specifically stimulate TPH2 activity might be identified. These could provide an alternative to the modern antidepressants which inhibit serotonin reuptake. The reuptake inhibition is accompanied with several side-effect caused by the non-specific nature of this treatment.[76]

1.4 Tetrahydrobiopterin

6*R*-L-erythro-5,6,7,8-tetrahydrobiopterin (BH_4) is an important co-substrate in several enzymes of metabolic importance, including the AAAHs, alkylglycerol mono-oxygenase, and nitric oxide synthases.[77] BH_4 is formed *de novo* from GTP in a sequence of three enzymatic steps.[77] The intracellular concentration of BH_4 in the brain has been found not to saturate TPH2 and is likely around or lower than $K_{m,BH4}$ (~20 µM [40]).[78]

In the reaction catalyzed by TPH, BH_4 is converted to 4a-carbinolamine tetrahydrobiopterin (4a-hydroxy-BH_4), Figure 1.5.[79] The product 4a-hydroxy-BH_4 is converted to quinonoid dihydrobiopterin (qBH_2), either spontaneously or catalytically by pterin-4a-carbinolamine dehydratase.[80] BH_4 is enzymatically regenerated from qBH_2 by an NAD(P)H-dependent oxidoreductase.[81] If qBH_2 is not regenerated, it will rearrange non-enzymatically to form 7,8-dihydrobiopterin (BH_2).[81] The role of BH_4 in the hydroxylation of tryptophan is further described and discussed in chapter 5.

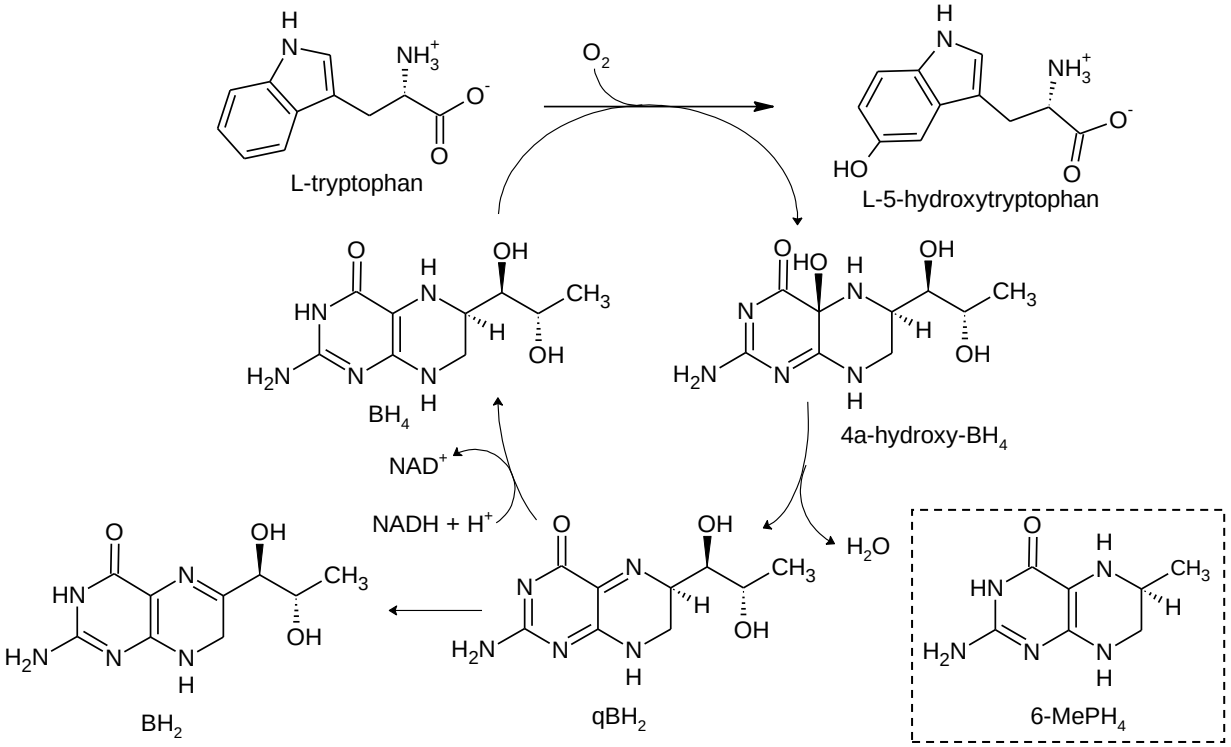

Figure 1.5. Schematic illustration of the recycling of co-substrate BH_4. Insert illustrates 6-methyl-5,6,7,8-tetrahydropterin (6-$MePH_4$)

The natural co-substrate of the AAAHs is BH_4 [82], however, earlier studies have used a co-substrate analogue 6-methyl-5,6,7,8-tetrahydropterin (6-$MePH_4$), Figure 1.5 (insert).

1.5 References

[14] Cao, J., Shi, F., Liu, X., Huang, G., and Zhou, M., 2010, Phylogenetic analysis and evolution of aromatic amino acid hydroxylase, *FEBS Lett. 584(23)*, 4775–4782.

[15] Kaneda, N., Kobayashi, K., Ichinose, H., Kishi, F., Nakazawa, A., Kurosawa, Y., Fujita, K., and Nagatsu, T., 1987, Isolation of a novel cDNA clone for human tyrosine hydroxylase: alternative RNA splicing produces four kinds of mRNA from a single gene, *Biochem. Biophys. Res. Commun. 146(3)*, 971-975.

[16] Walther, D. J., Peter, J.-U., Bashammakh, S., Hörtnagl, H., Voits, M., Fink, H., and Bader, M., 2003, Synthesis of serotonin by a second tryptophan hydroxylase isoform, *Science 299*, 76.

[17] Kaufman, S., 1963, The structure of the phenylalanine-hydroxylation cofactor, *Biochemistry 50*, 1085-1093.

[18] Wallick, D. E., Bloom, L. M., Gaffney, B. J., and Benkovic, S. J., 1984, Reductive activation of phenylalanine hydroxylase and its effect on the redox state of the non-heme iron, *Biochemistry 23*, 1295-1302.

[19] Fitzpatrick, P. F., 1989, The metal requirement of rat tyrosine hydroxylase, *Biochem. Biophys. Res. Commun. 161*, 211-215.

[20] Moran, G. R., Daubner, S. C., and Fitzpatrick, P. F., 1998, Expression and characterization of the catalytic core of tryptophan hydroxylase, *J. Biol. Chem. 273*, 12259-12266.

[21] Koehntop, K. D. and Emerson, J.P., 2005, The 2-His-1-carboxylate facial triad: a versatile platform for dioxygen activation by mononuclear non-heme iron(II) enzymes, *J. Biol. Inorg. Chem. 10(2)*, 87–93.

[22] Andersen, O. A., Stokka, A. J., Flatmark, T., and Hough, E., 2003, 2.0 Å Resolution crystal structures of the ternary complexes of human phenylalanine hydroxylase catalytic domain with tetrahydrobiopterin and 3-(2-thienyl)-L-alanine or L-norleucine: substrate specificity and molecular motions related to substrate binding, *J. Mol. Biol. 333*, 747–757.

[23] Andersen, O. A., Flatmark, T., and Hough, E., 2002, Crystal structure of the ternary complex of the catalytic domain of human phenylalanine hydroxylase with tetrahydrobiopterin and 3-(2-thienyl)-L-alanine, and its implications for the mechanism of catalysis and substrate activation, *J. Mol. Biol. 320(5)*, 1095-1108.

[24] Chow, M. S., Eser, B. E., Wilson, S. A., Hodgson, K. O., Hedman, B., Fitzpatrick, P. F., and Solomon, E. I., 2009, Spectroscopy and Kinetics of Wild-type and Mutant Tyrosine Hydroxylase: Mechanistic Insight into O2 Activation, *J. Am. Chem. Soc.131*, 7685-7698.

[25] Fitzpatrick, P. F., 1999, Tetrahydropterin-dependant amino acid hydroxylases, *Annu. Rev. Biochem. 68*, 355–381.

[26] Boadle-Biber, M.C., 1993, Regulation of serotonin synthesis, *Prog. Biophys. Molec. Biol. 60*, 1-15.

[27] Kaufman, S., 1959, Studies on the mechanism of the enzymatic conversion of phenylalanine to tyrosine, *J. Biol. Chem. 234*, 2677–2682.

[28] Udenfriend, S. and Cooper, J. R., 1952, The enzymatic conversion of phenylalanine to tyrosine, *J. Biol. Chem. 194*, 503-511.

[29] Al Hafid, N. and Christodoulou, J., 2015, Phenylketonuria: a review of current and future treatments, *Transl. Pediatr. 4(4)*, 304–317.

[30] Nagatsu, T., Levitt, M., and Udenfriend, S., 1964, Tyrosine hydroxylase the initial step in norepinephrine biosynthesis, *J. Biol. Chem. 239*, 2910-2917.

[31] Dunkley, P. R., Bobrovskaya, L., Graham, M. E., von Nagy-Felsobuki, E. I., and Dickson, P. W., 2004, Tyrosine hydroxylase phosphorylation: regulation and consequences, *J. Neurochem. 91(5)*, 1025-1043.

[32] McKinney, J., Teigen, K., Frøystein, N. A., Salaün, C., Knappskog, P. M., Haavik, J., and Martínez, A., 2001, Conformation of the substrate and pterin cofactor bound to human tryptophan hydroxylase. Important role of Phe313 in substrate specificity, *Biochemistry, 40*, 15591–15601.

[33] Daubner, S. C., Melendez, J., and Fitzpatrick, P. F., 2000, Reversing the substrate specificities of phenylalanine and tyrosine hydroxylase: aspartate 425 of tyrosine hydroxylase is essential for L-DOPA formation, *Biochemistry 39*, 9652–9661.

[34] Fitzpatrick, P. F., 1991, Studies of the rate-limiting step in the tyrosine hydroxylase reaction: alternate substrates, solvent isotope effects, and transition state analogs, *Biochemistry 30*, 6386-6391.

[35] Fisher, D. B. and Kaufman, S., 1973, The Stimulation of Rat Liver Phenylalanine Hydroxylase by Lysolecithin and α-Chymotrypsin, *J. Biol. Chem. 248*, 4345-4353.

[36] Lovenberg, W., Jequier, E., and Sjoerdsma, A., 1967, Tryptophan hydroxylation: measurement in pineal gland, brainstem, and carcinoid tumor, *Science 155*, 217-219.

[37] Amireault, P., Sibon, D., and Cote, F., 2013, Life without peripheral serotonin: insights from tryptophan hydroxylase 1 knockout mice reveal the existence of paracrine/autocrine serotonergic networks, *Chem. Neurosci. 4(1)*, 64–71.

[38] Murphy, K. L., Zhang, X., Gainetdinov, R. R., Beaulieu, J.-M., and Caron, M. G., 2008, A regulatory domain in the N terminus of tryptophan hydroxylase 2 controls enzyme expression, *J. Biol. Chem. 283*, 13216-13224.

[39] Tenner, K., Walther, D., and Bader, M., 2007, Influence of human tryptophan hydroxylase 2 N- and C-terminus on enzymatic activity and oligomerization, *J. Neurochem. 102*, 1887-1894.

[40] McKinney, J., Knappskog, P. M., and Haavik, J., 2005, Different properties of the central and peripheral forms of human tryptophan hydroxylase, *J. Neurochem. 92*, 311–320.

[41] Winge, I., McKinney, J.A., Ying, M., D'Santos, C. S., Kleppe, R., Knappskog, P. M., and Haavik, J., 2008, Activation and stabilization of human tryptophan hydroxylase 2 by phosphorylation and 14-3-3 binding, *Biochem. J. 410(1)*, 195-204.

[42] Kuhn, D. M., Arthur, R. Jr., and States, J. C., 1997, Phosphorylation and activation of brain tryptophan hydroxylase: identification of serine-58 as a substrate site for protein kinase A, *J. Neurochem. 68*, 2220–2223.

[43] Kuhn, D. M., Sakowski, S. A., Geddes, T. J., Wilkerson, C., and Haycock, J. W., 2007, Phosphorylation and activation of tryptophan hydroxylase 2: identification of serine-19 as the substrate site for calcium, calmodulin-dependent protein kinase II, *J. Neurochem. 103(4)*, 1567-1573.

[44] Aitken, A., 2006, 14-3-3 proteins: A historic overview, *Semin. Cancer Biol. 16(3)*, 162–172.

[45] Banik, U., Wang, G.A., Wagner, P.D., and Kaufman, S., 1997, Interaction of Phosphorylated Tryptophan Hydroxylase with 14-3-3 Proteins, *J. Biol. Chem. 272(42)*, 26219-26225.

[46] Ng, J., Papandreou, A., Heales, S. J., and Kurian, M. A., 2015, Monoamine neurotransmitter disorders--clinical advances and future perspectives, *Nat. Rev. Neurol. 10*, 567-584.

[47] Turlejski, K., 1996, Evolutionary ancient roles of serotonin: long-lasting regulation of activity and development, *Acta Neurobiol. Exp. 56(2)*, 619–636.

[48] Hasegawa, H. and Nakamura, K., 2009, Tryptophan Hydroxylase and Serotonin Synthesis Regulation, in Handbook of the Behavioral Neurobiology of Serotonin, edited by C.P. Müller, B.L. Jacobs, Academic press, Chapter 2.3, 183-202.

[49] Berger, M., Gray, J. A., and Roth, B. L., 2009, The expanded biology of serotonin, *Annu. Rev. Med. 60*, 355-366.

[50] Craig, D. A. and Martin, G. R., 1993, 5-HT1B receptors mediate potent contractile responses to 5-HT in rat caudal artery, *Br. J. Pharmacol. 109*, 609–611.

[51] Walther, D. J., Peter, J. U., Winter, S., Höltje, M., Paulmann, N., Grohmann, M., Vowinckel, J., Alamo-Bethencourt, V., Wilhelm, C. S., Ahnert-Hilger, G., and Bader, M., 2003, Serotonylation of small GTPases is a signal transduction pathway that triggers platelet alpha-granule release, *Cell 115(7)*, 851-862.

[52] Welford, R. W. D., Vercauteren, M., Trébaul, A., Cattaneo, C., Eckert, D., Garzotti, M., Sieber, P., Segrestaa, J., Studer, R., Groenen, P. M. A., and Nayler, O., 2016, Serotonin biosynthesis as a predictive marker of serotonin pharmacodynamics and disease-induced dysregulation, *Sci. Rep. 6*, 30059.

[53] Grider, J. R., Kuemmerle, J. F., and Jin, J. G., 1996, 5-HT released by mucosal stimuli initiates peristalsis by activating 5-HT4/5-HT1p receptors on sensory CGRP neurons, *Am. J. Physiol. 270*, 778–782.

[54] Gershon, M. D., 2003, Serotonin and its implication for the management of irritable bowel syndrome, *Rev. Gastroenterol. Disord. 3 (Suppl 2)*, 25–34.

[55] Fabre, A., Marchal-Sommé, J., Marchand-Adam, S., Quesnel, C., Borie, R., Dehoux, M., Ruffié, C., Callebert, J., Launay, J. M., Hénin, D., Soler, P., and Crestani, B., 2008, Modulation of bleomycin-induced lung fibrosis by serotonin receptor antagonists in mice, *Eur. Respir. J. 32(2)*, 426-436.

[56] Yadav, V. K., Balaji, S., Suresh, P. S., Liu, X. S., Lu, X., Li, Z., Guo, X. E., Mann, J. J., Balapure, A. K., Gershon, M. D., Medhamurthy, R., Vidal, M., Karsenty, G., and Ducy, P., 2010, Pharmacological inhibition of gut-derived serotonin synthesis is a potential bone anabolic treatment for osteoporosis, *Nat. Med. 16(3)*,308-312.

[57] Kulke, M. H., O'Dorisio, T., Phan, A., Bergsland, E., Law, L., Banks, P., Freiman, J., Frazier, K., Jackson, J., Yao, J. C., Kvols, L., Lapuerta, P., Zambrowicz, B., Fleming, D., and Sands, A., 2014, Telotristat etiprate, a novel serotonin synthesis inhibitor, in patients with carcinoid syndrome and diarrhea not adequately controlled by octreotide, *Endocr. Relat. Cancer 21(5)*, 705-714.

[58] Hornung, J. P., 2003, The human raphe nuclei and the serotonergic system, *J. Chem. Neuroanat. 26(4)*, 331-343.

[59] Brodie, B. B. and Shore, P. A., 1957, A concept for a role of serotonin and norepinephrine as chemical mediators in the brain, *Ann. N. Y. Acad. Sci. 66(3)*, 631-642.

[60] Lucki I., 1998, The spectrum of behavior influenced by serotonin, *Biol. Psychiatry 44*, 151-62.

[61] Zhang, X., Gainetdinov, R. R., Beaulieu, J. M., Sotnikova, T. D., Burch, L. H., Williams, R. B., Schwartz, D. A., Krishnan, K. R., and Caron, M. G., 2005, Loss-of-function mutation in tryptophan hydroxylase-2 identified in unipolar major depression, *Neuron 45(1)*, 11-16.

[62] Torrente, M. P., Gelenberg, A. J., and Vrana, K. E., 2012, Boosting serotonin in the brain: is it time to revamp the treatment of depression?, *J. Psychopharmacol. 26*, 629-635.

[63] Liu, Q., Yang, Q., Sun, W., Vogel, P., Heydorn, W., Yu, X., Hu, Z., Yu, W., Jonas, B., Pineda, R., Calderon-Gay, V., Germann, M., O'Neill, E., Brommage, R., Cullinan, E., Platt, K., Wilson, A., Powell, D., Sands, A., Zambrowicz, B., and Shi, Z., 2008, Discovery and Characterization of Novel Tryptophan Hydroxylase Inhibitors That Selectively Inhibit Serotonin Synthesis in the Gastrointestinal Tract, *J. Pharmacol. Exp. Ther. 325*, 47-55.

[64] Popova, N. K. and Kulikov, A.V., 2010, Targeting tryptophan hydroxylase 2 in affective disorder, *Expert Opin. Ther. Targets 14*, 1259-1271.

[65] Matthes, S., Mosienko, V., Bashammakh, S., Alenina, N., and Bader, M., 2010, Tryptophan hydroxylase as novel target for the treatment of depressive disorders, *Pharmocology 85*, 95-109.

[66] Walther, D. J. and Bader, M., 2003, A unique central tryptophan hydroxylase isoform, *Biochem. Pharmacol. 66*, 1673–1680.

[67] Satterlee, W. G., Serpick, A., and Bianchine, J. R., 1970, The Carcinoid Syndrome: Chronic Treatment with Para-Chlorophenylalanine, *Ann. Intern. Med. 72(6)*, 919-921.

[68] Engelman, K., Lovenberg, W., and Sjoerdsma, A., 1967, Inhibition of Serotonin Synthesis by Para-Chlorophenylalanine in Patients with the Carcinoid Syndrome, *N. Engl. J. Med. 277*, 1103-1108.

[69] Kvols, L. K., 1986, Metastatic carcinoid tumors and the carcinoid syndrome. A selective review of chemotherapy and hormonal therapy, *Am. J. Med. 81*, 49–55.

[70] Sjoerdsma, A., Lovenberg, W., Engelman, K., Carpenter, W. T., Wyatt, R. J., and Gessa, G. L., 1970, Serotonin now; clinical implications of inhibiting its synthesis with parachlorophenylalanine, *Ann. Intern. Med. 73*, 607-629.

[71] Weber, L. J., 1970, p-Chlorophenylalanine depletion of gastrointestinal 5-hydroxytryptamine, *Biochem. Pharmacol. 19*, 2169–2172.

[72] Koe, B. K. and Weissman, A., 1966, p-Chlorophenylalanine: a specific depletor of brain serotonin, *J. Pharmacol. Exp. Ther. 154*, 499–516.

[73] Goldberg, D. R., De Lombaert, S., Aiello, R., Bourassa, P., Barucci, N., Zhang, Q., Paralkar, V., Stein, A. J., Valentine, J., and Zavadoski, W., 2016, Discovery of acyl guanidine tryptophan hydroxylase-1 inhibitors, *Bioorg. Med. Chem. Lett. 26(12)*, 2855-2860.

[74] Goldberg, D. R., De Lombaert, S., Aiello, R., Bourassa, P., Barucci, N., Zhang, Q., Paralkar, V., Valentine, J., and Zavadoski, W., 2016, Discovery of spirocyclic proline tryptophan hydroxylase-1 inhibitors, *Bioorg. Med. Chem. Lett. 26*, 1124–1129.

[75] Petrassi, M., Barber, R., Be, C., Beach, S., Cox, B., D'Souza, A. M., Duggan, N., Hussey, M., Fox, R., Hunt, P., Jarai, G., Kosaka, T., Oakley, P., Patel, V., Press, N., Rowlands, D., Scheufler, C., Schmidt, O., Srinivas, H., Turner, M., Turner, R., Westwick, J., Wolfreys, A., Pathan, N., Watson, S., and Thomas, M., 2017, Identification of a Novel Allosteric Inhibitory Site on Tryptophan Hydroxylase 1 Enabling Unprecedented Selectivity Over all Related Hydroxylases, *Front. Pharmacol. 8*, 240.

[76] Immadisetty, K., Geffert, L. M., Surratt, C. K. and Madura, J. D., 2013, New design strategies for antidepressant drugs, *Expert Opin. Drug Discov. 8(11)*, 1399-1414.

[77] Werner, E. R., Blau, N., and Thöny, B., 2011, Tetrahydrobiopterin: biochemistry and pathophysiology, *Biochem J. 438(3)*, 397-414.

[78] Miwa, S., Watanabe, Y., and Hayaishi, O., 1985, 6R-L-erythro-5,6,7,8-tetrahydrobiopterin as a regulator of dopamine and serotonin biosynthesis in the rat brain, *Arch. Biochem. Biophys. 239(1)*, 234-241.

[79] Moran, G. R., Derecskei-Kovacs, A., Hillas, P. J., and Fitzpatrick, P. F., 2000, On the Catalytic Mechanism of Tryptophan Hydroxylase, *J. Am. Chem. Soc. 122(19)*, 4535–4541.

[80] Lazarus, R. A., Benkovic, S. J., and Kaufman, S., 1983, Phenylalanine hydroxylase stimulator protein is a 4a-carbinolamine dehydratase, *J. Biol. Chem. 258*, 10960–10962.

[81] Kaufman, S., 1961, The Nature of the Primary Oxidation Product Formed from Tetrahydropteridines during Phenylalanine Hydroxylation, *J. Biol. Chem. 236*, 804-810.

[82] Kaufman, S., 1963, The Structure of the Phenylalanine Hydroxylase Cofactor, *Proc. Natl. Acad. Sci. 50(6)*, 1085–1093.

Chapter 2

Purification of tryptophan hydroxylase

This chapter starts by introducing the background of TPH purification and how the purification strategy, utilized in this dissertation, has been optimized by previous students of the Metalloprotein Chemistry and Engineering Group at DTU. The optimized purification procedure is presented followed by a description of how the procedure has been applied to the different TPH variants. Results of purification of *h*TPH2 utilizing this procedure are subsequently presented. This is followed by a presentation and discussion of the purification yields obtained for the different TPH variants.

Outline

2.1 Introduction and background

For proper enzymatic characterization sufficient quantities of pure enzyme are required. Extraction from its original source is a tedious procedure and will often yield low quantities of the target enzyme. This is also the case for TPH, as it has been extracted only in low quantities from brain tissues [83-85] and purification or the extracts has resulted in low yields [86-89]. Recombinant expression of TPH1 from different mammalian species in *E. coli* has greatly increased the available quantities of active enzyme. Despite the increased quantities of TPH1, characterization has been hampered by its inherently poor stability.[90-93] Especially the N-terminal regulatory domain has been identified as the source of TPH instability and reduced solubility.[94] The quantity of stable enzyme was increased by recombinant expression of only the catalytic domain of TPH1 (cTPH1) in *E. coli.*[95] The amount of active TPH1 was increased ~10-fold compared to full-length. Furthermore, it was found that high ionic strength, in the form of 100 mM $(NH_4)_2SO_4$, greatly increases purification yields. A rapid and more convenient procedure for achieving pure catalytic domain of TPH1 in high quantities has subsequently been described by Nielsen *et al*.[96]

Purification strategies for full-length TPH have been optimized by expressing TPH variants as fusion protein, which enables very selective affinity chromatography. TPH1 has been expressed as a fusion protein with maltose binding protein [91,97], glutathione S-transferase [98], and Histidine-tag [99]. In all these cases, attempts to cleave the fusion protein and isolate active TPH1 were unsuccessful. In a study by McKinney *et al.*[100], fusion proteins of *human* TPH1 and TPH2 with 6xHis-MBP were expressed in *E. coli* and purified in

high yields. The fusion proteins were successfully cleaved with tobacco etch virus (TEV) protease. However, the purity of the cleaved TPH1 and TPH2 samples was low (50 and 80 % pure, respectively).

In the Metalloprotein Chemistry and Engineering Group at DTU, a method for purification of *chicken* cTPH1 and *human* cTPH2 expressed in *E. coli* was presented by M. S. Nielsen.[101] The procedure consists of two steps, anion exchange followed by gel filtration. J. Boesen optimized and applied this strategy successfully to *human* cTPH1.[102] J. Boesen furthermore fund that the regulatory domain of *h*TPH1 has a requirement for high ionic strength during purification.

Ion-exchange is excluded because of the requirement of *h*TPH1 for high salt concentration. Therefore, L. T. Haahr developed a purification procedure for *h*TPH1, which, instead of ion-exchange, includes an affinity chromatographic step using a MBP fusion protein.[103] This purification strategy allows the use of 300 mM $(NH_4)_2SO_4$, which has been found to stabilize the regulatory domain.[102] Successful cleavage of the fusion protein was achieved using *human* rhinovirus 3C protease (3CP). After cleavage, stable TPH was achieved which subsequently was further purified with additional affinity and gel filtration steps. This method was also applied successfully to purify the regulatory and catalytic domains of TPH1 (rc*h*TPH1).[103] This method was, however, non-successful in relation to TPH2 variants containing the regulatory domain.[103]

The purification strategy presented by L. T. Haahr includes two affinity purification steps and two gel filtration steps and has a duration of two days. The duration of the purification was significantly reduced, while the yield was increased, by performing on-column cleavage of the MBP-TPH fusion protein.[104] Using on-column cleavage with MBP-3CP, the purification procedure is reduced to one affinity step and one gel filtration step. In my master's project, this procedure was optimized to successfully purify rc*h*TPH2 in quantities suitable for enzymatic characterization.[105] The purification yield was found to increase significantly when the 47 N-terminal residues were removed.[105]

2.2 TPH variants and nomenclature

Throughout this dissertation, abbreviation of the different TPH variants will be used. As will be described in section 2.3.2, all TPH variants are expressed as fusion proteins with MBP. Before MBP is cleaved from the target TPH variant, the variant will be referred to as MBP-TPH. In total, 14 *human* TPH variants were purified according to the procedures described in section 2.3. In Table 2.1, description, abbreviation, molecular weight, and extinction coefficient at 280 nm (calculated using ProtParam [107]) for each variant are listed. In the abbreviation, the first letter(s) refers to the domains which are included in the TPH variant; "r" refers to the regulatory domain, "c" refers to the catalytic domain, and if no letters are included the full-length variant is referred to. The letter(s) in italic refers to the species from which the protein sequence originates from; i.e. "*h*" refers to *Homo sapiens* (human). NΔ followed by a number refers to truncation of that number of residues from the N-terminus.

2.3 Experimental procedures

The purification strategy and conditions used in this study, is based on the purification procedure developed by L. T. Haahr [103] which has been optimized by previous members of the Metalloprotein Chemistry and Engineering Group. A flow diagram of the procedure is presented in Figure 2.1.

2.3.1 Materials

All used chemicals were of analytical grade, and all solutions were prepared using water from an 18.2 MΩ·cm Milli-Q synthesis A10 Q-Gard system which was filtered through a 0.22 µm filter. Protein purification was performed on an ÄKTA purifier 100 from GE Healthcare. Utilized GE Healthcare column variants: HiLoad Superdex 200 26/60 pg, HiLoad Superdex 75 26/60 pg, and XK 16/20 column packed with 25 mL

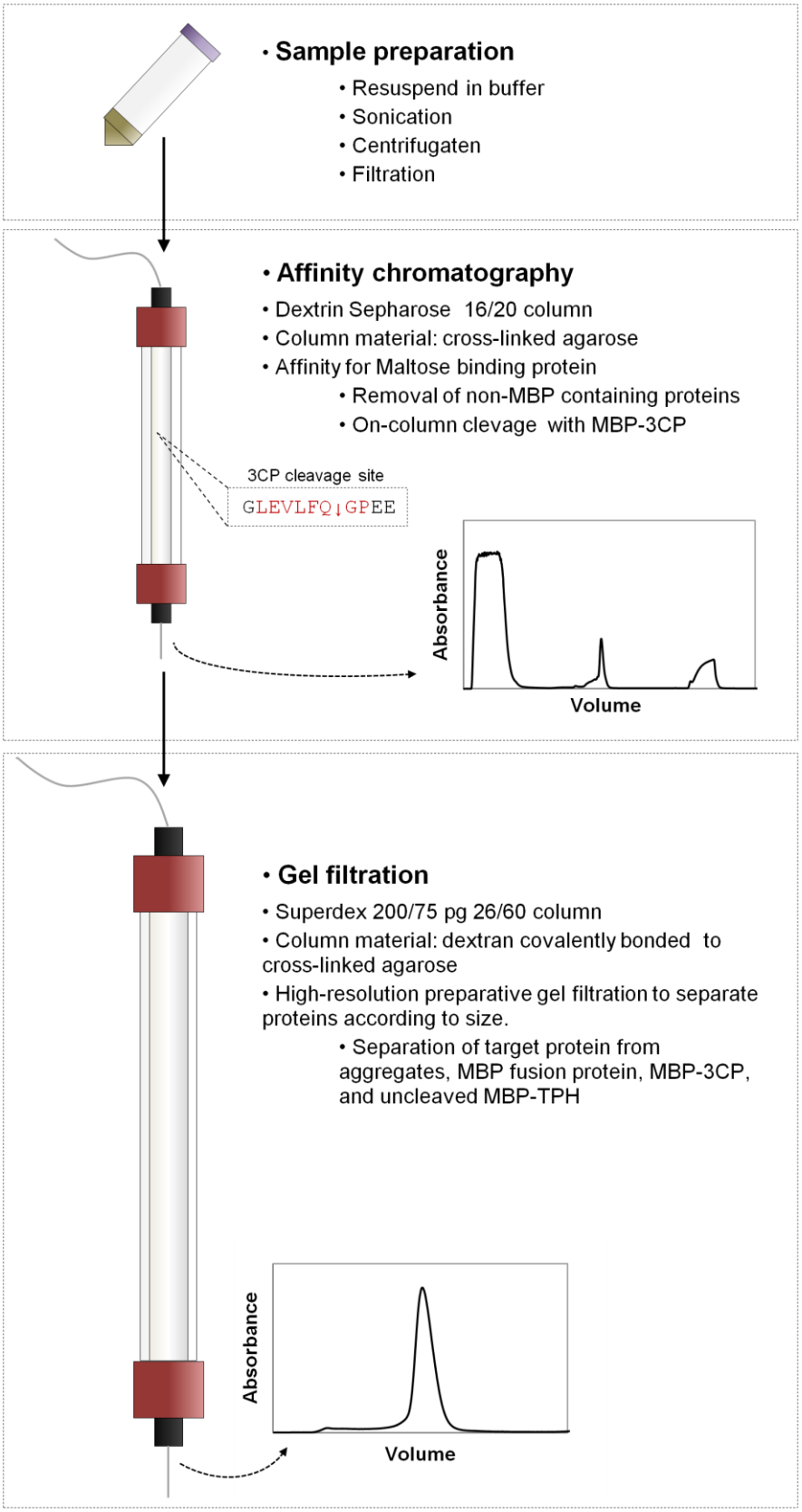

Figure 2.1. Flow chart presenting the general purification procedure of the MBP-TPH variants.

Dextrin Sepharose High Performance media. During purifications, all TPH containing solutions were kept in ice water, except during the chromatographic steps, which were performed at room temperature. Protein solutions were concentrated using an Amicon ultrafiltration cell with an Ultracell PL-3 membrane. Protein concentrations were determined by measuring the absorbance at 280 nm on an ND-1000 NanoDrop Spectrophotometer from Saveen Werner.

2.3.2 Cloning and expression of TPH variants

The expression of the TPH variants was conducted by laboratory technicians and the following procedure was used. Full-length cDNA optimized for expression in *E. coli* was obtained from GenScript. All proteins were expressed as maltose binding protein fusion proteins from the pET26 expression vector in *E. coli* BL21(DE3) (Novagen) cells. The sequences of the proteins expressed are given in Appendix B. The recombinant fusion proteins contain a cleavage recognition site for *human* rhinovirus 3C protease [106]. The construct encoding the different protein variants was obtained by PCR. The primers used are listed in the supporting information of Appendix A.1. All DNA sequences were verified by sequencing (Eurofins). Proteins were expressed at 20°C for 14 h as previously described [96].

2.3.3 Purification of c*h*TPH1 variants

E. coli cells from one or more 650 mL cultures were thawed from -80 °C and resuspended in buffer solution containing 20 mM TRIS/H_2SO_4, 100 mM $(NH_4)_2SO_4$, pH 8.0, to a volume of 40 mL (per 650 mL cell culture). The resuspended cell culture was lysed by sonication for 3x30 seconds using a Satorius Labsonic at 80 % amplitude, while kept in ice water. The lysed sample was centrifuged at 4 °C and 18,000 x g for 20 minutes. The supernatant was decanted to another tube and centrifuged a second time at 4 °C and 18,000 x g for 20 minutes, while the pellet was discarded. The supernatant was collected and filtered through a 0.45 µm filter. A volume of approximately 35 mL filtered supernatant was loaded with a flow-rate of 5 ml/min onto a Dextrin Sepharose column which was equilibrated with 5 column volumes of buffer solution. Following sample loading, an MBP-3CP solution was prepared by diluting MBP-3CP from stock with buffer solution to a concentration of 2.2 µM. 30 ml MBP-3CP solution was loaded onto the column with a flow-rate of 5 ml/min, and the column was incubated at room temperature for one hour. Once the flow (5 mL/min) was resumed, 10 mL of the protein-containing eluate was collected. The collected solution, containing target protein, was filtered through a 0.45 µm filter prior to loading on a HiLoad Superdex 200 prep grade column, which had been equilibrated with 2 column volumes of buffer solution. The same buffer solution from the affinity chromatography step was used as mobile phase using a flow-rate of 2.5 mL/min, and UV-detected (280 nm) peaks, containing the target protein, were collected. The concentration of the collected protein was determined by UV-Vis absorption at 280 nm utilizing theoretical extinction coefficients obtained from Expasy [107]. The samples were either concentrated by ultrafiltration prior to freezing in liquid nitrogen, or if the concentration of target protein was high enough in the eluate, the ultrafiltration was bypassed, and the protein solution was frozen in liquid nitrogen and stored at -80 °C.

2.3.4 Purification of rc*h*TPH1 and *h*TPH1

Purification of the rc*h*TPH1 and *h*TPH1 was conducted with the same procedure as described for c*h*TPH1, with the only difference being the buffer solution. These variants were purified in either 20 mM TRIS/H_2SO_4, 300 mM $(NH_4)_2SO_4$, pH 8.0 or 20 mM TRIS/H_2SO_4, 300 mM $(NH_4)_2SO_4$, 3 mM L-phenylalanine, pH 8.0 throughout the purification.

2.3.5 Purification of c*h*TPH2 variants

Purification of the c*h*TPH2 variants was conducted in 20 mM HEPES/NH_4OH, 100 mM $(NH_4)_2SO_4$, pH 7.0 with the same procedure as described for c*h*TPH1.

2.3.6 Purification of rc*h*TPH2

Purification of the rc*h*TPH2 variants was conducted in 20 mM HEPES/NH_4OH, 300 mM $(NH_4)_2SO_4$, 3 mM L-phenylalanine, pH 7.0 with the same procedure as described for c*h*TPH1. As rc*h*TPH2 could not be purified in the absence of L-phenylalanine, a method that uses two buffer solutions was used. The resuspension, lysis, and affinity chromatography step, was performed with a buffer containing 20 mM HEPES/NH_4OH, 300 mM $(NH_4)_2SO_4$, 3 mM L-phenylalanien, pH 7.0 and the gel filtration was performed with a buffer containing 20 mM HEPES/NH_4OH, 300 mM $(NH_4)_2SO_4$, pH 7.0. With this procedure the final purification product is assumed not to contain L-phenylalanine.

2.3.7 Purification of NΔ47-rc*h*TPH2 variants and *h*TPH2

Purification of NΔ47-rc*h*TPH2 variants and *h*TPH2 were conducted in either 20 mM HEPES/NH_4OH, 300 mM $(NH_4)_2SO_4$, pH 7.0 or 20 mM HEPES/NH_4OH, 300 mM $(NH_4)_2SO_4$, 3 mM L-phenylalanine, pH 7.0 with the same procedure as described for c*h*TPH1.

2.3.8 SDS-PAGE analysis

Evaluation of molecular weights and purity was conducted by sodium dodecyl sulfate polyacrylamide gel electrophoresis (SDS-PAGE). Proteins were resolved on Mini-PROTEAN TGX gels (7.5 %) from Bio-Rad run at 100 V for 75 min with a protein standard from Bio-Rad (no. 161-0304). Gels were stained with Coomassie Blue G-250 to visualize the proteins.

2.4 Introduction to TPH variants

In total 14 variants have been produced to characterize TPH (Table 2.1). Because all TPH variants were purified as fusion proteins with MBP, they contain two additional residues in the N-terminus (Gly and Pro). These residues originate from the recognition and cleavage site of 3CP, Figure 2.1. The design of the Y125A-, Y125L-, Y125W-c*h*TPH1, Y171A-, Y171W-c*h*TPH2, loop-swap-c*h*TPH1, and loop-swap-c*h*TPH2 variants is described in chapter 7. NΔ47-rc*h*TPH2 will be described in the following section.

2.4.1 Truncation of the N-terminus

Full-length *h*TPH2 and rc*h*TPH2 have proven to be challenging to purify in quantities sufficient for enzymatic characterization.[103,105] In pursuit of a *h*TPH2 variant with improved purification properties, attention was turned towards the crystal structure of phenylalanine hydroxylase. The structure of PAH from *rat* (PDB entry: 1PHZ) lacks interpretable electron density in the 18 N-terminal residues, suggesting that the terminus is mobile.[108,109] The mobility of the N-terminus has also been confirmed by an NMR study.[110] The mobility of this region could cause instability and promote aggregation. The termini of *rn*PAH and *h*TPH2 were aligned to identify a corresponding mobile region of *h*TPH2, Figure 2.2.

Figure 2.2 shows that the first 47 residues of *h*TPH2 align with the mobile 18 residues of *rn*PAH, which indicates that these residues of *h*TPH2 are mobile. *h*TPH2 has an additional 46 residues in the N-terminus compared to *h*TPH1. Unlike *h*TPH2, *h*TPH1 has been purified with high yields which also suggests that the N-terminus of *h*TPH2 induce instability or insolubility. Therefore, a mutant variant lacking 47 residues in the N-terminus, NΔ47-rc*h*TPH2, was expressed, purified, and characterized.

Table 2.1. Included domain, molecular weights, and theoretical extinction coefficients at 280 nm of the investigated TPH variants.

Domain(s)	Isoform	Abbreviation	Molecular weight (Da)	Extinction coefficient at 280 nm (M^{-1} cm^{-1})
Catalytic	TPH1	c*h*TPH1	36,220	33,350
Catalytic	TPH1	Y125W-c*h*TPH1	36,243	37,360
Catalytic	TPH1	Y125A-c*h*TPH1	36,128	31,860
Catalytic	TPH1	Y125L-c*h*TPH1	36,170	31,860
Catalytic	TPH1	Loop-swap-c*h*TPH1	36,250	33,350
Catalytic and regulatory	TPH1	rc*h*TPH1	47,816	33,350
Full-length	TPH1	*h*TPH1	51,008	33,350
Catalytic	TPH2	c*h*TPH2	36,339	39,310
Catalytic and regulatory	TPH2	rc*h*TPH2	52,574	51,800
Catalytic and regulatory	TPH2	NΔ47-rc*h*TPH2	47,434	44,810
Full-length	TPH2	*h*TPH2	56,080	53,290
Catalytic	TPH2	Loop-swap-c*h*TPH2	36,309	39,310
Catalytic	TPH2	Y171A-c*h*TPH2	36,247	37,820
Catalytic	TPH2	Y171W-c*h*TPH2	36,362	43,320

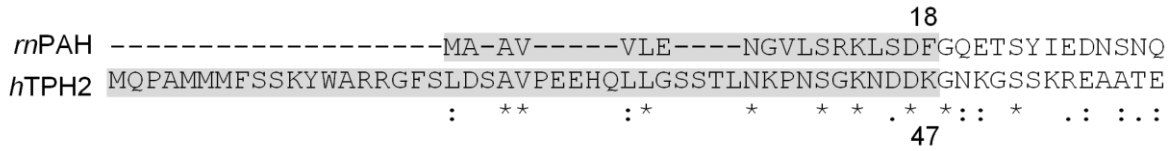

Figure 2.2. Alignment of *h*TPH2 and *rn*PAH, using Clustal Omega (only the first 60 residues shown). "-" marks a gap in the primary structure. "*" marks conserved residues, ":" marks conservation of residues with highly similar properties and "." marks conservation of residues with slightly similar properties. The grey background in the sequence of *rn*PAH illustrates the highly mobile part of the N-terminal region, for which no crystal structure is available. The gray background in *h*TPH2 illustrates the corresponding region.

2.5 Results of TPH purifications

2.5.1 Purification of TPH variants

All TPH variants were purified according to section 2.3. Purifications of c*h*TPH1, rc*h*TPH1, *h*TPH1, c*h*TPH2, NΔ47-rc*h*TPH2, and rc*h*TPH2 resulted in chromatograms, yields, and purity similar to the ones obtained in previous theses or dissertations.[101-103,105] Several mutant versions were constructed for c*h*TPH1 and c*h*TPH2; Loop-swap-c*h*TPH1, Y125A-c*h*TPH1, Y125L-c*h*TPH1, Y125W-c*h*TPH, Loop-swap-c*h*TPH2,

Y171A-c*h*TPH2, and Y171W-c*h*TPH2. The purpose of these mutations is described and discussed in chapter 7. All these mutant variants resulted in chromatograms very similar to the wild-type version (see Appendix C.2-10).

2.5.2 Purification of *h*TPH2

Full-length *h*TPH2 was purified in 20 mM HEPES/NH_4OH, 300 mM $(NH_4)_2SO_4$, 3 mM L-phenylalanine, pH 7.0. After lysis, centrifugation, and filtration, 35 mL supernatant was loaded on a dextrin sepharose column. The chromatogram from the affinity chromatographic step of *h*TPH2 is shown in Figure 2.3.

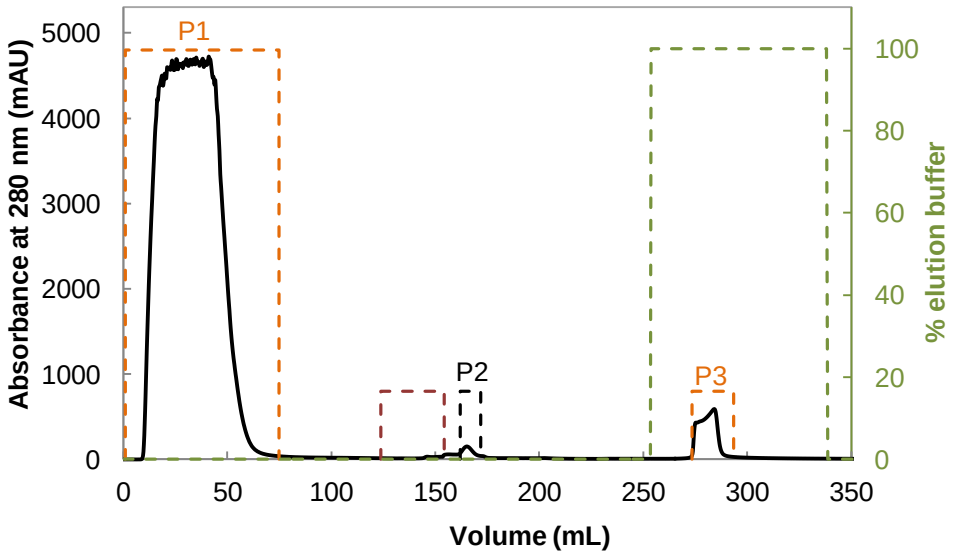

Figure 2.3. Chromatogram from affinity chromatography of *h*TPH2 using 20 mM HEPES/NH_4OH, 300 mM $(NH_4)_2SO_4$, 3 mM L-phenylalanine, pH 7.0 as mobile phase on a Dextrin Sepharose 16/12 column. The black line is the absorption at 280 nm. The red dashed line illustrates when MBP-3CP was loaded on the column. The green dashed line shows when the mobile phase was changed to elution buffer. The orange dashed lines indicate where samples for SDS-PAGE analysis were taken from P1 and P3. The black dashed line shows the collected protein from P2, which was also subjected to SDS-PAGE analysis.

First the flow-through of unwanted proteins was eluted. The SDS-PAGE analysis in Figure 2.4 shows that MPB-*h*TPH2 binds the column very well, as only small amounts of MBP-*h*TPH2 is found in Peak 1 (P1).

MPB-3CP was loaded and incubated for one hour. After the incubation period, P2 was eluted and collected. The SDS-PAGE analysis in Figure 2.4 shows that P2 contains *h*TPH2 with very low amounts of impurities. P3 contains MPB, MPB-3CP, and small amounts of MPB-*h*TPH2, which suggests incomplete cleavage. P2 from the chromatogram in Figure 2.3 was collected (10 mL) for further purification.

The 10 mL was loaded onto a gel filtration column resulting in two peaks eluting. Judged from the absence of a peak at the void volume (~108 mL) in the chromatogram in Figure 2.5, very small amounts of aggregate are formed. Two peaks are eluted at around 140 mL and 160 mL. The SDS-PAGE analysis shows that both peaks predominantly contain *h*TPH2. The elution volumes of P4 and P5 correspond to a higher ordered oligomer and tetramer, respectively.[103]

The yield of this purification was 1.9 mg/L cell culture. As large quantities are found in the pellet (P in Figure 2.4) after lysis and centrifugation, the low yield is probably accounted for by the low solubility of *h*TPH2.

The purification of *h*TPH2 was also conducted in a buffer solution that did not contain L-phenylalanine. The resulting chromatograms of this purification are very similar to the ones obtained with L-phenylalanine. The

chromatograms can be found in Appendix C.1. In the absence of L-phenylalanine, a purification yield of 0.4 mg/L cell culture was achieved. This yield is similar to the 0.6 mg/L cell culture obtained by L. T. Haahr using a 2 day off-column cleavage procedure.[103]

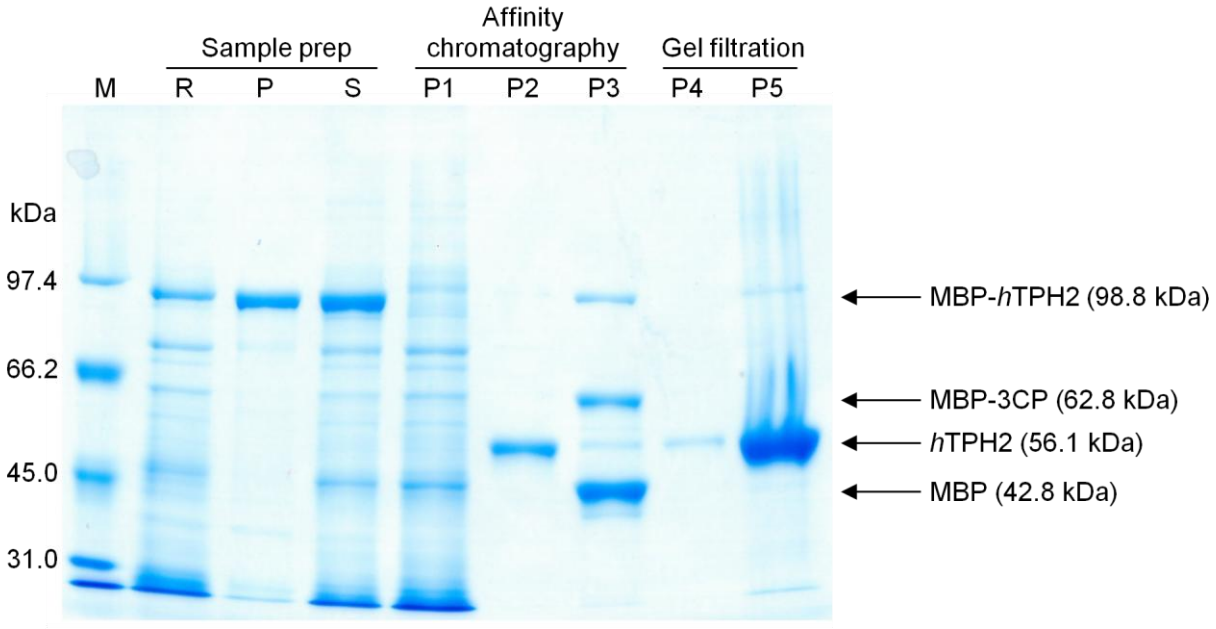

Figure 2.4. SDS-PAGE result of collected peaks from purification of *h*TPH2 using a buffer solution containing 20 mM HEPES/NH_4OH, 300 mM $(NH_4)_2SO_4$, 3 mM L-phenylalanine, pH 7.0. M: Molecular weight standard. R: Resuspension of cell culture (diluted 1:10). P: Resuspended pellet (diluted 1:10). S: Supernatant (diluted 1:10). P1: Flow-through of unwanted species (diluted 1:1). P2: Peak eluting after cleavage with MBP-3CP (diluted 1:1). P3: Peak from elution of MBP-bound species (diluted 1:1). P4 and P5: Peaks from gel filtration.

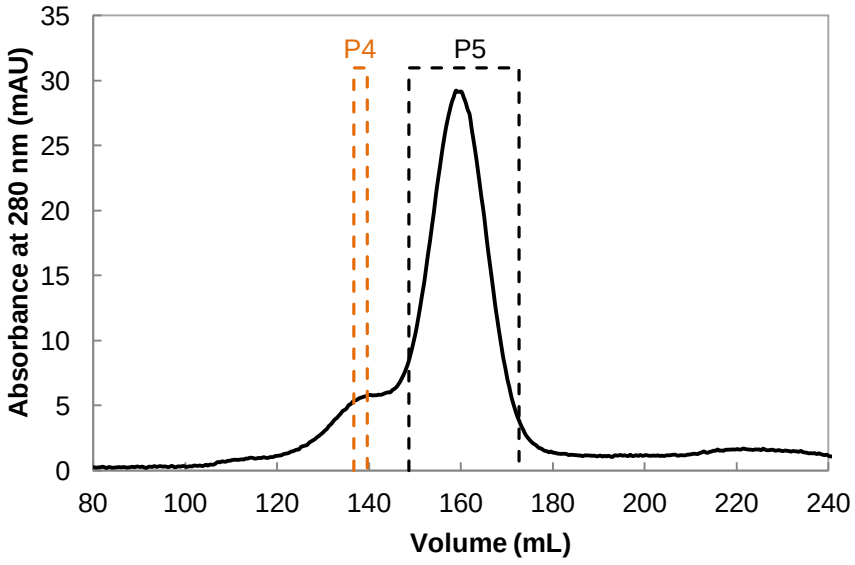

Figure 2.5. Chromatogram from gel filtration on a Hiload 26/600 Superdex 200 column of the collected protein from affinity chromatography in the purification of *h*TPH2 using 20 mM HEPES/NH_4OH, 300 mM $(NH_4)_2SO_4$, 3 mM L-phenylalanine, pH 7.0. The black line is the absorption at 280 nm. The orange dashed line indicates where sample for SDS-PAGE analysis was taken from P4. The black dashed line shows the collected protein from P5, which was also subjected to SDS-PAGE analysis.

2.6 Purification yields

The obtained purification yields differ significantly among the TPH variants. Some variants are purified in high yields while others are impossible to purify in quantities sufficient for enzymatic characterization. Tryptophan has been found to stabilize *h*TPH1 [97], but the presence of tryptophan complicates concentration determination and activity assays due to its absorption at 280 nm. For reasons described in chapter 3, phenylalanine was chosen as an alternative to tryptophan in the purification buffer solutions. In the following, Std and L-Phe buffers refer to buffer solutions without and with 3 mM L-phenylalanine, respectively.

2.6.1 Purification of TPH2 variants

Purification of c*h*TPH2 and the three mutant variants in 20 mM HEPES/NH_4OH, 100 mM $(NH_4)_2SO_4$, pH 7.0 resulted in yields between 10 and 16 mg/L cell culture. The purification yield of c*h*TPH2 did not change significantly when 3 mM L-phenylalanine was added to the purification buffer solution, Figure 2.6.

In the absence of L-phenylalanine, full-length *h*TPH2 was purified in very low quantities. Truncation of the C-terminal tetramerization domain resulted in a variant, rc*h*TPH2, which could not be isolated and concentrated in quantities suitable for characterization in Std buffer. Truncation of 47 residues in the N-terminus of the regulatory domain resulted in a variant, NΔ47-rc*h*TPH2, which could be purified in quantities comparable to c*h*TPH2.

With 3 mM L-phenylalanine in the buffer solution, the purification yield of *h*TPH2 was increased 5-fold (only based on one purification of each). When rc*h*TPH2 was purified with L-Phe buffer in the affinity chromatographic step and Std buffer in the gel filtration step, around 1 mg/L cell culture was achieved. This yield was increased 6-fold by using L-Phe buffer throughout the purification. The yield of NΔ47-rc*h*TPH2 was increased 4-fold by purifying with L-Phe buffer compared to Std buffer.

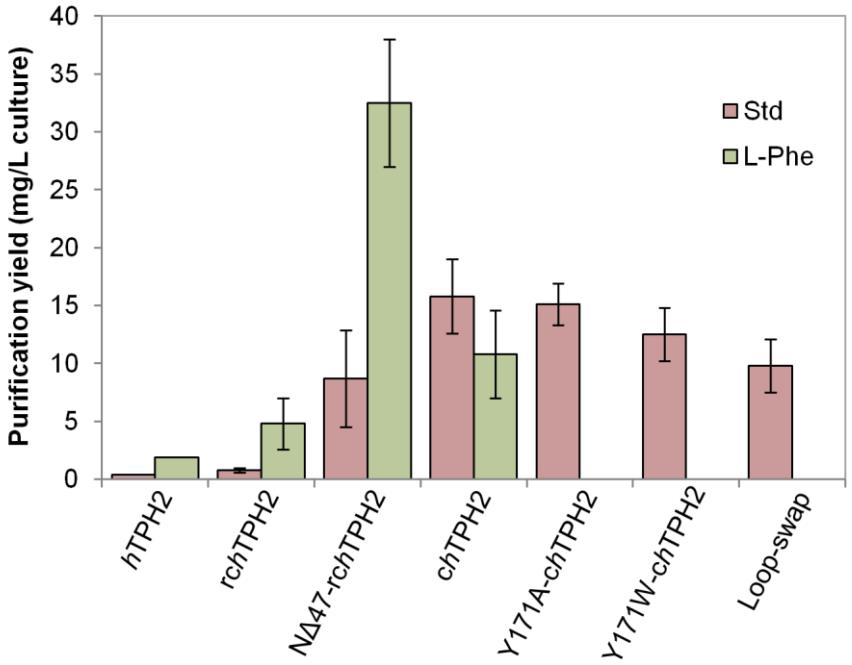

Figure 2.6. Average (±SD) yields obtained from purifications of the TPH2 variants (n=1-10). Red bars represent purifications using 20 mM HEPES/NH_4OH, 100 or 300 mM $(NH_4)_2SO_4$, pH 7.0 and green bars represent purifications using 20 mM HEPES/NH_4OH, 100 or 300 mM $(NH_4)_2SO_4$, 3 mM L-phenylalanine, pH 7.0 For data see Table D.1 in Appendix D.

The yields of variants containing the regulatory domain were increased significantly by introducing 3 mM L-phenylalanine to the purification buffer solution. It was investigated whether this was caused by an increase in the solubility of the variants. The solubility of the fusion proteins MBP-c*h*TPH2, MBP-rc*h*TPH2 and MBP-NΔ47-rc*h*TPH2 were analyzed by SDS-PAGE of cells lysed in either Std or L-Phe buffer, Figure 2.7. The SDS-PAGE analysis shows that the solubility of rc*h*TPH2 is rather low as great amounts are found in the insoluble fraction (P). In the absence of the regulatory domain, c*h*TPH2, the solubility increases significantly as the majority of the protein is found in the soluble fraction (S). Truncation of the 47 N-terminal residues resulted in increased solubility, however, still inferior to only the catalytic domain.

Addition of 3 mM phenylalanine to the buffer solution does not seem to have a profound effect on the solubility of any of the *h*TPH2 variants in Figure 2.7. Because the expression levels of the variants also seem equivalent, the profound differences in purification yield obtained in the absence and presence of phenylalanine do not seem to originate from a change in solubility.

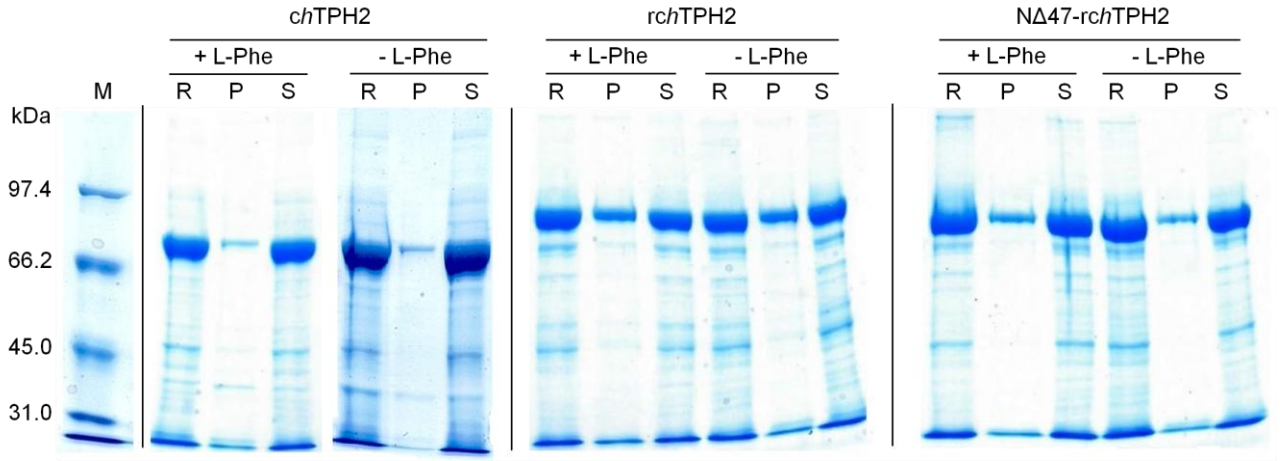

Figure 2.7. Solubility of *h*TPH2 variants. Comassie-blue stained SDS-PAGE gel (7.5 % acrylamide) from *E.coli* lysates showing total protein content in resuspension (R), pellet (P), and supernatant (S). A molecular weight marker with indicated weights is in the first lane. + L-Phe indicates the presence of 3 mM L-phenylalanine in the lysis buffer and - L-Phe indicates absence of L-phelynalanine.

2.6.2 Purification of TPH1 variants

All TPH1 variants comprising only the catalytic domain were purified in 20 mM TRIS/H_2SO_4, 100 mM $(NH_4)_2SO_4$, pH 8.0 while variants also comprising the regulatory domain were purified in 20 mM TRIS/H_2SO_4, 300 mM $(NH_4)_2SO_4$, pH 8.0. Increased ionic strength was used for *h*TPH1 and rc*h*TPH1 because J. Boesen found that these conditions stabilize the regulatory domain of TPH1.[102] Figure 2.8 shows that the yields of all the *h*TPH1 variants, besides Y125L-c*h*TPH1, are similar and ranges between 19 and 26 mg/L cell culture. Unlike *h*TPH2, variants of TPH1 which contain the regulatory domain are purified in high yields. Furthermore, 3 mM L-phenylalanine does not seem to have an effect on the purification yield of neither *h*TPH1 nor rc*h*TPH1.

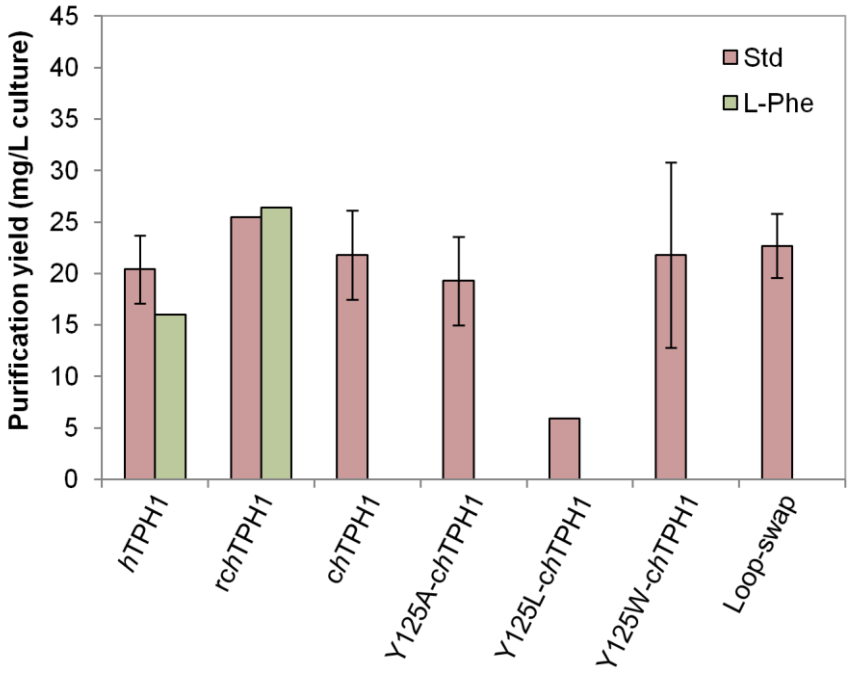

Figure 2.8. Average (±SD) yields obtained from purifications of the TPH1 variants (n=1-4). Red bars represent purifications using 20 mM TRIS/H_2SO_4, 100 or 300 mM $(NH_4)_2SO_4$, pH 8.0 and green bars represent purifications using 20 mM TRIS/H_2SO_4, 300 mM $(NH_4)_2SO_4$, 3 mM L-phenylalanine, pH 8.0 For data see Table D.1 in Appendix D.

2.7 Discussion

Characterization of both isoforms of TPH has been hampered by their inherent instability and solubility. Procedures enabling purification of quantities sufficient of enzymatic characterization of a variety of TPH variants has been developed by former student of the Metalloprotein Chemistry and Engineering Group at DTU.[101-103] The procedures are, however, not suitable for purifying *h*TPH2 variants containing the regulatory domain, as very low yields are obtained.[103] Even with the optimized procedure used in this dissertation, which only comprise one affinity chromatographic step, including on-column cleavage, followed by gel filtration, very low amounts were obtained.

Truncation of 47 residues in the N-terminus resulted in a variant that could be purified in quantities comparable to c*h*TPH2 which is sufficient for enzymatic characterization. In chapter 3, it is described that the thermostability of NΔ47-rc*h*TPH2 and rc*h*TPH2 are comparable. In this chapter, the SDS-PAGE analysis of MPB-NΔ47-rc*h*TPH2 and MPB-rc*h*TPH2, and MPB-c*h*TPH2 revealed that the solubility is significantly decreased by the presence of the regulatory domain but increased upon truncations of the N-terminus. The solubility of these variants is anticipated to be lowered in the absence of the MBP fusion partner. Judging from the observed purification yields, the influence of the N-terminus on the solubility might be even greater in the absence of the MBP fusion partner. Furthermore, L-phenylalanine did not have an effect on the solubility of the MBP-*h*TPH2 variants. Whether this is the case after cleavage of the fusion protein is unknown.

The presence of L-phenylalanine in the buffer solution significantly increased the purification yields of *h*TPH2 variants containing the regulatory domain. The yield of c*h*TPH2 was not increased, suggesting that L-phenylalanine has an effect only on the regulatory domain. Like rc*h*TPH2, addition of L-phenylalanine increased the yield of NΔ47-rc*h*TPH2. This suggests that L-phenylalanine does not exert its effect on the N-

terminus. The lower yield of c*h*TPH2 compared to NΔ47-rc*h*TPH2 purified in L-Phe buffer is caused by less efficient on-column cleavage of the fusion protein.[105]

With the two-step purification procedure used in this dissertation, *h*TPH1 and rc*h*TPH1 were purified with similar yields as previously obtained with the two day procedure (four-step procedure).[103] In contrast to the *h*TPH2 variants, L-phenylalanine had no influence on the purification yields of *h*TPH1 and rc*h*TPH1, suggesting that the stabilizing effect is isoform specific. This is unexpected considering the high sequence identity of the isoforms. The role of L-phenylalanine is explored in chapter 3 and 4.

2.8 Conclusion

In this chapter, it is demonstrated how full-length *human* TPH2 can be purified to homogeneity using a simple and fast two step procedure. The same holds true for a variety of deletion mutation variants and variants with single or multiple point mutations. Limited purification quantities are still obtained from purification of TPH2 variants containing the regulatory domain. The quantities can, however, be significantly increased by addition of 3 mM L-phenylalanine to the purification buffers. With the two-step purification procedure and addition of L-phenylalanine, around 30 mg NΔ47-rc*h*TPH2 is obtained per L cell culture. This quantity is sufficient for most experiments including crystallization attempts.

2.9 References

[83] Gal, E. M., Armstrong, J. C., and Ginsberg, B., 1966, The nature of in vitro hydroxylation of L-tryptophan by brain tissue, *J. Neurochem. 13(8)*, 643–654.

[84] Green, H. and Sawyer, J. L., 1966, Demonstration, characterization, and assay procedure of tryptophan hydroxylase in rat brain, *Anal. Biochem. 15(1)*, 53-64.

[85] Grahame-Smith, D. G., 1967, The Biosynthesis of 5-Hydroxytryptamine in Brain, *Biochem. J. 105*, 351-360.

[86] Jequier, E., Robinson, D. S., Lovenberg, P. W., and Sjoerdsma, A., 1969, Further Studies on Tryptophan Hydroxylase in Rat Brainstem and Beef Pineal, *Biochem. Pharmacol. 18*, 1071-1081.

[87] Tong, J. H. and Kaufman, S., 1975, Tryptophan Hydroxylase – Purification and some properties of the enzyme from rabbit hindbrain, *J. Biol. Chem. 250(11)*, 4152-4158.

[88] Joh. T. H., Shikimi, T., Pickel, V. M., and Reis, D. J., 1975, Brain tryptophan hydroxylase: Purification of, production of antibodies to, and cellular and ultrastructural localization in serotonergic neurons of rat midbrain, *Proc. Nat. Acad. Sci. 72(9)*, 3575-3579.

[89] D'Sa, C., Arthur, R., Jennings, I., Cotton, R. G. H., and Kuhn, D. M., 1996, Tryptophan hydroxylase: purification by affinity chromatography on calmodulin-sepharose, *J. Neurosci. Methods 69*, 149-153.

[90] Park, D. H., Stone, D. M., Kim, K. S., and Joh, T. H., 1994, Characterization of recombinant mouse tryptophan hydroxylase expressed in Escherichia coli, *Mol Cell Neurosci. 5(1)*, 87-93.

[91] Tipper, J. P., Citron, B. A., Ribeiro, P., and Kaufman, S., 1994, Cloning and expression of rabbit and human brain tryptophan hydroxylase cDNA in Escherichia coli, *Arch Biochem. Biophys. 315(2)*, 445-453.

[92] Yang, X-J. and Kaufman, S., 1994, High-level expression and deletion mutagenesis of human tryptophan hydroxylase, *Proc. Natl. Acad. Sci. USA 91*, 6659-6663.

[93] Vrana, K. E., Rucker, P. J., and Kumer, S. C., 1994, Recombinant rabbit tryptophan hydroxylase is a substrate for cAMP-dependent protein kinase, *Life Sci. 55*, 1045-1052.

[94] Carkaci-Salli, N., Flanagan, J. M., Martz, M. K., Salli, U., Walther, D. J., Bader, M., and Vrana, K. E., 2006, Functional domains of human tryptophan hydroxylase 2 (hTPH2), *J. Biol. Chem. 281*, 28105-28112.

[95] Moran, G. R., Daubner, S. C., and Fitzpatrick P. F., 1998, Expression and characterization of the catalytic core of tryptophan hydroxylase, *J. Biol. Chem. 273*, 12259-12266.

[96] Nielsen, M. S., Petersen, C. R., Munch, A., Vendelboe, T. V., Boesen, J., Harris, P., and Christensen, H. E. M., 2008, A simple two step procedure for purification of the catalytic domain of chicken tryptophan hydroxylase 1 in a form suitable for crystallization, *Protein Expr. Purif. 57*, 116-126.

[97] McKinney, J., Knappskog, P. M., Pereira, J., Ekern, T., Toska, K., Kuitert, B. B., Levine, D., Gronenborn, A. M., Martinez, A., and Haavik, J., 2004, Expression and purification of human tryptophan hydroxylase from Escherichia coli and Pichia pastoris, *Protein Expr. Purif. 33*, 185-194.

[98] D´Sa, C., Arthur, R. E., Jr., and Kuhn, D. M., 1996, Expression and deletion mutagenesis of tryptophan hydroxylase fusion proteins: delineation of the enzyme catalytic core, *J. Neurochem. 67*, 917-926.

[99] Mockus S. M., Kumer S. C., and Vrana K. E., 1997, Carboxyl terminal deletion analysis of tryptophan hydroxylase, *Biochim. Biophys. Acta 1342*, 132-140.

[100] McKinney, J., Knappskog, P. M., and Haavik, J., 2005, Different properties of the central and peripheral forms of human tryptophan hydroxylase, *J. Neurochem. 92*, 311-320.

[101] Nielsen, M. S., 2007, Expression, purification and characterization of tryptophan hydroxylase, Ph.D. thesis. Department of Chemistry, Technical University of Denmark, Kgs. Lyngby.

[102] Boesen, J., 2010, Cloning, expression, purification and characterization of tryptophan hydroxylase variants, Ph.D. thesis. Department of Chemistry, Technical University of Denmark, Kgs. Lyngby.

[103] Haahr, L. T., 2012, Purification and Characterization of Tryptophan Hydroxylase, Ph.D. thesis, Department of Chemistry, Technical University of Denmark, Kgs. Lyngby.

[104] Jones, S.E., 2013, Optimized purification and ITC characterization of full-length tryptophan hydroxylase, B.Sc. thesis, Department of Chemistry, Technical University of Denmark, Kgs. Lyngby.

[105] Tidemand K. D. and Hoeck, N., 2014, Characterization and stabilization of human tryptophan hydroxylase by rational protein engineering, M.Sc. thesis, Department of Chemistry, Technical University of Denmark, Kgs. Lyngby.

[106] Walker, P. A., Leong, L. E.C., Ng, P. W.P., Tan, S. H., Waller, S., Murphy, D., and Porter, A. G., 1994, Efficient and Rapid Affinity Purification of Proteins Using Recombinant Fusion Proteases, *Nat Biotechnol 12*, 601-605.

[107] Gasteiger, E., Hoogland, C., Gattiker, A., Duvaud, S., Wilkins, M. R., Appel, R. D., and Bairoch, A., 2005, Protein Identification and Analysis Tools on the ExPASy Server. The Proteomics Protocols Handbook, Humana Press, New York, USA.

[108] Kobe, B., Jennings, I. G., House, C. M., Michell, B. J., Goodwill, K. E., Santarsiero, B. D., Stevens, R. C., Cotton, R. G. H., and Kemp, B. E., 1999, Structural basis of autoregulation of phenylalanine hydroxylase, *Nat. Struct. Biol. 6(5)*, 442-448.

[109] Jaffe, E. K., Stith, L., Lawrence, S. H., Andrake, M., and Dunbrack Jr., R.L., 2013, A new model for allosteric regulation of phenylalanine hydroxylase: Implications for disease and therapeutics, *Arch. Biochem. Biophys. 530*, 73-82.

[110] Horne, J., Jennings, I. G., Teh, T., Gooley, P. R., and Kobe, B., 2002, Structural characterization of the N-terminal autoregulatory sequence of phenylalanine hydroxylase, *Protein Sci. 11*, 2041–2047.

Chapter 3

Stabilization of tryptophan hydroxylase 2

Tryptophan hydroxylase isoform 2 is notoriously known to suffer from low stability. In this chapter an attempt to overcome this issue is presented. This chapter concerns the identification of stabilizing ligands by utilizing differential scanning fluorimetry (DSF). The methodology behind DSF will be introduced and previous results obtained for the AAAHs using DSF will be presented.

DSF was used to investigate the effect of eight compounds on three TPH2 variants; c*h*TPH2, r*ch*TPH2, and NΔ47-r*ch*TPH2. The experimental DSF procedure used to determine TPH transition temperatures is presented. The results obtained from the small scale ligand screen using DSF is presented and discussed. To investigate if the unfolding is accompanied by enzymatic inactivation, thermal inactivation measurements were conducted. The obtained results are presented and discussed. The majority of the results presented in this chapter have been published in FEBS Open Bio (Appendix A.1)

Outline

3.1 Differential scanning fluorimetry

In chapter 2 it was discussed how characterization of TPH2 has been hampered by insufficient purification yields due to its instability and tendency to aggregate. Increased purification yields might be achieved through increasing the thermostability of the notoriously instable TPH2. The stability of a protein determines the equilibrium between the native folded state and an ensemble of semi-folded and unfolded states.[111] Increased stability can therefore be achieved through stabilization of the native state.[111] It is known that the native state can be stabilized by binding of specific ligands, thereby reducing the proteins propensity to unfold and aggregate.[112]

The increase in thermostability induced by a ligand can be quantified by measuring the change in unfolding temperature, T_m. The increase in T_m is proportional to the concentration of the ligand and the affinity of the ligand for the protein.[113] The change in T_m as a function of ligand concentration can be measured in a fast and high-throughput fashion by utilizing differential scanning fluorimetry.[114]

In DSF the thermal unfolding of a protein is monitored in the presence of a fluorescent dye.[114] The dyes used in DSF are highly fluorescent in a non-polar environment compared to in an aqueous solution. In this study, the dye SYPRO orange was used, Figure 3.1. In aqueous solution, the fluorescence of the hydrophobic moiety of SYPRO orange is quenched. When the temperature induced unfolding of the protein is initiated, hydrophobic patches from the core of the protein will be exposed. SYPRO orange will bind to these patches resulting in an increase in fluorescence.[114]

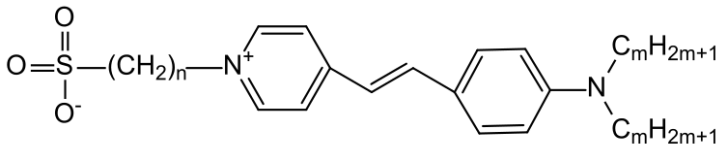

Figure 3.1. Structure of SYPRO® orange.

In the case of a two-state unfolding of a protein, the plot of fluorescence intensity as a function of temperature will yield a sigmoidal curve. Initially, the intensity is low as SYPRO orange does not bind folded protein. After unfolding, the protein sample will eventually aggregate resulting in quenching of the intensity.[114] The transition temperature can be calculated by fitting a Boltzmann sigmoidal (eq. 1) to the unfolding curve,

$$y = LL + \frac{UL - LL}{1 + \exp\left(\frac{T_m - x}{a}\right)} \qquad \text{(eq. 1)}$$

where LL and UL are the values of minimum and maximum intensities, respectively, and *a* denotes the slope of the curve at T_m.

3.2 AAAH stability

Differential scanning fluorimetry has been utilized in attempts to stabilize or identify potent ligands in all members of the AAAH family. Furthermore, DSF has been used to determine the change in stability introduced by point mutations.[115,116]

The transition temperature of full length *h*PAH has been found to range from 47.5 – 49.5 °C.[115,116] Substrate phenylalanine (>1 mM) has been found to increase T_m with 3.4 and 2.7 °C in PAH from *human* and *legionella pneumophila*, respectively.[116,117] T_m of the regulatory domain of *h*PAH, however, was increased by 21.7 °C with 1 mM phenylalanine.[118] The regulatory domains of *h*TPH1 and *h*TH were not stabilized by tryptophan and tyrosine, respectively.[118] Similar to PAH, the transition temperature is 55.5 °C for *h*TPH2 and range from 45.2 – 51.8 °C for full length *h*TH.[119-121]

DSF has been utilized to screen compound libraries in *h*PAH and *h*TH to identify compounds which increase T_m. Compounds were identified which increased T_m as much as 13.6 and 21.7 °C for *h*PAH and *h*TH, respectively.[115,121]

3.3 Experimental procedures

3.3.1 Differential scanning fluorimetry

The unfolding of the TPH2 variants was recorded with an Agilent Technologies Stratagene MX3005 P RT-PCR machine (λ_{ex} = 465 nm, λ_{em} = 610 nm). The ligand screen was performed with total volume of 25 µL in 96-well plates (polypropylene plates from Agilent Technologies). Each well was composed of protein at a

concentration of 1 µM, SYPRO orange at a concentration of 2X (diluted from SYPRO® 5000X stock from Sigma), and ligand (diluted in purification buffer) in a concentration range of 0.1 µM to 10 mM. Each plate contained control wells with the purification buffer with and without protein and ligand. Scans were carried out using a scan-rate of 1 °C/min, going from 20 °C to 95 °C. The thermograms were baseline corrected with MxPro QPCR Software and analyzed for transition temperatures with GraphPad Prism 6 utilizing a Boltzmann sigmoid fit (eq. 1). The obtained T_m-values as a function of substrate concentrations were fitted with eq. 2 [122],

$$T_{\mathrm{m}} = \frac{a[\mathrm{S}]}{K_{\mathrm{d}} + [\mathrm{S}]} + T_{\mathrm{m},0} \qquad \text{(eq. 2)}$$

where K_d is the dissociation constant of the substrate, $T_{m,0}$ is transition temperature at zero concentration of ligand, and a is the maximal increase in T_m, where $a + T_{m,0}$ is T_m at saturating compound concentration ($T_{m,max}$).

3.3.2 Heat induced inactivation

The rate of inactivation at 30 °C was determined by heating the protein in aliquots of 1300 µL to 30 °C in a water bath. The denaturation was stopped at a certain time point by cooling the protein solution in ice water. The enzymatic activity was determined at different time points with a continuous fluorescence assay described in details in chapter 6. The obtained data was fitted with one-exponential decay curves, and the rate constants, k, were calculated using an exponential function, $E_t = E_0 e^{-kt}$, where E_0 is the initial enzyme activity, and E_t is the activity after time t at 30 °C. From the decay rate constants, half lives ($t_{½}$) of the TPH samples were calculated using $t_{½} = \ln(2)/k$.

3.4 DSF results

The characterization of both isoforms of full length *h*TPH are very limited compared to that of PAH and TH. This is primarily caused, as described in chapter 2, by low purification yields of the TPH isoforms. Deletion of the regulatory domain significantly increases the purification yield [123], however the possibility to obtain knowledge about this domain is lost. The regulatory domains of all the AAAHs comprise a fold motif referred to as an ACT domain (see chapter 4). Such domains have been found to bind L-valine, L-serine, and L-phenylalanine.[118,124,125] To analyze if similar binding of ligands occur in the ACT domain of TPH2, the transition temperature was analyzed in the presence of different amino acids or amino acid derivatives. The change in T_m of the TPH2 variants was analyzed with eight compounds; L-phenylalanine, L-tryptophan, L-tyrosine, L-valine, L-serine, D-phenylalanine, 5-hydroxytryptophan (5-HTP), and 5-hydroxytryptamine (5-HT). All compounds were screened in a concentration range of 0.1µM-10mM except for L-Tyr which was screened from 0.1 µM-1.5 mM, due to limited solubility.

3.4.1 DSF results of c*h*TPH2

T_m was determined for c*h*TPH2 in purification buffer; 20 mM HEPES, 300 mM $(NH_4)_2SO_4$, pH 7.0. Representative examples of the DSF results of c*h*TPH2, in the presence of the highest tested concentrations of the ligands, are presented in Figure 3.2. The unfolding curves in Figure 3.2 show that c*h*TPH2 has an almost ideal two-state unfolding behavior with a transition temperature of 42.7 ± 1.3 °C.

Two-state unfolding was observed for all compounds except 5-HTP and 5-HT. These compounds appear to change the unfolding from two-state to continuous (see Figure 3.3 for example of continuous unfolding); hence, it was not possible to obtain a good fit with the eq. 1 and T_m-values were therefore not obtained for

these compounds. The remaining compounds did not have a significant effect on the unfolding behavior or T_m-value of c*h*TPH2, Figure 3.2.

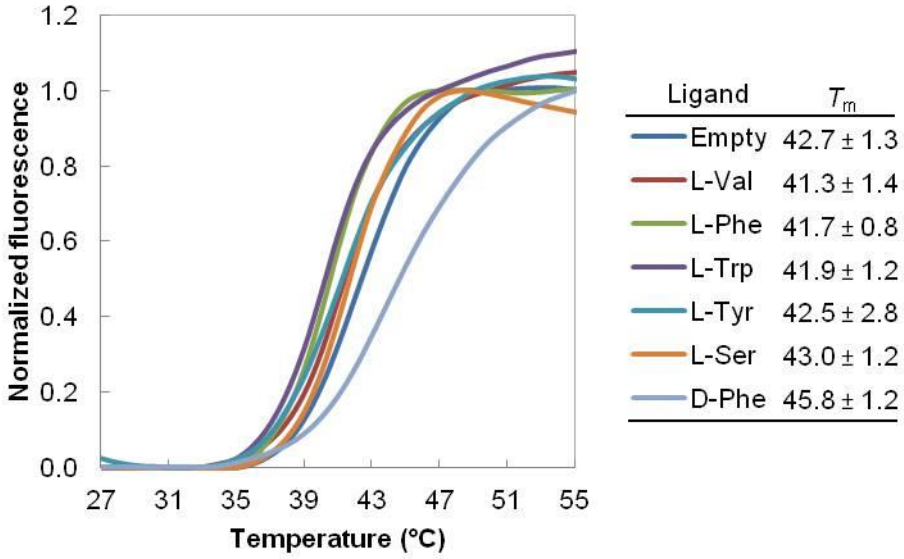

Figure 3.2. Normalized and baseline corrected differential scanning fluorimetry curves - ligand screen on c*h*TPH2 (enzyme concentration of 1 µM). Representative examples of the highest concentration of the compounds in the screen (1.5 mM for tyrosine and 10 mM for all other compounds). To the right T_m-values (n=3) of c*h*TPH2 with the respective compounds are listed in °C ± standard deviation.

3.4.2 DSF results of rc*h*TPH2

The transition temperature, T_m, was determined for rc*h*TPH2 in purification buffer; 20 mM HEPES/NH_4OH, 300 mM $(NH_4)_2SO_4$, pH 7.0. Containing the regulatory domain, rc*h*TPH2, gave rise to inconsistent and polyphasic unfolding curves from which no T_m-value could be obtained (Figure 3.3, solid line).

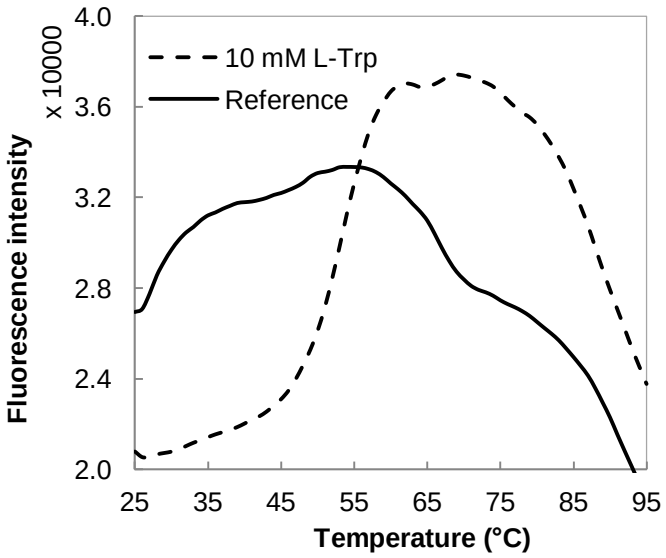

Figure 3.3. Representative examples of raw data from differential scanning fluorimetry of rc*h*TPH2 (enzyme concentration of 1 µM) with no ligand (solid line, reference) and with addition of 10 mM L-Trp (dashed line).

The ligand screen showed that L-Trp and L-Phe induced a change from continuous unfound to an apparent two-state unfolding, as represented in Figure 3.3. None of the other compounds, including D-Phe, were able to induce this change in unfolding. The T_m-value of rc*h*TPH2 was increased with increasing concentration of L-Phe or L-Trp, Figure 3.4.

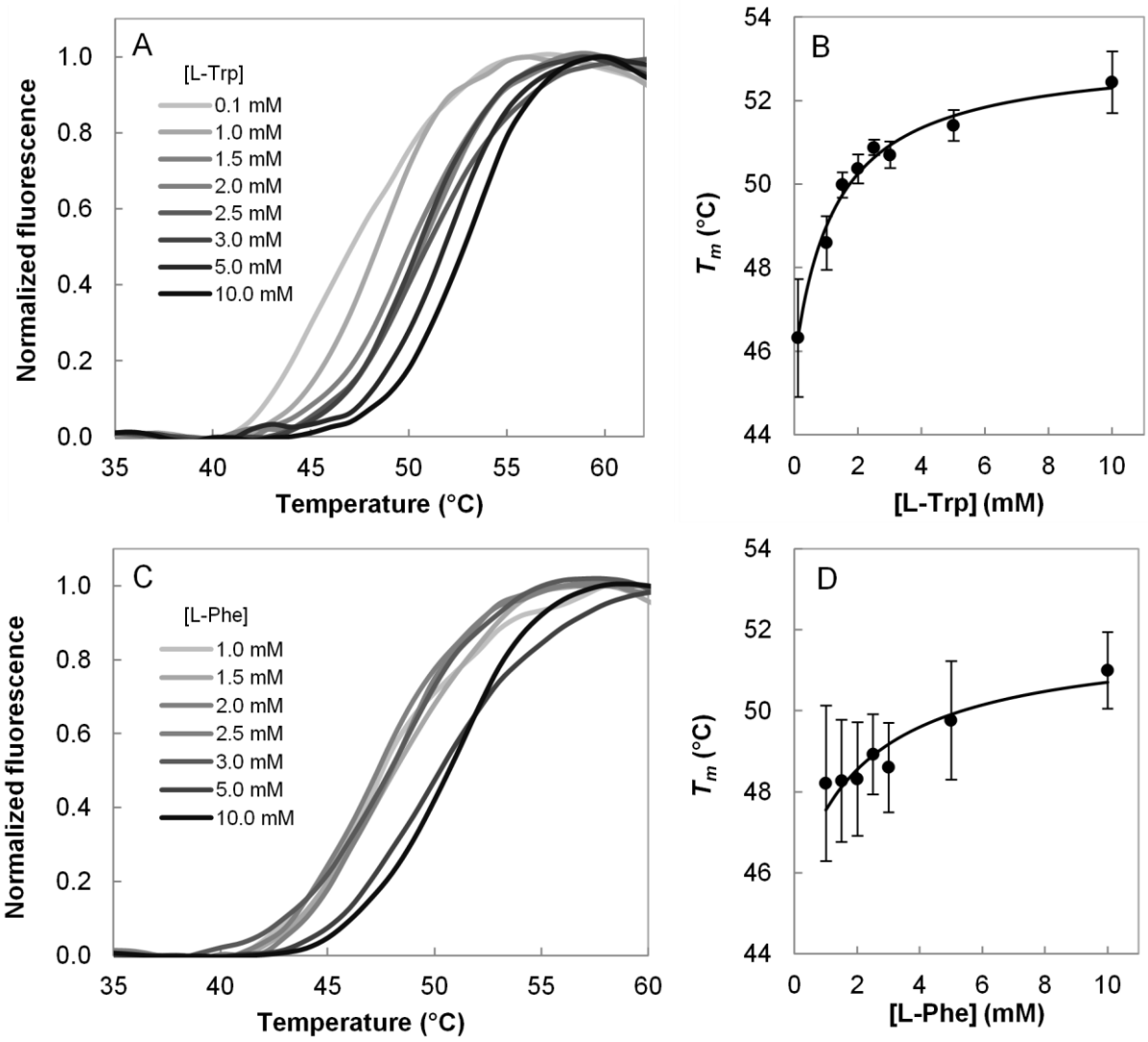

Figure 3.4. Representative normalized and baseline corrected DSF curves of rc*h*TPH2. A: DSF curves with different L-Trp concentration. B: T_m-values with increasing L-Trp concentration fitted with eq. 2. C: DSF curves with different L-Phe concentration. D: T_m-values with increasing L-Phe concentration fitted with eq. 2.

At 0.1 mM L-Trp, a T_m-value of 46.3 ± 1.4 °C was obtained for rc*h*TPH2. This was increased by 6.1 °C with the addition of 10.0 mM L-Trp. A K_d-value of tryptophan binding was estimated by fitting eq. 2 to the data presented in Figure 3.4 B. The utilized model (eq. 2) is the most simple for ligand binding and assumes a 1:1 binding ratio.[122] Furthermore, the model does not account for the change in temperature. A K_d-value of 1.3 mM, $T_{m,0}$-value of 45.7 °C and $T_{m,max}$-value of 53.1 °C were determined.

The transition temperature of rc*h*TPH2 was increased to 51.0 ± 0.9 °C by addition of 10.0 mM L-Phe (Figure 3.4 D). Insufficient data in the low concentration region was obtained to fit the T_m-values as a function of L-Phe concentration without constraints. $T_{m,0}$ was therefore constrained to the value obtained from the data presented in Figure 3.4 B. A K_d-value of 2.3 mM and $T_{m,max}$-value of 51.9 °C were determined.

Similar results were obtained for NΔ47-rc*h*TPH2. Continuous unfolding curves were also observed for NΔ47-rc*h*TPH2 in the absence of a ligand. L-Phe and L-Trp changed the unfolding to apparent two-state, comparable to the observations for rc*h*TPH2 (see Appendix E.1).

As both L-Trp and L-Phe gave rise to increased transition temperatures, a combination of the compounds was analyzed. At 10 mM L-Trp, rc*h*TPH2 has a T_m-value of only 0.7 °C from the calculated $T_{m,max}$, suggesting that saturation is almost attained. However, at 10 mM L-Trp addition of L-Phe seems to increase the T_m-value in a concentration-dependent manner, Figure 3.5.

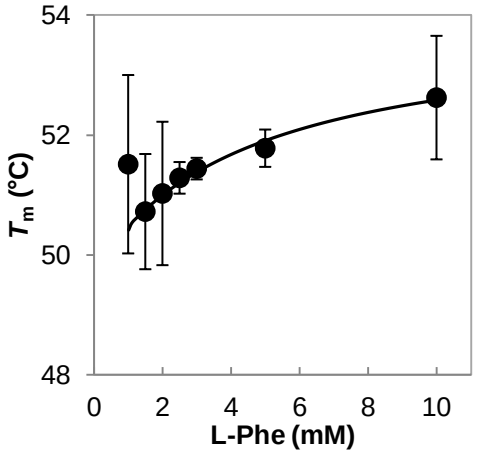

Figure 3.5. T_m-values of rc*h*TPH2 with increasing L-Phe concentration at a constant L-Trp concentration of 10 mM. Data is fitted with eq. 2, T_m at 1 mM L-Phe was omitted from the fit.

From the data in Figure 3.5, a $T_{m,max}$-value of 53.9 °C was determined (1.0 mM L-Phe omitted). The DSF data for L-Phe and L-Trp combination was produced on a different day than the data for only L-Trp. The data seems to be systematically lower from the day of the combinatorial study of L-Phe and L-Trp (Appendix E.2). The $T_{m,max}$-value obtained at 10 mM L-Phe in combination with 10 mM L-Trp is therefore lower than expected when comparing to the $T_{m,max}$-value obtained from addition of only L-Trp. Despite this fact and the large standard deviations, T_m seems to increase with increasing concentration of L-Phe at saturated concentration of L-Trp. This might suggest an additive effect of the ligand.

3.4.3 DSF results of c*h*TPH mutant variants

In chapter 7, mutations in an active site loop is made in both TPH isoforms and analyzed for changes in their kinetic parameters. The thermostability of these mutant variants of c*h*TPH1 and c*h*TPH2 was analyzed in 20 mM TRIS/H_2SO_4, 100 mM $(NH_4)_2SO_4$, pH 8.0 and 20 mM HEPES/NH_4OH, 100 mM $(NH_4)_2SO_4$, pH 7.0, respectively. Representative examples of the unfolding curves of the TPH variants are presented in Figure 3.6.

The transition temperatures obtained for the c*h*TPH variants are summarized in Figure 3.6. The transition temperature of c*h*TPH1 is determined to 41.4 ± 0.2 ºC. This value corresponds well with previous results.[126] Mutations of Tyr125 to alanine or tryptophan or the three loop-swap mutations only resulted in subtle changes in the transition temperature.

Together with the other c*h*TPH variants the transition temperature of c*h*TPH2 was determined again (previous section in this chapter – different buffer solution). The T_m-value was determined to 42.1 ± 0.3 ºC which corresponds well with the previous result. As was the case of c*h*TPH1, the substitution of tyrosine to alanine or tryptophan in position 171 or the three loop-swap mutations only resulted in small changes in the T_m-value.

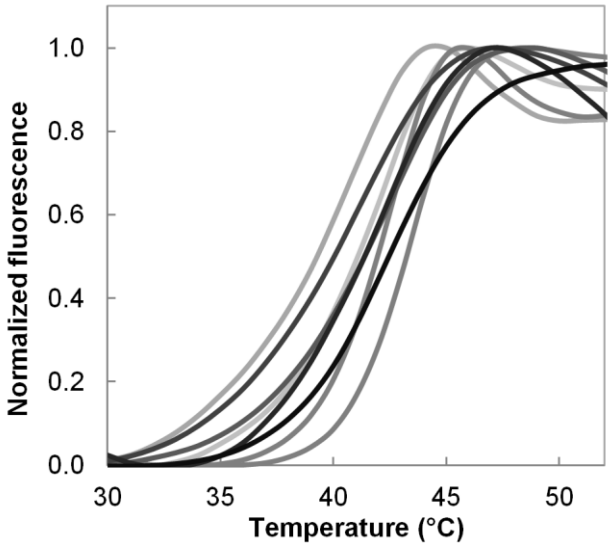

Variant	T_m
c*h*TPH1	41.4 ± 0.2
Y125A-c*h*TPH1	40.1 ± 0.2
Y125W-c*h*TPH1	43.3 ± 0.1
Loop-swap-c*h*TPH1	42.1 ± 0.2
c*h*TPH2	42.1 ± 0.3
Y171A-c*h*TPH2	40.5 ± 0.3
Y171W-c*h*TPH2	41.3 ± 0.5
Loop-swap-c*h*TPH2	42.4 ± 0.1

Figure 3.6. Representative normalized and baseline corrected DSF curves of c*h*TPH variants. To the right T_m-values (n=4-6) of the c*h*TPH variants are listed in °C ± standard deviation.

3.5 Inactivation results

3.5.1 Inactivation of *h*TPH2 variants

As an alternative to the thermal unfolding measurements, the rates of inactivation at 30 °C was analyzed under the same buffer conditions; 20 mM HEPES/NH_4OH, 300 mM $(NH_4)_2SO_4$, pH 7.0. This assay reveals whether the unfolding is associated with loss of function and if the dye gives rise to artifacts. The influence of L-Phe on the inactivation rates of c*h*TPH2, NΔ47-rc*h*TPH2, and rc*h*TPH2 was analyzed. The results in the absence and presence of 3 mM L-Phe are presented in Figure 3.7 A-C.

From the data in Figure 3.7 A, a half-life at 30 °C ($t_{½}$) of 203 ± 40 min was determined for c*h*TPH2. With 3 mM L-Phe, the $t_{½}$ is 193 ± 29 min. L-Phe does therefore not change the inactivation rate of c*h*TPH2. This result is consistent with the result obtained from the DSF experiments.

The data in Figure 3.7 B and C show that rc*h*TPH2 and NΔ47-rc*h*TPH2 display $t_{½}$-values of only 15 ± 2 and 18 ± 3 min, respectively. The presence of the regulatory domain hence results in a >10-fold increase in the inactivation rate. The N-terminus, however, do not seem to have an influence on the inactivation rate.

In contrast to c*h*TPH2, L-Phe has a significant impact on the $t_{½}$-values of the variants containing the regulatory domain. The $t_{½}$-vaules were increased to 41 ± 3 min for rc*h*TPH2 and 49 ± 5 min for NΔ47-rc*h*TPH2. Again, these results correlate with the observations from the DSF experiments, where L-Phe increased the transition temperature of variants containing the regulatory domain.

The half-life of full-length *h*TPH2 was also determined in the presence of L-Phe, Figure 3.7 D. Here a $t_{½}$-value of 30.3 ± 3.3 min was obtained, suggesting that tetrameric *h*TPH2 is slightly less stable under the used conditions compared to dimeric rc*h*TPH2 and NΔ47-rc*h*TPH2 (oligomeric states are further discussed in chapter 4).

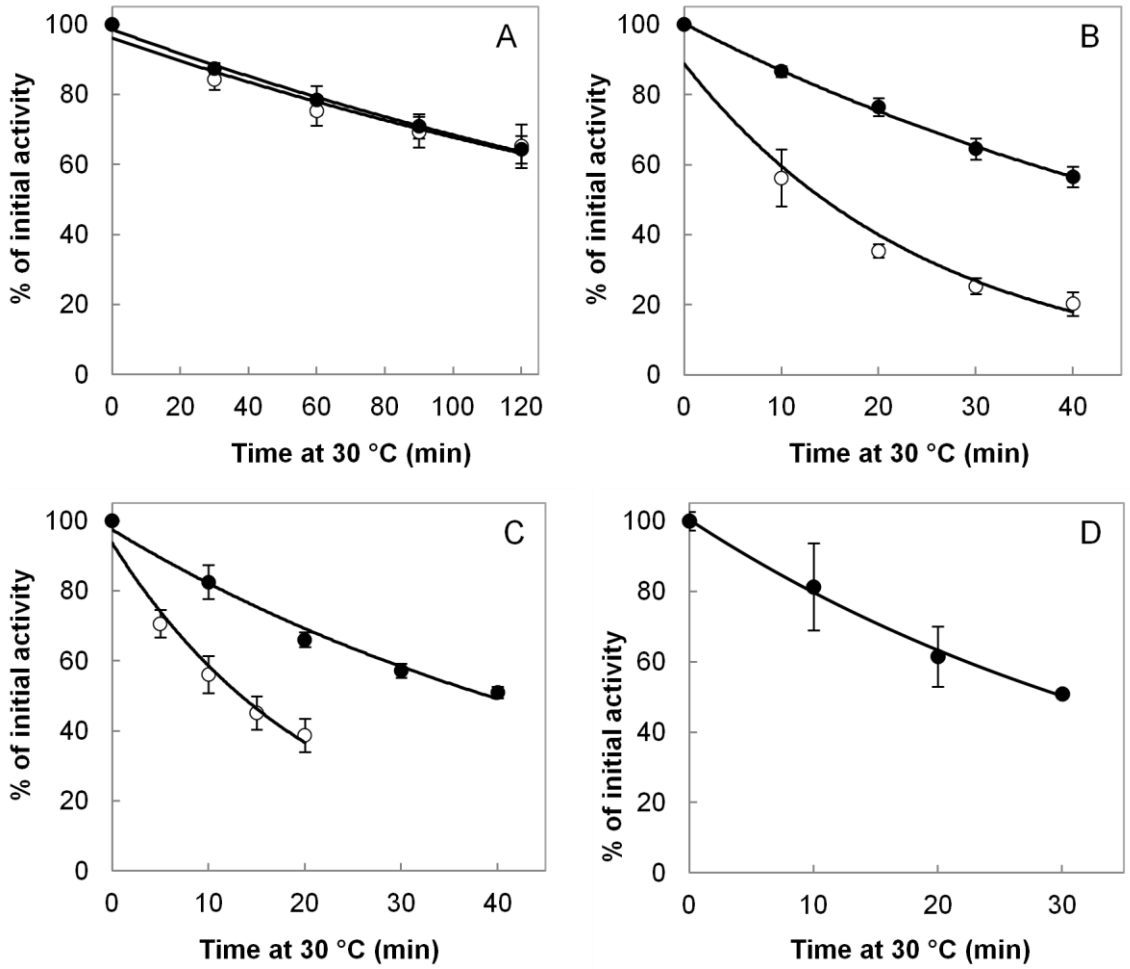

Figure 3.7. Heat inactivation of TPH2 variants; A: c*h*TPH2 (n=3), B: NΔ47-rc*h*TPH2 (n=3), C: rc*h*TPH2 (n=3), and D: *h*TPH2 (n=2) with 3 mM L-phe (closed circles) or no ligand (open circles). Enzyme samples (5 µM) were incubated at 30 °C, and residual activity in % of initial activity at t_0 was assayed in time intervals.

3.5.2 Inactivation of *h*TPH1

The inactivation rate of full-length *h*TPH1 was analyzed in 20 mM TRIS/H_2SO_4, 300 mM $(NH_4)_2SO_4$, pH 8.0. The results are presented in Figure 3.8 and show that *h*TPH1 is not inactivated at 30 °C within two hours.

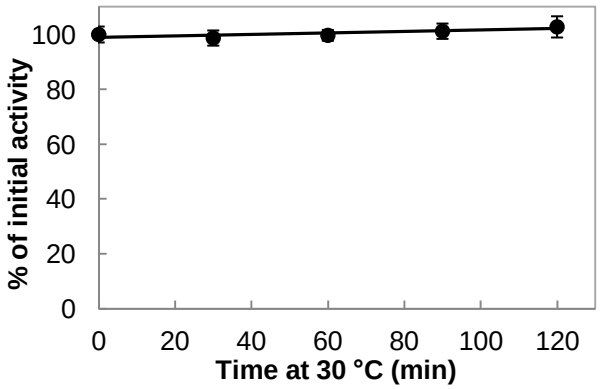

Figure 3.8. Heat inactivation of *h*TPH1 (n=3). Enzyme samples (5 µM) were incubated at 30 °C, and residual activity in % of initial activity at t_0 was assayed in time intervals.

3.6 Discussion

Characterization of the TPH isoforms, especially TPH2, has been limited because of inherent instability and tendency to aggregate. Utilizing differential scanning fluorimetry, it was identified that L-Phe and L-Trp changed the unfolding behavior of TPH2 variants containing the regulatory domain from continuous and polyphasic to apparent two-state. The change in unfolding behavior was accompanied by a significant increase in thermal stability which, as described in chapter 2, resulted in a several fold increase in purification yields.

The observed transition temperatures of c*h*TPH1 and c*h*TPH2 were similar and corresponds with values previously observed.[126] DSF measurements were conducted for c*h*TPH2 at 100 mM and 300 mM $(NH_4)_2SO_4$ and resulted in the same T_m-value, suggesting that 100 mM is sufficient for c*h*TPH2 stability.

The transition temperature of c*h*TPH2 did not increase in the presence of ligands. In contrast, L-Phe and L-Trp increased the T_m-values of rc*h*TPH2 and NΔ47-rc*h*TPH2. This implies that the ligands stabilize through binding in the regulatory domain and do not seem to involve the 47 N-terminal residues. In the presence of these ligands, the TPH2 variants display T_m-values comparable to the ones observed for *h*PAH and *h*TH (in the absence of ligands).[115,116,120,121] A greater T_m-value (55.5 °C) has been determined for full-length *h*TPH2, despite similar buffer conditions; 20 mM HEPES, 200 mM NaCl, pH 7.0.[119] The assay, however, contained 2.5 % DMSO, and 8-anilino 1-naphthalenesulfonic acid (ANS) was used as the dye.[119] Furthermore, the TPH sample was purified according to a purification procedure by McKinney *et al*.[127], where 10 % glycerol (v/v) is included. Glycerol has a known stabilizing effect and tendency to bind the catalytic site of TPH.[126]

In line with the observations in the DSF experiments, only variants containing the regulatory domain displayed an increased $t_{½}$-value at 30 °C in the presence of L-Phe. For rc*h*TPH2 and NΔ47-rc*h*TPH2, $t_{½}$ was increased ~3-fold, whereas c*h*TPH2 was not significantly influenced by L-Phe. The very short half-lives determined in this study, are comparable to values previously determined for *h*TPH2 variants [123,128,129] and confirms that TPH2 is instable and hence a challenge to characterize. In contrast, it was demonstrated that *h*TPH1 is very thermostable, as it maintained full activity upon incubation at 30 °C for 2 hours. Longer half-lives has also been observed for the more stable *h*TH, which is therefore more thoroughly characterized.[130,131]

When the DSF results are compared to the inactivation results, it is noticed that in the presence of L-Phe c*h*TPH2 has a lower T_m but a higher $t_{½}$ than e.g. rc*h*TPH2. This might be explained by the presence of dye in the DSF measurements which might reduce the apparent stability of isolated catalytic domain. This is, however, unlikely, as the raw fluorescence intensity data shows that c*h*TPH2 and rc*h*TPH2 start from the same intensity level compared to the baseline. This suggests that the dye does not bind one variant more than the other prior to unfolding. Alternatively, c*h*TPH2 retains activity upon the unfolding transition observed in the DSF. The activity might then be lost upon aggregation which is achieved at greater temperatures.

From the DSF experiments K_d-values for L-Trp (1.3 mM) and L-Phe (2.3 mM) were obtained in the milli molar range, suggesting very low affinity of these ligands. The substrate dissociation constant in the AAAHs are usually in the low micro molar range.[126,132,133] The observed K_d-values are therefore around two orders of magnitude larger than expected for substrates binding in the active site. This suggests that the increase in T_m occur through binding of L-Trp and L-Phe in a low affinity site. Such an allosteric site has been identified in PAH, where T_m similarly has been found to increase with increasing L-Phe concentration.[118,134] In this low affinity site of PAH, L-Phe displays a K_d-value of 174 ± 9 µM [134], which similarly is significantly higher than values observed for binding in the active site [135]. Binding of L-Phe in the allosteric site of PAH is associated with dimerization of the regulatory domains.[118,134] The influence of L-Trp and L-Phe on the oligomeric state of TPH2 upon binding in a potential allosteric site will be discussed in chapter 4.

3.7 Conclusion

This chapter describes how differential scanning fluorimetry was utilized to identify tryptophan and phenylalanine as thermostabilizing ligands for *h*TPH2 variants containing the regulatory domain. The results show that the regulatory domain is involved in the induced thermostability, as binding of the amino acids only has an effect on variants comprising this domain. It was demonstrated that the binding to the *h*TPH2 variants is specific, as only one of the stereoisomers of phenylalanine increased the transition temperature.

3.8 References

[111] Branden, C. and Tooze, J., 2009, Introduction to Protein Structure, 2nd edition, Garland Publishing, New York, USA.

[112] Vedadi, M., Niesen, F. H., Allali-Hassani, A., Fedorov, O. Y., Finerty, P. J. Jr, Wasney, G. A., Yeung, R., Arrowsmith, C., Ball, L. J., Berglund, H., Hui, R., Marsden, B. D., Nordlund, P., Sundstrom, M., Weigelt, J., and Edwards, A. M., 2006, Chemical screening methods to identify ligands that promote protein stability, protein crystallization, and structure determination, *Proc. Natl. Acad. Sci. 103(43)*, 15835-15840.

[113] Matulis, D., Kranz, J. K., Salemme, F. R., and Todd, M. J., 2005, Thermodynamic stability of carbonic anhydrase: measurements of binding affinity and stoichiometry using ThermoFluor, *Biochemistry 44(13)*, 5258-5266.

[114] Niesen, F. H., Berglund, H., and Vedadi, M., 2007, The use of differential scanning fluorimetry to detect ligand interactions that promote protein stability, *Nat. Protoc. 2*, 2212–2221.

[115] Pey, A. L., Ying, M., Cremades, N., Velazquez-Campoy, A., Scherer, T., Thöny, B., Sancho, J., and Martinez, A., 2008, Identification of pharmacological chaperones as potential therapeutic agents to treat phenylketonuria, *J. Clin. Invest. 118(8)*, 2858-2867.

[116] Gersting, S. W., Staudigl, M., Truger, M. S., Messing, D. D., Danecka, M. K., Sommerhoff, C. P., Kemter, K. F., and Muntau, A. C., 2010, Activation of phenylalanine hydroxylase induces positive cooperativity toward the natural cofactor, *J. Biol. Chem. 285(40)*, 30686-30697.

[117] Aubi, O., Flydal, M. I., Zheng, H., Skjærven, L., Rekand, I., Leiros, H. K., Haug, B. E., Cianciotto, N. P., Martinez, A., and Underhaug, J., 2015, Discovery of a Specific Inhibitor of Pyomelanin Synthesis in Legionella pneumophila, *J. Med. Chem. 58(21)*, 8402-8412.

[118] Patel, D., Kopec, J., Fitzpatrick, F., McCorvie, T. J., and Yue, W. W., 2016, Structural basis for ligand-dependent dimerization of phenylalanine hydroxylase regulatory domain, *Sci. Rep. 6*, 23748.

[119] Calvo, A. C., Scherer, T., Pey, A. L., Ying, M., Winge, I., McKinney, J., Haavik, J., Thöny, B., and Martinez, A., 2010, Effect of pharmacological chaperones on brain tyrosine hydroxylase and tryptophan hydroxylase 2, *J. Neurochem. 114(3)*, 853-863.

[120] Korner, G., Noain, D., Ying, M., Hole, M., Flydal, M. I., Scherer, T., Allegri, G., Rassi, A., Fingerhut, R., Becu-Villalobos, D., Pillai, S., Wueest, S., Konrad, D., Lauber-Biason, A., Baumann, C. R., Bindoff, L. A., Martinez, A., and Thöny, B., 2015, Brain catecholamine depletion and motor impairment in a Th knock-in mouse with type B tyrosine hydroxylase deficiency, *Brain 138(10)*, 2948-2963.

[121] Hole, M., Underhaug, J., Diez, H., Ying, M., Røhr, Å. K., Jorge-Finnigan, A., Fernàndez-Castillo, N., García-Cazorla, A., Andersson, K. K., Teigen, K., and Martinez, A., 2015, Discovery of compounds that protect tyrosine hydroxylase activity through different mechanisms, *Biochim. Biophys. Acta 1854(9)*, 1078-1089.

[122] Copeland, R. A., 2000, Enzymes: A Practical Introduction to Structure 2nd ed., Mechanism, and Data Analysis, Chapter 4 - Protein-Lingand Binding Equilibria, Wiley-VCH, Inc., New York.

[123] Carkaci-Salli, N., Flanagan, J. M., Martz, M. K., Salli, U., Walther, D. J., Bader, M., and Vrana, K. E., 2006, Functional Domains of Human Tryptophan Hydroxylase 2 (hTPH2), *J. Biol. Chem. 281*, 28105-28112.

[124] Chen, L., Chen, Z., Zheng, P., Sun, J., and Zeng, A. P., 2012, Study and reengineering of the binding sites and allosteric regulation of biosynthetic threonine deaminase by isoleucine and valine in Escherichia coli, *Appl. Microbiol. Biotechnol. 97*, 2939-2949

[125] Schuller, D. J., Grant, G. A., and Banaszak, L. J., 1995, The allosteric ligand site in the V-max-Type cooperative enzyme phosphoglycerate dehydrogenase, *Nat. Struct. Biol. 2*, 69-76.

[126] Haahr, L.T., 2012, Purification and Characterization of Tryptophan Hydroxylase, Ph.D. thesis, Department of Chemistry, Technical University of Denmark, Kgs. Lyngby.

[127] McKinney, J., Knappskog, P. M., and Haavik, J., 2005, Different properties of the central and peripheral forms of human tryptophan hydroxylase, *J. Neurochem. 92*, 311–320.

[128] Winge, I., McKinney, J. A., Knappskog, P.M., and Haavik, J., 2007, Characterization of wild-type and mutant forms of human tryptophan hydroxylase 2, *J. Neurochem. 100*, 1648–1657.

[129] Cichon, S., Winge, I., Mattheisen, M., Georgi, A., Karpushova, A., Freudenberg, J., Freudenberg-Hua, Y., Babadjanova, G., Van Den Bogaert, A., Abramova, L. I., Kapiletti, S., Knappskog, P. M., McKinney, J., Maier, W., Jamra, R. A., Schulze, T. G., Schumacher, J., Propping, P., Rietschel, M., Haavik, J., and Nöthen, M. M., 2008, Brain-specific tryptophan hydroxylase 2 (TPH2): a functional Pro206Ser substitution and variation in the 50-region are associated with bipolar affective disorder, *Hum. Mol. Genet. 17(1)*, 87–97.

[130] Bezem, M. T., Baumann, A., Skjærven, L., Meyer, R., Kursula, P., Martinez, A., and Flydal, M. I., 2016, Stable preparations of tyrosine hydroxylase provide the solution structure of the full-length enzyme, *Sci. Rep. 6*, 30390.

[131] Royo, M., Daubner, S. C., and Fitzpatrick, P. F., 2005, Effects of Mutations in Tyrosine Hydroxylase Associated With Progressive Dystonia on the Activity and Stability of the Protein, *Proteins 58(1)*, 14–21.

[132] Pey, A. L. and Martinez, A., 2005, The activity of wild-type and mutant phenylalanine hydroxylase and its regulation by phenylalanine and tetrahydrobiopterin at physiological and pathological concentrations: An isothermal titration calorimetry study, *Mol. Genet. Metab. 86*, 43–53.

[133] Erlandsen, H., Pey, A. L., Gámez, A., Pérez, B., Desviat, L. R., Aguado, C. Koch, R., Surendran, S., Tyring, S., Matalon, R., Scriver, C. R., Ugarte, M., Martínez, A., and Stevens, R. C., 2004, Correction of kinetic and stability defects by tetrahydrobiopterin in phenylketonuria patients with certain phenylalanine hydroxylase mutations, *Proc. Natl. Acad. Sci. 101(48)*, 16903–16908.

[134] Meisburger, S. P., Taylor, A. B., Khan, C. A., Zhang, S., Fitzpatrick, P. F., and Ando, N., 2016, Domain Movements upon Activation of Phenylalanine Hydroxylase Characterized by Crystallography and Chromatography-Coupled Small-Angle X‑ray Scattering, *J. Am. Chem. Soc. 138*, 6506−6516.

[135] Ronau, J. A., Paul, L. N., Fuchs, J. E., Liedl, K. R., Abu-Omar, M. M., and Das, C., 2014, A conserved acidic residue in phenylalanine hydroxylase contributes to cofactor affinity and catalysis, *Biochemistry 53(43)*, 6834-6848.

Chapter 4

Subunit assembly of TPH variants

This chapter concerns the quaternary structure of tryptophan hydroxylase and how the domains are involved in the inter-subunit assembly. The three domains in the aromatic acid hydroxylases are introduced and their roles on the quaternary structure are presented and discussed. As very limited knowledge prevails on especially the regulatory domain of the TPH isoforms, the structure and function of the homologues regulatory domain in PAH will be presented.

Analytical gel filtration was utilized to analyze the oligomeric state of three TPH2 variants; c*h*TPH2, rc*h*TPH2, and NΔ47-rc*h*TPH2. The experimental procedure to determine the oligomeric state is presented. In chapter 3, it was described how it was found that ligands increase the thermostability of TPH2 variants containing the regulatory domain. In this chapter, the influence of these ligands on the oligomeric state of the TPH2 variants are presented and discussed. The majority of the results presented in this chapter have been published in FEBS Open Bio (Appendix A.1)

Outline

4.1 The AAAH domains

All mammalian aromatic amino acid hydroxylases (AAAHs) consists of three domains; An N-terminal regulatory domain, a catalytic domain, and a C-terminal tetrameriztion domain.[136] The AAAHs consist of a similar number of amino acid residue in the catalytic and tetramerization domains, whereas the number of residues in the regulatory domains vary significantly.[137-139] The number of residues in the domains of the AAAHs are presented in Figure 4.1, these number may, however, vary in literature as domain borders are not rigid entities.

TPH1	99	314	31
TPH2	145	314	31
PAH	118	309	25
TH	153	302	42

Figure 4.1. Schematic representation of the amino acid residue distribution of the regulatory domain (blue), catalytic domain (green), and tetramerization domain (yellow) of the *human* aromatic amino acid hydroxylases. The numbers indicate the number of amino acid residues in the individual domains.

Table 4.1 shows the sequence identities of the three domains in the AAAHs based on the length presented in Figure 4.1. The catalytic domains are highly conserved with sequence identities ranging from 60 to 81 %, whereas the regulatory and tetramerization domains have significantly lower sequence identities. The TPH isoforms are very homologous and both share a higher sequence identity with PAH compared to TH. The high sequence identities suggest that the structure and function of the domains in the AAAHs are similar.

Table 4.1. Sequence identity matrix of the domains in the aromatic amino acid hydroxylases. The values are given as % identities in the regulatory / catalytic / tetramerization domains, respectively. Values are obtained from Clustal Omega multiple sequence alignments.[140]

	TPH1	TPH2	PAH
TPH2	48 / 81 / 39		
PAH	34 / 65 / 12	30 / 66 / 20	
TH	21 / 60 / 19	17 / 63 / 15	23 / 64 / 24

4.1.1 Tetramerization domain

The AAAHs form homotetramers through dimers of dimers.[141] The assembly of subunits into a tetramer is accomplished using a common folding motif, in which repeats of hydrophobic residues are positioned in an α-helix with a distance of four or three amino acid residues. This 4-3 repeat of hydrophobic residues produces a hydrophobic face on the α-helix which can interact with other such helices, forming coiled coils through hydrophobic interactions.[142] The 4-3 repeat motif has been identified in the C-terminus of all members of the AAAH family.[142,143]

No full-length crystal structure exists of either of the isoforms of TPH. However, full-length structures *rat* PAH have been published.[144,145] These structures confirm a tetrameric assembly, which is held together by coiled coils, Figure 4.2. Crystal structures of the catalytic and tetramerization domains of *rat* TH [139,146] show an identical assembly.

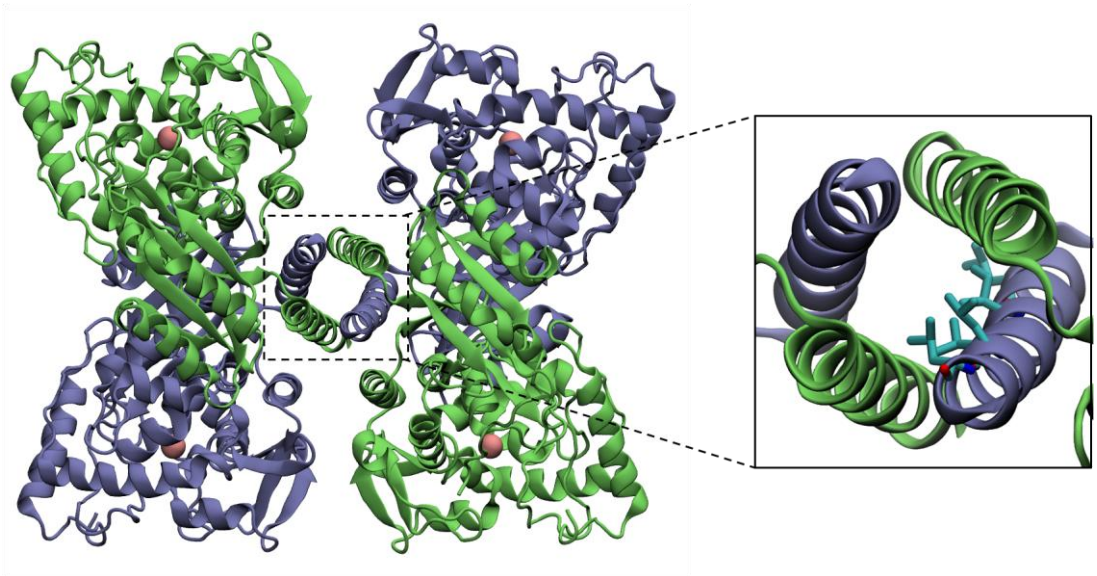

Figure 4.2. Cartoon illustration of the tetrameric structure of full-length *rat* phenylalanine hydroxylase (PDB entry: 5FGJ). Subunits A and B are shown in blue and subunits C and D are shown in green. Iron atoms are shown as pink spheres. The zoom-in shows the residues (Leu430, Ile437, Val441, Leu444, and Leu448) of the 4-3 hydrophobic repeat motif of subunit A.

Size exclusion chromatography has shown that both isoforms of TPH elute at volumes corresponding to tetramers.[147,148] Because of the high sequence identity of the TPH isoforms with PAH and TH, it is expected that they form similar quaternary structures.[149]

The role of the tetramerization domain has been confirmed by deletion mutant variants of both isoforms. Removal of the 4-3 hydrophobic repeat (CΔ17), renders TPH1 incapable of forming tetramers and monomers are predominantly found.[147] This is also the case in TPH2, where deletion of 19 residues in the C-terminus (CΔ19) results in monomers.[143]

4.1.2 Regulatory domain

The N-terminal regulatory domain is the most diverse among the AAAHs. The role of this domain is very poorly studied in the case of TPH. However, structural and functional information can be gathered from studies of PAH and TH.

The N-terminal regulatory domains of PAH and TH comprise a characteristic βαββαβ-fold motif, referred to as an ACT domain (named after aspartate kinase, chorismate mutase, and TyrA [150]).[151,152] ACT domains are present in several proteins and are in many cases involved in regulative mechanisms triggered by amino acid binding.[153] Binding of an amino acids to an ACT domain often occurs at domain interfaces and results in conformational changes.[154] From sequence analysis, TPH has also been proposed to contain an ACT domain. [150,155]

Compared to the C-terminal domain, the effect of the regulatory domain on the macromolecular assembly is less clear. It has been found that the first 41 residues of the N-terminus of TPH1 are necessary for tetramer formation, as truncation of these residues (NΔ41) predominantly results in a monomeric form.[156] In contrast, it has also been found that the tetrameric assembly was retained upon truncation of the regulatory domain of TPH1 (NΔ98).[157] A similar observation has been made for TPH2, where a tetramer is observed after truncation of the regulatory domain (NΔ150).[158]

Isolated regulatory domain of TPH1 (r*h*TPH1), has been found to forms a stable dimer that does not undergo a monomer-dimer equilibrium. Furthermore, it was found that L-phenylalanine had no influence on the dimer.[159] Similarly, it has been found that L-tryptophan does not thermally stabilize r*h*TPH1, suggesting that L-tryptophan does not bind the regulatory domain of *h*TPH1.[138]

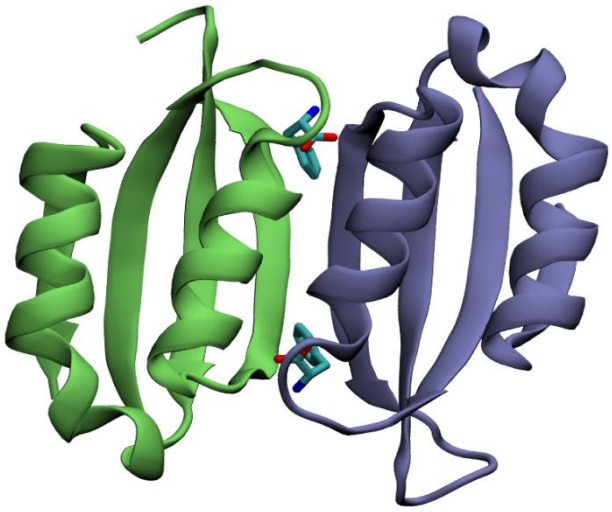

Figure 4.3. Crystal structure of *human* rPAH (PDB entry: 5FII). Cartoon representation of the r*h*PAH dimeric structure, one subunit is colored blue (chain A) and one is colored green (chain C). L-phenylalanine ligands are shown in sticks.

In PAH, the role of the regulatory domain is more thoroughly studied. Isolated regulatory domain of PAH (residue 1 to 117; rPAH) elutes as a dimer from a gel filtration column.[160] This dimer has been crystallized with bound L-phenylanine, identifying the binding pocket of L-phenylalanine at the subunit-subunit interface of the dimer, Figure 4.3.[138]

Initial sedimentation velocity experiments of rPAH showed that it undergoes a monomer–dimer equilibrium (K_{eq} = 46 ± 35 µM) that is shifted towards dimer in the presence of L-phenylalanine (K_d = 8 µM; obtained from global fit with a model including binding of two molecules of L-phenylalanine).[161] NMR experiments on isolated regulatory domain of PAH (residue 25 to 117; rPAH) in solution have verified that L-phenylalanine binds at the interface of the domains.[162]

4.1.3 Catalytic domain

The catalytic domain is more thoroughly studied and crystal structures of this domain reside in the protein data bank for all the AAAHs (tables with all structures are found in chapter 7). Isolating the catalytic domain upon truncation of both the regulatory and tetramerization domains of TPH1 or TPH2 (NΔ101/CΔ28 or NΔ150/CΔ24), results in predominately monomer.[158,163] Crystallization of the catalytic domain of TPH1 has therefore resulted in a monomeric structures.[164,165]

4.1.4 PAH activation

In recent years, the purpose of the observed dimerization of the regulatory domains has been unraveled. It is well documented that phenylalanine hydroxylase is activated cooperatively by preincubation with L-phenylalanine.[166] However, different mechanisms have been proposed to explain this cooperative activation. It has been proposed that this activation is caused by binding of L-phenylalanine in the active site [167,168], an allosteric binding site in the interface of the regulatory and catalytic domains[151,169], or in an allosteric site in the interface of two regulatory domains from adjacent subunits in the tetramer. The last scenario will be discussed in the following, as recent literature has supported this model.

As described for isolated regulatory domain, dimerization of regulatory domains is also believed to occur in full-length PAH. Two crystal structures of full-length *rat* PAH were recently published by different groups.[145,170] Both structures represent a tetramer which is arranged as a dimer of dimers, placing the regulatory domains on each side of the tetrameric assembly, Figure 4.4. Both structures present an auto-inhibited form in which the N-terminus partially blocks access to the active site, Figure 4.4. Removal of the N-terminus (NΔ30) in PAH results in increased activity, and preincubation with L-phenylalanine is no longer required for activation.[171] These observations confirm the inhibitory role of the N-terminus.

Jaffe *et al*.[172], have proposed that PAH exists in equilibrium between a high activity tetramer and a low activity tetramer. The interchange between these forms is associated with L-phenylalanine binding in the allosteric site in the regulatory domain. It is proposed that L-phenylalanine binding induce a conformational change involving a rotation of the regulatory domain with respect to the catalytic domain, allowing two regulatory domains to form a dimer. This movement propagate to the N-terminus, which is removed from the active site, resulting in increased enzymatic activity, Figure 4.5.[172] This model is supported by a hydrogen/deuterium exchange study in which L-phenylalanine was found to alter the interaction between the regulatory and catalytic domains.[173] In further support, SEC-SAXS experiments show that L-phenylalanine induces rearrangements of the regulatory domains of tetrameric PAH.[145,170] Based on SAXS-curves with varied concentration of L-phenylalanine, a binding constant of 174 ± 9 µM was determined [145], in agreement with results from a kinetic study of the allosteric activation.[174]

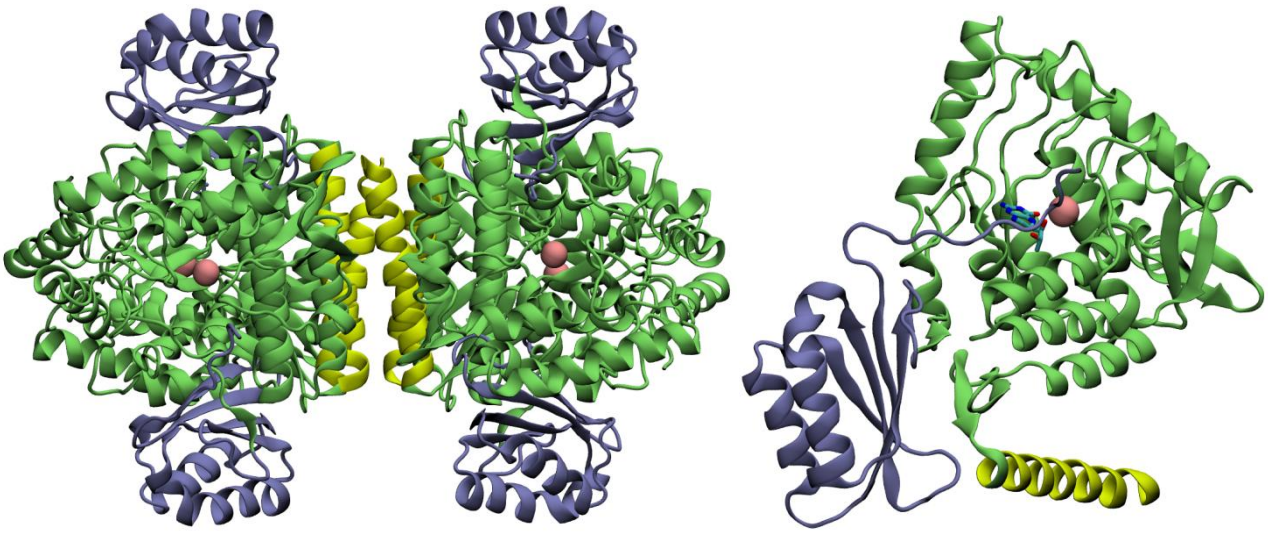

Figure 4.4. Cartoon illustration of the tetrameric structure of full-length *rat* phenylalanine hydroxylase (PDB entry: 5FGJ). Regulatory domains are colored blue, catalytic domains are colored green, and tetramerization domains are colored yellow. Left: side view of full-length tetramer. Right: One subunit of the tetramer illustrating how the N-terminus blocks asses of the active site. BH_4 is shown in sticks and is superimposed from the crystal structure of the catalytic domain of *human* PAH (PDB entry: 1J8U).

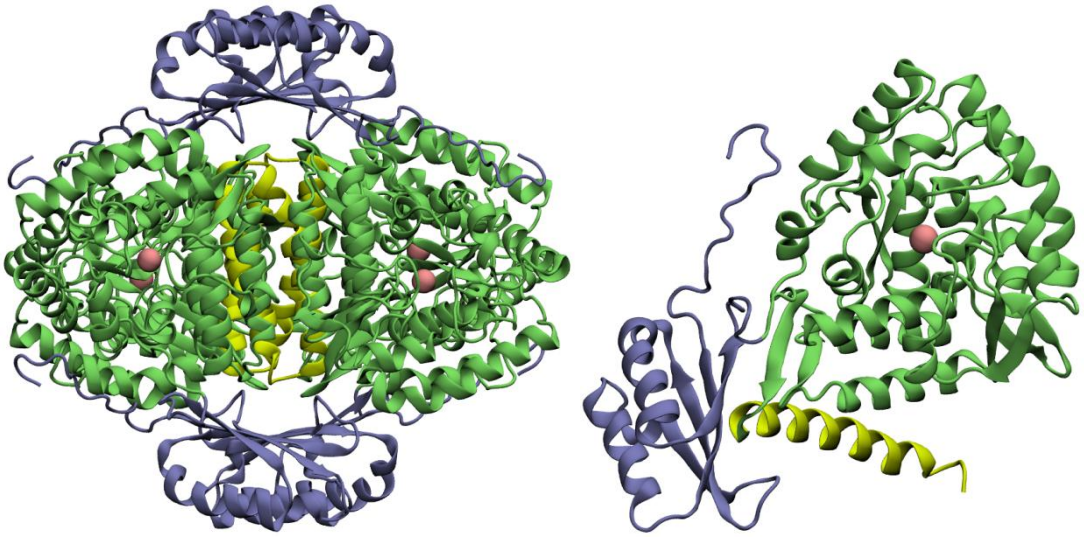

Figure 4.5. Cartoon illustration of a model structure of tetrameric full-length PAH after binding of L-phenylalanine in the allosteric site (Theoritical model – supporting information of [172]). Regulatory domains are colored blue, catalytic domains are colored green, and tetramerization domains are colored yellow. Left: Side view of full-length tetramer model. Right: One subunit of the tetramer model illustrating how the N-terminus is removed from the entrance of the active site.

In support of an allosteric model, it was been confirmed that activation of *rat* PAH does not require binding of L-phenylalanine in the active site.[145,175] All together, activation of PAH is believed to occur through dimerization of the regulatory domains upon binding of L-phenylalanine in the allosteric site, which induces a conformational change that displaces the N-terminus from the active site, resulting in increased access of the substrate.

For TPH, it has been found that truncation of the N-terminus of TPH2 (NΔ44-TPH2) resulted in an almost 4-fold increase in activity compared to full-length TPH2.[143] This suggests an inhibitory function of the N-terminus similar to the one observed for PAH. As no structural information is available for the regulatory domain of the TPH isoforms, it is hard to predict how the N-terminus facilitates this inhibitory function. Based on the length of the N-terminal domains of PAH, TPH1, and TPH2 (Figure 4.1), it can be hypothesized that the N-terminus of TPH2 might similarly block access to the active site, while the N-terminus of TPH1 is unable to, due to insufficient length. This could explain the lower activity of TPH2 compared to TPH1, as the 46 residue extension of the N-terminus in TPH2 is the main difference between the highly homologous enzymes.[176]

4.2 Experimental procedure - analytical gel filtration

The oligomeric state of the TPH2 variants was analyzed by performing analytical gel filtration utilizing a Superdex 200 10/300 GL column. Before the samples were loaded, the column was equilibrated with two column volumes of buffer. For c*h*TPH2, 20 mM HEPES/NH_4OH, 100 mM $(NH_4)_2SO_4$, pH 7.0 was used as the buffer solution (referred to as Std buffer) and for rc*h*TPH2 and NΔ47-rc*h*TPH2 20 mM HEPES/NH_4OH, 300 mM $(NH_4)_2SO_4$, pH 7.0 was used (referred to as Std buffer). When the influence of L-phenylalanine, D-phenylalanine, or L-tryptophan was investigated, the amino acids were added to the buffer solutions prior to column equilibration. When 3 mM L-Phe was added to the buffer solution, it is referred to as Phe buffer. The amino acids were similarly added to the TPH samples and allowed to equilibrate for 20 min before loading onto the column. Samples were loaded with a 500 µL loop and analyzed at a flow rate of 0.5 mL/min. A calibration curve of molecular weight versus elution volume was obtained from GE Healthcare [177].

The obtained chromatograms were deconvoluted using PeakFit v4.12. The chromatograms were fitted with the lowest possible number of peaks, and peaks at elution volumes corresponding to molecular weights lower than monomer were not introduces. The peaks were fitted using chromatography and Eval4 Area Tailed peak type. Tailed was chosen as even mono-disperse solutions deviate from a perfect Gaussian shape. From the areas under the curves of the deconvoluted peaks, the equilibrium dissociation constant, K_{eq}, was determined using eq. 1. For derivation of eq.1 see Appendix A.1.

$$K_{\mathrm{eq}} = \frac{2 * \mathrm{AUC_M^2} \frac{[\mathrm{M}]_{\mathrm{total}}}{\mathrm{DF}}}{\mathrm{AUC_D} * (\mathrm{AUC_D} + \mathrm{AUC_M})} \qquad \text{(eq. 1)}$$

In eq. 1 AUC_M and AUC_D are the areas under the curve of the peaks representing the monomer and dimer, respectively. $[M]_{total}$ is the concentration of the loaded sample and DF is the dilution factor. The dilution factor during elution was measured by the width at half-height of the peak divided by the sample load volume [178]. This was performed only on mono-disperse solutions. The mole fraction of dimer, f_D, at a specific concentration of TPH, was determined from eq. 2. For derivation of eq. 2 see Appendix A.1.

$$f_{\mathrm{D}} = \frac{\frac{1}{4}\left(4 * \frac{[\mathrm{M}]_{\mathrm{total}}}{\mathrm{DF}} + K_{\mathrm{eq}} - 1 * \sqrt{K_{\mathrm{eq}}^2 + 8 * K_{\mathrm{eq}} * \frac{[\mathrm{M}]_{\mathrm{total}}}{\mathrm{DF}}}\right)}{\frac{[\mathrm{M}]_{\mathrm{total}}}{\mathrm{DF}}} \qquad \text{(eq. 2)}$$

4.3 Results – oligomeric state of *h*TPH2 variants

In chapter 2, *h*TPH2 was found to elute as a tetramer, with no evidence of dimer or monomer. In this section, analytical gel filtration results of variants with deletion of the tetramerization domain (CΔ31), rc*h*TPH2, NΔ47-rc*h*TPH2, and c*h*TPH2, are presented and discussed. In chapter 3, it was discussed how L-phenylalanine and L-tryptophan increased the thermostability of rc*h*TPH2 and NΔ47-rc*h*TPH2 and resulted in a two-state unfolding behaviors typically observed for mono-disperse samples. In the following, the influence of the thermostabilizing ligands on the oligomeric states of the TPH variants lacking the tetramerization domain are investigated.

4.3.1 Analytical gel filtration – c*h*TPH2

The results of analytical gel filtration of c*h*TPH2 in either Std buffer or Phe buffer are presented in Figure 4.6 as black or orange peaks, respectively.

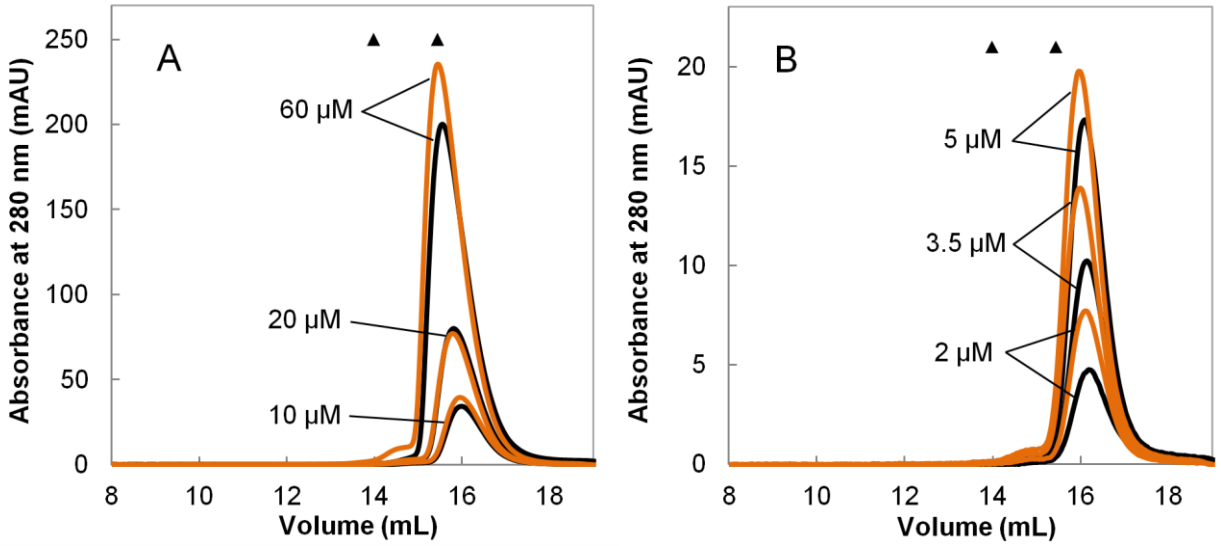

Figure 4.6. Size exclusion chromatography of c*h*TPH2, with no ligand (black) and with the addition of 3 mM L-phenylalanine (orange). The markers (▲) indicate the expected elution volumes of a dimer and a monomer, respectively.[177] Protein loading concentrations are indicated in the chromatograms. A: High loading concentration range. B: Low loading concentration range.

The chromatogram in Figure 4.6 shows that c*h*TPH2 elutes at a volume of ~16 mL corresponding to the molecular weight of a monomer (36.2 kDa). c*h*TPH2 was found to elute as a monomer independent of loading concentration ranging of 2 to 60 µM. Furthermore, 3 mM L-phenylalanine did not induce any change in the elution pattern of the mono-disperse solution.

To test if there was a saturation of the UV-detector, the maximum UV absorbance as a function of loading concentration was analyzed. In Figure 4.7 the correlation between loading concentrations of c*h*TPH2 in Phe buffer and peak heights (maximum absorption) is shown. The peak heights were found to be related directly to the loading concentration, which means that saturation of the detector does not occur. This was also the case for c*h*TPH2 in Std buffer and NΔ47-rc*h*TPH2 in Phe buffer (Appendix F.1 and F.2).

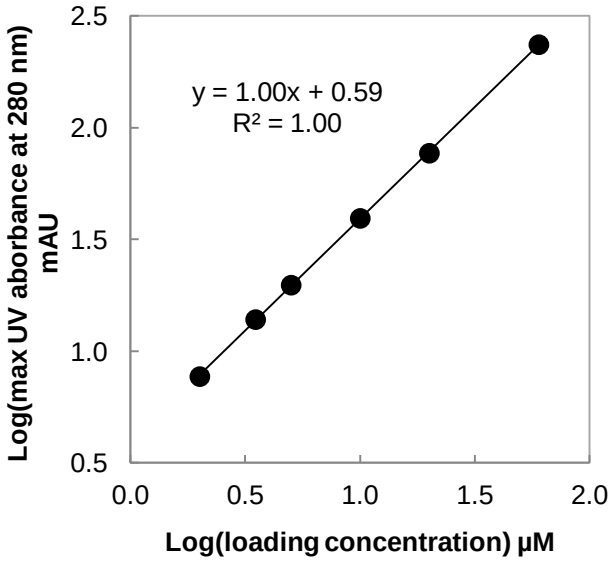

Figure 4.7. Max height of elution peak (max UV_{280nm} response) as a function of c*h*TPH2 loading concentration.

During loading, separation, and elution the concentration of protein will be lowered by a dilution factor compared to the loading concentration. To know the actual concentration of TPH on the column the dilution factor was calculated as width at half-height of the peak divided by the sample load volume.[178] The dilution factors calculated from analytical gel filtrations of c*h*TPH2 in Std or Phe buffer and NΔ47-rc*h*TPH2 in Phe buffer are presented in Table 4.2.The dilution factor was calculated based on those chromatograms, as they resulted in mono-disperse samples (only one peak, Figure 4.6 and Figure 4.8). The dilution factor is on average 1.9 ± 0.1 and is not dependent on the loading concentration.

Table 4.2. Dilution factor of samples loaded on a Superder200 10/300 GL column. Dilution factors calculated from width at half-height (mL) divided by loading volume (mL). Std and Phe for c*h*TPH2 refers to 20 mM HEPES/NH_4OH, 100 mM $(NH_4)_2SO_4$, pH 7.0 or 20 mM HEPES/NH_4OH, 100 mM $(NH_4)_2SO_4$, 3 mM L-phenylalanine, pH 7.0, respectively. Phe for NΔ47-rc*h*TPH2 refers to 20 mM HEPES/NH_4OH, 300 mM $(NH_4)_2SO_4$, 3 mM L-phenylalanine, pH 7.0

Loading conc. (µM)	c*h*TPH2 (Std)	c*h*TPH2 (Phe)	NΔ47-rchTPH2 (Phe)
	Dilution factor		
60.0	2.0	1.9	1.9
20.0	1.9	1.9	1.8
10.0	1.8	1.9	1.8
5.0	1.8	1.8	2.0
3.5	1.7	1.7	2.0
2.0	1.8	1.8	2.1

4.3.2 Analytical gel filtration – NΔ47-rc*h*TPH2

The results of analytical gel filtration of NΔ47-rc*h*TPH2 in either Std buffer or Phe buffer are presented in Figure 4.8 as black or orange peaks, respectively. In the absence of L-phenylalanine the chromatogram of NΔ47-rc*h*TPH2 results in two overlapping peaks with elution volumes of ~13 and ~15 mL corresponding to molecular weights of a dimer (94.9 kDa) and monomer (47.4 kDa), respectively. The elution peaks are gradually shifted from predominantly dimer to a mixture of monomer and dimer with decreasing loading

concentration. This illustrates that NΔ47-rc*h*TPH2 is in a concentration-dependent monomer-dimer equilibrium.

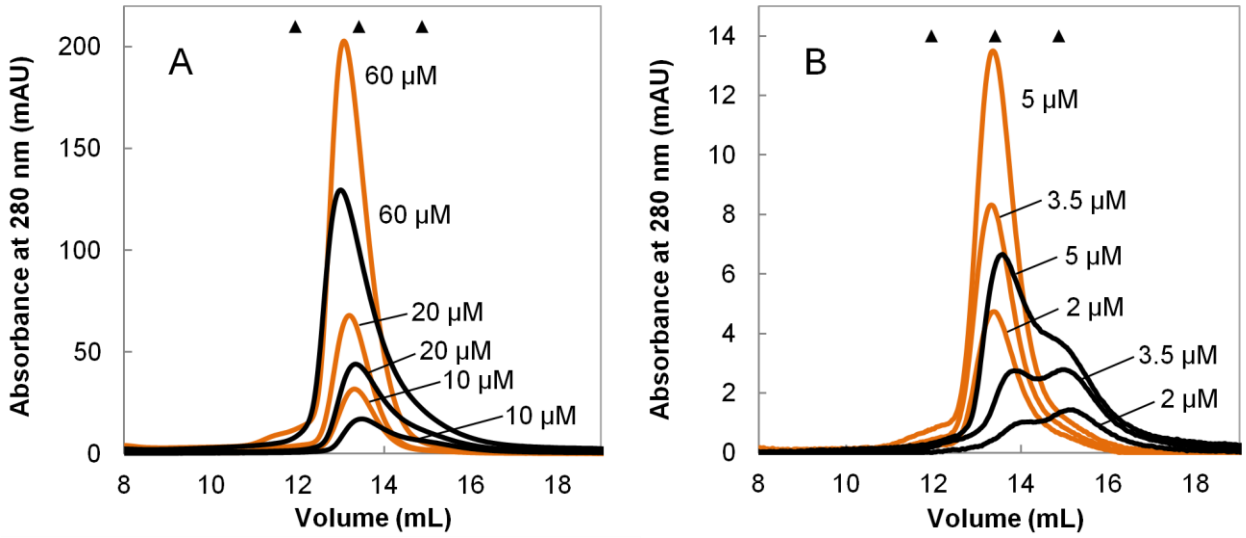

Figure 4.8. Size exclusion chromatography of NΔ47-rc*h*TPH2 without added L-Phe (black lines) and with added L-Phe (orange lines). The markers (▲) indicate the expected elution volume of (from left to right) a tetramer, a dimer, and a monomer, respectively.[177] Protein loading concentrations are indicated in the chromatograms. A: High loading concentration range. B: Low loading concentration range.

As the peaks in Figure 4.8 are not baseline separated, the chromatograms were deconvoluted. To assess the relative amounts of monomer and dimer the AUCs of the peaks were calculated based on the deconvoluted chromatograms. Figure 4.9 shows an example of a deconvoluted chromatogram of NΔ47-rc*h*TPH2 with a loading concentration of 2 µM.

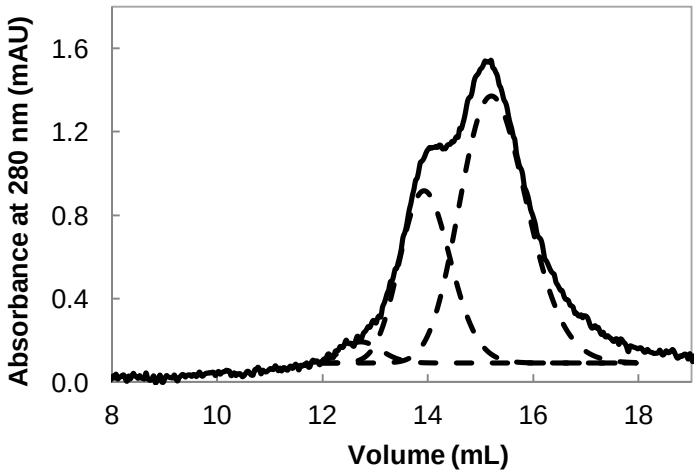

Figure 4.9. PeakFit deconvolution of the chromatogram of NΔ47-rc*h*TPH2 (2 µM) in 20 mM HEPES/NH_4OH, 300 mM $(NH_4)_2SO_4$, pH 7.0. The solid line represents data and dashed lines represent deconvoluted peaks.

From the extracted AUCs, while taking the determined dilution factor into account, the monomer-dimer equilibrium dissociation constant, K_{eq}, can be determined using eq. 1. The equilibrium dissociation constants calculated from the six loading concentrations of NΔ47-rc*h*TPH2 are presented in Table 4.3.

Table 4.3. Equilibrium dissociation constant, K_{eq}, of the dimerization of NΔ47-rc*h*TPH2 in 20 mM HEPES/NH_4OH, 300 mM $(NH_4)_2SO_4$, pH 7.0 determined at different loading concentrations.

Loading conc. (μM)	K_d (μM)
60.0	1.28
20.0	1.15
10.0	1.36
5.0	1.26
3.5	1.27
2.0	1.30

From Table 4.3, an average K_{eq}-value of 1.3 ± 0.1 μM can be calculated for the dimerization of NΔ47-rc*h*TPH2 in absence of L-phenylalanine. The mole fraction of dimer, f_D, at a specific NΔ47-rc*h*TPH2 concentration can be calculated from the determined concentration of monomer and dimer. f_D as a function of NΔ47-rc*h*TPH2 concentration is presented in Figure 4.10. The same dissociation constant of 1.3 μM can be obtained from a nonlinear regression of the data in Figure 4.10 with eq. 2.

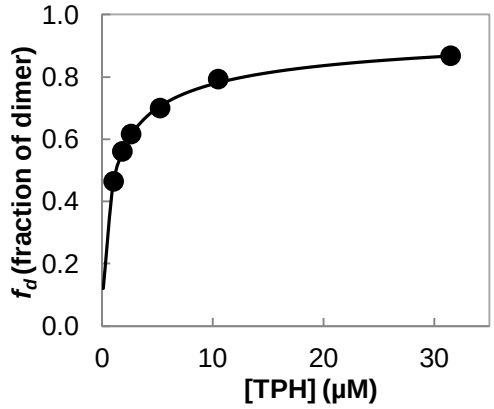

Figure 4.10. Fraction of dimer as a function of NΔ47-rc*h*TPH2 concentration (loading concentration divided by dilution factor). The solid line represents the nonlinear regression with equation 2.

The effect of L-phenylalanine on the monomer-dimer equilibrium was analyzed by performing analytical gel filtration on NΔ47-rc*h*TPH2 samples with addition of 3 mM L-phenylalanine. The results are presented in the chromatogram in Figure 4.8 (orange peaks). It is evident that the presence of 3 mM L-phenylalanine shifts the monomer-dimer equilibrium towards dimer. The dimerizing effect of L-phenylalanine is obvious at a loading concentration of 2 μM NΔ47-rc*h*TPH2. Here the equilibrium is shifted from predominately monomer to almost exclusively dimer. A K_{eq}-value of 0.2 ± 0.1 μM was obtained for the dimerization of NΔ47-rc*h*TPH2 in the presence of 3 mM L-phenylalanine. Only loading concentrations of 2, 3.5, 5, and 10 μM were used to calculate this value, as no monomer was observed upon deconvolution of the chromatograms of loading concentrations 20 and 60 μM.

The concentration dependency of L-phenylalanine was analyzed by performing analytical gel filtration on NΔ47-rc*h*TPH2 with a loading concentration of 2 μM at varied concentrations of L-phenylalanine. Results with 1, 2, and 3 mM L-phenylalanine are presented in Figure 4.11. The dimerizing effect of L-phenylalanine is obvious as the equilibrium is shifted towards dimer with increase concentration. K_{eq}-values of 1.2, 0.7 and 0.2 μM were obtained for 1, 2, and 3 mM L-phenylalanine, respectively.

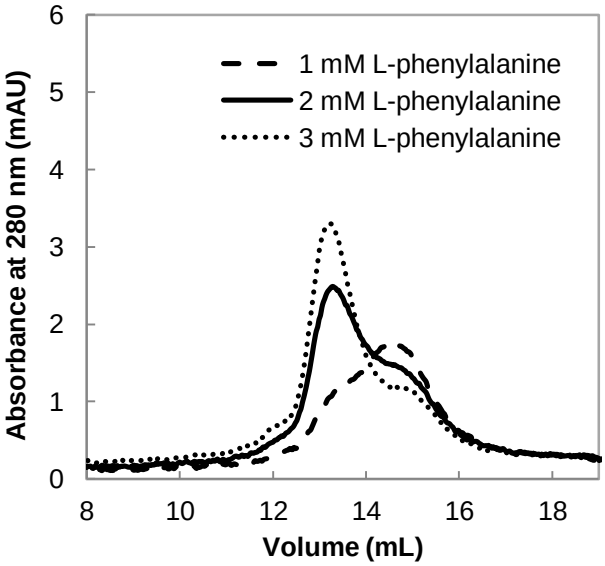

Figure 4.11. Size exclusion chromatography results of NΔ47-rc*h*TPH2 with 1 mM L-phe (dashed line), 2 mM L-phe (solid line), or 3 mM L-phe (dotted line).

In chapter 3, L-tryptophan was found to increase the thermostability of NΔ47-rc*h*TPH2, while D-phenylalanine had no influence on the stability. To see if this correlates with a dimerizing effect, analytical gel filtrations of NΔ47-rc*h*TPH2 were conducted in the presence of 0.5 and 1.0 mM L-tryptophan and 3 mM D-phenylalanine. The results are presented in Figure 4.12.

The influence of L-tryptophan at 3 mM could not be studied by analytical gel filtration with a UV-Vis detector because the absorption by L-tryptophan overlaps with that of the protein (primarily tryptophan). This results in high background noise, which limits the measurements to either high protein concentrations or low L-tryptophan concentrations. As a consequence, the influence of L-tryptophan was investigated at 0.5 and 1 mM. Even at these concentrations a lot of noise is observed in the chromatograms, Figure 4.12 B and C. Due to noise limitations, measurements at 1 mM L-tryptophan with NΔ47-rc*h*TPH2 concentrations lower than 5 µM could not be conducted.

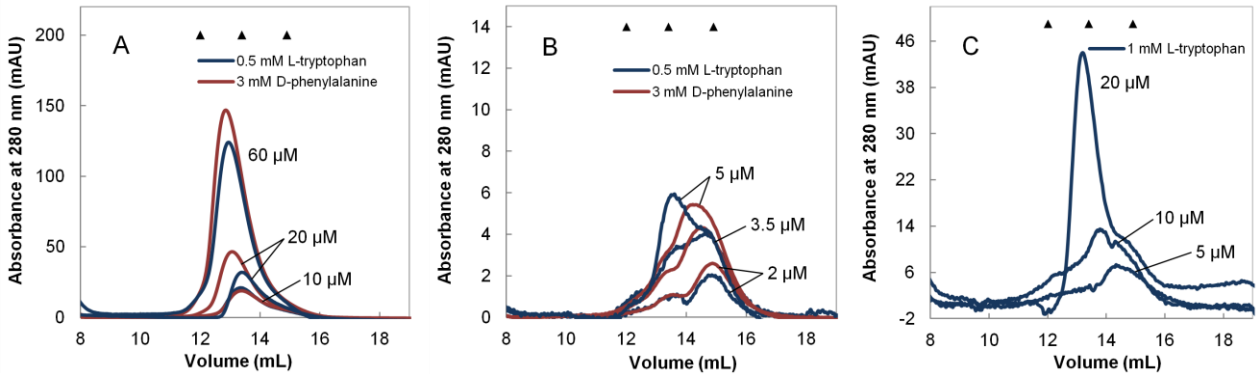

Figure 4.12. Size exclusion chromatography results of NΔ47-rc*h*TPH2 with L-tryptophan or D-phenylalanine. Protein loading concentrations are indicated in the chromatograms. The markers (▲) indicate the expected elution volumes of a tetramer, a dimer, and a monomer, respectively. A: High loading concentration range with addition of 0.5 mM L-tryptophan (blue) or 3 mM D-phenylalanine (red). B: Low loading concentration range with addition of 0.5 mM L-tryptophan (blue) or 3 mM D-phenylalanine (red). C: Addition of 1 mM L-tryptophan.

From Figure 4.12 A and B it is evident that 0.5 mM L-tryptophan or 3 mM D-phenylalanine do not shift the equilibrium to predominantly dimer as observed for 3 mM L-phenylalanine. From the monomer-dimer

distribution obtained at the six concentrations of NΔ47-rc*h*TPH2, dimerization K_{eq}-values of 1.6 ± 0.7 µM and 1.8 ± 0.9 µM were determined for L-tryptophan and L-phenylalanine addition, respectively. Hence, neither 3 mM D-phenylalanine nor 0.5 mM L-tryptophan have a significant impact on the monomer-dimer equilibrium.

In the chromatograms of NΔ47-rc*h*TPH2 in the presence of 1 mM L-tryptophan (Figure 4.12 C) significant levels of noise are present. However, based on the elution volumes it seems that the majority of the protein is present as monomer at loading concentrations of 5 and 10 µM.

4.3.3 Analytical gel filtration – rc*h*TPH2

The results of analytical gel filtration of rc*h*TPH2 in either Std buffer or Phe buffer are presented in Figure 4.13 as black or orange peaks, respectively. As for NΔ47-rc*h*TPH2, the monomer-dimer equilibrium of rc*h*TPH2 is found to shift significantly towards dimer in the presence of 3 mM L-phenylalanine. This result demonstrates that the effect of L-phenylalanine does not involve the N-terminus.

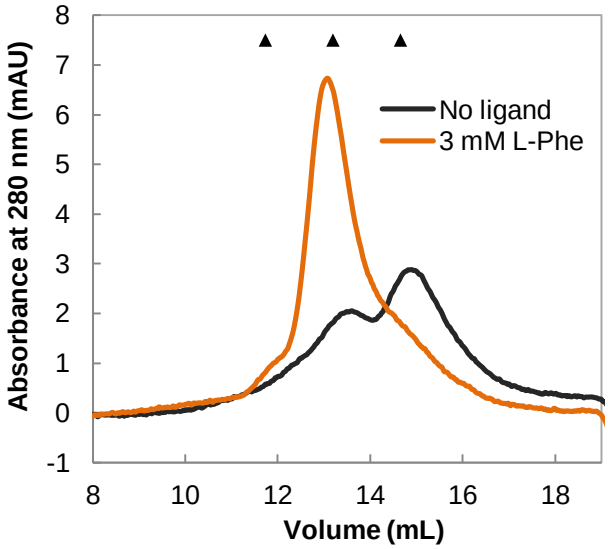

Figure 4.13. Size exclusion chromatography of rc*h*TPH2 (loading concentration of 2 µM), with no ligand (black line) and with the addition of 3 mM L-Phe (orange line). The markers (▲) indicate the expected elution volumes of a tetramer, a dimer, and a monomer, respectively.

4.3.4 Analytical gel filtration – c*h*TPH mutant variants

In chapter 7, a mutational study is conducted on an active site loop of both TPH isoforms. Here, point mutations of residue 125 in c*h*TPH1 and 171 in c*h*TPH2 were conducted. To assure that the mutations did not result in changes in the oligomeric state of the catalytic domain of the TPH isoforms analytical gel filtration was performed.

The chromatograms display that all TPH variants of the two isoforms are monodisperse, Figure 4.14. The c*h*TPH1 variants elute at volumes from 15.5 to 15.6 mL (n=3) while the c*h*TPH2 variants from 15.7 to 15.8 mL (n=3) (data found in Appendix F.3). These results show that all the TPH variants reside as monomers and that no significant changes within each variant occur as a consequence of mutation. Despite the slightly higher molecular weights of the c*h*TPH2 variants (36274 to 36362 Da) compared to c*h*TPH1 counterparts (36128 to 36250 Da), they elute at a slightly greater elution volume, which indicate that the c*h*TPH2 variants are more compact.

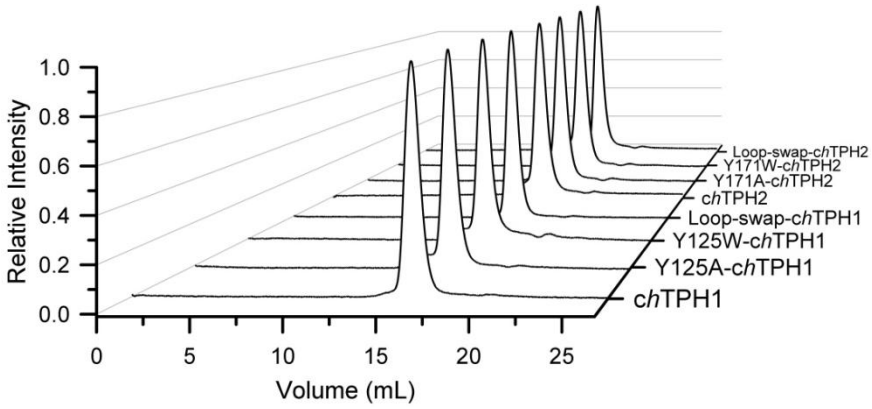

Figure 4.14. Normalized size exclusion chromatography results of the c*h*TPH variants.

4.4 Discussion

Full-length TPH2 exists as tetramers with no sign of dimer or monomer. In this study, deletion of the regulatory and tetramerization domains resulted in a mono-disperse solution with retention volume corresponding to the molecular weight of a monomer. This finding is in consensus with previous studies on the catalytic domain of TPH.[157,158,179] When only the tetramerization domain is deleted, a concentration-dependent monomer-dimer equilibrium is established. This result demonstrates that the dimerization is caused by the regulatory domain as c*h*TPH2 was found only as a monomer.

The equilibrium dissociation constant of the dimerization of NΔ47-rc*h*TPH2 was determined to 1.3 ± 0.1 µM. This value is lower than 46 ± 35 µM determined for the dimerization of the regulatory domain of PAH.[161] The lower value might be explained by the presence of the catalytic domain. Two C-terminal β-strands in the catalytic domain of PAH have been found to be important for dimer formation.[180] These β-strands are also present in the C-terminal of the cataltyic domain of TPH2. The strands are found buried at the interface between two catalytic domains in the crystal structyre of ct*h*TPH2 (PDB entry: 4V06).

The ability of the regulatory domain to facilitate dimerization in a TPH variant containing the catalytic domain has not previously been studied. Very little is known in regards to the regulatory domain and there is no data available in the literature on dimerization of isolated regulatory domain of TPH2. However, isolated regulatory domain of TPH1 forms a stable dimer.[138,159] This observation together with the results obtained for NΔ47-rc*h*TPH2 indicate that the regulatory domain of TPH might be involved in a dimerization mechanism similar to the one observed for PAH. The result of dimerization in PAH has been hypothesized to be the origin of the cooperative L-phenylalanine activation mechanism.[172] No evidence has been presented for a similar cooperative activation of TPH. This leaves the question of whether the observed dimerization in TPH2 is *in vivo* relevant or just an inherited trade which can only be detected *in vitro*.

In chapter 3, it was demonstrated that NΔ47-rc*h*TPH2 was thermostabilized by L-phenylalanine but not by D-phenylalanine. In agreement with these observations, this chapter demonstrates that of the two stereoisomers of phenylalanine only L-phenylalanine caused a shift in the monomer-dimer equilibrium. The DSF results with L-phenylalanine showed that the unfolding of NΔ47-rc*h*TPH2 was changed from polyphasic to two-state. Such a change has previously been shown in a DSF study to indicate increased mono-dispersity and stability.[181] This correlates well with a change from a mixture of monomer and dimer to exclusively dimer.

The fact that only one stereoisomer of phenylalanine induces dimerization and thermostabilization suggests that it is caused by specific binding of phenylalanine rather than its amphiphilic nature. The binding affinity of

this specific binding must, however, be very low as 3 mM is required to obtain complete dimerization. Low affinity is also observed in full-length PAH as a K_d-value for L-phenylalanine binding in the allosteric site is 174 ± 9 µM and 1 mM is required for full effect.[145] One could speculate that L-phenylalanine is not the most potent ligand for allosteric binding in TPH. The more obvious ligand would be L-tryptophan which was also found to thermostabilize NΔ47-rc*h*TPH2 and induce two-state unfolding at concentration <1 mM. However, tryptophan did not induce a change in the monomer-dimer equilibrium at concentration of 1 mM. This suggests that stabilization occurs through a different mechanism.

In a study by Patel *et al*., it was demonstrated that, among the regulatory domains of TH, PAH, and TPH1, only PAH is thermostabilized by its natural substrate.[138] This suggests that only the regulatory domain of PAH binds substrate. Furthermore, the oligomeric state of r*h*TPH1 was not influenced by L-Phe (1 mM).[159] In line with these results, analytical gel filtration on NΔ47-rc*h*TPH2 shows that L-tryptophan most likely does not bind in the regulatory domain of TPH2, whereas L-phenylalanine does. This indicates that TPH2 might have an allosteric site in the regulatory domain that TPH1 does not have. This hypothesis is supported by observations from TPH purifications (chapter 2), where it was found that purification yields were significantly increased for TPH2 variants containing the regulatory domain, whereas the yield of the TPH1 variants were not influenced. However, it might also be the case that only TPH2 is able to bind phenylalanine in the regulatory domain, but both isoforms are able to bind a so far unknown ligand.

Phylogenetically PAH and TPH2 are related [182] which might mean that TPH2 has just retained the ability to bind L-phenylalanine in the regulatory domain. This cannot be ruled out, however, the affinities of PAH and TPH2 for L-phenylalanine are presumably not very different which implies an importance of the conserved site.

TPH is able to catalyze hydroxylation of L-phenylalanine [163], which means that it binds in the catalytic site. L-phenylalanine did not cause dimerization of the catalytic domain; however, it opens up the possibility that active site binding somehow affects the regulatory domain. To confirm that dimerization is not induced by active site binding more experiments have to be conducted. Studies should be conducted on isolated regulatory domain of TPH2. If L-phenylalanine induces dimerization or increase T_m for this variant, the allosteric binding site hypothesis would be strengthened. Alternatively, mutations of substrate binding residues would diminish active site binding, and dimerization experiments on this mutant variant could reveal whether active site binding was involved.

4.5 Conclusion

In this chapter, it is demonstrated that isolated catalytic domain of *h*TPH2 exists as a monomer while the presence of the regulatory domain induces a monomer-dimer equilibrium with a K_{eq}-value of 1.3 µM. This equilibrium is shifted significantly towards dimer in the presence of 3 mM L-phenylalanine resulting in a mono-disperse solution. Of the two stereoisomers of phenylalanine, only L-phenylalanine induces dimerization which demonstrates that the change in equilibrium is caused by specific binding.

4.6 References

[136] Fitzpatrick, P.F., 1999, Tetrahydropterin-dependant amino acid hydroxylases, *Annu. Rev. Biochem. 68*, 355–381

[137] Windahl, M. S., Boesen, J., Karlsen, P.E., and Christensen, H.E.M., 2009, Expression, Purification and Enzymatic Characterization of the Catalytic Domains of Human Tryptophan Hydroxylase Isoforms, *Protein J. 28(9-10)*, 400–406

[138] Patel, D., Kopec, J., Fitzpatrick, F., McCorvie, T. J., and Yue, W. W., 2016, Structural basis for ligand dependent dimerization of phenylalanine hydroxylase regulatory domain, *Sci. Rep. 6*, 23748.

[139] Goodwill, K. E., Sabatier, C., Marks, C., Raag, R., Fitzpatrick, P. F., and Stevens, R. C., 1997, Crystal structure of tyrosine hydroxylase at 2.3 Å and its implications for inherited neurodegenerative diseases, *Nat. Struct. Biol. 7*, 578-585.

[140] Sievers, F., Wilm, A., Dineen, D. G., Gibson, T. J., Karplus, K., Li, W., Lopez, R., McWilliam, H., Remmert, M., Söding, J., Thompson, J. D., and Higgins, D., 2011, Fast, scalable generation of high-quality protein multiple sequence alignments using Clustal Omega, *Mol. Syst. Biol. 7*, 539.

[141] Fitzpatrick, P. F., 2015, Structural insights into the regulation of aromatic amino acid hydroxylation, *Curr. Opin. Struct. Biol. 35*, 1–6.

[142] Liu, X. and Vrana, K.E., 1991, Leucine zippers and coiled-coils in the aromatic acid hydroxylases, *Neurochem. Int. 18(1)*, 27-31.

[143] Tenner, K., Walther, D., and Bader, M., 2007, Influence of human tryptophan hydroxylase 2 N- and C-terminus on enzymatic activity and oligomerization, *J. Neurochem. 102(6)*, 1887–1894.

[144] Arturo, E.C., Gupta, K., Heroux, A., Stith, L., Cross, P.J., Parker, E.J., Loll, P.J., and Jaffe, E.K., 2016, The First Structure of a Full-Length Mammalian Phenylalanine Hydroxylase Reveals the Architecture of an Auto-inhibited Tetramer, *Proc. Natl. Acad. Sci. 113* 2394-2399.

[145] Meisburger, S.P., Taylor, A.B., Khan, C.A., Zhang, S., Fitzpatrick, P.F., and Ando, N., 2016, Domain Movements upon Activation of Phenylalanine Hydroxylase Characterized by Crystallography and Chromatography-Coupled Small-Angle X-ray Scattering, *J. Am. Chem. Soc. 138*, 6506-6516.

[146] Goodwill, K.E., Sabatier, C., and Stevens, R.C., 1998, Crystal Structure of Tyrosine Hydroxylase with Bound Cofactor Analogue and Iron at 2.3 Å Resolution: Self-Hydroxylation of Phe300 and the Pterin-Binding Site, *Biochemistry 37*, 13437-13445.

[147] Mockus S. M., Kumer S. C., and Vrana K. E., 1997, Carboxyl terminal deletion analysis of tryptophan hydroxylase, *Biochim. Biophys. Acta 1342*, 132-140.

[148] Haahr, L. T., 2012, Purification and Characterization of Tryptophan Hydroxylase, Ph.D. thesis, Department of Chemistry, Technical University of Denmark, Kgs. Lyngby.

[149] Jiang, G. C.-T., Yohrling, G. J., Schmitt, I. V. J. D., and Vrana, K. E., 2000, Identification of Substrate Orienting and Phosphorylation Sites Within Tryptophan Hydroxylase Using Homology-based Molecular Modeling, *J. Mol. Biol. 302*, 1005-1017.

[150] Aravind, L. and Koonin, E. V., 1999, Gleaning Non-trivial Structural, Functional and Evolutionary Information About Proteins by Iterative Database Searches, *J. Mol. Biol. 287*, 1023-1040.

[151] Kobe, B., Jennings, I. G., House, C. M., Michell, B. J., Goodwill, K. E., Santarsiero, B. D., Stevens, R. C., Cotton, R. G., and Kemp, B. E., 1999, Structural basis of autoregulation of phenylalanine hydroxylase, *Nat. Struct. Mol. Biol. 6*, 442–448.

[152] Zhang, S., Huang, T., Ilangovan, U., Hinck, A. P., and Fitzpatrick, P. F., 2014, The solution structure of the regulatory domain of tyrosine hydroxylase, *J. Mol. Biol. 426*, 1483-1497.

[153] Fitzpatrick, P.F., 2012, Allosteric regulation of phenylalanine hydroxylase, *Arch. Biochem. Biophys. 519(2)*, 194-201.

[154] Lang, E. J. M., Cross, P. J., Mittelstädt, G., Jameson, G. B., and Parker, E. J., 2014, Allosteric ACTion: the varied ACT domains regulating enzymes of amino-acid metabolism, *Curr. Opin. Struct. Biol. 29*, 102-111.

[155] Liberles, J. S., Thórólfsson, M., and Martínez, A., 2005, Allosteric mechanisms in ACT domain containing enzymes involved in amino acid metabolism, *Amino Acids 28(1)*, 1-12.

[156] Yohrling, G. J., Mockus, S. M., and Vrana, K. E., 1999, Identification of Amino-Terminal Sequences Contributing to Tryptophan Hydroxylase Tetramer Formation, *J. Mol. Neurosci. 12*, 23-34.

[157] D´Sa, C., Arthur, R. E., Jr., and Kuhn, D. M., 1996, Expression and deletion mutagenesis of tryptophan hydroxylase fusion proteins: delineation of the enzyme catalytic core, *J. Neurochem. 67*, 917-926.

[158] Carkaci-Salli, N., Flanagan, J. M., Martz, M. K., Salli, U., Walther, D. J., Bader, M., and Vrana, K. E., 2006, Functional Domains of Human Tryptophan Hydroxylase 2 (hTPH2), *J. Biol. Chem. 281(38)*, 28105-28112.

[159] Zhang, S., Hinck, C. S., and Fitzpatrick, P. F., 2016, The regulatory domain of human tryptophan hydroxylase 1 forms a stable dimer, *Biochem. Biophys. Res. Commun. 476*, 457-461.

[160] Li, J., Ilangovan, U., Daubner, S. C., Hinck, A. P., and Fitzpatrick, P. F., 2011, Direct evidence for a phenylalanine site in the regulatory domain of phenylalanine hydroxylase, *Arch. Biochem. Biophys. 505*, 250-255.

[161] Zhang, S., Roberts, K. M., and Fitzpatrick, P. F., 2014, Phenylalanine binding is linked to dimerization of the regulatory domain of phenylalanine hydroxylase, *Biochemistry 53*, 6625-6627.

[162] Zhang, S. and Fitzpatrick, P. F., 2016, Identification of the Allosteric Site for Phenylalanine in Rat Phenylalanine Hydroxylase, *J. Biol. Chem. 291(14)*, 7418–7425.

[163] Moran, G. R., Daubner, S. C., and Fitzpatrick, P. F., 1998, Expression and Characterization of the Catalytic Core of Tryptophan Hydroxylase, *J. Biol. Chem. 273*, 12259-12266.

[164] Wang, L., Erlandsen, H., Haavik, J., Knappskog, P. M., and Stevens, R. C., 2002, Three-Dimensional Structure of Human Tryptophan Hydroxylase and Its Implications for the Biosynthesis of the Neurotransmitters Serotonin and Melatonin, *Biochemistry 41(42)*, 12569-12574.

[165] Windahl, M. S., Petersen, C. R., Christensen, H. E. M., and Harris, P., 2008, Crystal Structure of Tryptophan Hydroxylase with Bound Amino Acid Substrate, *Biochemistry 47*, 12087–12094.

[166] Fisher, D. B. and Kaufman, S., 1973, The Stimulation of Rat Liver Phenylalanine Hydroxylase by Lysolecithin and α-chymotrypsin, *J. Biol. Chem. 248*, 4345–4353.

[167] Andersen, O. A., Stokka, A. J., Flatmark, T., and Hough, E., 2003, 2.0 Å Resolution crystal structures of the ternary complexes of human phenylalanine hydroxylase catalytic domain with tetrahydrobiopterin and 3-(2-thienyl)-L-alanine or L-norleucine: substrate specificity and molecular motions related to substrate binding, *J. Mol. Biol. 333*, 747–757.

[168] Thórólfsson, M., Ibarra-Molero, B., Fojan, P., Petersen, S. B., Sanchez-Ruiz, J. M., and Martínez, A., 2002, L-Phenylalanine Binding and Domain Organization in Human Phenylalanine Hydroxylase: A Differential Scanning Calorimetry Study, *Biochemistry 41*, 7573−7585.

[169] Carluccio, C., Fraternali, F., Salvatore, F., Fornili, A., and Zagari, A., 2016, Towards the identification of the allosteric Phe-binding site in phenylalanine hydroxylase, *J. Biomol. Struct. Dyn. 34(3)*, 497-507.

[170] Arturo, E. C., Gupta, K., Héroux, A., Stith, L., Cross, P. J., Parker, E. J., Loll, P. J., and Jaffe, E. K., 2016, First structure of full-length mammalian phenylalanine hydroxylase reveals the architecture of an autoinhibited tetramer, *Proc. Natl. Acad. Sci. 113(9)*, 2394-2399.

[171] Jennings, I. G., Teh, T., and Kobe, B., 2001, Essential role of the N-terminal autoregulatory sequence in the regulation of phenylalanine hydroxylase, *FEBS Lett. 488*, 196-200.

[172] Jaffe, E. K., Stith, L., Lawrence, S. H., Andrake, M., and Dunbrack, R. L. Jr., 2013, A new model for allosteric regulation of phenylalanine hydroxylase: implications for disease and therapeutics, *Arch. Biochem. Biophys. 530*, 73-82.

[173] Li, J., Dangott, L. J., and Fitzpatrick, P. F., 2010, Regulation of phenylalanine hydroxylase: conformational changes upon phenylalanine binding detected by hydrogen/deuterium exchange and mass spectrometry, *Biochemistry 49*, 3327-3335.

[174] Knappskog, P. M., Flatmark, T., Aarden, J. M., Haavik, J., and Martínez, A., 1996, Structure/function relationships in human phenylalanine hydroxylase - Effect of terminal deletions on the oligomerization, activation and cooperativity of substrate binding to the enzyme, *Eur. J. Biochem. 242*, 813−821.

[175] Roberts, K. M., Khan, C. A., Hinck, C. S., and Fitzpatrick, P. F., 2014, Activation of Phenylalanine Hydroxylase by Phenylalanine Does Not Require Binding in the Active Site, *Biochemistry 53*, 7846−7853.

[176] McKinney, J., Knappskog, P. M., and Haavik, J., 2005, Different properties of the central and peripheral forms of human tryptophan hydroxylase, *J. Neurochem, 92(2)*, 311-320.

[177] Calibration curve obtained from: GE Healthcare, Gel Filtration Calibration Kit LMW, Gel Filtration Kit HMW, Data File 28-4073-84-AA.

[178] Manning, L. R., Jenkins, W. T., Hess, J. R., Vandegriff, K., Winslow, R. M., and Manning, J. M., 1999, Subunit dissociations in natural and recombinant hemoglobins, *Protein Science 5*, 775-781.

[179] Nielsen, M. S., 2007, Expression, purification and characterization of tryptophan hydroxylase, Ph.D. thesis. Department of Chemistry, Technical University of Denmark, Kgs. Lyngby.

[180] Erlandsen, H., Fusetti, F., Martinez, A., Hough, E., Flatmark, T., and Stevens, R.C., 1997, Crystal structure of the catalytic domain of human phenylalanine hydroxylase reveals the structural basis for phenylketonuria, *Nat. Struct. Biol. 4*, 995–1000.

[181] Chari, A., Haselbach, D., Kirves, J. M., Ohmer, J., Paknia, E., Fischer, N., Ganichkin, O., Möller, V., Frye, J. J., Petzold, G., Jarvis, M., Tietzel, M., Grimm, C., Peters, J. M., Schulman, B. A., Tittmann, K., Markl, J., Fischer, U., and Stark, H., 2015, ProteoPlex: stability optimization of macromolecular complexes by sparse-matrix screening of chemical space, *Nat. Methods 12*, 859-865.

[182] Cao, J., Shi, F., Liu, X., Huang, G., and Zhou, M., 2010, Phylogenetic analysis and evolution of aromatic amino acid hydroxylase, *FEBS Lett. 584(23)*, 4775–4782.

Chapter 5

Reaction mechanism of TPH

This chapter concerns the reaction mechanism of the TPH isoforms. In chapter 1, it was introduced how TPH catalyzes the reaction of tryptophan to 5-hydroxytryptophan utilizing 6*R*-L-erythro-5,6,7,8-tetrahydrobiopterin (BH_4) and O_2. In the following, a more detailed reaction mechanism including the role of BH_4 and iron will be presented.

During conversion from a substrate to a product, one or more reaction intermediates are formed transiently. During a 3 month research stay in Prof. Edward I. Solomon's group at Stanford University, stopped-flow kinetic experiments were conducted on c*h*TPH2 in pursuit of such reaction intermediates. Stopped-flow absorbance spectroscopy will be introduced, and results obtained utilizing this method will be presented and discussed.

Outline

5.1 The reaction mechanism of TPH

The TPH isoforms are nonheme iron-dependent monooxygenases which catalyze the insertion of one oxygen atom from O_2 into the aromatic ring of tryptophan. In this process, BH_4 accepts the second oxygen atom from O_2, forming 4a-hydroxy-BH_4, Figure 5.1.[183] 4a-hydroxy-BH_4 has been observed in the reaction of all the AAAHs [184-186], and it is believed that the enzymes share a common catalytic mechanism of hydroxylation.[187] 4a-hydroxy-BH_4 is converted to qBH_2 which in turn is reduced back to BH_4, as described in chapter 1.

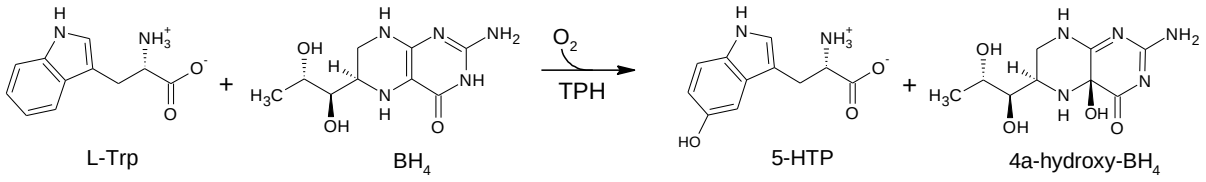

Figure 5.1. Schematic illustration of the TPH catalyzed reaction.

The reaction in Figure 5.1 is believed to occur through two consecutive steps; reaction between the active site Fe^{II}, O_2, and BH_4 to form a reactive hydroxylating intermediate, followed by hydroxylation of tryptophan. The hydroxylating intermediate in the first part of the reaction is believed to be a ferryl oxo species ($Fe^{IV}O$), as Fe^{IV} has been observed experimentally in the reactions of TH and PAH.[188,189]

Preceding the formation of $Fe^{IV}O$, the reaction is believed to occur through a Fe^{II}-peroxypterin intermediate, Figure 5.2.[190] Such an intermediate is attractive because heterolytic cleavage of the oxygen-oxygen bond would result in 4a-hydroxy-BH_4 and $Fe^{IV}O$ directly. The presence of such an intermediate is supported by a study of PAH with tyrosine as substrate. Here, unproductive consumption of BH_4 and O_2 results in H_2O_2 which is consistent with the breakdown of a peroxypterin intermediate.[191,192] This intermediate has never been isolated experimentally, however, evidence of an intermediate species preceding the formation of $Fe^{IV}O$ has been detected for the TPH1 catalyzed reaction.[193]

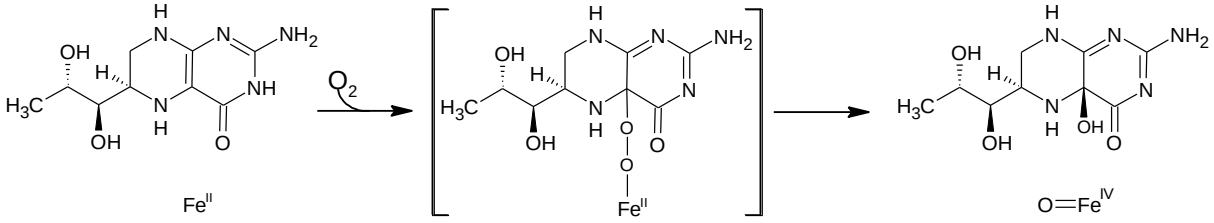

Figure 5.2. Scheme illustrating the reaction of Fe^{II}, O_2, and BH_4 to yield $Fe^{IV}O$ and 4a-hydroxy-BH_4 through a Fe^{II}-peroxypterin intermediate.

In the second half of the reaction, the electrophilic $Fe^{IV}O$ intermediate undergoes a nucleophilic attack from the aromatic ring of tryptophan which results in formation of a C-O bond, Figure 5.3.[188] The aromaticity of the ring is restored by a 1,2-hydride shift followed by a loss of a hydrogen to yield 5-HTP.[186]

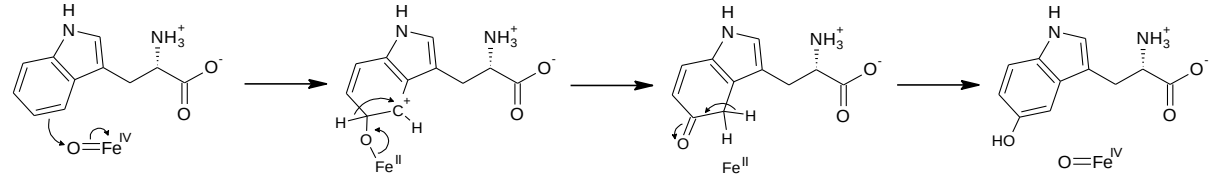

Figure 5.3. Scheme illustrating the mechanism by which tryptophan is hydroxylated by the $Fe^{IV}O$ intermediate.

5.2 Stopped-flow absorbance spectroscopy

Stopped-flow absorbance spectroscopy is a useful method to investigate the kinetics of a reaction in a timescale of milliseconds to seconds.[194] In this time range, detailed information of a reaction pathway can be obtained. If e.g. a reaction intermediate has unique spectral properties, its formation and decay can be monitored providing time-resolved information on the reaction.

In stopped-flow absorbance spectroscopy, two reactants are expelled from a set of syringes into a mixer where the reaction is initiated. This reaction mixture is rapidly transferred into an observation cell which is irradiated with a light source. The absorption of the mixture in the observation cell is measured as a function of time by an absorbance detector, e.g. photodiode array detector, Figure 5.4.[195]

The data produced in a stopped-flow experiment comprise progress curves of the monitored molecular processes. The analysis of such progress curves for a reaction can yield rate constants of the molecular processes. Under pseudo-first-order conditions (the monitored reactant is in great excess over the other reactant) the kinetic traces can be fitted to an exponential function or a sum of exponential functions, and the

observed rate constant(s), k_{obs}, can be determined. The rate constant can then be obtained from the slope of the linear plot of k_{obs} versus ligand concentration.[195]

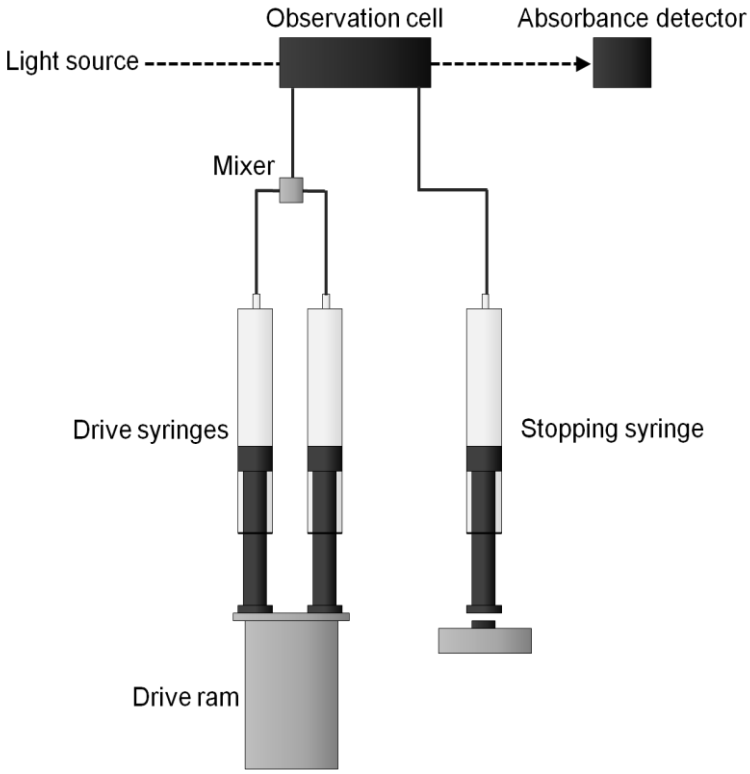

Figure 5.4. Schematic diagram of a stopped-flow absorbance spectroscopy setup.

5.3 Stopped-flow kinetics of the AAAHs

The reaction mechanisms of TH, PAH, and TPH1 have been investigated utilizing stopped-flow absorbance spectroscopy. In most studies, the ternary complex, E•Fe^{II}•pterin•substrate, is mixed under single-turnover conditions with an O_2 solution to initiate the reaction. The reaction is then followed by continuously measuring the absorbance at various wavelengths as the reactants and intermediates have distinctive absorbance spectra.

Utilizing stopped-flow kinetic experiments, the reaction of *rat* TH was fit to a model comprising the consecutive steps; reversible binding of O_2, formation of 4a-hydroxy-6MePH_3 (6MePH_4 is a BH_4 analogue), formation of DOPA from tyrosine, and dehydration of 4a-hydroxy-6MePH_3 to q-6MePH_2.[196] Another study on *rat* TH supported this model and furthermore found that k_{cat} depends on the viscosity of the medium, suggesting that product release is the rate-limiting step in the reaction.[197]

In a stopped-flow kinetic study of *rabbit* cTPH1, it was found that the first events in the reaction upon mixing TPH•Fe^{II}•6-MePH_4•tryptophan with oxygen were reversible O_2 binding, followed by the formation of a transient intermediate with maximal absorbance at 420 nm.[193] Furthermore, the rate of decay of the intermediate matched the rate of formation of 4a-hydroxy-6-MePH_4, suggesting that the intermediate precedes formation of $Fe^{IV}O$. A rapid-quench technique was used to determine the rate of 5-hydroxytryptophan (5-HTP) formation. Formation of 5-HTP comprised a burst-phase followed by slow steady-state phase which is presumably limited by the rate of product release.

Evidence of such an intermediate is supported by a study of *rat* PAH.[198] Here, stopped-flow kinetics was used to monitor binding events prior to formation of the ternary complex. This was achieved by monitoring absorption changes at different combinations of PAH, BH_4, and phenylalanine in the absence of O_2. It was found that the first steps in the reaction are binding of BH_4, followed by phenylalanine and then reversible binding of O_2. In a similar study of bacterial PAH, the reaction mechanism was found to be initiated by random binding order of pterin and phenylalanine, favored by pterin binding first, followed by binding of O_2.[199]

5.4 Experimental procedure

The TPH samples for the stopped-flow experiments were prepared anaerobic in a glovebox. The concentration of the TPH sample was determined by UV-vis absorption with ε_{280} = 39310 M^{-1} cm^{-1}. The sample was added two equivalents of freshly prepared sodium dithionite to reduce the active site iron. The dithionite was removed by buffer exchange using centrifugation with 10 kDa filters. After buffer exchange, the protein concentration was determined and diluted to the desired concentration with a buffer solution comprising 150 mM HEPES/NaOH, 100 mM $(NH_4)_2SO_4$, 20 w/v% sucrose, pH 7.0.

Stopped-flow experiments were conducted using an Applied Photophysics SX20 stopped-flow absorption spectrophotometer (~2 ms dead time and cell path length of 1 cm) equipped with a Hg/Xe Arc lamp and outfitted with PEEK tubing. The temperature was maintained at 4 °C using a water temperature bath (Fisher Scientific Isotemp 3016). The experiments were performed in an anaerobic glovebox. Both drive syringes of the stopped-flow instrument were degassed with 50 mM sodium dithionite for ~2 h and washed with anaerobic water and buffer solution.

To the anaerobic protein samples, tryptophan and BH_4 were added in concentrations corresponding to 0.95 mole equivalents. The O_2-solutions were prepared by mixing an O_2-saturated buffer solution with an anaerobic buffer solution. The O_2 saturated solution (~2 mM) was prepared by sparging a buffer solution with O_2 in an ice bath for >30 min. The ternary complex (125 µM) was loaded into one drive syringe and a buffer solution with a desired O_2 concentration was loaded into the other. The absorption was monitored with a photodiode array detector.

5.5 Stopped-flow kinetic results – c*h*TPH2

Stopped-flow kinetic experiments were conducted on c*h*TPH2 in pursuit of a reaction intermediate preceding formation of 4a-hydroxy-BH_4. The initial results from this experiment revealed that a transient species with a strong absorption peak with maximum at 442 nm was formed, Figure 5.5 A and B. BH_4 and 4a-hydroxy-BH_4 do not have any absorbance peaks in the range of > 440 nm.[200] Hence, at wavelengths greater than 440 nm the spectral changes of these species do not interfere with the spectrum of the intermediate. The time-resolved spectrum in Figure 5.5 C provides a clear evidence for the formation and decay of an intermediate.

To investigate the O_2-dependence of the rates of formation and decay of the intermediate, the stopped-flow experiment was repeated with different concentrations of oxygen, Figure 5.6 A. The O_2 concentration was varied from 16 to 500 µM (0.25 to 8 mole equivalents). At all O_2 concentrations, the change in absorbance at 442 nm as a function of time is biexponential. The time traces in Figure 5.6 A were therefore fitted with eq. 1;

$$A_t = A_1 e^{-k_{1,obs}t} + A_2 e^{-k_{2,obs}t} \qquad \text{(eq. 1)}$$

where A_t is absorbance at a given time, A_i (i=1,2) is the amplitude of the phase, and $k_{i,obs}$ (i=1,2) is the observed rate constant of the phase at a given O_2 concentration. Figure 5.6 A shows that eq. 1 fits very well to the kinetic data, except for the absorbance trace at 500 µM O_2 which deviates at around 1 sec. From the fits, $k_{1,obs}$ and $k_{2,obs}$ values were extracted at the various O_2 concentrations and plotted in Figure 5.6 B.

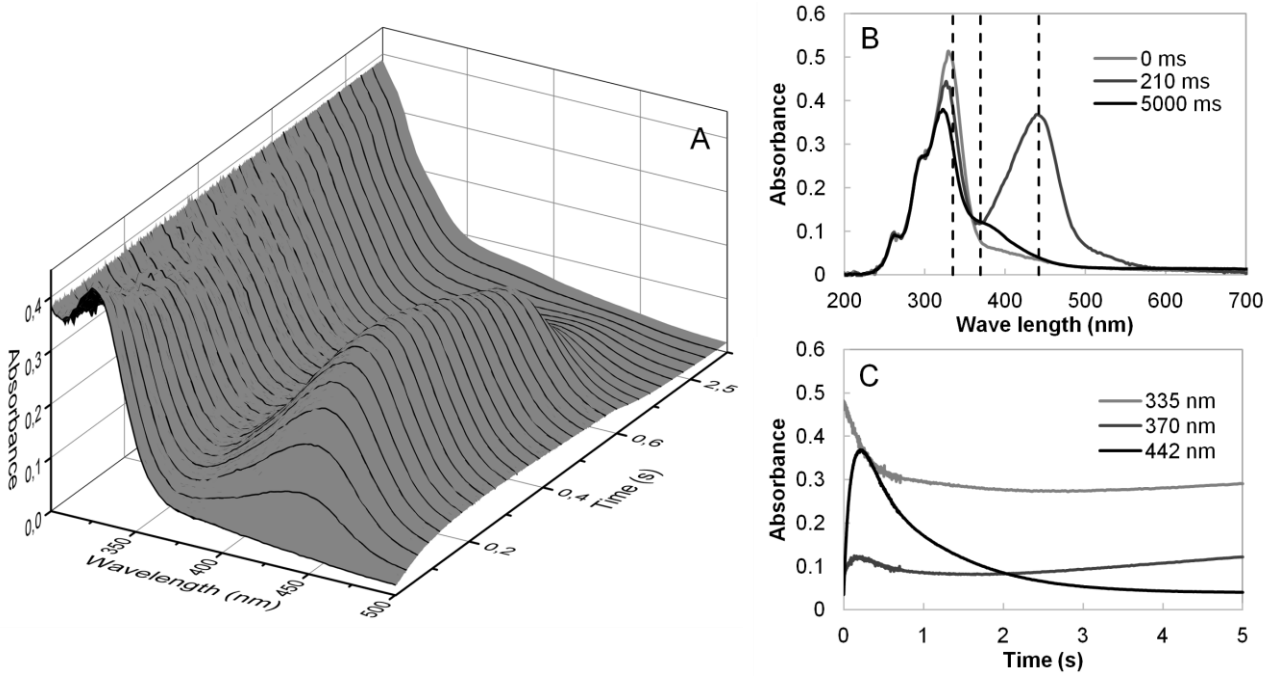

Figure 5.5. Stopped-flow kinetic results of 125 µM c*h*TPH2 in 150 mM HEPES/NaOH, 100 mM $(NH_4)_2SO_4$, 20 w/v%, pH 7.0. In the assay the concentrations of Trp, BH4, and O_2 were 120, 120, and 250 µM, respectively. A: 3D plot of raw data acquired from a single experiment. B: Replot of data in A at only three time values. Dashed lines represent chosen wavelengths where significant changes in the spectra were observed. C: Time traces of the selected wavelengths in B.

To obtain the actual rate constants, the data in Figure 5.6 B was fitted with eq. 2 and eq. 3.[198,201,202] Eq. 2 describes a direct correlation between the observed rate constants and the concentration of O_2, which corresponds to a simple second-order reaction where k_1 and k_{-1} are rate constants of the forward and reverse reactions, respectively. Eq. 3 describes a rapid initial binding event, which does not induce a change in absorption, followed by a reaction, where k_1, k_{-1}, and K_d are the rate constants of the forward and reverse reactions and the dissociation constant, respectively.

$$k_{\mathrm{obs}} = k_1[\mathrm{O_2}] + k_{-1} \qquad \text{(eq. 2)}$$

$$k_{\mathrm{obs}} = k_{-1} + \frac{k_1[\mathrm{O_2}]}{K_\mathrm{d} + [\mathrm{O_2}]} \qquad \text{(eq. 3)}$$

Fitting the $k_{1,obs}$–values (closed circles) of intermediate formation with eq. 3 resulted in a significantly better fit compared to eq. 2 ($p < 0.05$, F-test). The fit resulted in k_1 and k_{-1} values of 17.1 $M^{-1}s^{-1}$ and 7.5 s^{-1}, respectively, and a K_d-value of 0.4 mM. This implies that the steps in the formation of the intermediate are reversible O_2 binding followed by a reaction between O_2 and presumably BH_4 and Fe^{II}.

The observed rate constants of the decay of the intermediate, k_{2obs}, showed a linear dependence on the O_2 concentration, Figure 5.6 B (open circles). The linear relation suggests that the decay of the intermediate occur via a simple second-order reaction. By fitting with eq. 2, k_2 and k_{-2}-values of 4.0 $M^{-1}s^{-1}$ and 0.65 s^{-1} were obtained, respectively.

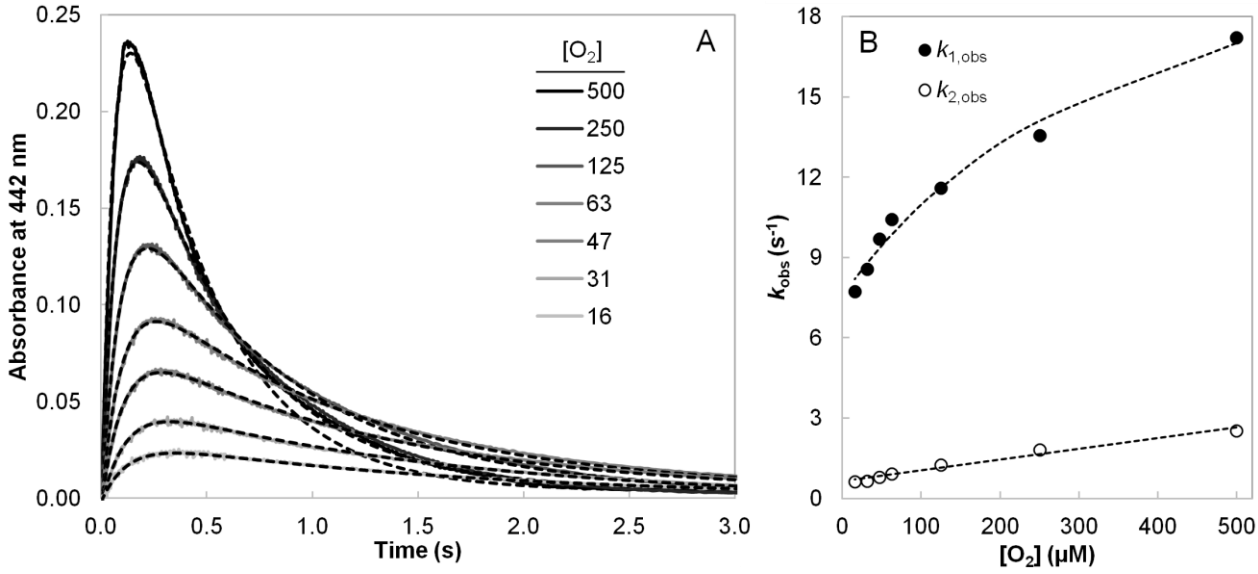

Figure 5.6. Stopped-flow traces showing the formation of an intermediate in the reaction of c*h*TPH2. A: Baseline subtracted kinetic traces measured at 442 nm at different O_2 concentrations. B: Rate constants derived with eq. 1, for the two phases at the various O_2 concentrations. The measurements were conducted at 62.5 µM c*h*TPH2, 60 µM tryptophan, and 60 µM BH_4 in 150 mM HEPES/NaOH, 100 mM $(NH_4)_2SO_4$, 20 w/v%, pH 7.0.

5.6 Discussion

The reaction mechanisms of the AAAHs have been studied extensively. Despite great efforts, the first half of the reaction mechanism involving formation of $Fe^{IV}O$ remains elusive. A reaction intermediate which precedes the formation of the observable 4a-hydroxy-BH_4 has been proposed in several studies.[183,187] The first evidence of such an intermediate was presented by Pavon *et al.*[193] This species displayed a maximum absorbance at 420 nm and an extinction coefficient of only 220 M^{-1} cm^{-1} at this wavelength. The identity of this species is undetermined but Fe-peroxy-6-MePH_4 is a plausible candidate.

In the present study, the presence of a transient species with a strong absorption feature at ~440 nm was identified. BH_4, 4a-hydroxy-BH_4, and q-BH_2 do not have any absorption features above ~400 nm.[200,203] This strongly suggests that the observed transient species is a reaction intermediate preceding the formation of 4a-hydroxy-BH_4 and hence also $Fe^{IV}O$.

The fit of the hyperbolic saturation curve observed for the rate constants of formation suggests that the reaction of the intermediate consists of an O_2 binding step followed by reaction of O_2 with presumably Fe^{II} and BH_4. This observation is in agreement with the proposed reaction mechanism of *rabbit* TPH1, *rat* TH, and PAH from *rat* and *chromobacterium violaceum*.[183,193,197,199]

In the current study, very high yield of the intermediate was obtained. A change in absorption monitored at 442 nm was measured to as much as ~0.4 absorption units during the reaction. This is ~40-fold greater than the change in absorbance observed in the study by Pavon *et al* [193], which suggests that significantly higher yield was obtained under the conditions chosen in this current study. The difference in absorption and probably yield might be explained by choice of e.g. TPH variant and co-substrate. In the current study, c*h*TPH2 was investigated together with the natural co-substrate BH_4. In the study by Pavon *et al*. [193], *rabbit* cTPH1 was used together with the co-substrate analogue 6-MePH_4.

The identity of the intermediate is still undetermined but Fe^{II}-peroxy-BH_4 is a likely candidate. The high yield obtained in this study enables isolation of the intermediate by rapid freeze-quench techniques. By isolating the intermediate, its identity can conclusively be determined by e.g. raman spectroscopy.

5.7 Conclusion

The reaction mechanisms of especially PAH and TH have been studied extensively, and consensus it that a transient species if formed prior to formation of 4a-hydroxy-BH_4. This transient species is hypothesized to be Fe^{II}-peroxy-BH_4, however, this has never been verified experimentally. In this chapter, it was demonstrated that under the chosen conditions for c*h*TPH2, the transient intermediate is formed in quantities sufficient for characterization by e.g. raman spectroscopy. The identity of the intermediate is still undetermined. However, the presented results promote future identification of the intermediate.

5.8 References

[183] Roberts K. M. and Fitzpatrick, P. F., 2013, Mechanisms of tryptophan and tyrosine hydroxylase, *IUBMB Life 65(4)*, 350-357.

[184] Lazarus, R. A., Dietrich, R. F., Wallick, D. E., and Benkovic, S. J., 1981, On the mechanism of action of phenylalanine hydroxylase, *Biochemistry 20(24)*, 6834-6841.

[185] Dix, T. A., Kuhn, D. M., and Benkovic, S. J., 1987, Mechanism of oxygen activation by tyrosine hydroxylase, *Biochemistry 26(12)*, 3354-3361.

[186] Moran, G. R., Derecskei-Kovacs, A., Hillas, P. J., and Fitzpatrick, P. F., 2000, On the Catalytic Mechanism of Tryptophan Hydroxylase, *J. Am. Chem. Soc. 122(19)*, 4535–4541.

[187] Fitzpatrick, P. F., 2003, Mechanism of Aromatic Amino Acid Hydroxylation, *Biochemistry 42(48)*, 14083–14091.

[188] Eser, B. E., Barr, E. W., Frantom, P. A., Saleh, L., Bollinger, J. M. Jr, Krebs, C., and Fitzpatrick, P. F., 2007, Direct spectroscopic evidence for a high-spin Fe(IV) intermediate in tyrosine hydroxylase, *J. Am. Chem. Soc. 129(37)*, 11334-11335.

[189] Panay, A. J., Lee, M., Krebs, C., Bollinger Jr, J. M., and Fitzpatrick, P. F., 2011, Evidence for a High Spin Fe(IV) Species in the Catalytic Cycle of a Bacterial Phenylalanine Hydroxylase, *Biochemistry 50(11)*, 1928–1933.

[190] Dix, T. A., Bollag, G. E., Domanico, P. L., and Benkovic, S. J., 1985, Phenylalanine hydroxylase: absolute configuration and source of oxygen of the 4a-hydroxytetrahydropterin species, *Biochemistry 24(12)*, 2955-2958.

[191] Davis, M. D. and Kaufman, S., 1989, Evidence for the formation of the 4a-carbinolamine during the tyrosine-dependent oxidation of tetrahydrobiopterin by rat liver phenylalanine hydroxylase, *J. Biol. Chem. 264(15)*, 8585-8596.

[192] Davis, M. D. and Kaufman, S., 1991, Studies on the partially uncoupled oxidation of tetrahydropterins by phenylalanine hydroxylase, *Neurochem. Res. 16(7)*, 813-819.

[193] Pavon, J. A., Eser, B., Huynh, M. T., and Fitzpatrick, P. F., 2010, Single turnover kinetics of tryptophan hydroxylase: evidence for a new intermediate in the reaction of the aromatic amino acid hydroxylases, *Biochemistry 49(35)*, 7563-7571.

[194] Connors, K. A., 1990, Chapter 4 - Fast Reasction, in Chemical kinetics: the study of reaction rates in solution, Wiley VCH, New York, N.Y, USA.

[195] Wang, R.-Y., 2013, Rapid Scan, Stopped-Flow Kinetics, in Applications of Physical Methods to Inorganic and Bioinorganic Chemistry, 1 ed, edited by R. A. Scott and C. M. Lukehart, Wiley-Blackwell, New York, N.Y, USA.

[196] Chow, M. S., Eser, B. E., Wilson, S. A., Hodgson, K. O., Hedman, B., Fitzpatrick, P. F., and Solomon, E. I., 2009, Spectroscopy and kinetics of wild-type and mutant tyrosine hydroxylase: mechanistic insight into O2 activation, *J. Am. Chem. Soc. 131(22)*, 7685-7698.

[197] Eser, B. E. and Fitzpatrick, P. F., 2010, Measurement of Intrinsic Rate Constants in the Tyrosine Hydroxylase Reaction, *Biochemistry 49 (3)*, 645–652.

[198] Roberts, K. M., Pavon, J. A., and Fitzpatrick, P.F., 2013, Kinetic mechanism of phenylalanine hydroxylase: intrinsic binding and rate constants from single-turnover experiments, *Biochemistry 52(6)*, 1062-1073.

[199] Subedi, B. P. and Fitzpatrick, P. F., 2016, Kinetic Mechanism and Intrinsic Rate Constants for the Reaction of a Bacterial Phenylalanine Hydroxylase, *Biochemistry 55 (49)*, 6848–6857.

[200] Moran, G. R., Daubner, S. C., and Fitzpatrick, P. F., 1998, Expression and Characterization of the Catalytic Core of Tryptophan Hydroxylase, *J. Biol. Chem. 273(20)*, 12259-12266.

[201] Frantom, P. A., Seravalli, J., Ragsdale, S. W., and Fitzpatrick, P. F., 2006, Reduction and Oxidation of the Active Site Iron in Tyrosine Hydroxylase: Kinetics and Specificity, *Biochemistry 45(7)*, 2372–2379.

[202] Nakatani, H. and Hiromi, K., 1980, Analysis of signal amplitude in stopped-flow method for enzyme-ligand systems, *J. Biochem. 87(6)*, 1805-1810.

[203] Moran, G. R. and Fitzpatrick, P. F., 1999, A Contentious Fluorescence Assay for Tryptophan Hydroxylase, *Anal. Biochem. 266*, 148-152.

Chapter 6

Steady-state kinetic mechanism

Enzyme kinetics is a fundamental part of enzymology and deals with the rates of enzyme catalyzed reactions. In enzyme kinetics, it is possible to deduce a kinetic mechanism of the reaction by measuring the initial reaction velocities at variable substrate and product concentrations. The kinetic mechanism is the order of which substrates bind the enzyme and products leave the enzyme. Knowing the mechanism of an enzyme gives great insight into how it works and helps to predict how the enzyme behaves and is controlled in living organisms.

In this chapter, general enzyme kinetics is discussed and more advanced kinetic mechanisms and velocity equations are presented. The activity assay for determining initial rates of TPH is introduced and the experimental procedure is presented. Steady-state kinetic data for c*h*TPH1 is presented and kinetic models are fitted to the observed data and discussed in detail. Some of the results presented in this chapter have been included in a submitted manuscript. (Appendix A.2)

Outline

6.1 Kinetic analysis

The simplest kinetic model of an enzyme catalyzed reaction involving a single substrate may be represented by the mechanism:

$$E + S \underset{k_{-1}}{\overset{k_1}{\rightleftharpoons}} ES \xrightarrow{k_2} E + P$$

This model can be analyzed with the Michaelis-Menten equation (eq. 1) which is applicable under steady-state conditions.[204] Here, v_0 is initial velocity, [S] is the initial substrate concentration, V_{max} is velocity at saturated [S], K_m is a constant that describe the substrate concentration as which the reaction rate is half of V_{max}.

$$v_0 = \frac{V_{\max}[S]}{K_m + [S]} \qquad \text{(eq. 1)}$$

$$v_0 = \frac{V_{\max}[\mathrm{S}]}{K_{\mathrm{m}} + [\mathrm{S}] + \frac{[\mathrm{S}]^2}{K_{\mathrm{i}}}} \qquad \text{(eq. 2)}$$

Steady-state is reached when the ES complex is formed and decomposed at the same rate and occurs shortly after mixing enzyme and substrate, and constitutes the time interval when the rate of reaction is constant with time. If the concentration of S is much greater than E, the concentration of free S will be approximately equal to the total substrate added. Hence during the time period of the measurement, the concentration of the ES complex is approximately constant. As the initial rate is measured, the reverse reaction of product formation can be ignored.[205] At a fixed low concentration of enzyme, a series of experiments in which only [S] is varied can be conducted. Under these conditions, the initial reaction velocity will increase until it reaches a substrate independent velocity. From this type of data, V_{max} and K_m can be determined by fitting eq. 1 to the rate as a function of [S]. In cases where S binds an unproductive form of the enzyme, substrate inhibition will be apparent. If substrate inhibition occurs at elevated concentration of S, eq. 2 can be utilized, where K_i is the substrate inhibition constant.[206] The values of V_{max}, K_m, and K_i will be apparent values in the case of multi-substrate enzymes.

6.1.1 Multi-substrate reactions

In multi-substrate enzymes, V_{max} and K_m can only be determined if saturation is reached for all substrates. This is often not possible and apparent values are determined instead. These values will depend on the concentration of the fixed substrates. When multiple substrates are involved in a reaction, more complicated mechanisms will apply. In cases where binding and dissociation of the substrates occur very rapidly compared to the catalytic step, the reaction is said to follow a rapid equilibrium mechanism.[207] Here, dissociation constants can be obtained. If the catalytic step is not rate limiting, a steady-state reaction, where all enzyme species reach a steady-state concentrations, is observed. Here Michaelis constants are obtained rather than dissociation constants. A steady-state reaction can either follow a sequential or a Ping Pong mechanism. In a sequential mechanism, all substrates must bind to the enzyme before any product is released. In a sequential mechanism substrates can either bind in an ordered or random fashion. If a product is released between the additions of two substrates, the mechanism is defined as a Ping Pong mechanism.[208]

TPH catalyses a ter bi reaction as it uses three substrates, BH_4, O_2, and Trp, to produce two products, 4a-hydroxy-BH_4, and HO-Trp. Discrimination between enzymatic mechanisms with three substrates can occur through graphical methods. In the method described by Viola and Cleland [209], one substrate is held at saturation (>100K_m) while the other substrates are varied. Alternatively, each substrate can be varied separately at fixed concentrations of the other two substrates maintained at a constant concentration ratio.[210] The obtained data can govern mechanistic information based on graphical appearance. However, kinetic parameters should be determined with great caution from these double reciprocal plots (Lineweaver-Burk plots) because the data points will be weighted differently.[211] The parameters are more accurately determined by fitting an appropriate velocity equation to the measured initial velocities using non-linear regression.

In this study, the concentration of O_2 was not varied, and the reaction catalyzed by TPH is therefore treated as a bi bi reaction. In the following, some common bi bi reactions will be described and illustrated using Cleland nomenclature [212], where A and B represent substrates, P and Q represent products, k_x are rate constants, K_A and K_B are dissociation constants for A and B, and $K_{m,A}$ and $K_{m,B}$ represent Michaelis constants for A and B. As TPH1 exhibits substrate tryptophan inhibition, substrate inhibition in the following mechanisms will also be considered.

6.1.2 Kinetic mechanisms

6.1.2.1 Sequential mechanisms

If A and B bind in an obligatory order before products P and Q are formed, the reaction follows an *ordered bi bi mechanism*, illustrated in Scheme 1. In the absence of products, the velocity equation is given as eq. 3.[208] K_A is the dissociation constant of A to free enzyme (k_{-1}/k_1).

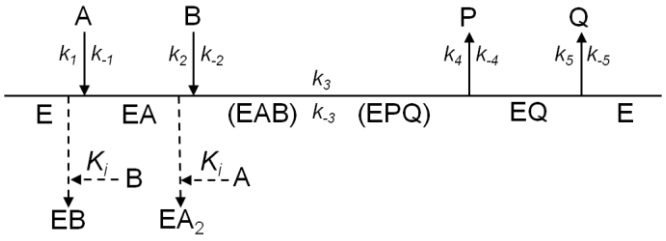

Scheme 1

If K_A is not much smaller that $K_{m,A}$ the slopes of the double reciprocal plots of *v* versus the concentration of varied substrate will increase linearly with decreasing concentration of the fixed substrate. In cases where $K_A << K_{m,A}$, the slopes of the plots will appear parallel.

$$v = \frac{V_{\max}[\mathrm{A}][\mathrm{B}]}{K_\mathrm{A}K_{\mathrm{m,B}} + K_{\mathrm{m,A}}[\mathrm{B}] + K_{\mathrm{m,B}}[\mathrm{A}] + [\mathrm{A}][\mathrm{B}]} \qquad \text{(eq. 3)}$$

Two different competitive substrate inhibition mechanisms can occur in ordered bi bi mechanisms; formation of a dead-end EB complex or a dead-end EA_2 complex (dotted arrows in Scheme 1). In the former, B bind free enzyme to form a dead-end complex, while in the latter two molecules of A bind the enzyme to form a dead-end complex. In the presence of a dead-end inhibitor, the velocity equation is modified by multiplying the factor $(1+[\mathrm{I}]/K_\mathrm{i})$ with the terms in the denominator representing the enzyme form which combines with the inhibitor.[208] In the presence of substrate inhibition, the velocity equations will take the form of eq. 4 and eq. 5 for EB and EA_2, respectively.[208]

$$v = \frac{V_{\max}[\mathrm{A}][\mathrm{B}]}{K_\mathrm{A}K_{\mathrm{m,B}}\left(1+\frac{[\mathrm{B}]}{K_\mathrm{i}}\right) + K_{\mathrm{m,A}}[\mathrm{B}]\left(1+\frac{[\mathrm{B}]}{K_\mathrm{i}}\right) + K_{\mathrm{m,B}}[\mathrm{A}] + [\mathrm{A}][\mathrm{B}]} \qquad \text{(eq. 4)}$$

$$v = \frac{V_{\max}[\mathrm{A}][\mathrm{B}]}{K_\mathrm{A}K_{\mathrm{m,B}} + K_{\mathrm{m,A}}[\mathrm{B}] + K_{\mathrm{m,B}}[\mathrm{A}]\left(1+\frac{[\mathrm{A}]}{K_\mathrm{i}}\right) + [\mathrm{A}][\mathrm{B}]} \qquad \text{(eq. 5)}$$

In the case of EB dead-end formation, the double reciprocal *v* versus [A] plots will be linear at all concentrations of B. The slopes will be affected by the concentration of B; with increasing concentration the slope will decrease, pass through a minimum, and then start to increase as substrate inhibition becomes more pronounced (Figure 6.1 a). The slope of the plots is described by eq. 6.[208]

$$slope_{1/[\mathrm{A}]} = \frac{K_{\mathrm{m,A}}}{V_{\max}K_\mathrm{i}}[\mathrm{B}] + \frac{K_\mathrm{A}K_{\mathrm{m,B}}}{V_{\max}}[\mathrm{B}]^{-1} + \frac{K_{\mathrm{m,A}}}{V_{\max}}\left(1+\frac{K_\mathrm{A}K_{\mathrm{m,B}}}{K_{\mathrm{m,A}}K_\mathrm{i}}\right) \qquad \text{(eq. 6)}$$

The inhibition by B is obvious from the 1/*v* versus 1/[B] plot, which will pass through a minimum and then curve up as they approach the 1/*v*-axis (Figure 6.1 b). At low concentrations of A, these plots will appear linear only at high values of 1/[B]. With saturating concentrations of A, the inhibition is overcome and the

plots are linear. The slopes of these plots will decrease with increasing [A]. Similar plots will occur in the case of EA_2 complex formation.

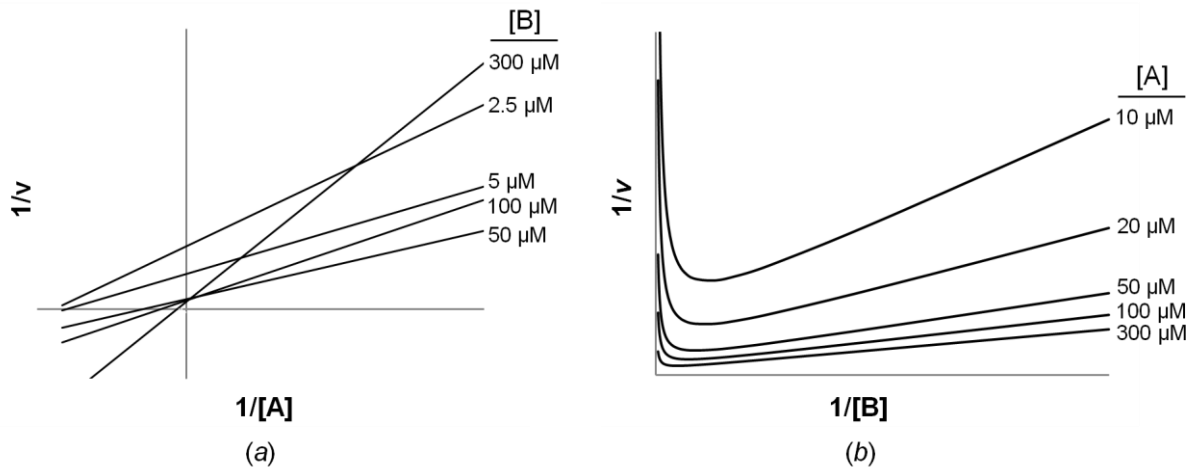

Figure 6.1. Theoretical plots illustrating substrate inhibition by B in an ordered sequential bi bi mechanism (V_{max} = 200, $K_{m,A}$ = 20, $K_{m,B}$ = 50, K_i = 20, K_A = 50). (*a*) Double reciprocal plot of *v* versus [A] at different concentrations of B. (*b*) Double reciprocal plot of *v* versus [B] at different concentrations of A.

6.1.2.2 Ping Pong mechanism

If a product is released between binding of A and B, the mechanism is called Ping Pong. The *Ping Pong mechanism* is illustrated in Scheme 2, where F is modified enzyme (i.e. covalently modified by accepting a molecule from substrate A). This type of mechanism is common in group transfer reactions, where the enzyme is covalently modified. In the absence of products, the velocity equation is given as eq. 7.[208]

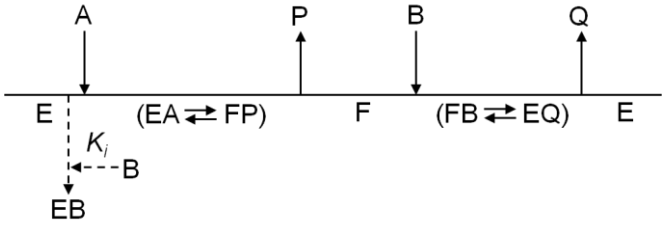

Scheme 2

If the enzyme follows a Ping Pong mechanism, the double reciprocal plots of *v* versus [A] or [B] will be linear, and with increasing concentration of the fixed substrate the plots will be parallel shifted to lower 1/*v* intercept until $1/V_{max}$ is reached. The properties that account for the parallel plots are, however, not always the formation of a covalent enzyme intermediate, but might be the occurrence of a kinetically irreversible step between binding of the substrates.[213]

$$v = \frac{V_{\max}[\mathrm{A}][\mathrm{B}]}{K_{\mathrm{m,A}}[\mathrm{B}] + K_{\mathrm{m,B}}[\mathrm{A}] + [\mathrm{A}][\mathrm{B}]} \qquad \text{(eq. 7)}$$

$$v = \frac{V_{\max}[\mathrm{A}][\mathrm{B}]}{K_{\mathrm{m,A}}[\mathrm{B}]\left(1 + \frac{[\mathrm{B}]}{K_{\mathrm{i}}}\right) + K_{\mathrm{m,B}}[\mathrm{A}] + [\mathrm{A}][\mathrm{B}]} \qquad \text{(eq. 8)}$$

Competitive substrate inhibition can occur in a Ping Pong mechanism if B can bind F as well as E, see dotted arrow in Scheme 2. This will result in the modified velocity eq. 8.[208] At low concentrations of B, the 1/*v* versus 1/[A] plots will appear parallel as usual. As the fixed concentrations of B increases, the slope of the plots will increase linearly and the 1/v-axis intercept will decrease to the limit of $1/V_{max}$, Figure 6.2 a.

Opposed to a sequential mechanism, the secondary plot of slope$_{1/A}$ versus 1/[B] will be linear. The 1/*v* versus 1/[B] plots will appear parallel at high 1/[B] values but pass through a minimum and increase as they approach the 1/*v*-axis.

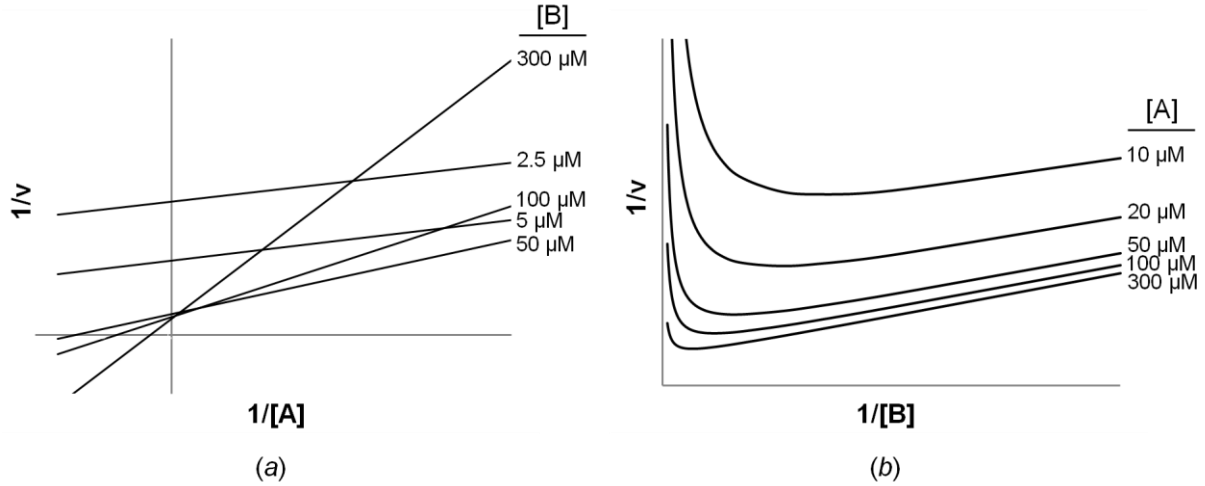

Figure 6.2. Theoretical plots illustrating substrate inhibition by B in a Ping Pong bi bi mechanism (V_{max} = 200, $K_{m,A}$ = 20, $K_{m,B}$ = 50, K_i = 20). (*a*) Double reciprocal plot of *v* versus [A] at different concentrations of B. (*b*) Double reciprocal plot of *v* versus [B] at different concentrations of A.

6.1.2.3 Rapid equilibrium random mechanism

If A and B bind in random order and the catalytic step is rate limiting, the system can be described as a *rapid equilibrium random bireactant system,* as illustrated in Scheme 3.

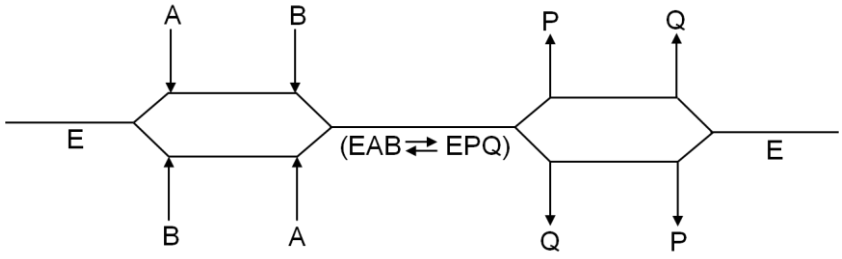

Scheme 3

The velocity equation, derived under rapid equilibrium assumptions, is given as eq. 9.[214] K_{iA} and K_A are the dissociation constant of A to free enzyme and EB complex, respectively. The slopes of the double reciprocal plots of *v* versus the concentration of varied substrate will increase linearly with decreasing concentration of the fixed substrate.

$$v = \frac{V_{\max}[\mathrm{A}][\mathrm{B}]}{K_{\mathrm{iA}}K_{\mathrm{B}} + K_{\mathrm{A}}[\mathrm{B}] + K_{\mathrm{B}}[\mathrm{A}] + [\mathrm{A}][\mathrm{B}]} \qquad \text{(eq. 9)}$$

$$v_{\mathrm{i}} = \frac{V_{\max}[\mathrm{A}][\mathrm{B}]}{K_{\mathrm{iA}}K_{\mathrm{B}}\left(1 + \frac{[\mathrm{B}]}{K_{\mathrm{i}}}\right) + K_{\mathrm{A}}[\mathrm{B}]\left(1 + \frac{[\mathrm{B}]}{\alpha K_{\mathrm{i}}}\right) + K_{\mathrm{B}}[\mathrm{A}] + [\mathrm{A}][\mathrm{B}]} \qquad \text{(eq. 10)}$$

If one substrate has affinity for the binding site of the other substrate, dead-end BE or BEB complexes can form. In this case, the velocity equation will take the form of eq. 10, where α is a factor describing the change in dissociation constant for binding of the second B, and K_i is the inhibition constant of B binding in A's site. In the case of inhibition, the slopes in a 1/*v* versus 1/[A] plot will decrease with increasing concentrations of

[B] but eventually start to increase, and the 1/*v* versus 1/[B] will pass through a minimum and then curve up as it approaches the 1/*v*-axis, similarly to an ordered sequential mechanism in Figure 6.1.

6.1.2.4 Hybrid Ping Pong-ordered mechanism

In special cases, hybrids of a Ping Pong bi bi mechanism and an ordered or sequential mechanism can occur. Steady-state kinetic data obtained for c*h*TPH1 suggest such a case, and a *hybrid Ping Pong-ordered mechanism* is therefore presented. In such a mechanism, A can bind in an ordered fashion and participate in a Ping Pong mechanism by donating a group to E. Alternatively, B can bind EA and the reaction will occur through a sequential mechanism, see Scheme 4. In the sequential mechanism the group can be passed from A to B directly or it can be passed from A to E and then from E to B.[208]

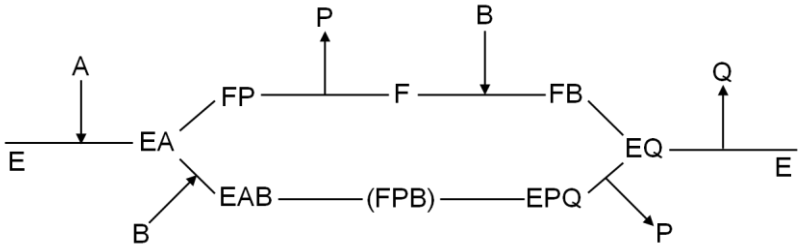

Scheme 4

A reaction mechanism similar to the one in Scheme 4, has been proposed by Mannervik [215,216]. Here the velocity eq. 11 was proposed, where V_1, V_2, and K_3 and K_4 are constants. In the total sequence, A adds once while B adds twice and the velocity equation thus contains the $[B]^2$ terms. When the concentration of B is low, the $[B]^2$ terms can be neglected and the equation will degenerate to the velocity equation of a Ping Pong mechanism (eq. 7).

$$v = \frac{V_1[\mathrm{A}][\mathrm{B}] + V_2[\mathrm{A}][\mathrm{B}]^2}{K_{\mathrm{m,A}}[\mathrm{B}] + K_{\mathrm{m,B}}[\mathrm{A}] + [\mathrm{A}][\mathrm{B}] + K_3[\mathrm{B}]^2 + K_4[\mathrm{A}][\mathrm{B}]^2} \qquad \text{(eq. 11)}$$

When competitive substrate inhibition, by binding of a second molecule of A (dead-end EA_2 complex), is observed the velocity equation is modified to eq. 12.[217]

$$v = \frac{V_1[\mathrm{A}][\mathrm{B}] + V_2[\mathrm{A}][\mathrm{B}]^2}{K_{\mathrm{m,A}}[\mathrm{B}] + K_{\mathrm{m,B}}[\mathrm{A}]\left(1 + \frac{[\mathrm{A}]}{K_{\mathrm{i}}}\right) + [\mathrm{A}][\mathrm{B}] + K_3[\mathrm{B}]^2 + K_4[\mathrm{A}][\mathrm{B}]^2} \qquad \text{(eq. 12)}$$

Alternatively, competitive substrate inhibition can occur through formation of a dead-end EB complex. The velocity equation for such a model is obtained by multiplying the terms in the denominator representing free enzyme with $(1+[B]/K_i)$.[218] By this operation eq. 11 is modified to eq. 13.

$$v = \frac{V_1[\mathrm{A}][\mathrm{B}] + V_2[\mathrm{A}][\mathrm{B}]^2}{K_{\mathrm{m,A}}[\mathrm{B}]\left(1 + \frac{[\mathrm{B}]}{K_{\mathrm{i}}}\right) + K_{\mathrm{m,B}}[\mathrm{A}] + [\mathrm{A}][\mathrm{B}] + K_3[\mathrm{B}]^2 + K_4[\mathrm{A}][\mathrm{B}]^2} \qquad \text{(eq. 13)}$$

In these hybrid mechanisms with substrate inhibition, the 1/*v* versus 1/[A] plots will appear parallel at high 1/[A] values but pass through a minimum and increase as they approach the 1/*v*-axis, Figure 6.3 b. Similar to a regular Ping Pong mechanism, the 1/*v* versus 1/[B] plots will appear parallel at low concentrations of A, but as the fixed concentrations of A increase the slope of the plots will increase and the 1/v-axis intercept will

decrease to the limit of $1/V_{max}$ (Figure 6.3 a). However, the difference is that at low values of 1/[B] the curves will deviate from linearity. This effect is more pronounced at low concentrations of A, Figure 6.3 a.

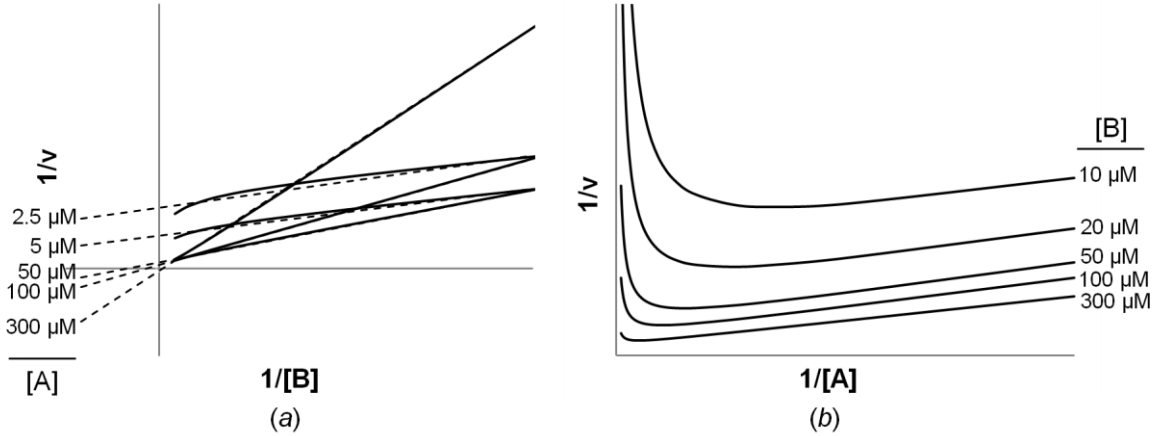

Figure 6.3. Theoretical plots illustrating substrate inhibition by A in a hybrid Ping Pong-ordered bi bi mechanism (V_{max} = 200, $K_{m,A}$ = 20, $K_{m,B}$ = 50, K_i = 50, K_3 = 0.05, K_4 = 0.001). (*a*) Double reciprocal plot of *v* versus [B] at different concentrations of A. (*b*) Double reciprocal plot of *v* versus [A] at different concentrations of B.

6.1.3 Statistical model comparison

To compare the fits of the kinetic models, an F-test was used.[219] This test accounts for the fact that it is easier to fit a complicated model with more parameters compared to a simple model. To determine if a more complicated model, despite the greater number of parameters, is statistically superior, the F-ratio is used. The F-ratio is defined as follows,

$$F = \frac{\frac{SS_{\text{null}} - SS_{\text{alt}}}{SS_{\text{alt}}}}{\frac{DF_{\text{null}} - DF_{\text{alt}}}{DF_{\text{alt}}}}$$

where SS_{null} and SS_{alt} are the sum of squares of deviation of the data points from the null hypothesis model and alternative model, respectively. DF_{null} and DF_{alt} are the degrees of freedom of the null hypothesis model and alternative model, respectively.The DF-values equal the number of data points minus the number of fitted parameters. From the F-ratio a *p*-value can be calculated.[219]

6.2 Steady-state kinetics of c*h*TPH1

In this following, the kinetic mechanism of c*h*TPH1 is investigated. The assay for determining TPH activity and the experimental procedure is presented. The present knowledge about the kinetic mechanism of the aromatic amino acid hydroxylases is outlined. The mechanistic insight is mainly based on studies on PAH and TH because a very limited amount of data has been published on TPH. Steady-state kinetic results of c*h*TPH1 will be presented, analyzed graphically and by non-linear regression, and discussed.

6.2.1 TPH assay

The activity of TPH was assayed by continuously monitoring the fluorescence of 5-hydroxytryptophan formed in the presence of substrates, as described by Moran and Fitzpatrick [220]. This assay is based on the different spectral characteristics of tryptophan and 5-hydroxytryptophan. The hydroxylation of tryptophan results in shift of the UV-absorbance transitions to longer wavelengths, Figure 6.4. At 300 nm the absorbance is almost exclusive for 5-hydroxytryptophan which makes excitation at this wavelength suitable

for monitoring product formation. The emission was monitored at 330 nm, as the emission maximum of 5-hydroxytryptophan is at 330 nm when excited at 300 nm.[220]

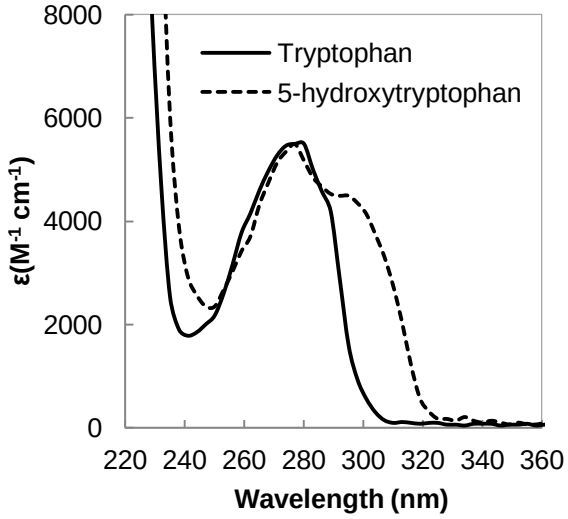

Figure 6.4. Absorbance spectra of tryptophan and 5-hydroxytryptophan measured in 10 mM HCl.

To stabilize TPH and to ensure continuous product formation, several components are added to the assay. TPH is only active when iron is in its ferrous form, and $(NH_4)_2Fe(II)(SO_4)_2{\cdot}6H_2O$ is therefore added in excess to insure that all TPH is loaded with Fe^{2+}. $(NH_4)_2SO_4$ has been found to stabilize TPH [221], hence additional $(NH_4)_2SO_4$ is added. Catalase is added to consume the H_2O_2 which is formed upon autooxidation of BH_4 to qBH_2. BH_4 has a high absorption at 300 nm and the fluorescence signal from 5-hydroxytryptophan is reduced by BH_4 attenuating the incoming light. A constant amount of BH_4 is therefore desirable, and the reducing agent dithiothreitol (DTT) is added to ensure a constant concentration of BH_4 throughout the assay. Furthermore, DTT maintains iron in its reduced form. Because of the concentration dependent reduction of the 5-hydroxytryptophan fluorescence signal caused by BH_4, standard curves of 5-hydroxytryptophan fluorescence at all BH_4 concentrations were produced (see Appendix G.1).

6.2.2 Experimental procedure

Activity measurements were conducted on a Varian Cary Eclipse fluorescence spectrophotometer. The excitation and emission wavelengths were 300 and 330 nm, respectively and slit widths of 5 nm were used. The photomultiplier tube voltage was set to 650 V. The measurements were done in a 10.00 x 10.00 mm QS quartz cuvette (2500 µL total). The spectrophotometer is equipped with a temperature controlled cuvette holder with magnetic stirring. The concentration of O_2 in the assay was determined using a MI-730 Oxygen electrode and an OM-4 Oxygen Meter from Microelectrodes, Inc., Londonderry, NH, USA. The O_2 concentration was controlled as described by Nielsen *et al*.[222] The electrode was calibrated in a cuvette containing 50 mM HEPES/NH_4OH, 200 mM $(NH_4)_2SO_4$, pH 7.0 at 15 °C. In the calibration, the zero set point was obtained by sparging with N_2 until saturation and the 100 % O_2 point was obtained by sparging with O_2 until saturation. At 15 °C and 101.325 kPa, the solubility of O_2 at (100 %) was assumed to be equal to1528 µM.[223] The desired O_2 concentration was obtained by sparging with a mixture of N_2 and O_2. Mixing of the gases was performed with Mass Flow controllers model 5850 TR from Brooks Instruments B. V. Veenendaal, Holland. The gas flow controllers were operated using a monitor model 0152 from Brooks Instruments. In addition to the cuvette containing the reaction mixture, a reference cuvette was used to monitor the O_2 concentration. When the reaction cuvette was added enzyme and BH_4, the reference cuvette was added equivalent volumes of water.

All measurement were performed under the following conditions; 50 mM HEPES/NH_4OH, 200 mM $(NH_4)_2SO_4$, pH 7.0, 0.025 g/L (8823 U/mg) catalase, 25 µM $(NH_4)_2Fe(II)(SO_4)_2•6H_2O$, and 7 mM DTT. The concentration of tryptophan and BH_4 varied. (6R)-5,6,7,8-tetrahydro-L-biopterin dihydrochloride (BH_4) was bought from Schircks Laboratories, Jona, Switzerland. All other chemicals used were analytical grade obtained from Sigma-Aldrich and all solutions were prepared using 18.2 MΩ•cm water from a Milli-Q synthesis A10 Q-Gard system (Millipore).
Protein solutions, stored at -80 °C, were thawed and diluted to 5 µM in the buffer in which they were purified. Stock solutions of catalase, Trp, and BH_4 were thawed from -20 °C and used together with freshly prepared DTT and $(NH_4)_2Fe(II)(SO_4)_2•6H_2O$ solutions. The concentrations of the tryptophan and BH_4 stocks were determined by UV-Vis using $\varepsilon_{(278)}$ = 5500 $M^{-1}cm^{-1}$ and $\varepsilon_{(266)}$ = 18000 $M^{-1}cm^{-1}$ (2 M HCl), respectively.[220] Buffer, water, $(NH_4)_2Fe(II)(SO_4)_2•6H_2O$, DTT, and tryptophan were added to the reaction cuvette and the equivalent volume of buffer and water was added to the reference cuvette.
Both cuvettes were sealed with lids using parafilm, and gas tubes were inserted through holes in the lids into the solutions. The reference cuvette was added an O_2 electrode and both cuvettes were stirred at 15 °C until the desired concentration of O_2 was reached. Then the tubes were pulled up over the surface of the solution, purging the head space to maintain the O_2 concentration. Catalase and TPH were added to the reaction cuvette, while water was added to the reference cuvette. After addition, the solutions were stirred for another 2 min before the reaction was initiated by the addition of BH_4. The initial rate slope (intensity/min) of the monitored fluorescence signal was quantified using Varian spectrophotometer software. Quantification occurred through linear regression on a manually placed interval of minimum 0.04 min of the initial curve. The initial rates were converted to µM 5-hydroxytryptopan per minute by dividing with the slopes of the standard curve at the given BH_4 concentration.
Standard curves were produced by measuring the fluorescence of 5-hydroxytryptophan (0.5 - 20 µM) in 50 mM HEPES/NH_4OH, 200 mM $(NH_4)_2SO_4$, pH 7.0 at various BH_4 concentration (10 – 750 µM). The concentration of 5-hydroxytryptophan was determined in 10 mM HCl using $\varepsilon_{(278)}$ = 5500 $M^{-1}cm^{-1}$.[220] The standard curves can be found in Appendix G.1.

6.2.3 AAAH – Kinetic mechanism

The fundamental mechanisms of aromatic amino acid hydroxylation by the AAAH members have been under investigation for decades. Despite great efforts to dissect the mechanism, ambiguities still exist. Of the AAAHs, PAH and TH have been more thoroughly studied by steady-state kinetic assays and spectroscopy.

6.2.3.1 Evidence for Ping Pong mechanism

Based on steady-state kinetic measurements, Ikeda *et al.*[224] have found that *bovine* TH follows a Ping Pong mechanism in which the substrates bind in a ordered fashion where pterin (6,7-Dimethyl-5,6,7,8-tetrahydropterine, $DMPH_4$) binds before Tyr. Here it was found that the first step of the reaction occurs between TH and pterin and the second step is aerobic oxidation of Tyr.
From *bovine* TH, parallel lines in a double reciprocal Lineweaver-Burk plot of velocity against BH_4 concentration at varied Tyr concentrations were obtained by Oka et al., similarly suggesting a Ping Pong mechanism.[225] Substrate inhibition by Tyr was observed and it was found that Tyr inhibition was decreased by increased concentrations of BH_4. At concentrations of BH_4 up to a limit of 220 uM, Tyr at 50 µM was inhibitory. At higher BH_4 concentrations, Tyr at this concentration was not inhibitory. This resulted in biphasic curves in the Lineweaver-Burk plots with BH_4. For this reason, two different K_m values of the substrates were obtained depending on whether the concentration of BH_4 was lower or higher than the threshold of 220 µM. The biphasic behavior was explained by the potential presence of two enzyme forms or two different conformations.
In support of a Ping Pong mechanism is the observation that in *rat* TH, oxidation of BH_4 can occur in the absence of substrate Tyr at pH of 8.2 with rates only two fold lower than in the presence of Tyr.[226] The oxidation occurs at slower rates at pH 7.2 and not at all at pH 6.5.[226,227] The reaction between TH, pterin,

and O_2, in the absence of Tyr is supported by the gradually lower hydroxylation yield of substrate Tyr observed when Tyr is added as the last substrate in the reaction.[226] This suggests the breakdown of a reactive intermediate formed by TH, pterin, and O_2.

6.2.3.2 Evidence for sequential mechanism

The mechanism of *rat* TH has also been studied by Fitzpatrick [227], where 6-MePH_4, O_2, and Tyr were varied pairwise with the third substrate at non-saturating concentrations. This study finds the order of binding being 6-MePH_4, O_2, and Tyr and that Tyr forms a dead-end complex with TH at high concentrations. The reaction mechanism is, however, contradicting the observations from *bovine* TH, as intersecting lines are found in the double reciprocal plots. This suggests an ordered sequential mechanism involving a quaternary complex with all three substrates bound.
The mechanism has also been probed by stopped-flow absorbance spectroscopy. Single turn-over kinetic analysis was performed on PAH from *Chromabacterium violaceum* by Subedi *et al*.[228] Here absorbance traces upon pterin binding under anaerobic conditions and formation of reaction intermediates were used in combination with rapid mixing chemical quenching for detection of Tyr, to decipher the mechanism. The obtained data was fitted with a mechanistic model in which pterin and Phe bind in a random order, favored by pterin binding first, followed by reversible O_2 binding. No evidence of Phe substrate inhibition is presented. In contrast, a steady-state kinetic analysis of PAH from *Chromabacterium violaceum* showed that the enzyme follows a sequential mechanism in which DMPH_4 binds first followed by Phe and then O_2. Here substrate inhibition by Phe was observed but only at concentrations greater than 1 mM.[229]
A similar single-turnover study using stopped-flow absorbance spectroscopy was made by Roberts *et al.* for a truncated *rat* PAH variant lacking the N-terminal regulatory domain.[230] Here, it is found that a productive ternary complex is formed in an ordered sequential fashion where BH_4 binds before Phe. O_2 binds the ternary complex and initiates the reaction. Here it is proposed that both BH_4 and Phe (K_d value = 1.3 mM) can form an inhibitory binary complex upon binding to free PAH.
The same sequential mechanism, in which O_2 binds after formation of a ternary complex, has been proposed in a study by Chow *et al*., where X-ray absorbance spectroscopy and magnetic circular dichorism were utilized to find that Fe(II) in *rat* TH undergoes a six-coordinate (6C) to five-coordinate (5C) conversion only when both Tyr and 6-MePH_4 is bound.[231] The 5C geometry is assumed to be the active state of the active site which is able to bind O_2 and initiate reaction. This type of O_2-activation has been observed in other O_2-activating nonheme iron enzymes.[232]
Single turn-over kinetics has also been carried out for the catalytic domain of *rabbit* TPH1.[233] In this study, a model in which a ternary complex, TPH•6-MePH_4•Trp, is formed followed by equilibrium binding of O_2, fits the data. No evidence of Trp substrate inhibition is presented.

Binding of BH_4 as the first substrate is consistent with finding in TPH1 where inhibitors display uncompetitive inhibition towards 6-MePH_4, which indicates that the pterin binds first.[234] Additionally, the crystal structure of *chicken* TPH (PDB entry: 3E2T) shows that binding of L-tryptophan results in a closed conformation, which indicates the formation of a dead-end complex.[235]

Collectively, the kinetic mechanism of the AAAH's has been studied with a number of methods with contradictory conclusions. In general, it seems that the most recent beliefs are in favor of an ordered sequential mechanism where the order of binding is pterin, amino acid substrate, and O_2. Several of these studies are, however, conducted with very high substrate concentrations (typically 0.5 mM+ range) [228,230,231,233] and with 6-MePH_4 instead of BH_4.

6.2.4 Steady-state kinetic results of c*h*TPH1

Kinetic parameters for c*h*TPH1 were determined according to the method of Viola *et al*.[209], in which the concentration of BH_4 and Trp are varied while the concentration of O_2 is held at constant. Ideally, in this

method O_2 concentration would be at saturation level (>100K_m). However, this is not possible because of the solubility of O_2. The kinetics experiments in this section are performed with an O_2 concentration of 500 µM to enable comparison with data produced previously in the Metalloprotein Chemistry and Engineering Group at DTU.[222,236] The derived kinetic parameters are therefore apparent values throughout this section. The apparent $K_{m,O2}$ for c*h*TPH1, at 70 µM tryptophan and 300 µM BH_4, is 109 ± 7 µM [236], which means that the O_2 concentration in this study is ~5-fold $K_{m,O2}$.

To explore the kinetic mechanism of TPH1, the initial velocity of c*h*TPH1 were determined at various tryptophan and BH_4 concentrations. The concentrations of the substrates were varied in a concentration matrix of fourteen tryptophan concentrations and six BH_4 concentrations. This data is presented in Figure 6.5.

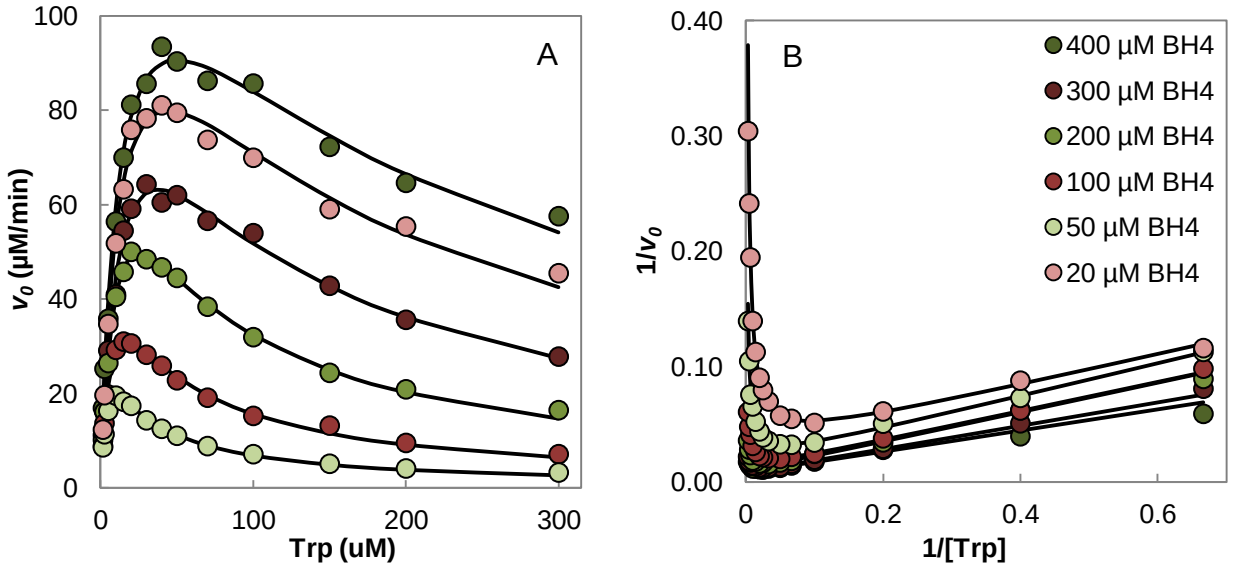

Figure 6.5. Initial velocity of c*h*TPH1 against tryptophan concentration at fixed concentrations of BH_4. The oxygen concentration was 500 µM in all measurements. The plots are fitted with eq. 2.

Figure 6.5 A shows that the data deviates from the classical hyperbolic curve and can be fitted very well with eq. 2 which describes linear substrate inhibition resulting from dead-end complex formation between substrate and a nonproductive enzyme form.[218] Similarly, Figure 6.5 B does not represent a family of straight lines, rather the double reciprocal plots are only linear at high values of 1/[Trp]. As the plots approach the 1/v_0-axis they pass through a minimum and bend upward which is expected when substrate inhibition is occurring. The linear parts (high 1/[Trp]) of the 1/v_0 versus 1/[Trp] plots seem parallel. Parallel lines in this plot only occur in mechanisms that follow a Ping Pong system (section 6.1.2.2, Figure 6.2 b). However, in sequential mechanisms where K_A<<$K_{m,A}$ the K_A term in eq. 7 will be insignificant and the plots will appear parallel. Because of the non-linear nature of the double reciprocal plots, slopes (K_m/V_{max}) and intercepts (1/V_{max}) are hard to determine graphically. Apparent V_{max}, $K_{m,Trp}$, and K_i values were, therefore, determined by fitting velocity equation 2 to the data. The obtained values were used to produce the secondary plots in Figure 6.6.

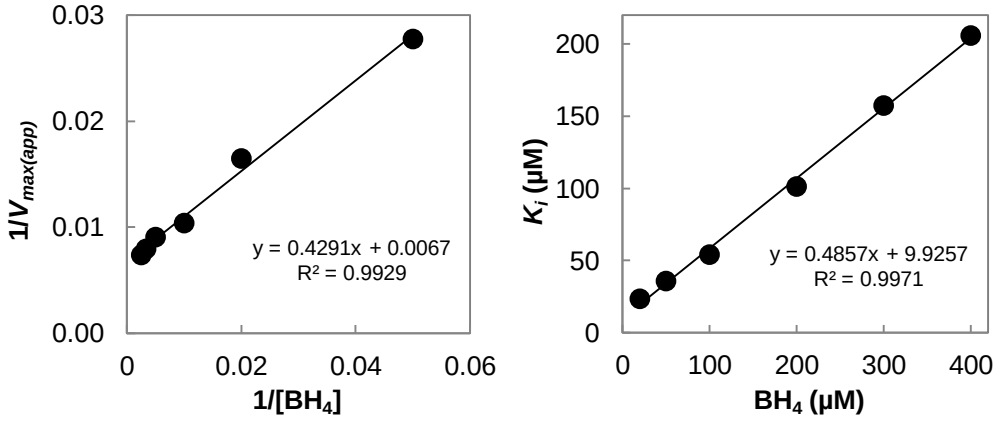

Figure 6.6. Secondary plots of V_{max} and K_i-values obtained from fitting the plots in Figure 6.5 with eq. 2.

The secondary plots show that c*h*TPH1 displays BH_4 concentration-dependent substrate inhibition. At low fixed concentrations of BH_4 (20 µM), c*h*TPH1 has an apparent K_i of 24 µM, while at high concentration (400 µM) the apparent K_i is increased to 206 µM. The apparent V_{max} also increase with increasing concentration of BH_4. Here a value for V_{max} can be determined to 149 µM/min from the interception with the $1/V_{max}$-axis. $K_{m,Trp}$ also seems to be BH_4 concentration-dependent (Table 6.1).

Table 6.1. Apparent kinetic parameters for c*h*TPH1 determined from fitting the kinetic data in Figure 6.5 with eq. 2.

	BH_4 (µM)					
	20	**50**	**100**	**200**	**300**	**400**
V_{max} **(µM/min)**	36	61	96	110	126	135
$K_{m,Trp}$ **(µM)**	4.9	8.7	12.2	14.1	12.7	12.5
K_i **(µM)**	24	36	54	102	158	206

When the data in Figure 6.5 is replotted as v_0 versus [BH_4], the plots in Figure 6.7 are obtained. The plots have the classic hyperbolic shape and eq. 1 fits well. From visual inspection, it is clearly seen that both V_{max} and $K_{m,BH4}$ are increased with increasing concentration of tryptophan and that there are no sign of substrate inhibition. The values of V_{max} and $K_{m,BH4}$ were determined using eq. 1, and are summarized in Table 6.2.

Table 6.2. Apparent kinetic parameters for c*h*TPH1 determined from fitting the kinetic data in Figure 6.7 with eq. 1.

	Trp (µM)													
	1.5	**2.5**	**5**	**10**	**15**	**20**	**30**	**40**	**50**	**70**	**100**	**150**	**200**	**300**
V_{max} **(µM/min)**	14	22	37	59	81	102	117	145	146	159	207	215	268	1071
$K_{m,BH4}$ **(µM)**	22	28	36	49	79	114	152	237	252	344	571	791	1227	6989

The concentration of tryptophan clearly has an influence on the value of $K_{m,BH4}$. At low concentration of tryptophan (1.5 µM) $K_{m,BH4}$ is 22 µM while at 70 µM tryptophan, which is considered standard in TPH assays, $K_{m,BH4}$ is 344 µM. The kinetic parameters determined at higher concentrations of tryptophan are unreliable because only v_0-values at BH_4 concentrations well below $K_{m,BH4}$ are determined. Hence, only $K_{m,BH4}/V_{max}$ values are reliable.

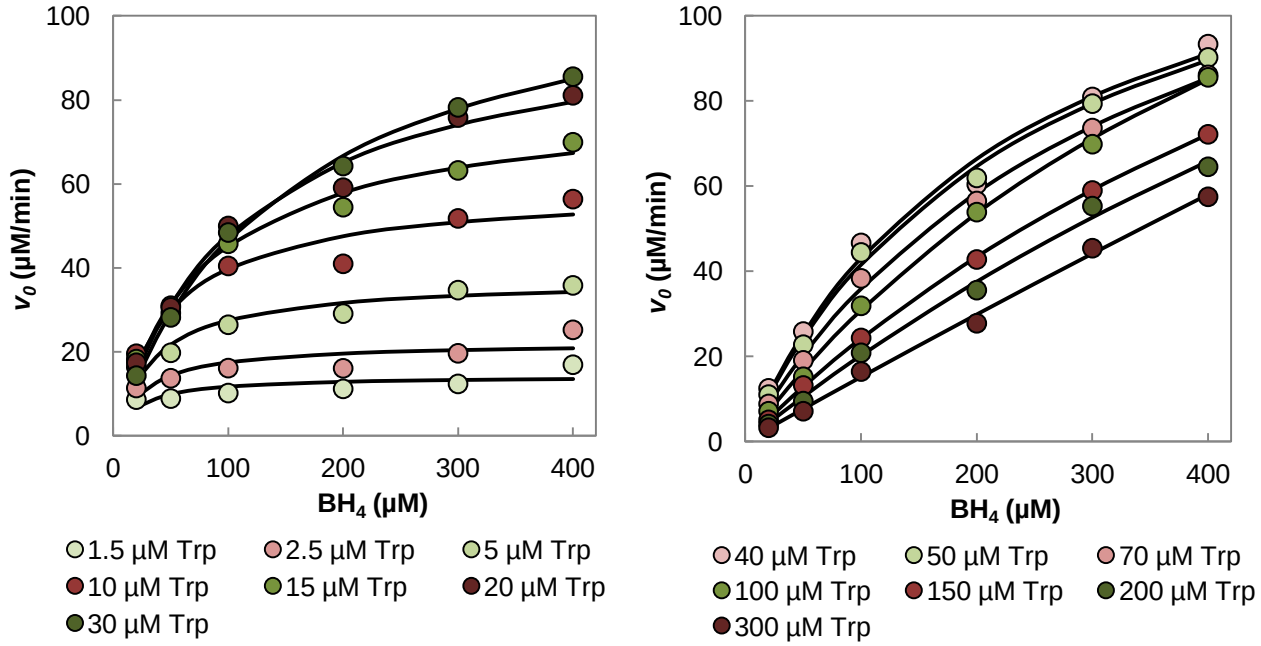

Figure 6.7. Initial velocity of c*h*TPH1 against BH_4 concentration at fixed concentrations of tryptophan. The oxygen concentration was 500 µM in all measurements. The plots are fitted to eq. 1.

The data from Figure 6.7 is replotted as $1/v_0$ versus $1/[BH_4]$ in Figure 6.8 A. For clarity, only the two highest and lowest tryptophan concentrations are included in the plot. Plots of all the concentrations can be found in Appendix G.2. The values of $K_{m,BH4}/V_{max}$ ($slope_{1/BH4}$) were calculated from values in Table 6.2, and are presented in Figure 6.8 B as a function of [Trp].

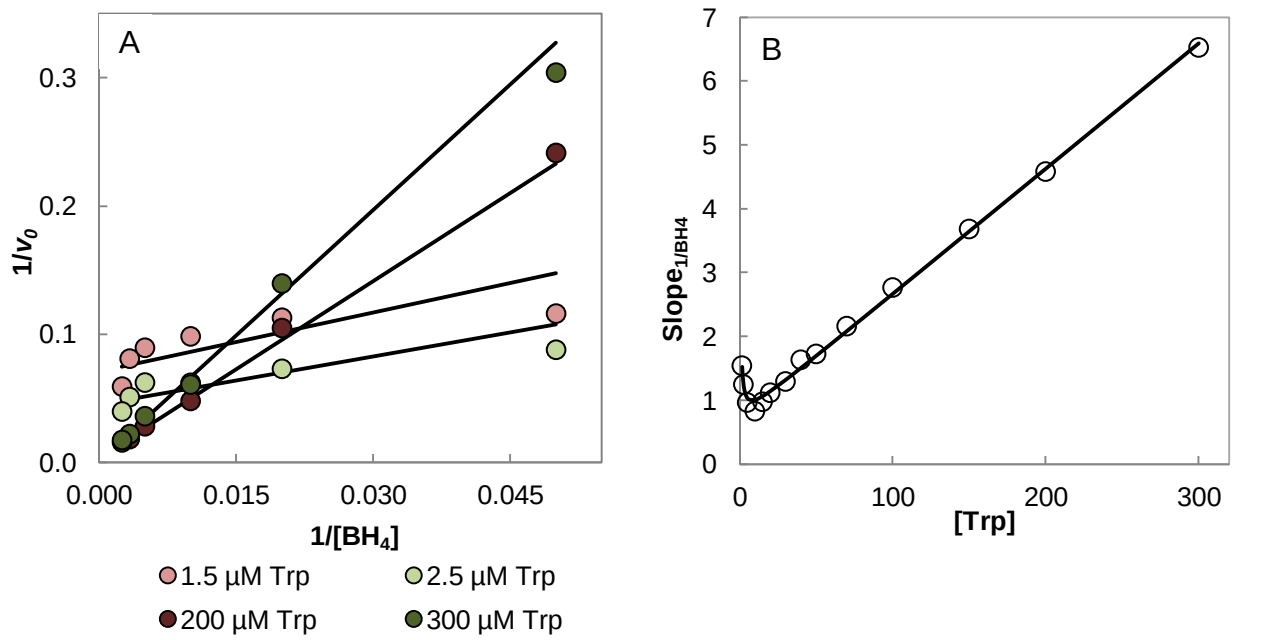

Figure 6.8. (a) Double reciprocal v_0 versus $[BH_4]$ plots of the two highest and lowest concentrations of tryptophan from Figure 6.7. Data is fitted with eq. 1. (b) Slopes (K_m/V_{max}) obtained from fits with eq. 1 of data from Figure 6.7, and are fitted with eq. 6.

Figure 6.8 B shows that the slopes of the plots in Figure 6.8 A are not linearly correlated with the concentration of Trp, as is expected in the case of a Ping Pong mechanism. A $slope_{1/[B]}$ versus [A] plot that

passes through a minimum and bends up is indicative of a sequential mechanism, Figure 6.1 a. The deviation from linearity of the $slope_{1/BH4}$-plot occurs at very low tryptophan concentrations, which is indicative of a very small value of K_A.

Noteworthy is, that at low tryptophan concentration in Figure 6.8 A (1.5 and 2.5 µM Trp), the data deviates from linearity. This phenomenon is expected from a hybrid Ping Pong-ordered mechanism, see Figure 6.3 (section 6.1.2.4). The dataset was therefore split into two datasets to test if the data represent two distinct mechanisms, which is the case in a hybrid Ping Pong-ordered system. One dataset contained initial velocities from combinations of all tryptophan concentrations with the BH_4 concentrations 20, 50, and 100 µM and the second dataset with 200, 300, and 400 µM BH_4. Both datasets were fitted with eq. 1 for every tryptophan concentration, and the slopes (K_m/V_{max}) were calculated, Figure 6.9. The obtained kinetic parameters can be found in Appendix G.3.

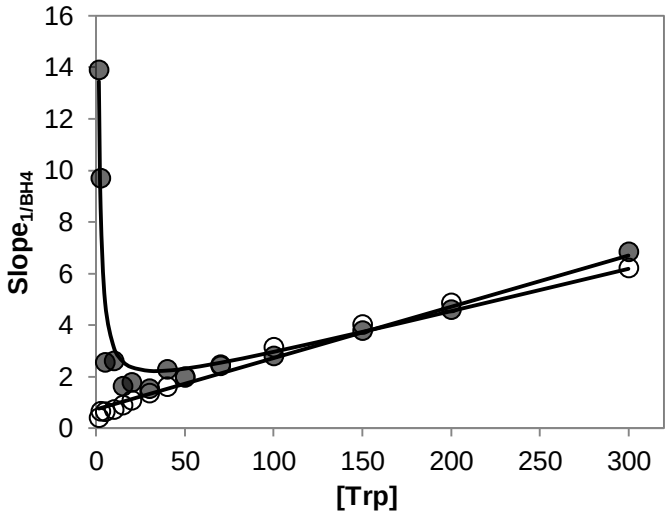

Figure 6.9. Slopes (K_m/V_{max}) obtained from fits with eq. 1 of data from Figure 6.7 split into two datasets. White circles represent slopes obtained from the dataset containing [BH_4] = 20, 50, and 100 µM (fitted with eq. 6) and gray circles represent slopes obtained from the dataset containing [BH_4] = 200, 300, and 400 µM (fitted with linear regression).

Figure 6.9 shows that the two parts of the dataset result in different fits. Using the dataset with low concentrations of BH_4 (white circles), results in $slope_{1/BH4}$-values which are linearly increasing with tryptophan concentration. This trend is expected for a Ping Pong mechanism. With the dataset containing high concentrations of BH_4 (gray circles), the $slope_{1/BH4}$-values are clearly not linear. Here, the $slope_{1/BH4}$-values decrease, pass through a minimum, and increase linearly with increasing [Trp]. This trend is expected for a sequential mechanism.

6.2.4.1 Data analysis by global fitting on split dataset

Based on the graphical interpretation and fitting with eq. 1 and 2, the mechanism cannot conclusively be decided. From analyzing the entire dataset a sequential mechanism with a small K_A compared to $K_{m,A}$ seems favorable. However, when the dataset is split into high and low concentrations of BH_4, a mechanism that branches into a Ping Pong and a sequential pathway seems attractive.
To evaluate which mechanism the kinetic data represents, global fitting with the two-substrate equations was conducted for the two datasets. The datasets were fitted to the velocity equations describing *i*) dead-end EB complex formation in a Ping Pong mechanism, *ii*) dead-end EB complex formation in a sequential mechanism, and *iii*) dead-end EA_2 complex formation in a sequential mechanism. The resulting parameters of the fits are summarized in Table 6.3.

Table 6.3. Kinetic parameters derived from fitting the data with a Ping Pong mechanism (eq. 7), a sequential mechanism with a dead-end EB complex (Seq. EB - eq. 4), and a sequential mechanism with a dead-end EA_2 complex (Seq. EA_2 - eq. 5). Parameters have been derived for two datasets; one containing initial velocities at BH_4 concentrations of 20, 50 and 100 µM and one containing initial velocities at BH_4 concentrations of 100, 200, and 300 µM. The model error is given by the sum of squared residuals. *: F-test, p<0.01.

	Mechanism	V_{max} (µM/min)	$K_{m,Trp}$ (µM)	$K_{m,BH4}$ (µM)	K_i (µM)	K_A (µM)	Error
Low [BH_4] range	Ping Pong EB	314	42	208	32	-	59.4
	Seq. EB	314	42	208	32	0	59.4
	Seq. EA_2	314	42	208	32	0	59.4
High [BH_4] range	Ping Pong EB	299	31	426	92	-	245.7
	Seq. EB	236	17	235	64	124	207.3*
	Seq. EA_2	236	17	268	73	8.0	207.3*

From Table 6.3, it can be seen that at low concentrations of BH_4 all the mechanism have the same parameters and the same model errors. When fitting the data to the sequential mechanisms, the parameter K_A is reduced to zero, which results in a collapse of eq. 4 and 5 into eq. 7, describing a Ping Pong mechanism. At high BH_4 concentrations, fits to the sequential mechanisms result in better models compared to the Ping Pong mechanism, as the error is 16 % lower (F = 14.6, p<0.01). The sequential mechanisms result in identical model errors and both give reasonable kinetic parameters (µM range). One sequential mechanism can therefore not be chosen over the other based on these fits.

6.2.4.2 Data analysis by global fitting on entire dataset

Global fits to the entire dataset were conducted to test if the data represents one of the branching mechanisms presented in Figure 6.10 and Figure 6.11. In Figure 6.10, the reaction can either occur through a Ping Pong or a sequential mechanism depending on the concentration of tryptophan, and substrate inhibition is caused by formation of a dead-end EB (TPH•Trp) complex formed if tryptophan binds before BH_4 (hybrid EB mechanism).

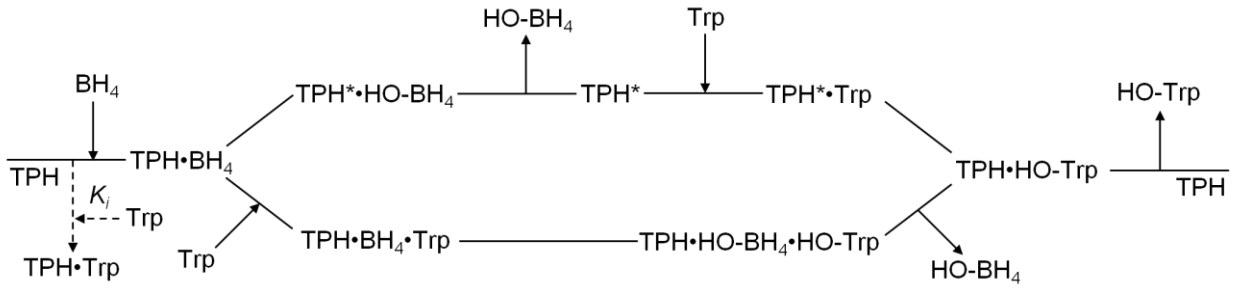

Figure 6.10. Basic scheme for a branching mechanism of c*h*TPH1. The scheme corresponds to a hybrid Ping Pong-ordered mechanism with a dead-end TPH•Trp complex (EB). TPH* indicates a TPH that has undergone an irreversible change (e.g. formation of $Fe^{IV}O$). Upper path represents a Ping Pong mechanism and the lower path represents a sequential mechanism.

Figure 6.11 present a reaction in which the concentration of BH_4 determines the reaction mechanism, and substrate inhibition occurs through binding of a second tryptophan forming a dead-end TPH*•Trp_2 complex

(hybrid E*A_2 mechanism). In this mechanism, the upper path is not a conventional Ping Pong mechanism where a product is released before the next substrate binds. Rather it represents a mechanism in which an irreversible change occurs in TPH after binding of tryptophan. Such an irreversible change can account for data which appear to represent a Ping Pong mechanism.[213]

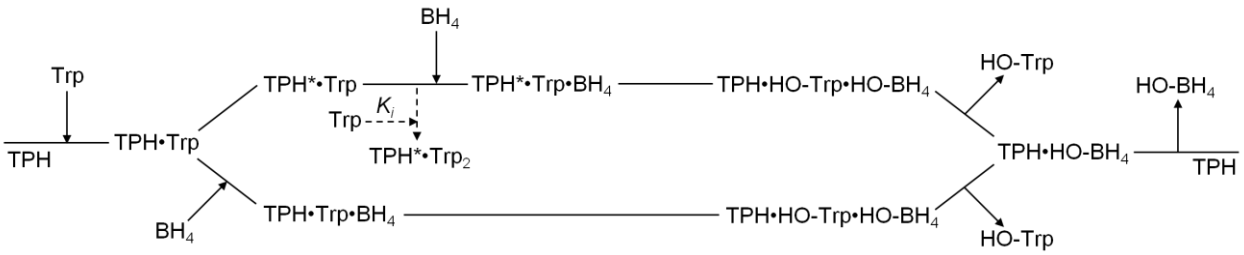

Figure 6.11. Basic scheme for a branching mechanism of c*h*TPH1. The scheme corresponds to a hybrid Ping Pong-ordered mechanism with a dead-end TPH*•Trp_2 complex (E*A_2). TPH* indicates a TPH that has undergone an irreversible change (e.g. loop closure). Upper path represents a Ping Pong mechanism and the lower path represents a sequential mechanism.

For comparison, the full dataset was fitted with the six different mechanisms including the branched mechanisms. In Figure 6.12 fits are shown for a Ping Pong mechanism (solid line), the hybrid E*A_2 mechanism (dashed lines), and the hybrid EB mechanism (dotted lines). The sequential mechanisms resulted in identical fits, as K_A was reduced to zero resulting in a reduction of the equations to that of a Ping Pong mechanism. Similarly, the equation of a rapid equilibrium random mechanism is collapsed into the equation of a Ping Pong mechanism by reducing K_A to zero and α to one. For this reason, identical kinetic parameters were obtained for the four mechanisms (Table 6.4). Based on this analysis of the conventional non-branched mechanisms, a Ping Pong mechanism fits the total dataset best.

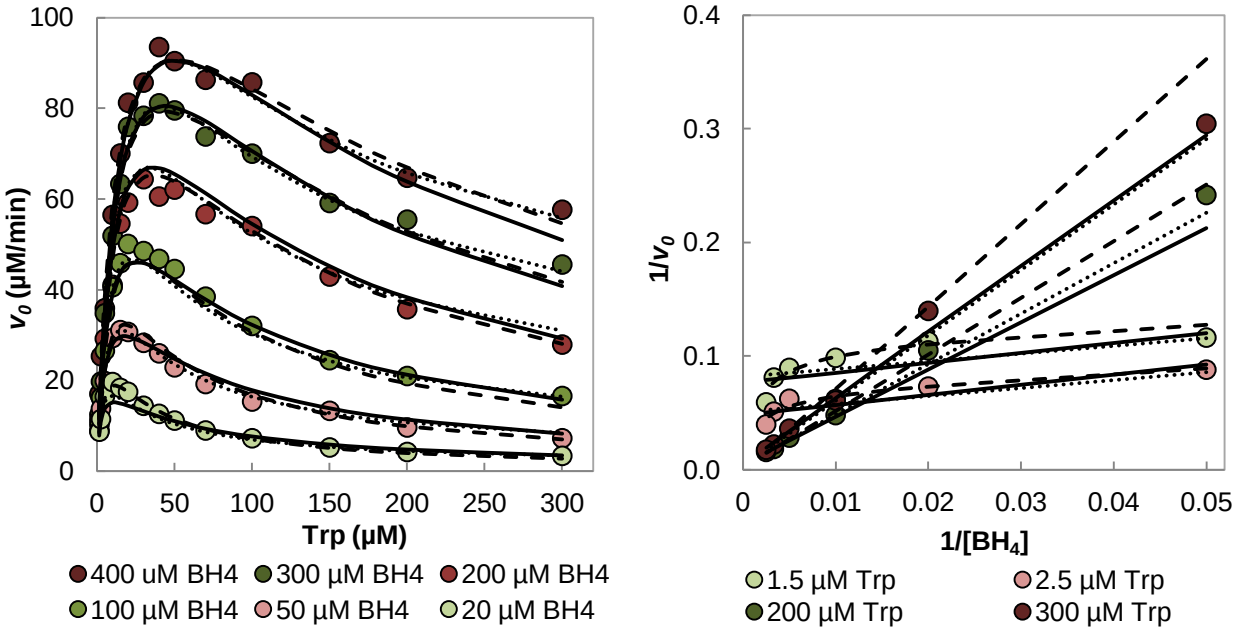

Figure 6.12. Global fits to initial velocity measurements for c*h*TPH1. The oxygen concentration was 500 µM in all measurements. Left: initial velocities versus tryptophan concentration at fixed concentration of BH_4. Right: double reciprocal plots of v_0 versus [BH_4]. The plots are fitted with eq. 7 (Ping Pong mechanism - solid lines), eq. 12 (Hybrid Ping Pong-ordered E*A_2 mechanism - dashed lines), or eq. 13 (Hybrid Ping Pong-ordered EB mechanism - dotted lines).

When the dataset is fitted with the hybrid E*A_2 model (eq.11), the fit improves (F = 17.8, p<0.01) compared to the fit with a Ping Pong mechanism (Table 6.4). From a visual inspection of the fits in Figure 6.12, it is obvious that the hybrid E*A_2 model results in better fits at low tryptophan concentrations. This hybrid model is also able to account for the deviation from linearity observed in the $1/v_0$ versus 1/[BH_4] plots at low tryptophan concentrations. The deviation from linearity is the result of the $[B]^2$ terms becoming negligible at low BH_4 concentrations, which results in eq. 11 being reduced to eq. 7 (Ping Pong). The kinetic parameters derived from this model are presented in Table 6.4. Fitting this hybrid model to the data results in a redundancy of K_3 as it is zero. The hybrid EB model also results in an improved global fit (F = 6.1, p<0.01) compared to that of a Ping Pong mechanism, Table 6.4. Fitting this model to the data results in a redundancy of K_4.

Table 6.4. Kinetic parameters derived from global fits. Parameters are derived from fitting with a Ping Pong mechanism with dead-end EB (eq. 7), a sequential mechanism with a dead-end EB complex (Seq. EB - eq. 4), a sequential mechanism with a dead-end EA_2 complex (Seq. EA_2 - eq. 5), a rapid equilibrium random mechanism with dead-end EB and BEB formation (Rapid eq. EB – eq. 9), a hybrid Ping Pong-ordered mechanism with dead-end EA_2 formation (Hybrid EA_2 – eq. 12), and a hybrid Ping Pong-ordered mechanism with dead-end EB formation (Hybrid EB – eq. 13) to all the data. The model error is given by the sum of squared residuals. *: F-test, p<0.01.

Mechanism	V_{max} µM/min	V_2 min^{-1} $µM^{-1}$	$K_{m,Trp}$ µM	$K_{m,BH4}$ µM	K_i µM	K_A µM	K_3	K_4 $µM^{-1}$	α	Error
Ping Pong EB	213	-	23	181	51	-	-	-	-	551
Seq. EB	213	-	23	181	51	0	-	-	-	551
Seq. EA_2	213	-	23	181	51	0	-	-	-	551
Rapid eq. EB	213	-	23	181	51	0	-	-	1	551
Hybrid E*A_2	117	0.2	18	46	17	-	0	$7e10^{-4}$	-	325*
Hybrid EB	210	0.3	24	135	52	-	2.8	0	-	445*

6.3 Discussion of kinetic results

The kinetic mechanism has not unambiguously been determined for the aromatic amino acid hydroxylases. Several studies of the mechanism have been conducted for PAH and TH but with conflicting conclusions. In the case of TPH, very little is known about the fundamental mechanism of both isoforms. In this study, elucidation of the catalytic mechanism of c*h*TPH1 has been carried out by measuring the initial reaction velocity at different combinations of BH_4 and tryptophan concentrations.

Global fit of the conventional mechanisms to all the kinetic data obtained in this study yields the best fit with a Ping Pong mechanism in which BH_4 binds before tryptophan and where tryptophan acts as an inhibitor upon binding prior to BH_4. This order of substrate binding is in agreement with the majority of studies conducted on the AAAHs.[224,225,227,229,230,233] The same Ping Pong mechanisms has been proposed for TH [224,225], where a BH_4 concentration-dependent substrate tryptophan inhibition constant was also observed [225]. However, other studies conducted on the AAAHs, including a study of *rabbit* TPH1, find the mechanism to be sequential.[227-231,233]

A graphical analysis shows that the secondary plot of $slope_{1/BH4}$ versus [Trp] gives a non-linear relationship, which suggests that the reaction follows a sequential mechanism. In the double reciprocal $1/v_0$ versus 1/[BH_4] plots, it is noteworthy that the plots are not linear at low concentrations of tryptophan. This unusual feature has also been observed for TH.[225] Oka *et al.*[225] found that at low tyrosine concentrations the $1/v_0$ versus 1/BH_4 plots were non-linear, and deviation from linearity occurred at ~0.2 mM BH_4. The data was

therefore analyzed separately for velocity data obtained at respectively higher or lower than 0.2 mM BH_4. Similar data has been recorded for i.e. pytuvate carboxylase, glutathione reductase, hypoxathine phosphoribosyltransferase, and glutathione S-transferase A.[217,237-239]

When data obtained in this study is expressed in terms of a low and a high BH_4 concentration ranges, two different kinetic mechanisms are obtained. At low concentrations of BH_4, the reaction seems to follow a Ping Pong (dead-end EB) mechanism and at high concentrations a sequential mechanism. One sequential mechanism cannot be chosen over the other based on fitting with EB or EA_2 dead-end models. Formation of a EA_2 complex is less likely, as ITC experiments have shown that tryptophan only binds once (n = 1) in *h*TPH1.[240] In the kinetic study on *rabbit* cTPH1 [233], very high substrate concentrations ([6-MePH_4] =1–1.5 mM and [Trp]=0.5–1.0 mM) were used. The high substrate concentrations might explain the sequential mechanism they observed for *rabbit* cTPH1.

A switch in mechanism, as a function of substrate concentration, has been observed for glutathione reductase and hypoxathine phosphoribosyltransferase.[217,238] Here, a mechanism that branches into either a Ping Pong or a sequential mechanism after binding of substrate A, were applied to account for the deviation of linearity in the double reciprocal plots. Such a mechanism has been denoted a hybrid Ping Pong-ordered mechanism.[208]

A hybrid Ping Pong-ordered model where tryptophan binds as the first substrate (hybrid E^*A_2) fit the data obtained for c*h*TPH1 very well. According to this model, at low BH_4 concentrations the reaction occurs through a Ping Pong mechanism where tryptophan binds to TPH and induces an irreversible step. Such an irreversible change, which accounts for the Ping Pong kinetics, does not have to be a covalent modification of TPH, but can be a kinetically irreversible step that occurs before binding of BH_4. Such a step can e.g. be a large conformational change which forward direction is much faster than the reverse direction, and where the reverse step is much slower than the kinetic steps of the mechanism.[213] Binding of tryptophan as the first substrate is supported by observations of Nielsen for isoform 2.[241] Here steady-state kinetic data for c*h*TPH2 indicates a sequential mechanism with ordered binding of tryptophan followed by random binding of BH_4 or O_2. The data is, however, not statistically sufficient for a conclusive determination of the mechanism. In literature, a substantial amount of experimental evidence has been presented which documents that BH_4 binds before amino acid substrate.[224,225,227,229,230,233] ITC data for *h*TPH1 do not indicate that substrate tryptophan binds to multiple sites of the catalytic domain.[240] Furthermore, binding of two substrates has to the best of my knowledge never been observed for any for the AAAHs. Together, these observations render this mechanism unlikely despite the improved fit.

A global fit with a hybrid Ping Pong-ordered model, in which BH_4 binds first (hybrid EB), also results in a significantly improved fit compared to a Ping Pong mechanism. In this hybrid mechanism, the reaction can occur through a Ping Pong mechanism at low tryptophan concentrations. BH_4 will bind first and undergo an irreversible reaction before binding of tryptophan. This correlates well with accepted reaction path catalyzed by TPH, where BH_4 react with O_2 and Fe(II) to form a reactive $Fe^{IV}O$ species which subsequently reacts with tryptophan.[242] Alternatively, at high tryptophan concentrations the reaction can occur through a sequential mechanism where both BH_4 and tryptophan bind before a reaction with O_2 takes place. This reaction path is in agreements with one observed in the study on *rabbit* TPH1 which was conducted at high tryptophan concentrations.[233]

To truly understand the mechanism of c*h*TPH1, initial velocities should be measured at different concentrations of O_2. This is unfortunately a difficult task and could not be done within the timeframe of this project. Product inhibition studies with BH_2 and 5-hydroxytryptophan are also needed to distinguish between the possible mechanisms. Product inhibition studies could especially be informative if $K_A << K_{m,A}$. Here it is very difficult to distinguish between an ordered sequential mechanism and a Ping Pong mechanism as they will yield very similar plots. The presented data should also be produced for c*h*TPH2. c*h*TPH2 is not subject to substrate tryptophan inhibition and analysis of this isoform will therefore be more straight forward. The

high sequence identity implies that the isoforms will follow the same mechanism; this is, however, not given as they display very different kinetic behaviors.

6.4 Conclusion

Knowledge about the steady-state kinetic mechanism of the TPH isoforms is very limited. In this chapter, two hybrid Ping Pong mechanisms resulted in improved fits to the experimental data compared to the reaction mechanisms by which the reaction has been described for TH and PAH. Based on observations from literature, one of the models is highly unlikely and can be discarded. The most plausible steady-state kinetic mechanism of c*h*TPH1 is therefore a hybrid Ping Pong-ordered mechanism in which the reaction can either occur through a Ping Pong or a sequential mechanism depending on the concentration of tryptophan.

6.5 References

[204] Cornish-Bowden, A., 1976, Principles of enzyme kinetics, Chapter 2, Introduction to Enzyme Kinetics. Butterworth Co Ltd, London.

[205] Zubay, G., 1988, Biochemistry, 2nd edition, Chapter 8, Macmillan Publishing Company, New York.

[206] Cornish-Bowden, A., 1976, Principles of enzyme kinetics, Chapter 4, Inhibitors and Activators. Butterworth Co Ltd, London.

[207] Segel, I. H., 1975, Rapid equilibrium bireactant and terreactant systems, Chapter 6, Enzyme kinetics, behavior and analysis of rapid equilibrium and steady-state enzyme systems. John Wiley and Son, Inc., New York.

[208] Segel, I. H., 1975, Steady-state kinetics of multireactant enzymes, Chapter 9, Enzyme kinetics, behavior and analysis of rapid equilibrium and steady-state enzyme systems,. John Wiley and Son, Inc., New York.

[209] Viola, R. E. and Cleland, W. W., 1982, Initial velocity analysis for terreactant mechanisms, *Methods Enzymol. 87*, 353-366.

[210] Rudolph, F. B., Purich, D. L., and Fromm, H. J., 1968, Coenzyme A-linked Aldehyde Dehydrogenase from Escherichia coli, *J. Biol. Chem. 243*, 5539-5545.

[211] Leskovac, V., 2003, Statistical Analysis of Initial Rate and Binding Data, Chapter 18, Comprehensive enzyme kinetics, Kluwer Academic/Plenum Press, New York.

[212] Cleland, W. W., 1963, The kinetics of enzyme-catalyzed reactions with two or more substrates or products, I. nomenclature and rate equations, *Biochim. Biophys. Acta 67*, 104-137.

[213] Grabner, G. K. and Switzer, R. L., 2002, Kinetic Studies of the Uracil Phosphoribosyltransferase Reaction Catalyzed by the Bacillus subtilis Pyrimidine Attenuation Regulatory Protein PyrR, *J. Biol. Chem. 278(9)*, 6921-6927.

[214] Leskovac, V., 2003, Enzyme Activation, Chapter 7, Comprehensive enzyme kinetics, Kluwer Academic/Plenum Press, New York.

[215] Mannervik, B., 1973, A Branching Mechanism of Glutathione Reductase, *Biochem. Biophys. Res. Commun. 51(4)*, 1151-1158.

[216] Mannervik, B.,1975, Nonlinear Regression Methods In Design of Experiments and Mathematical Modelling. Applications to the analysis of the Steady-State Kinetics of Glutathione Reductase, *BioSystems 7*, 101-119.

[217] Montero, S., de Arriaga, D., Busto, F., and Soler, J., 1990, A study of the Kinetic Mechanism followed by Glutathione Reductase from Mycelium of Phycomyces Blakesleeanus, *Arch. Biochem. Biophys. 278(1)*, 52-59.

[218] Leskovac, V., 2003, Substrate Inhibition and Mixed Dead-End and Product Inhibition, Chapter 11, Comprehensive enzyme kinetics, Kluwer Academic/Plenum Press, New York.

[219] Motulsky, H. and Christopoulos, A., 2004, Fitting models to biological data using linear and nonlinear regression, a practical guide to curve fitting, Oxford University Press, Oxford, England.

[220] Moran, G. R. and Fitzpatrick P. F., 1999, A continuous fluorescence assay for tryptophan hydroxylase, *Anal. Biochem. 266*, 148-152.

[221] Moran, G. R., Daubner, S. C., and Fitzpatrick, P. F., 1998, Expression and Characterization of the Catalytic Core of Tryprophan Hydroxylase, *J. Biol. Chem. 273*, 12259-12266.

[222] Nielsen, M. S., Petersen, C. R., Munch, A., Vendelboe, T. V., Boesen, J., Harris, P., and Christensen, H. E. M., 2008, A simple two step procedure for purification of the catalytic domain of chicken tryptophan hydroxylase 1 in a form suitable for crystallization, *Protein Expr. Purif. 57*, 116–126.

[223] Battino, R., 1981, IUPAC Solubility data series, Vol. 7, Oxygen and Ozone, Pergamon Press, Oxford, England.

[224] Ikeda, M., Fahien, L. A., and Udenfriend, S., 1966, A Kinetic Study of Bovine Adrenal Tyrosine Hydroxylase, *J. Biol. Chem. 241*, 4452-4456.

[225] Oka, K., Kato, T., Sugimoto, T., Matsuura, S., and Nagatsu, T., 1981, Kinetic properties of tyrosine hydroxylase with natural tetrahydrobiopterin as cofactor, *Biochim. Biophys. Acta 661*, 45-53.

[226] Dix, T. A., Kuhn, D. M., and Benkovic, S. J., 1987, Mechanism of Oxygen Activation by Tyrosine Hydroxylase, *Biochemistry 26*, 3354-3361.

[227] Fitzpatrick, P. F., 1991, Steady-State Kinetic Mechanism of Rat Tyrosine Hydroxylase, *Biochemistry 30*, 3658-3662.

[228] Subedi, B. S. and Fitzpatrick, P. F., 2016, Kinetic Mechanism and intrinsic Rate Constant for the Reaction of a Bacterial Phenylalanine Hydroxylase, *Biochemistry 55*, 6848-6857.

[229] Volner, A., Zoidakis, J., and Abu-Omar, M. M., 2003, Order of substrate binding in bacterial phenyalanine hydroxylase and its mechanistic implication for pterin-dependent oxygenases, *J. Biol. Inorg. Chem. 8*, 121-128.

[230] Roberts, K. M., Pavon, J. A., and Fitzpatrick, P. F., 2013, Kinetic mechanism of phenylalanine hydroxylase: intrinsic binding and rate constants from single-turnover experiments, *Biochemistry 52*, 1062−1073.

[231] Chow, M. S., Eser, B. E., Wilson, S. A., Hodgson, K. O., Hedman, B., Fitzpatrick, P. F., and Solomon, E. I., 2009, Spectroscopy and Kinetics of Wild-type and Mutant Tyrosine Hydroxylase: Mechanistic Insight into O2 Activation, *J. Am. Chem. Soc.131*, 7685-7698.

[232] Solomon, E. I., Brunold, T. C., Davis, M. I., Kemsley, J. N., Lee, S.-K., Lehnert, N., Neese, F., Skulan, A. J., Yang, Y.-S., and Zhou, J., 2000, Geometric and Electronic Structure/Function Correlations in Non-Heme Iron Enzymes, *Chem. Rev. 100*, 235-349.

[233] Pavon, J. A. Eser, B., Huynh, M. T., and Fitzpatrick, P. F., 2010, Single Turnover Kinetics of Tryptophan Hydroxylase: Evidence for a New Intermediate in the Reaction of the Aromatic Amino Acid Hydroxylases, *Biochemistry 49*, 7563-7563.

[234] Cianchetta, G., Stouch, T., Yu, W., Shi, Z., Tari, L. W., Swanson, R. V., Hunter, M. J., Hoffman, I. D., and Liu, Q., 2010, Mechanism of Inhibition of Novel Tryptophan Hydroxylase Inhibitors Revealed by Co-crystal Structures and Kinetic Analysis, *Curr. Chem. Genomics 4*, 19-26.

[235] Windahl, M. S., Petersen, C. R., Christensen, H. E. M., and Harris, P., 2008, Crystal structure of tryptophan hydroxylase with bound amino acid substrate, *Biochemistry 47(46)*, 12087-12094.

[236] Windahl, M. S., Boesen, J., Karlsen, P. E., and Christensen H. E. M., 2009, Expression, Purification and Enzymatic Characterization of the Catalytic Domains of Human Tryptophan Hydroxylase Isoforms, *Protein J.* 28, 400–406.

[237] McClure, W. R., Lardy, H. A., and Kneifel, H. P., 1971, Rat Liver Pyruvate Carboxylase, *J. Biol. Chem. 246(11)*, 3569-3578.

[238] Krenitsky, T. A. and Papaioannou, R., 1969, Human Hypoxanthine Phosphoribosyltransferase, *J. Biol. Chem. 244(5)*, 1271-1277.

[239] Pabst, M. J., Habig, W. H., and Jakoby, W. B., 1974, Glutathion S-transferase, *J. Biol. Chem. 249(22)*, 7140-7150.

[240] Jones, S. E., 2012, Optimized purification and ITC characterization of full-length tryptophan hydroxylase, B.Sc. thesis. Department of Chemistry, Technical University of Denmark, Kgs. Lyngby.

[241] Nielsen, M. S., 2007, Expression, purification and characterization of tryptophan hydroxylase, Ph.D. thesis. Department of Chemistry, Technical University of Denmark, Kgs. Lyngby.

[242] Roberts, K. M. and Fitzpatrick, P. F., 2013, Mechanisms of Tryptophan and Tyrosine Hydroxylase, *IUBMB Life 65(4)*, 350-357.

Chapter 7

A kinetic study of an active site loop

This chapter concerns the steady-state kinetics of the catalytic domains of TPH1 and TPH2. In this chapter, the current knowledge about the catalytic domains and the substrate binding sites of the TPH isoforms will be presented. Structural information will be presented on a putatively important active site loop in the AAAHs.

So far, the results obtained for the TPH isoforms have been very similar. In chapter 2 through 4 it was presented that the catalytic domains of the highly homologous TPH isoforms behave very similar in terms of purification yields, thermostability, and oligomeric state. In this chapter, different kinetic properties of the isoforms will be presented and discussed. As a result of sequence and structural analyses of the TPH isoforms, several mutations in the isoforms are conducted. Steady-state kinetic results obtained for these mutant variants will be presented and discussed. Some of the results presented in this chapter have been included in a submitted manuscript. (Appendix A.2)

Outline

7.1 The catalytic domain

The tertiary structures of the catalytic domains of both TPH isoforms are known. In total, eight crystal structures of the catalytic domain of TPH1 has been published.[243-247] The binding pockets of substrate and co-substrate are also well defined, as structures that include BH_2 [243] or tryptophan [244] are available. The six remaining structures include bulky inhibitors in the active site. Only one structure of TPH2 has been uploaded to the protein data bank (PDB entry: 4V06) while an article based on this structure has not yet been published. This structure comprises the catalytic and tetramerization domains and has an imidazole bound to the active site iron.

Because of the high sequence identity, the crystal structures of the catalytic domains of *human* TPH1 (PDB entry: 1MLW [243]) and *human* TPH2 (PDB entry: 4V06) display a root mean squared deviation of the C_α-atoms ($RMSD_{C\alpha}$) of only 1.1 Å. The high sequence identity (81 %) and hence very similar ternary structures suggest that very similar substrate binding poses can be expected for the two isoforms. Similarly, the catalytic domain of *chicken* TPH1 has a sequence identity of 91 % and 83 % with TPH1 and TPH2,

respectively. In the following, the presented structural information will, therefore, be based on TPH1, but presumed to apply for both isoforms.

The catalytic domains of the TPH isoforms have a basketlike structure with an active site consisting of a ~12 Å long and ~7 Å wide channel, Figure 7.1.[243] The channel is intersected by the position of an iron atom, which separates the binding pockets of the substrate and co-substrate.

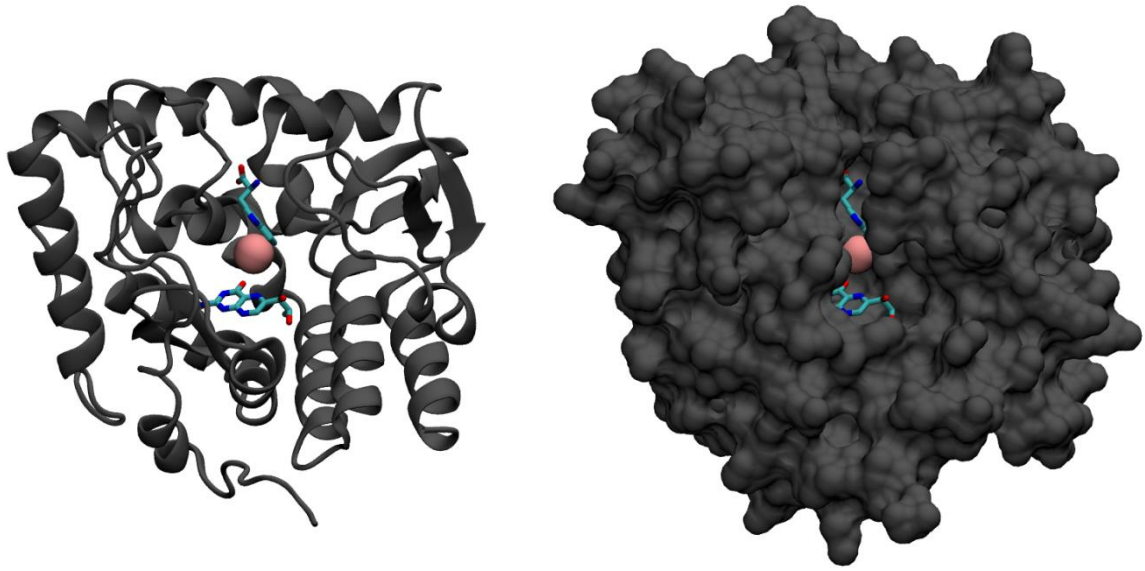

Figure 7.1. The catalytic domain of *human* TPH1 (PDB entry: 1MLW) with bound BH_2 and tryptophan. For illustrative purposes tryptophan has been superimposed from the structure of *chicken* TPH1 (PDB entry: 3E2T). Iron is shown as a pink sphere. Left: Cartoon representation of the catalytic domain illustrating the secondary and tertiary structure of the domain. Right: Surface representation of the catalytic domain illustrating the active site channel.

In the crystal structures of c*h*TPH1 which include inhibitors, the amino acid moiety of the inhibitors binds in the same pose as observed for tryptophan in *chicken* TPH1.[245] This confirms the binding pose of substrate tryptophan observed in *chicken* TPH1.

7.1.1 The tryptophan binding pocket

Based on the crystal structure of *chicken* TPH1, tryptophan binding is stabilized by several polar and hydrophobic interactions. The polar interactions occur through the carboxylate group of tryptophan which interacts with the side chains of Arg257 and Ser336 and the backbone of Thr265. Additionally, the indole nitrogen atom in the side chain of tryptophan interacts with the backbone of Ile366, Figure 7.2.[244] Deeper into the binding pocket, residues involved in hydrophobic interactions reside, these include; the side chains of Tyr235, Thr265, Pro268, His272, Phe313, Phe318, and Ile366. At the very bottom of the binding channel the active site iron atom resides at a distance of 4 Å to substrate tryptophan.

All residues involved in tryptophan binding are conserved between *human* TPH1 and TPH2. In contrast, Tyr235, Phe313, and Ile366 are not conserved in PAH and TH, and Thr265 is not conserved in TH.[244] These residues have been found to have an important role in substrate selectivity. The corresponding identity of Tyr235 in PAH and TH is leucine, and mutations of Tyr235 to alanine or leucine in TPH1 result in reduced activity and increased K_m for tryptophan.[248] This suggests that Tyr235 is important for substrate orientation and specificity.[248] Furthermore, it was found that these mutations eliminate the substrate inhibition of TPH1.[248] Phe313 corresponds to a tryptophan residue in both PAH and TH. Mutation of Phe313 to tryptophan results in a reduction of the preference of TPH1 for substrate tryptophan over

phenylalanine. This is caused by a reduction of the size of the hydrophobic binding pocket.[249] The residue Ile366 in TPH is a valine in PAH and an aspartic acid in TH. Mutation of the corresponding residue in PAH shows that this residue is important for substrate specificity. It is believed that it plays a role in controlling the shape of the hydrophobic pocket for the side chain of the substrate.[250]

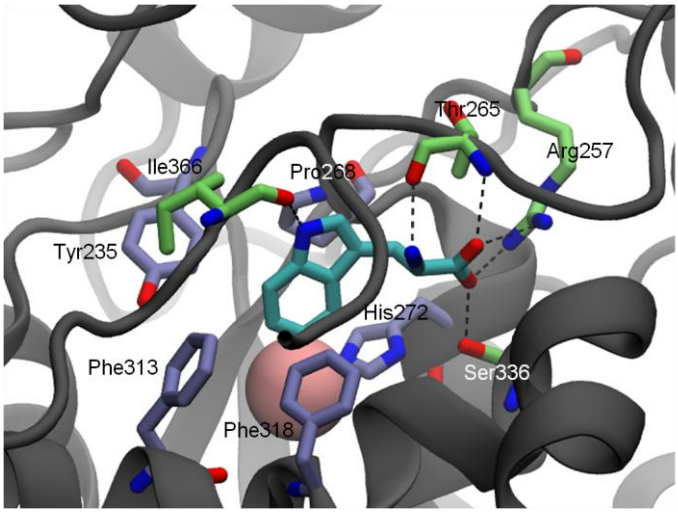

Figure 7.2. Cartoon representation (PDB entry: 3E2T) of the residues involved in tryptophan binding in *chicken* cTPH1. Residues involved in polar and hydrophobic interactions are colored green and blue, respectively. Iron is shown in pink and tryptophan in cyan. Dashed lines indicate hydrogen bonding distance.

$K_{m,Trp}$-values for TPH1 have been found to range from 8 to 48 µM [248,249,251-259], and for TPH2 from 15 to 77 µM [252,254,258,260-264]. These values are very similar, as expected for highly conserved binding pockets. No difference is observed between $K_{m,Trp}$-values obtained for full-length compared to variants comprising only the catalytic domain when they are directly compared.[256,259,260]

7.1.2 The BH_4 binding pocket

The crystal structure of c*h*TPH1 (PDB entry: 1MLW) [243] reveals the residues involved in co-substrate binding, Figure 7.3. Hydrogen bonds are formed between the backbone of Leu236 and Gly234 and the co-substrate. The co-substrate also interacts with Glu273, via hydrogen bonding mediated by two water molecules. Figure 7.3 shows that the co-substrate is held in place by several water molecules which form a hydrogen bonding network in the active site. The co-substrate is furthermore held in place by π-π interactions with Tyr235 and Phe241. In *h*PAH, BH_2 and BH_4 are found to bind in the same orientation and position as observed for BH_2 in c*h*TPH1.[265,266]

As is the case in the tryptophan binding pocket, all residues involved in BH_4 binding are conserved between *human* TPH1 and TPH2 and similar $K_{m,BH4}$-values are therefore expected. This is, however, not the case as $K_{m,BH4}$-values for TPH1 have been found to range from 27 to 324 µM [248,251-257,259] and for TPH2 from 6 to 80 µM [252,254,260-264]. There is a very broad range of $K_{m,BH4}$-values especially for TPH1. This might indicate that the $K_{m,BH4}$-value is sensitive to substrate concentrations, buffer solutions conditions, etc. It is therefore tough to compare different studies. Upon direct comparison in the same study, a 10-fold difference in the $K_{m,BH4}$-values for the two isoforms was observed.[252] Studies that compare full-length TPH to variants containing only the catalytic domain find no differences in the observed $K_{m,BH4}$-values.[256,259,260]

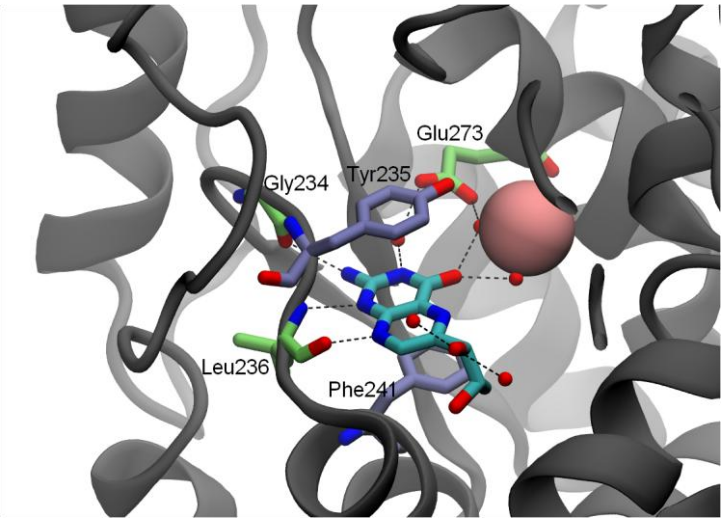

Figure 7.3. Residues in the active site of *human* cTPH1 (PDB entry: 1MLW) involved in BH_2 binding. Iron is shown in pink, BH_2 in cyan, and water molecules in red. Residues involved in hydrogen bonding are represented in green and residues with π-stacking interactions are shown in blue. Dashed lines indicate hydrogen bonding distance.

7.1.3 Active site loop

Common for the AAAHs is two intrinsically disordered loop regions lining the active site. These loops can either exist in an open or closed conformation dependent on active site occupancy. The role of these active site loops have been the subject of several studies, however, still remains unclear. In the following, information on these loop regions gathered from crystal structures and mutational studies of all the AAAHs is presented.

7.1.3.1 Active site loops of TPH

In *h*TPH1 the active site loop regions comprise Leu124-Asp139 and Ile367-Thr369. In total eight structures of cTPH1 are deposited in the PDB, Table 7.1. Four of these have insufficient electron density to solve the full structure of the active site Leu124-Asp139 loop [245,247] which indicates high mobility. Two recently published structures have density in the loops.[246,247] However, these structures include bulky inhibitors in the active site which perturbs the position of the loops. These structures will therefore not be considered in the discussion of the loop positions. The remaining two structures; c*h*TPH1 (PDB entry: 1MLW) and *chicken* cTPH1 (PDB entry: 3E2T) have well resolved active site loops.

When the crystal structures of c*h*TPH1 with bound BH_2 is compared to *chicken* cTPH1 with bound tryptophan and imidazole, a profound structural difference is observed within the loop regions lining the active site pocket.[244] The two structures reveal an open conformation and a closed conformation, respectively. In the closed conformation the loop regions close around the active site, Figure 7.4 a. This closure is observed upon L-tryptophan binding in the absence of BH_4. However, imidazole is bound in the BH_4 binding pocket, which might mimic binding of co-substrate.[244]

The crystal structure of ct*h*TPH2 (PDB entry: 4V06) has imidazole bound in the same position as in *chicken* cTPH1. ct*h*TPH2 displays an open conformation very similar to the structure of c*h*TPH1, suggesting that imidazole alone does cause loop closure. Whether the loop closure occurs solely upon binding of substrate or a combination of substrate and co-substrate is not known.

Table 7.1. Crystal structures of tryptophan hydroxylase isoform 1 and 2. In the header, substrate and co-substrate refers to presence of a (co-)substrate/(co-)substrate analogue in their respective binding sites. Open/closed refers to an open or closed conformation of the active site loops. AA in/out refers to Tyr125/Tyr171 pointing towards the active site or away from active site. *: part of the BH_4 binding pocket is also occupied by the inhibitor. **: Inhibitor interacts with loop and perturbs the position of Tyr125.

PDB entry	AAAH	Domain(s)	Species	Metal	Substrate	Co-substrate	Open/closed	AA in/out	Ref
1MLW	TPH1	c	*Human*	Fe^{3+}	-	BH_2	Open	In	[243]
3E2T	TPH1	c	*Chicken*	Fe^{3+}	L-tryptophan	imidazole	Closed	Out	[244]
3HF6	TPH1	c	*Human*	Fe^{3+}	Inhibitor A	*	No density	-	[245]
3HF8	TPH1	c	*Human*	Fe^{3+}	Inhibitor B	*	No density	-	[245]
3HFb	TPH1	c	*Human*	Fe^{3+}	Inhibitor C	*	No density	-	[245]
5J6D	TPH1	c	*Human*	Fe^{3+}	Inhibitor D	TRIS, *	Closed	In**	[246]
5I01	TPH1	c	*Human*	Fe^{3+}	Inhibitor E	*	Open	Out**	[247]
5TPG	TPH1	c	*Human*	Fe^{3+}	Inhibitor F	TRIS, *	No density	-	[247]
4V06	TPH2	c/t	*Human*	Fe^{3+}	-	imidazole	Open	Out	-

BH_2: 7,8-dihydrobiopterin, TRIS: 2-amino-2-hydroxymethyl-propane-1,3-diol, Inhibitor A: 4-(4-amino-6-{[(1R)-1-naphthalen-2-ylethyl]amino}- 1,3,5-triazin-2-yl)-L-phenylalanine, Inhibitor B: 4-{2-amino-6-[(1R)-2,2,2-trifluoro-1-(3'- fluorobiphenyl-4-yl)ethoxy]pyrimidin-4-yl}- L-phenylalanine, Inhibitor C: 4-(5-{[(2'-methylbiphenyl-2-yl)methyl]amino}pyrazin- 2-yl)-L-phenylalanine, Inhibitor D: 4-[(N-{[2-(3-methoxyphenoxy)-6-(piperidin- 1-yl)phenyl]methyl}carbamimidoyl)carbamoyl]- L-phenylalanine, Inhibitor E: (3~{S})-8-[2-azanyl-6-[(1~{R})-1-(4-chloranyl- 2-phenyl-phenyl)-2,2,2-tris(fluoranyl)ethoxy]pyrimidin- 4-yl]-2,8-diazaspiro[4.5]decane-3-carboxylic acid, Inhibitor F: (3S)-8-(2-amino-6-{(1R)-1-[5-chloro-3'-(methylsulfonyl)[1,1'- biphenyl]-2-yl]-2,2,2-trifluoroethoxy}pyrimidin- 4-yl)-2,8-diazaspiro[4.5]decane-3-carboxylic acid.

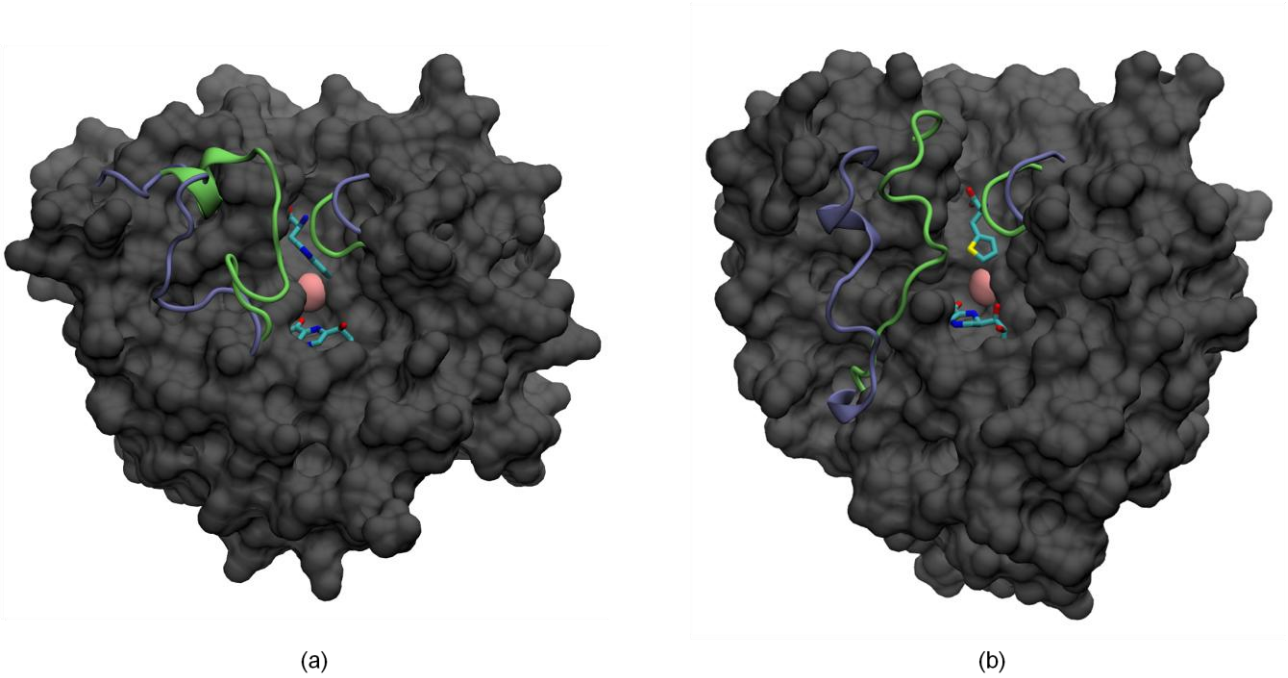

Figure 7.4. Representations of closed and open structures of tryptophan hydroxylase and phenylalanine hydroxylase. (a) Relative positions of the active site loops Leu123-Asp138 and Ile366-Thr368 in *chicken* cTPH1 (PDB entry: 3E2T) in which substrate tryptophan and imidazole are bound (green loops) and in c*h*TPH1 (PDB entry: 1MLW) in which BH_2 is bound (blue loops). (b) Relative positions of the active site loops Asn133-His146 and Val379-Phe382 in c*h*PAH (PDB entry: 1KW0) in which substrate analogue 3-(2-thienyl)-L-alanine and BH_4 are bound (green loops) and in c*h*PAH (PDB entry: 1J8U) in which BH_4 is bound (blue loops). Iron is shown in pink, substrate and co-substrate in cyan. For illustration, the binding pockets include (co-)substrate/(co-)substrate analogue.

7.1.3.2 Active site loops of PAH

In total, 41 crystal structures including the catalytic domain of PAH have been deposited in the PDB. Hence, more structural information has been gathered on the active site loop of PAH.

In PAH, binding of BH_4 causes only subtle structural changes in the BH_4 binding pocket and no large structural changes are observed.[266] However, binding of BH_4 and an L-phenylalanine analogue in PAH results in large structural changes, Figure 7.4 b.[267,268] The structural changes are primarily in the active site loop containing residue 133-141, which is found to close around the active site corresponding to the observation in TPH1.

In all structures of PAH, this loop either exists in an open or closed conformation dependent upon active site occupancy, Table 7.2. In Table 7.2, only crystal structures from mammalian sources are presented. The remaining structures are of PAH from *Chromobacterium violaceum*, *Colwellia psychrerythraea*, *Legionella pneumophila*, or *Dictyostelium discoideum*. The active site loop regions of structures from these species are not conserved and will therefore not be considered. A table which includes these structures can be found in Appendix H.

Table 7.2. Crystal structures of phenylalanine hydroxylase from mammalian species. In the header, substrate and co-substrate refers to presence of a (co-)substrate/(co-)substrate analogue in their respective binding sites. Open/closed refers to an open or closed conformation of the active site loops. AA in/out refers to Phe138 pointing towards the active site or away from active site. *: lack residues 137-139.

PDB entry	Domain(s)	Species	Metal	Substrate	Co-substrate	Open/closed	AA in/out	Ref
1PAH	c	*Human*	Fe^{3+}	-	-	Open	Out	[271]
3PAH	c	*Human*	Fe^{3+}	-	D-adrenaline	Open	Out	[272]
4PAH	c	*Human*	Fe^{3+}	-	L-norepinephrine	Open	Out	[272]
5PAH	c	*Human*	Fe^{3+}	-	L-dopamine	Open	Out	[272]
6PAH	c	*Human*	Fe^{3+}	-	L-DOPA	Open	Out	[272]
1PHZ	r/c	*Rat*	Fe^{3+}	-	-	No density	-	[273]
2PHM	r/c	*Rat*	Fe^{3+}	-	-	No density	-	[273]
2PAH	c/t	*Human*	Fe^{3+}	-	-	No density	-	[274]
1DMW	c	*Human*	Fe^{3+}	-	BH_2	Open	Out	[265]
1J8T	c	*Human*	Fe^{2+}	-	-	Open	Out	[266]
1J8U	c	*Human*	Fe^{2+}	-	BH_4	Open	Out	[266]
1LRM	c	*Human*	Fe^{3+}	-	BH_2	Open	Out	-
1KW0	c	*Human*	Fe^{2+}	3-(2-thienyl)-L-alanine	BH_4	Closed	In	[267]
1MMK	c	*Human*	Fe^{2+}	3-(2-thienyl)-L-alanine	BH_4	Closed	In	[268]
1MMT	c	*Human*	Fe^{2+}	L-norleucine	BH_4	Closed	In	[268]
1TDW	c	*Human*	Fe^{3+}	-	-	Open	Out	[275]
1TG2	c	*Human*	Fe^{3+}	-	BH_2	Open	Out	[275]
4ANP	c	*Human*	Fe^{3+}	-	Compound 1	Open	Out	[276]
5DEN	r/c/t	*Rat*	Fe^{3+}	-	-	No density	-	[277]
5EGQ	r/c/t	*Rat*	-	-	-	No density	-	[278]
5FGJ	r/c/t	*Rat*	Fe^{3+}	-	-	Open*	-	[278]

BH_2: 7,8-dihydrobiopterin, BH_4: 5,6,7,8-tetrahydrobiopterin, Compound 1 (pharmacological chaperone): 5,6-dimethyl-3-(4-methyl-2-pyridinyl)-2-thioxo-2,3-dihydrothieno[2,3-d]pyrimidin-4(1H)-one.

Table 7.2 shows that structures of mammalian PAH exist in an open conformation, unless iron, L-phenylalanine analogue, and BH_4 are present. In contrast to the catalytic domain, there is no crystal structure of full-length PAH which includes substrates. However, a similar functional importance of the loop has been found in the catalytic domain and the full-length tetramer.[269] This is further supported by a spectroscopic study on full-length *h*PAH.[270]

7.1.3.3 Active site loops of TH

The corresponding active site loop of TH comprises residues 178-193. Three crystal structures including the catalytic domain of TH reside in the PDB, Table 7.3. As was the case with PAH, no significant structural differences are detectable between *rat* TH with no substrates (PDB entry: 1TOH) [279] and with BH_2 (PDB entry: 2TOH) [280]. However, TH with no substrates do not have density in the active side loop [279], while TH with BH_2 has density in most of the loop but miss residue 183 to 185 [280]. The conformation of the part of the loop which is resolved, resembles the conformation of the loop observed in the PAH with BH_4 bound (open conformation). The last crystal structure is from *human* and comprises the catalytic and tetrameric domains and include a Zn^{2+} atom in the active site (PDB entry: 2XSN). The active site loop in this structure neither adopts an open nor closed conformation, but something in between. No publication follows the structure.

Table 7.3. Crystal structures of tyrosine hydroxylase. In the header, substrate and co-substrate refers to presence of a (co-)substrate/(co-)substrate analogue in their respective binding sites. Open/closed refers to an open or closed conformation of the active site loops. AA in/out refers to Tyr184 pointing towards the active site or away from active site. *No electron density for residue 183-185. **Not as open as observed in PAH (PDB entry: 1J8U) or TPH (PDB entry: 1MLW).

PDB entry	Domain(s)	Species	Metal	Substrate	Co-substrate	Open/closed	AA in/out	Ref
1TOH	c/t	*Rat*	Fe^{3+}	-	-	No density	-	[279]
2TPH	c/t	*Rat*	Fe^{3+}	-	BH_2	Open*	-	[280]
2XSN	c/t	*Human*	Zn^{2+}	-	-	Open**	In	-

BH_2: 7,8-dihydrobiopterin.

Tyrosine in the center of the active site loop

It is well established that open and closed conformations of the AAAHs exist. However, information regarding the role of this loop TPH is very scarce. Again, more information has been gathered on the other two members of the enzyme family.

In TH, the importance of this loop has been investigated by alanine-scanning. It was found that residues in the center of the loop, especially Phe184 (corresponding to Tyr125 in TPH1), have an effect on the kinetic parameters.[281] Phe184 was found to be important for substrate binding and catalysis, as a F184A mutation resulted in a 20-fold decrease in V_{max} and a 4-fold decrease in $K_{m,Tyr}$.[281] Further, the mutation resulted in a decrease from 37 ± 7 to 21 ± 3 in $K_{m,6\text{-}MePH4}$, and increased unproductive breakdown of the hydroxylating intermediate.[281]. Fluorescence anisotropy experiments on TH, in which Phe184 was mutated to a tryptophan, showed that binding of a BH_4 analogue resulted in decreased mobility of this residue.[282] This was interpreted as a closure of the active site loop, which contradicts observations from the crystal structures.

The function of the corresponding residue Tyr138 in *human* PAH has very recently been investigated.[269] Mutation of this residue results in reduced V_{max} and catalytic efficiency ($k_{cat}/[S]_{0.5}$) in both full-length and isolated catalytic domain of PAH.[269] Tyr138 is also found to play a role in the L-phenylalanine induced substrate activation for PAH. Furthermore, it is suggested that Gln134-Ile135 and Asp143-Ala144 act as hinge regions for the active site loop.[269]

7.2 Sequence and structural analysis of the active site loop of TPH

From studies on TH and PAH, it has been deduced that the loop, and especially the aromatic amino acid in the center of the loop, is important for the kinetics of the enzymes. The corresponding residues in TPH1 and 2 are Tyr125 and Tyr171, respectively. The significance of these residues has not previously been investigated. In the following sections, sequence and structural analyses are presented with the purpose of identifying possible explanations to the different kinetic properties of the two TPH isoforms.

7.2.1 Structural differences of the TPH isoforms

The TPH isoforms have a sequence identity of 81 % in the catalytic domains and their crystal structures show an $RMSD_{C\alpha}$ of only 1.1 Å. Despite these similarities, the isoforms display very different kinetic properties.

The kinetic differences might originate from non-conserved residues in the catalytic site. The sequences were therefore aligned to identify non-conserved residues, Figure 7.5. From the sequence alignment is seems that non-conserved residues are scattered over the entire sequence, but lower conservation is seemingly observed towards the terminals. The result of the alignment was depicted on the tertiary structure of c*h*TPH1 to visualize if some of the non-conserved residues were located in the active site or confined to specific locations on the structure. Figure 7.6 illustrates the structural positions of the 19 % non-conserved residues (in orange) in the catalytic domains of the *human* TPH isoforms.

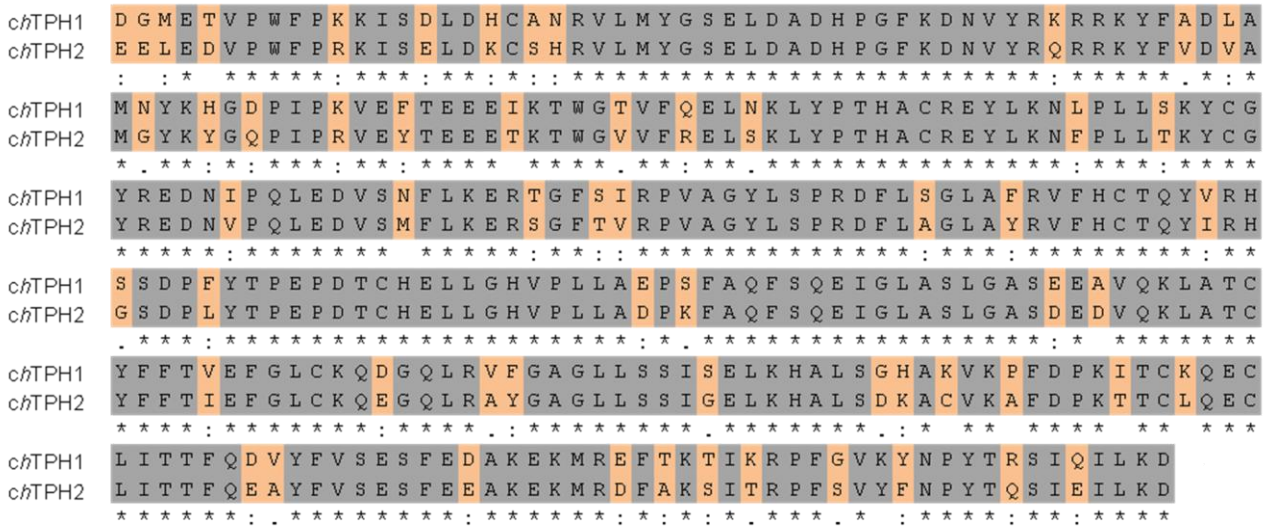

Figure 7.5. Clustal Omega alignment of c*h*TPH1 and c*h*TPH2. Conserved residues are shown in gray and non-conserved residues are shown in orange.

It appears that the non-conserved residues are randomly distributed mainly on the surface of the protein. To determine the degree of conservation in the active site, residues within 10 Å of the active site iron were investigated. Figure 7.6 shows that the conservation of residues within the catalytic sites is very high. Within 10 Å of the active site iron, only 2 (red residues) out of 37 residues are not conserved, and these residues are distant from the binding pockets of the substrate and co-substrate.

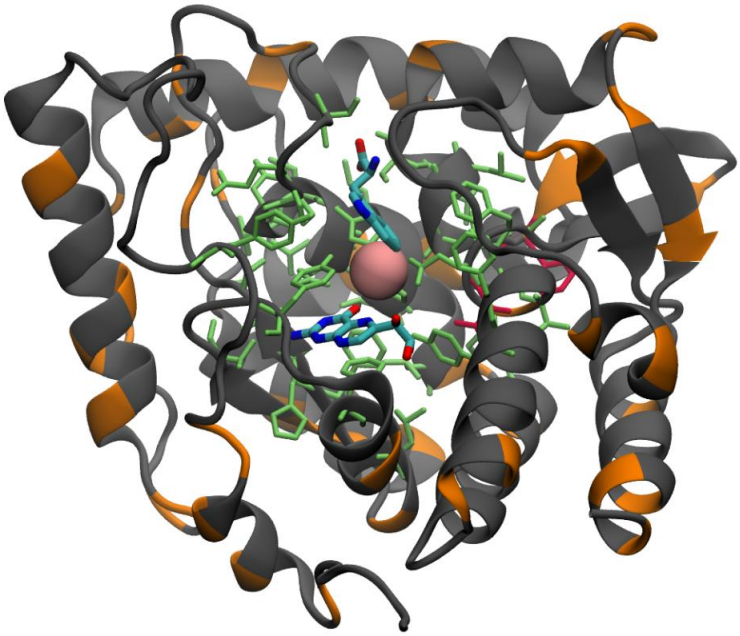

Figure 7.6. Crystal structure of *human* c*h*TPH1 with BH_2 and iron (PDB entry: 1MLW) and L-tryptophan (superimposed from *chicken* TPH1, PDB entry: 3E2T [244]). Orange secondary structure indicates the position of non-conserved residues and gray indicates conserved residue positions between the isoforms. Residues in red or green are non-conserved or conserved residues within 10 Å of active site iron, respectively. For illustration, the binding pockets include substrate and co-substrate analogue.

Figure 7.6 shows that the kinetic differences are most likely not explained by non-conserved residues in the active site, as these are neither clustered in one area nor located close to the substrate or co-substrate binding sites. The alignment does, however, not reveal anything about the position and orientation of residues. Therefore, differences in the crystal structures of the isoforms determined by $RMSD_{C\alpha}$ were analyzed in Figure 7.7. In Figure 7.7, high and low structural similarities are colored green and red, respectively.

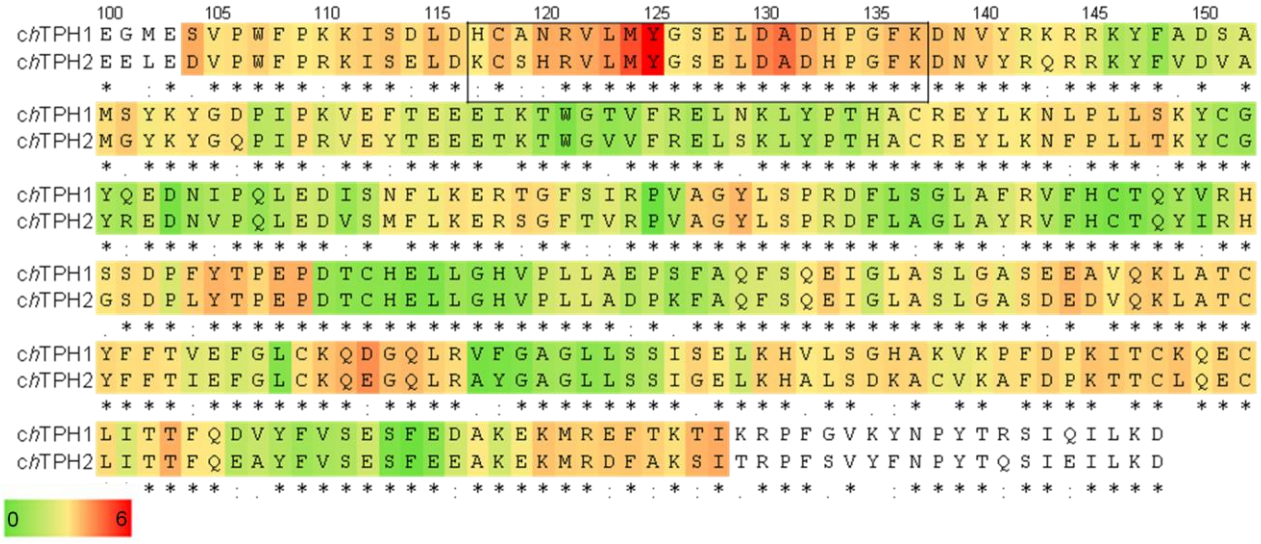

Figure 7.7. Sequence alignment of the catalytic domains of TPH1 and TPH2 (Clustal Omega 1.2.3 - * = identical, : = very similar, . = similar). The color scale (green is low and red is high) in the alignment shows the RMSD (unit Å) of the C_α-atoms calculated based on c*h*TPH1 (PDB entry: 1MLW) and c*h*TPH2 (PDB entry: 4V06). The black box indicates the sequence of the active site loop. The numbering of the sequence is based on TPH1.

Figure 7.7 shows that a stretch of sequence with high sequence identity displays relatively high $RMSD_{C\alpha}$-values compared to the rest of the structure. This stretch corresponds to the loop lining the active site, Figure 7.8. Especially tyrosine 125 in the center of the loop displays a high $RMSD_{C\alpha}$-value (5.2 Å) despite the fact that both structures are in open conformations. This loop spans residue 117-137 of TPH1 and 163-183 of TPH2.

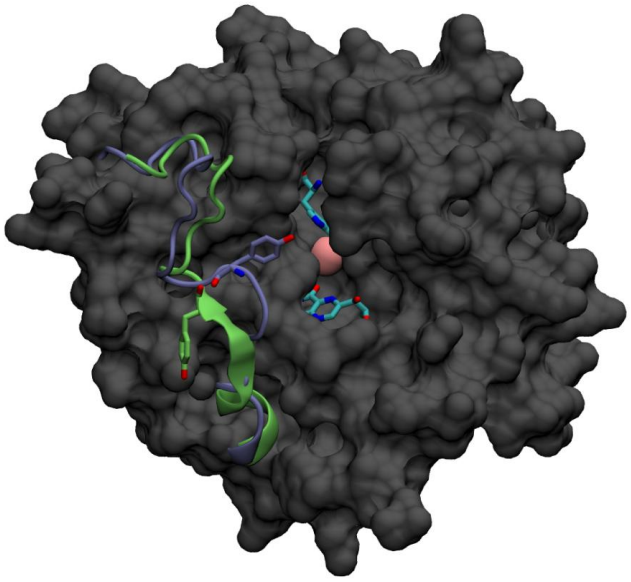

Figure 7.8. Crystal structure of c*h*TPH1 (PDB entry: 1MLW) with gray surface. The active site loop of c*h*TPH1 is shown in green with Tyr125 displayed as sticks and the loop of c*h*TPH2 (superimposed from PDB entry: 4V06) is shown in blue with Tyr171 displayed as sticks. In the active site, L-tryptophan (superimposed from PDB entry: 3E2T) and BH_2 are shown as sticks, and iron is shown as a pink sphere. For illustrative purposes, the binding pockets include substrate and co-substrate analogue.

Figure 7.8 shows that both isoforms are in an open conformation but the side chain of the tyrosine residue in the center of the loop is oriented towards the active site in c*h*TPH1 and is pointing away from the active site in ct*h*TPH2. To verify these different orientations, the structures of the loops and the orientation of the tyrosine residues, in the crystal structures, were assessed by B-factor and electron density in the loops.

A high value of the B-factor is associated with high mobility and low crystallographic resolution.[283] Figure 7.9 shows the B-factors obtained from the PDB-files of the crystal structures of c*h*TPH1 (PDB entry: 1MLW, 1.71 Å resolution) and ct*h*TPH2 (PDB entry: 4V06, 2.63 Å resolution). The average B-factor of the C_α-atoms in c*h*TPH1 is 23.0 $Å^2$ while for the loop it is 30.0 $Å^2$ (Tyr125 is 30.3 $Å^2$). In ct*h*TPH2, the average B-factor of the C_α-atoms is 64.1 $Å^2$ while for the loop it is 54.8 $Å^2$ (Tyr171 is 53.0 $Å^2$). In c*h*TPH1 the B-factor of the loop is slightly higher than the average value, while in ct*h*TPH2 the value is lower than the average. Based on the B-factors, the orientations of the loops of the isoforms seem to be well ordered.

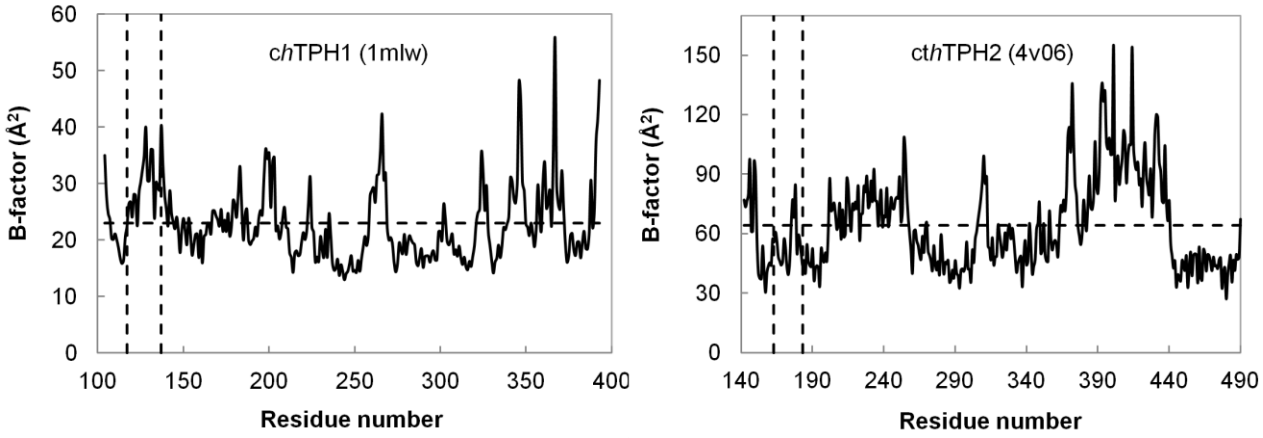

Figure 7.9. B-factor of the crystal structure of c*h*TPH1 (PDB entry: 1MLW, 1.71 Å resolution) and ct*h*TPH2 (PDB entry: 4V06, 2.63 Å resolution). The horizontal dashed lines represent the average B-factor of the structures and the vertical dashed lines represent the loop boarders.

The electron densities were also investigated to further assess the structure in the loop regions, Figure 7.10. The $2F_o$-F_c electron density maps of the crystal structures show that the structures of the loops in both isoforms are well resolved.

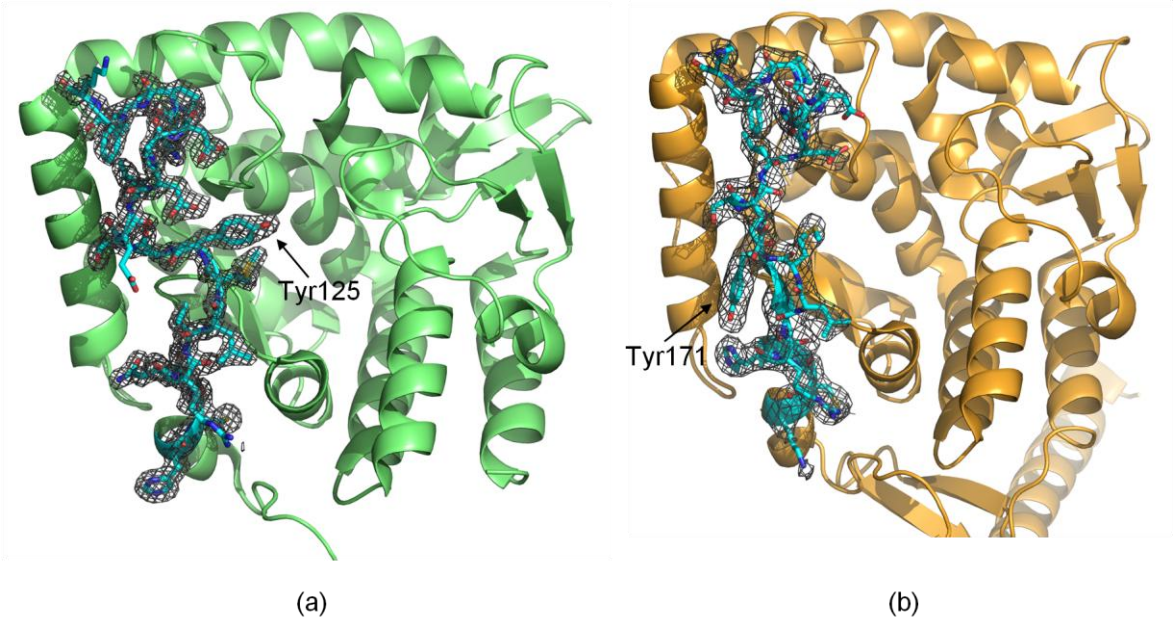

Figure 7.10. Density in the active site loops of the TPH isoforms. (a) Crystal structure of TPH1 (PDB entry: 1MLW) with $2F_o$-F_c density map on the loop comprising residue 117 to 137. (b) Crystal structure of TPH2 (PDB entry: 4V06, chain A) with $2F_o$-F_c density map on the loop comprising residue 163 to 183. The mesh map of the loop is contoured at 1.0 σ and within 1.6 Å of the selected atoms.

Judged from the B-factors and the electron densities of the active site loops, the orientation of the loops and Tyr125/171 seem to be well defined.

7.2.2 Mutations of tyrosine in the active site loop

In the previous section, it was identified that a tyrosine residue in the center of the active site loop has different orientations in the open conformation of the two TPH isoforms. It is also known that the

corresponding residue in TH and PAH has a profound influence on the kinetic properties of the hydroxylases. It was investigated whether this residue might have different roles on the kinetic properties in the two TPH isoforms, as a consequence of their different orientations. To decipher the role of the tyrosine residue it was mutated in both TPH isoforms. The identification of suitable residues for mutation is presented in chapter 8.

The tyrosine residues in both isoforms were mutated to alanine, leucine, or tryptophan. Each variant was expressed in *E. coli* and purified to homogeneity without complications (chapter 2). The variants are referred to as Y125A-c*h*TPH1, Y125L-c*h*TPH1, Y125W-c*h*TPH1, Y171A-c*h*TPH2, Y171L-c*h*TPH2, and Y171W-c*h*TPH2 in the following. All these variants elute as mono-disperse monomers (chapter 4) and have identical thermostability (chapter 3).

7.3 Substrate inhibition of TPH

In chapter 4, it is described that the isoforms of TPH has a sequence identity in the catalytic domain of 81 % and shown that the catalytic domains of both isoforms prevail as monomers. Despite these similarities, the isoforms have been shown to display very different kinetic properties. Especially, one feature of the kinetic discrepancies is interesting; TPH1 exhibits significant substrate inhibition while TPH2 does not.

Full-length *human* TPH1 has been found to be substrate tryptophan inhibited.[251] Direct comparison of the *human* TPH1 variants; full-length *h*TPH1, ct*h*TPH1, and rc*h*TPH1 shows that all variants exhibit comparable substrate inhibition.[259] Similar observations have been made in TH, where substrate inhibition was retained after deletion of the regulatory domain (NΔ132 or NΔ157) or deletion of both the regulatory and tetramerization domain (NΔ157/CΔ43).[284] This implies that the inhibition mechanism does not involve the tetramerization or regulatory domains. A study on the catalytic domains of both isoforms showed that only isoform 1 displays substrate tryptophan inhibition.[252] The substrate inhibition constant, K_i, was determined to 72 ± 7 µM.[252] Substrate inhibition has similarly been identified in the catalytic domain of *rabbit* TPH1, where a K_i-value of 146 ± 14 µM was obtained.[253]

While it is clear that TPH1 is substrate inhibited it is less so for TPH2. Conflicting results have been reported for substrate tryptophan inhibition of *human* TPH2. Several studies have found that *h*TPH2 is not subjected to substrate inhibition [260,262,263], while others have found inhibition constants of 418 ± 107 µM [261] or 970 ± 328 µM [254]. When the isoforms are directly compared in the same study, it was found that TPH1 displays a ~2.5 fold lower K_i compared to *h*TPH2.[254] A variety of enzymes are substrate inhibited, but only at substrate concentrations much greater than what is observed *in-vivo*.[285] Judged from the very high K_i-values, this is probably the case for TPH2. In contrast, the observed K_i-values of TPH1 are in a physiologically relevant range.[286]

7.4 Steady-state kinetics results of c*h*TPH variants

Steady-state kinetic measurements were conducted on c*h*TPH1, c*h*TPH2, and the mutant variants in which the tyrosine residue in the center of the active site loop was mutated to alanine, leucine, or tryptophan. The experimental procedure and data analysis utilized to determine the kinetic parameters are described in chapter 6. To enable comparison, the non-varied substrate concentrations were chosen based on previous measurements performed by M. S. Nielsen.[287] The oxygen concentration was fixed at 500 µM, L-tryptophan at 70 µM, and BH_4 at 300 µM. In this section, apparent kinetic parameters are determined given that saturated concentrations of the non-varied substrates are not obtained. Saturated condition cannot be achieved because O_2 has limited solubility, BH_4 has a strong absorption at the excitation wavelength used in the assay, and L-tryptophan displays substrate inhibition.

c*h*TPH1 is purified at pH 8.0 and c*h*TPH2 is purified at pH 7.0. To compare the isoforms, the kinetic measurements were conducted in the same buffer solution (pH 7.0) in the kinetic assay. It was found that

c*h*TPH1 has a 50 % (n = 3) higher activity at pH 7.0 compared to at pH 8.0 (data not shown). At low BH_4 concentrations very high values of intensity/min were observed. It was tested if different results were obtained at a lower photomultiplier tube voltage. Within statistical error, the same kinetic parameters were determined at 650 V and 585 V (data not shown). In the following all measurements were therefore conducted at 650 V.

The results of the steady-state kinetic measurements are presented in Figure 7.11 and Table 7.4. In agreement with results obtained by Windahl *et al.*[252], c*h*TPH1 displays substrate inhibition while c*h*TPH2 does not. At these substrate concentrations, a substrate inhibition constant, K_i, of 165 ± 18 µM was obtained for c*h*TPH1. Furthermore, it was also confirmed that c*h*TPH1 displays a 10-fold higher $K_{m,BH4}$ compared to c*h*TPH2.

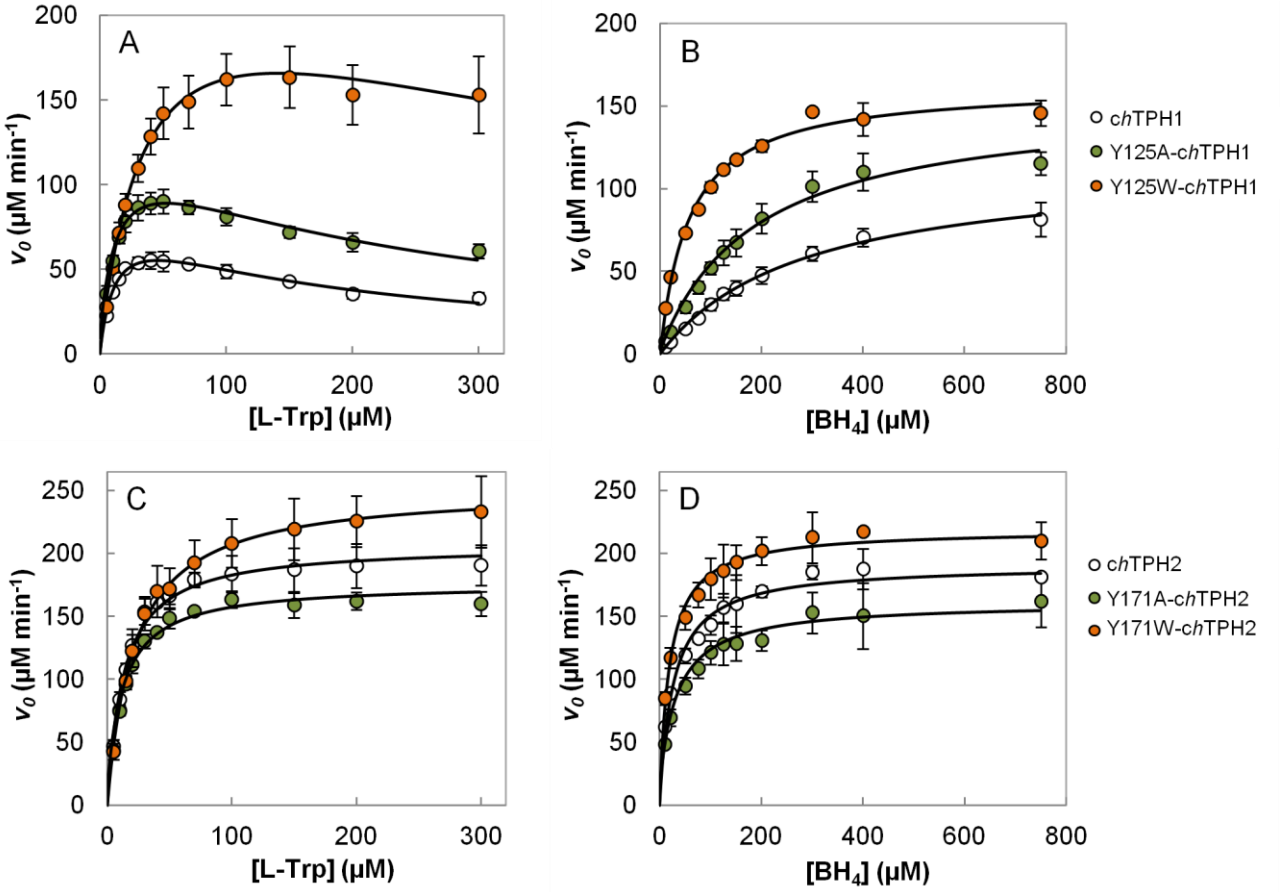

Figure 7.11. Initial rates of c*h*TPH1 variants (panel A and B) and c*h*TPH2 variants (panel C and D) as function of L-tryptophan or BH_4 concentration. Each measurement is reported as an average with standard deviation of three to five independent experiments. The TPH concentration was 0.8 µM in all measurements.

Initial studies showed that the mutant variant Y125L-c*h*TPH1 displayed the same kinetic parameters (data not shown) as Y125A-c*h*TPH1, but resulted in lower purification yields (chapter 2). For this reason, Y125L-c*h*TPH1 will not be considered in the following.

Panel A and B of Figure 7.11 show that the mutations of Tyr125 in c*h*TPH1 to alanine or tryptophan have a big impact on the kinetic plots. The plots were fitted with either the Michaelis Menten (eq. 1, chapter 6) equation or a modified version which considers substrate inhibition (eq. 2, chapter 6). The derived kinetic parameters are summarized in Table 7.4. Mutation to alanine results in a ~35 % reduction of $K_{m,BH4}$, while mutation to tryptophan results in a 5-fold reduction. The Y125W-c*h*TPH1 also induce a change in $K_{m,Trp}$.

The mutations also have an effect on the apparent tryptophan inhibition constant, K_i. Mutation to alanine increases the K_i-value by ~40 % while mutation to tryptophan results in a greater than 3-fold increase. Hence, mutations of Tyr125 in the active site loop significantly reduce the substrate inhibition observed in c*h*TPH1. This reduced substrate inhibition is obvious from panel A in Figure 7.11.

Beside the reduced $K_{m,BH4}$ and increased K_i-values, $k_{cat,Trp}$ is also found to change with the mutations. $k_{cat,Trp}$ is increased by 50 % and 3-fold by mutation to alanine and tryptophan, respectively.

Table 7.4. Kinetic parameters of c*h*TPH1 and c*h*TPH2 and mutation variants. Parameters are given as averages with standard deviations of at least three independent experiments from at least two purification batches. **: $p<0.01$, *: $p<0.05$ compared to wild-type.

	L-tryptophan			BH_4	
Variant	k_{cat} (µM min^{-1})	K_i (µM)	K_m (µM)	K_m (µM)	k_{cat} (µM min^{-1})
c*h*TPH1	108 ± 10	165 ± 18	12.7 ± 1.4	285 ± 15	145 ± 17
Y125A-c*h*TPH1	164 ± 10**	227 ± 21*	12.6 ± 0.5	188 ± 19**	192 ± 13*
Y125W-c*h*TPH1	315 ± 55**	544 ± 126**	36.7 ± 4.6**	57 ± 5**	203 ± 9*
Loop-swap-c*h*TPH1	178 ± 12**	189 ± 27	13.9 ± 2.7	240 ± 42	191 ± 18*
c*h*TPH2	258 ± 20	-	13.1 ± 1.3	26.7 ± 0.9	239 ± 12
Y171A-c*h*TPH2	220 ± 9	-	12.1 ± 1.3	31.1 ± 6.0	201 ± 27
Y171W-c*h*TPH2	315 ± 34	-	21.7 ± 1.5**	19.2 ± 3.4	274 ± 16
Loop-swap-c*h*TPH2	212 ± 4	497 ± 54	14.0 ± 0.7	37.6 ± 8.1	145 ± 8**

For c*h*TPH2, mutations from tyrosine to alanine or tryptophan do not result in any significant changes in the kinetic parameters, apart from an increase in $K_{m,Trp}$ for Y171W-c*h*TPH2. These observations correlate well with the different orientations of the tyrosine residue seen in the two crystal structures in Figure 7.8. In c*h*TPH1, the tyrosine residue is in vicinity of the active site and influences the kinetics of the enzyme, whiles in c*h*TPH2 the tyrosine residue point away from the active site which results in a less pronounced effect on the kinetics.

7.4.1 Steady-state kinetics – Loop-swap mutations

Mutations of the tyrosine residue in the center of the active site loop have different outcome on the kinetics of TPH1 and TPH2. This is most likely explained by the different orientations of the tyrosine residue, suggesting that the active site loops play different roles in the isoforms. It was therefore investigated how come this residue faces the active site in TPH1, while pointing away from the active site in TPH2.

Figure 7.7 shows that of the 21 residues in the active site loops, only three residues are not conserved between isoform 1 and 2. These residues are positioned at the very beginning of the loop, Figure 7.12. To examine whether these residues contribute to the different orientations of the tyrosine residue, the three non-conserved residues in c*h*TPH1 were mutated to the corresponding residues of the c*h*TPH2 sequence and vice versa. In c*h*TPH1, His117, Ala119, and Asn120 were mutated to Lys, Ser, and His (variant referred to as loop-swap-c*h*TPH1), respectively, while the opposite mutations were performed in position 163, 165, and 166 of c*h*TPH2 (variant referred to as loop-swap-c*h*TPH2).

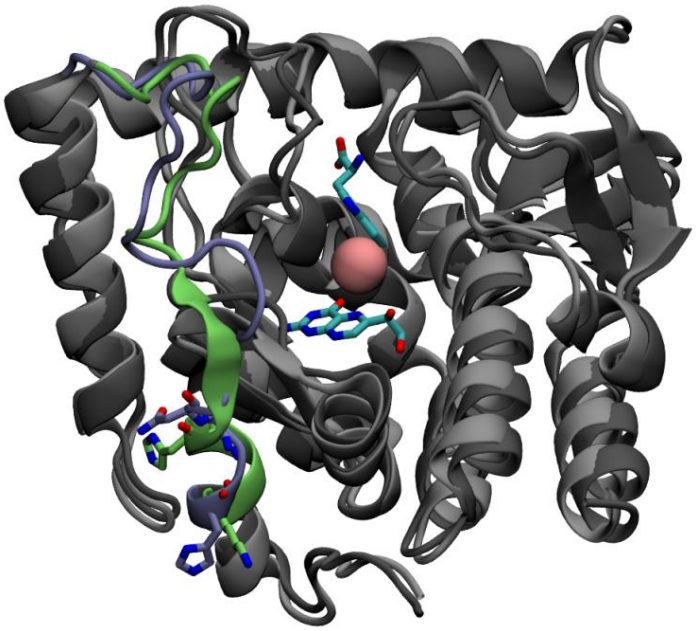

Figure 7.12. Loop-swap mutations in c*h*TPH1 and c*h*TPH2. Crystal structures of c*h*TPH1 (dark gray – PDB entry: 1MLW) and chTPH2 (light gray – PDB entry: 4V06). The active site loop of c*h*TPH1 is shown in green with His117, Ala119, and Asn120 displayed as green sticks and the loop of c*h*TPH2 is shown in blue with Lys163, Ser165, and His166 displayed as blue sticks. In the active site L-tryptophan (superimposed from PDB entry: 3E2T) and BH_2 are shown as sticks, and iron is shown as a pink sphere. For illustration, the binding pockets include substrate and co-substrate analogue.

The kinetic results of the loop-swap mutation are presented in Figure 7.13 and the kinetic parameters are summarized in Table 7.4. In c*h*TPH1, the loop-swap mutations result in only modest changes in the kinetic parameters. $k_{cat,Trp}$ is increased by 65 %, K_i is slightly increased, and $K_{m,BH4}$ is slightly decreased. The changes in the latter two parameters are statistically insignificant but change in the same fashion as observed for the Tyr125 mutations; $K_{m,BH4}$ decreases, K_i increases, and k_{cat} increases.

In c*h*TPH2, the loop-swap mutations similarly only introduce subtle changes to the kinetic parameters. $k_{cat,BH4}$ is increased and $K_{m,BH4}$ is slightly increased. However, the loop-swap mutations in c*h*TPH2 result in introduction of substrate tryptophan inhibition with a K_i-value of 497 ± 54 µM (Figure 7.13, panel C). In c*h*TPH1, K_i and $K_{m,BH4}$ seem to be inversely related. This correlates with the observations in loop-swap-c*h*TPH2 where $K_{m,BH4}$ is increased as substrate inhibition is observed.

These results strongly suggest that the inhibition mechanism, which is only observed for c*h*TPH1, can be traced to the loop lining the active site. The induced substrate inhibition suggests that the three mutations change the orientation of the loop. Its orientation might approach the orientation observed in c*h*TPH1, which enables it to participate in the inhibition mechanism.

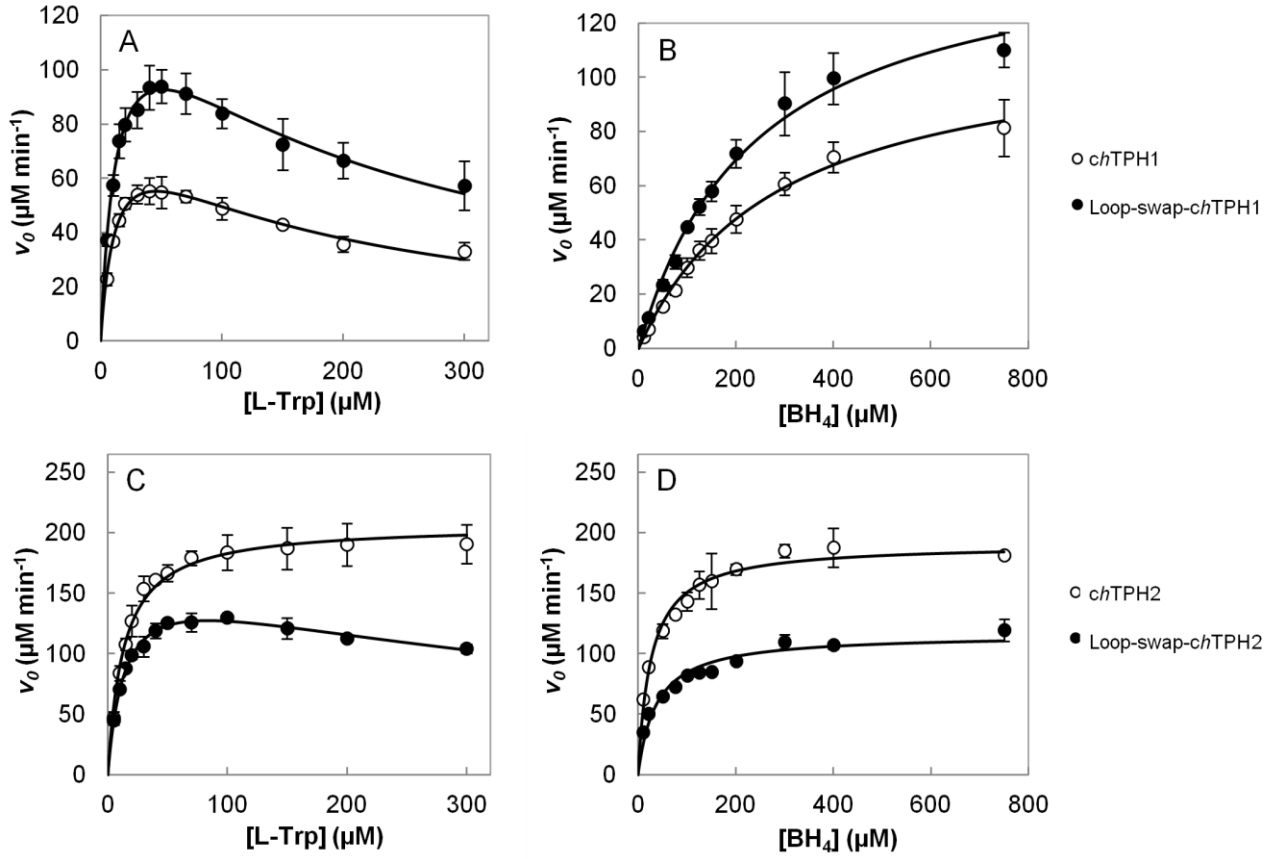

Figure 7.13. Initial rates of c*h*TPH1, loop-swap-c*h*TPH1 (panel A and B), c*h*TPH2, and loop-swap-c*h*TPH2 (panel C and D) as function of L-tryptophan or BH_4 concentration. Each measurement is reported as an average with standard deviation of three independent experiments. The TPH concentration was 0.8 µM in all measurements.

7.4.1.1 TPH active site loop conservation

The kinetic results of the loop-swap variants suggest that the non-conserved residues are important for the function of the loop in the isoforms. The degree of conservation was therefore analyzed. The conservation was analyzed using a logo plot [288] with sequences of TPH1 and TPH2 from 61 and 63 vertebrate species, respectively. The sequences of the TPH isoforms were obtained from an NCBI protein search “tryptophan 5 hydroxylase 1/2 AND vertebrates" accessed on 21.04.2017. The results are shown as a logo plot in Figure 7.14. The logo plot shows that the sequence of the entire loop is highly conserved among species, suggesting that this loop has a specialized function.

The sequence comparison across species shows that His117, Ala119, and Asn120 of TPH1 are 13, 100, and 97 % conserved, respectively (n = 61 vertebrates). In TPH2 Lys163, Ser165, and His166 are conserved 75, 100, and 33 %, respectively (n = 63 vertebrates). Of the residues in TPH1, Ala119 and Asn120 show a high degree of conservation, while for TPH2, Ser165 is highly conserved. This implies that these residues are important for proper loop orientation and function.

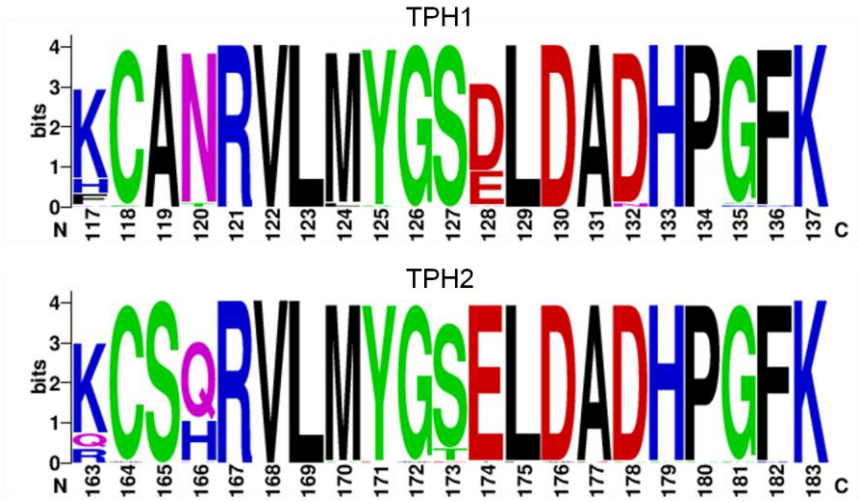

Figure 7.14. Logo plots of the loops lining the active sites of TPH1 (top) and TPH2 (bottom). The overall height of a column indicates the sequence conservation at a given position and the height of a symbol within the column indicates the relative frequency of that amino acid in that position.

7.5 Discussion

The kinetic data presented in this chapter shed light on the different kinetic properties that are displayed by the TPH isoforms despite their high sequence identity and tertiary structure. For wild-type c*h*TPH1 and c*h*TPH2 identical $K_{m,Trp}$-values and a 10-fold difference in $K_{m,BH4}$-values were obtained. Furthermore, a ~2-fold greater k_{cat} was observed for c*h*TPH2 compared to c*h*TPH1. These kinetic parameters correspond well with previous observations.[252] The observed substrate inhibition constant for c*h*TPH1 is also in agreement with previously determined values.[252,287]

The sequence and structural analyses of the two isoforms revealed that the biggest difference between the crystal structures is in the tyrosine residue in the active site loop. Mutation of this residue results in significant changes in the kinetic parameters of only c*h*TPH1. This implies that this residue has a functional importance in TPH1. This is supported by findings in PAH and TH where the corresponding residues Tyr138 and Phe184 have been found to be important for proper enzymatic function.[269,281]

Crystal structures of TPH and PAH have clearly revealed the presence of an open and a closed conformation. In the crystal structure of c*h*TPH1, the loop is in an open conformation and Tyr125 points towards the active site. From the crystal structures of PAH it is observed that the corresponding residue, Tyr138, is only oriented towards the active site in the closed conformation. Here, Tyr138 is only ~6 Å away from the iron atom resulting in a closed conformation [268] while the distance is ~10 Å in c*h*TPH1 (open confirmation). A similar conformation is observed in TH (PDB entry: 2XSN) where Phe184 is positioned in the loop facing the active site. The role of the loop closing mechanism is poorly understood. For PAH, it has been suggested that the closing mechanism might protect the co-substrate to enable a high degree of coupling efficiency.[269] Similarly, the loop in TH has been proposed to exclude water from the active site to avoid reaction between the hydroxylating intermediate and water molecules before hydroxylation of substrate takes place.[266,281,289] A similar functional importance is supported by the very high sequence conservation among vertebrate species observed for both TPH isoforms. The influence of the loop on the substrate inhibition mechanism is further investigated and discussed in chapter 8.

For PAH, it was predicted that residue 134-135 constitute a hinge region which facilitates movement of the active site loop.[269] This region corresponds to residue 121-122 in TPH1 and 167-168 in TPH2. This is very close to the non-conserved residues Ala119-Asn120 and Ser165-His166 which were mutated in this

study. This suggests that the loop-swap mutations were made in, or close to, one of the proposed hinge regions. It can be hypothesized that movement of the tyrosine residue in the loop requires a functional hinge region which is only observed in TPH1. The loop-swap mutations might have enhanced this hinge region, enabling loop movement, which might explain the induced substrate inhibition in loop-swap-c*h*TPH2.

Besides c*h*TPH1, substrate inhibition is also observed in TH. For TH, substrate inhibition is observed at tyrosine concentrations higher than 50 µM [290]. The tyrosine concentration in the brain has been found to vary as much as a factor of two.[291] Substrate inhibition of TH has been proposed to explain the lack of L-dopa concentration fluctuations as a consequence of increased tyrosine concentration upon food intake.[285] Tryptophan concentrations are around 60 µM in the blood [286] which is close to the tryptophan concentration at which the maximum velocity of TPH1 is achieved in this study. This suggests that substrate inhibition could play a role in the TPH1 regulation *in vivo*. It is possible that a corresponding mechanism observed for TH is ensuring that the production of 5-HT does not rise to high levels in the peripheral tissues, which is associated with several diseases.[292] The concentration of tryptophan in the brain is in the range of 25-35 µM [293] which is close to the observed $K_{m,Trp}$ of c*h*TPH2. The velocities of 5-HTP production and in turn serotonin production are, therefore, very sensitive to changes in brain tryptophan concentration.[293,294] This might explain the lack of substrate inhibition observed in TPH2, as rapid responses are desirable in the brain. It could be speculated that different regulatory mechanisms of the two isoforms have evolved to accommodate the diverse need for serotonin biosynthesis in different tissues.

7.6 Conclusion

Despite high sequence identity and very similar tertiary structure of the c*h*TPH isoforms, only c*h*TPH1 is substrate inhibited. In this chapter, it was presented how the orientations of a tyrosine residue in the active site loop are different in the isoforms. Steady-state kinetic results demonstrated that mutation of this residue only significantly change the kinetic parameters of c*h*TPH1, meaning that this residue have different properties in the two isoforms. The inhibition constant was significantly increased upon mutation of Tyr125, revealing that this residue, and hence the active site loop, plays a role in the inhibition mechanism. This was confirmed by the loop-swap mutations which introduced substrate inhibition in c*h*TPH2.

7.7 References

[243] Wang, L., Erlandsen, H., Haavik, J., Knappskog, P.M., and Stevens, R.C., 2002, Three-dimensional structure of human tryptophan hydroxylase and its implications for the biosynthesis of the neurotransmitters serotonin and melatonin, *Biochemistry 41(42)*, 12569-12574.

[244] Windahl, M. S., Petersen, C. R., Christensen, H. E. M., and Harris, P., 2008, Crystal structure of tryptophan hydroxylase with bound amino acid substrate, *Biochemistry 47*, 12087-12094.

[245] Cianchetta, G., Stouch, T., Yu, W., Shi, Z.-C., Tari, L. W., Swanson, R.V., Hunter, M.J., Hoffman, I.D., and Liu, Q., 2010, Mechanism of Inhibition of Novel Tryptophan Hydroxylase Inhibitors Revealed by Co-crystal Structures and Kinetic Analysis, *Curr. Chem. Genomics 4*, 19-26.

[246] Goldberg, D. R., De Lombaert, S., Aiello, R., Bourassa, P., Barucci, N., Zhang, Q., Paralkar, V., Stein, A. J., Valentine, J., and Zavadoski, W., 2016, Discovery of acyl guanidine tryptophan hydroxylase-1 inhibitors, *Bioorg. Med. Chem. Lett. 26*, 2855-2860.

[247] Goldberg, D. R., De Lombaert, S., Aiello, R., Bourassa, P., Barucci, N., Zhang, Q., Paralkar, V., Stein, A.J., Holt, M., Valentine, J., and Zavadoski, W., 2017, Optimization of spirocyclic proline tryptophan hydroxylase-1 inhibitors, *Bioorg. Med. Chem. Lett. 27,* 413-419.

[248] Jiang, G. C. T., Yohrling, G. J., Schmitt, I. V. J. D., and Vrana, K. E., 2000, Identification of Substrate Orienting and Phosphorylation Sites Within Tryptophan Hydroxylase Using Homology-based Molecular Modeling, *J. Mol. Biol. 302*, 1005-1017.

[249] McKinney, J., Teigen, K., Frøystein, N., Salaün, C., Knappskog, P. M., Haavik, J., and Martínez, A., 2001, Conformation of the Substrate and Pterin Cofactor Bound to Human Tryptophan Hydroxylase. Important Role of Phe313 in Substrate Specificity, *Biochemistry 40(51)*, 15591-15601.

[250] Daubner, S. C., Melendez, J., and Fitzpatrick, P. F., 2000, Reversing the substrate specificities of phenylalanine and tyrosine hydroxylase: aspartate 425 of tyrosine hydroxylase is essential for L-DOPA formation, *Biochemistry 39*, 9652–9661.

[251] McKinney, J., Knappskog, P. M., Pereira, J., Ekern, T., Toska, K., Kuitert, B. B., Levine, D., Gronenborn, A. M., Martinez, A., and Haavik, J., 2004, Expression and purification of human tryptophan hydroxylase from Escherichia coli and Pichia pastoris, *Protein Expr. Purif. 33*, 185–194.

[252] Windahl, M. S., Boesen, J., Karlsen, P. E., and Christensen, H. E. M., 2009, Expression, Purification and Enzymatic Characterization of the Catalytic Domains of Human Tryptophan Hydroxylase Isoforms, *Protein J. 28*, 400–406.

[253] Moran, G. R., Daubner, S.C., and Fitzpatrick, P. F., 1998, Expression and Characterization of the Catalytic Core of Tryptophan Hydroxylase, *J. Biol. Chem. 273*, 12259-12266.

[254] McKinney, J., Knappskog, P. M., and Haavik, J., 2005, Different properties of the central and peripheral forms of human tryptophan hydroxylase, *J. Neurochem. 92*, 311-320.

[255] Kowlessur, D. and Kaufman, S., 1999, Cloning and expression of recombinant human pineal tryptophan hydroxylase in Escherichia coli: purification and characterization of the cloned enzyme, *Biochim. Biophys. Acta 1434*, 317-330.

[256] D´Sa, C., Arthur, R. E., Jr., and Kuhn, D. M., 1996, Expression and deletion mutagenesis of tryptophan hydroxylase fusion proteins: delineation of the enzyme catalytic core, *J. Neurochem. 67*, 917-926.

[257] Nielsen, M. S., Petersen, C. R., Munch, A., Vendelboe, T. V., Boesen, J., Harris, P., and Christensen, H. E. M., 2008, A simple two step procedure for purification of the catalytic domain of chicken tryptophan hydroxylase 1 in a form suitable for crystallization, *Protein Expr. Purif. 57(2)*, 116-126.

[258] Tenner, K., Walther, D., and Bader, M., 2007, Influence of human tryptophan hydroxylase 2 N- and C-terminus on enzymatic activity and oligomerization, *J. Neurochem. 102(6)*, 1887–1894.

[259] Yang, X. J. and Kaufman, S., 1994, High-level expression and deletion mutagenesis of human tryptophan hydroxylase, *Proc. Natl. Acad. Sci. 91(14)*, 6659–6663.

[260] Carkaci-Salli, N., Flanagan, J. M., Martz, M. K., Salli, U., Walther, D.J., Bader, M., and Vrana, K. E., 2006, Functional Domains of Human Tryptophan Hydroxylase 2 (hTPH2), *J. Biol. Chem. 281*, 28105-28112.

[261] Winge, I., McKinney, J. A., Knappskog, P. M., and Haavik, J., 2007, Characterization of wild-type and mutant forms of human tryptophan hydroxylase 2, *J. Neurochem. 100*, 1648–1657.

[262] Cichon, S., Winge, I., Mattheisen, M., Georgi, A., Karpushova, A., Freudenberg, J., Freudenberg-Hua, Y., Babadjanova, G., Van Den Bogaert, A., Abramova, L. I., Kapiletti, S., Knappskog, P. M., McKinney, J., Maier, W., Jamra, R. A., Schulze, T. G., Schumacher, J., Propping, P., Rietschel, M., Haavik, J., and Nöthen, M. M., 2008, Brain-specific tryptophan hydroxylase 2 (TPH2): a functional Pro206Ser substitution and variation in the 5'-region are associated with bipolar affective disorder, *Hum. Mol. Genet. 17(1)*, 87-97.

[263] Winge, I., McKinney, J. A., Ying, M., D'Santos, C. S., Kleppe, R., Knappskog, P. M., and Haavik, J., 2008, Activation and stabilization of human tryptophan hydroxylase 2 by phosphorylation and 14-3-3 binding, *Biochem. J. 410(1)*, 195-204.

[264] Carkaci-Salli, N., Salli, U., Tekin, I., Hengst, J. A., Zhao, M. K., Gilman, T. L., Andrews, A. M., and Vrana, K. E., 2014, Functional characterization of the S41Y (C2755A) polymorphism of tryptophan hydroxylase 2, *J. Neurochem. 130(6)*, 748-758.

[265] Erlandsen, H., Bjørgo, E., Flatmark, T., and Stevens, R. C., 2000, Crystal structure and site-specific mutagenesis of pterin-bound human phenylalanine hydroxylase, *Biochemistry 39(9)*, 2208-2217.

[266] Andersen, O. A., Flatmark, T., and Hough, E., 2001, High resolution crystal structures of the catalytic domain of human phenylalanine hydroxylase in its catalytically active Fe(II) form and binary complex with tetrahydrobiopterin, *J. Mol. Biol. 314*, 279-291.

[267] Andersen, O. A., Flatmark, T., and Hough, E., 2002, Crystal structure of the ternary complex of the catalytic domain of human phenylalanine hydroxylase with tetrahydrobiopterin and 3-(2-thienyl)-L-alanine, and its implications for the mechanism of catalysis and substrate activation, *J. Mol. Biol. 320(5)*, 1095-1108.

[268] Andersen, O. A., Stokka, A. J., Flatmark, T., and Hough, E., 2003, 2.0 Å resolution crystal structures of the ternary complexes of human phenylalanine hydroxylase catalytic domain with tetrahydrobiopterin and 3-(2-thienyl)-L-alanine or L-norleucine: substrate specificity and molecular motions related to substrate binding, *J. Mol. Biol. 333(4)*, 747-757.

[269] Leandro, J., Stokka, A. J., Teigen, K., Andersen, O. A., and Flatmark, T., 2017, Substituting Tyr138 in the active site loop of human phenylalanine hydroxylase affects catalysis and substrate activation, *FEBS Open Bio 7(7)*, 1026-1036.

[270] Kemsley, J. N., Wasinger, E. C., Datta, S., Mitić, N., Acharya, T., Hedman, B., Caradonna, J. P., Hodgson, K. O., and Solomon, E. I., 2002, Spectroscopic and Kinetic Studies of PKU-Inducing Mutants of Phenylalanine Hydroxylase: Arg158Gln and Glu280Lys, *J. Am. Chem. Soc. 125*, 5677-5686.

[271] Erlandsen, H., Fusetti, F., Martinez, A., Hough, E., Flatmark, T., and Stevens, R.C., 1997, Crystal structure of the catalytic domain of human phenylalanine hydroxylase reveals the structural basis for phenylketonuria, *Nat. Struct. Biol. 4*, 995-1000.

[272] Erlandsen, H., Flatmark, T., Stevens, R.C., and Hough, E., 1998, Crystallographic analysis of the human phenylalanine hydroxylase catalytic domain with bound catechol inhibitors at 2.0 A resolution, *Biochemistry 37*, 15638-15646.

[273] Kobe, B., Jennings, I.G., House, C.M., Michell, B.J., Goodwill, K.E., Santarsiero, B.D., Stevens, R.C., Cotton, R.G., and Kemp, B.E., 1999, Structural basis of autoregulation of phenylalanine hydroxylase, *Nat. Struct. Biol. 6*, 442-448.

[274] Fusetti, F., Erlandsen, H., Flatmark, T., and Stevens, R.C., 1998, Structure of tetrameric human phenylalanine hydroxylase and its implications for phenylketonuria, *J. Biol. Chem. 273*, 16962-16967.

[275] Erlandsen, H., Pey, A. L., Gamez, A., Perez, B., Desviat, L. R., Aguado, C., Koch, R., Surendran, S., Tyring, S., Matalon, R., Scriver, C. R., Ugarte, M., Martinez, A., and Stevens, R.C., 2004, Correction of kinetic and stability defects by tetrahydrobiopterin in phenylketonuria patients with certain phenylalanine hydroxylase mutations, *Proc. Natl. Acad. Sci. 101*, 16903-16908.

[276] Torreblanca, R., Lira-Navarrete, E., Sancho, J., and Hurtado-Guerrero, R., 2012, Structural and Mechanistic Basis of the Interaction between a Pharmacological Chaperone and Human Phenylalanine Hydroxylase, *Chembiochem 13*, 1266-1269.

[277] Arturo, E. C., Gupta, K., Heroux, A., Stith, L., Cross, P. J., Parker, E. J., Loll, P. J., and Jaffe, E. K., 2016, First structure of full-length mammalian phenylalanine hydroxylase reveals the architecture of an autoinhibited tetramer, *Proc. Natl. Acad. Sci. 113*, 2394-2399.

[278] Meisburger, S. P., Taylor, A. B., Khan, C. A., Zhang, S., Fitzpatrick, P. F., and Ando, N., 2016, Domain Movements upon Activation of Phenylalanine Hydroxylase Characterized by Crystallography and Chromatography-Coupled Small-Angle X-ray Scattering, *J. Am. Chem. Soc. 138*, 6506-6516.

[279] Goodwill, K. E., Sabatier, C., Marks, C., Raag, R., Fitzpatrick, P. F., and Stevens, R.C., 1997, Crystal structure of tyrosine hydroxylase at 2.3 Å and its implications for inherited neurodegenerative diseases, *Nat. Struct. Biol. 4*, 578-585.

[280] Goodwill, K. E., Sabatier, C., and Stevens, R. C., 1998, Crystal structure of tyrosine hydroxylase with bound cofactor analogue and iron at 2.3 Å resolution: self-hydroxylation of Phe300 and the pterin-binding site, *Biochemistry 37*, 13437-13445.

[281] Daubner, S. C., McGinnis, J. T., Gardner, M., Kroboth, S. L., Morris, A. R., and Fitzpatrick, P. F., 2006, A Flexible Loop in Tyrosine Hydroxylase Controls Coupling of Amino Acid Hydroxylation to Tetrahydropterin Oxidation, *J. Mol. Biol. 359*, 299–307.

[282] Sura, G. R., Lasagna, M., Gawandi, V., Reinhart, G. D., and Fitzpatrick, P. F., 2006, Effects of Ligands on the Mobility of an Active-Site Loop in Tyrosine Hydroxylase as Monitored by Fluorescence Anisotropy, *Biochemistry 45*, 9632-9638.

[283] Lovell, S. C., Davis, I. W., Arendall, W. B. 3rd, de Bakker, P. I., Word, J. M., Prisant, M. G., Richardson, J. S., and Richardson, D. C., 2003, Structure validation by Calpha geometry: phi,psi and Cbeta deviation, *Proteins 50(3)*, 437–450.

[284] Ribeiro, P., Wang, Y., Citron, B. A., and Kaufman, S., 1993, Deletion Mutagenesis of Rat PC12 Tyrosine Hydroxylase Regulatory and Catalytic Domains, *J. Molec. Neurosci. 4(2)*, 125-139.

[285] Reed, M. C., Lieb, A., and Nijhout, H. F., 2010, The biological significance of substrate inhibition: A mechanism with diverse functions, *Bioessays 32*, 422–429.

[286] Breum, L., Rasmussen, M. H., Hilsted, J., and Fernstrom, J. D., 2003, Twenty-four–hour plasma tryptophan concentrations and ratios are below normal in obese subjects and are not normalized by substantial weight reduction, *Am. J. Clin. Nutr. 77*, 1112–1118.

[287] Nielsen, M.S., 2007, Expression, Purification and Characterisation of Tryptophan Hydroxylases, Ph.D. thesis, Department of Chemistry, Technical University of Denmark, Kgs. Lyngby.

[288] Crooks, G.E., Hon, G., Chandonia, J. M., and Brenner, S.E., 2004, WebLogo: A sequence logo generator, *Genome Research 14*, 1188-1190.

[289] Frantom, P. A. and Fitzpatrick, P. F., 2003, Uncoupled forms of tyrosine hydroxylase unmask kinetic isotope effects on chemical steps, *J. Am. Chem. Soc. 125(52)*, 16190-16191.

[290] Quinsey, N. S., Luong, A. Q., and Dickson, P. W., 1998, Mutational Analysis of Substrate Inhibition in Tyrosine Hydroxylase, *J. Neurochem. 71(5)*, 2132-2138.

[291] Fernstrom, J. D. and Faller, D. V., 1978, Neutral amino acids in the brain: changes in response to food ingestion, *J. Neurochem. 30*, 1531-1538.

[292] Amireault, P., Sibon, D., and Coté, F., 2013, Life without Peripheral Serotonin: Insights from Tryptophan Hydroxylase 1 Knockout Mice Reveal the Existence of Paracrine/Autocrine Serotonergic Networks, *Chem. Neurosci. 4,* 64−71.

[293] Fernstrom, J. and Fernstrom, M., 1995, Brain tryptophan concentrations and serotonin synthesis remain responsive to food consumption after the ingestion of sequential meals, *Am. J. Clin. Nutr. 61*, 312–319.

[294] Knott, P. J. and Curzon, G., 1972, Free Tryptophan in Plasma and Brain Tryptophan Metabolism, *Nature 239*, 452-453.

Chapter 8

In silico analysis - inhibition of *h*TPH1

In chapter 7, it was determined that c*h*TPH1 is substrate inhibited and that Tyr125 plays a significant role in the inhibition mechanism. In this chapter, molecular dynamics (MD) simulations are utilized in an attempt to understand the substrate inhibition mechanism on a structural level.

In the following, homology modeling and molecular dynamics simulations are briefly introduced, and the experimental procedures for building the initial TPH structures and setting up the MD simulations are presented. The resulting MD trajectories are analyzed in pursuit of understanding the underlying mechanism of substrate inhibition. Some of the results presented in this chapter have been included in a submitted manuscript. (Appendix A.2)

Outline

8.1 Homology modeling

To conduct a molecular dynamics simulation, a starting three-dimensional (3D) structure of the protein of interest is needed. In the absence of an experimental structure, homology modeling can be used to predict a 3D protein model, which will provide insight into the structure and function of the protein.[295]

In homology modeling, the tertiary structure of a protein is predicted based on the general observation that proteins with homologous sequences have similar structures. The longer and the more identical the sequence is, to that of an experimentally determined protein structure (template), the better the model. A protein domain with sequence identity >30 % is considered a homologous template.[296]

The process of homology modeling of a target protein consists of the following consecutive steps [297,298]; *i*) Identifying sequence homologues in the PDB utilizing a sequence search tool such as BLAST [299]. The most complete structure with the highest possible similarity score is chosen as a template. *ii*) Aligning the sequences of the target and template proteins using an alignment tool e.g. Clustal Omega [300]. *iii*) Building the model of the target protein based on the 3D structure of the template protein by transferring the position of every atom, which match in the sequence alignment. *iv*) Performing energy minimization to alleviate bad bond angles, atomic interactions, and to improve local geometries.

8.2 Molecular dynamics simulations

To investigate the structure-function relationship and dynamics of proteins on an atomic level, molecular dynamic simulations can be a useful tool. MD is a method based on classical mechanics which allows the description of large systems such as proteins or protein complexes on time scales typically of nano- to microseconds.[301] On this time scale e.g. atomic fluctuations, side-chain rearrangements, and loop movement can be observed.[302,303]

In MD simulations, the positions and momenta of all atoms in a system are calculated as a function of time by integrating Newton's equation of motion in discrete time steps. The equation of motion for a system consisting of N particles, which interact via a potential $\partial U(\vec{r}_i)$, $i = 1,\ldots,N$ can be formulated as follows [304]:

$$\vec{F}_i = \frac{d^2 \vec{r}_i}{dt^2} m_i \qquad \text{(eq. 1)}$$

where the forces are given as

$$\vec{F}_{i \to j} = -\nabla_{\vec{r}_i} U(r_{ij}) = -\frac{\partial U(r_{ij})}{\partial \vec{r}_i} \qquad \text{(eq. 2)}$$

In eq. 1 and 2, $U(r_{ij})$, m_i and $\vec{r}_i$ are the pair potential, mass and position of i'th atoms, respectively. In three dimensions, eq. 1 results in 3 N second-order differential equations. To numerically solve these equations to give $r(t)$, an integration algorithm is used which successively advances the system through discrete time steps.[305] Integration algorithms, such as the leap-frog [306] and velocity Verlet [307], are derived from Taylor expansions of the positions $r(t)$ and velocities $v(t)$. The different algorithms use different combinations of Taylor expansions of velocities $v(t)$, $v(t+\delta t)$, $v(t-\delta t)$.

In each integration cycle of e.g. the velocity Verlet algorithm, the first steps are to calculate the velocities one half time step ahead $v(t+\delta t/2)$ and then calculate the positions one time step ahead $r(t+\delta t)$. Then the accelerations one time step ahead $a(t+\delta t)$ are derived from the interaction potential using $r(t+\delta t)$. In the end of a cycle, the velocities one time step ahead $v(t+\delta t)$ are calculated from $v(t+\delta t/2)$ and $a(t+\delta t)$, and a new cycle can be initiated.[304]

The integration algorithm needs initial position and velocities for each atom in the system. The initial positions of the atoms are provided by the coordinate file extracted from e.g. a 3D protein structure from the PDB. The initial velocities are usually assigned from the Maxwell-Boltzmann distribution at a given temperature.[305] The result of integrating eq. 1 is a trajectory that describes how positions and velocities of the atoms in the system vary with time. When initiating an MD calculation, a time interval, Δt, between updates of atomic positions is chosen. Furthermore, force field, solvent model, ions, pH, temperature, and pressure have to be defined.

8.2.1 Force field

In MD simulations, electrons are not treated explicitly. Instead, the nucleus and the electrons are combined in one particle resulting in atoms modeled as spheres with point charges.[308] The forces between the atoms are calculated using a force field. A force field is a collection of mathematical functions with associated parameters which describe the interaction between different types of atoms as a function of their coordinates. The parameters in a force field are typically determined from experimental data and from quantum mechanical calculations.[309] The majority of force fields include six potential energy terms which can be divided into bonded interactions and nonbonded interactions. The bonded interaction terms represent the intramolecular potential energies given by the molecular geometry i.e. variation in bond length, bond angle, torsion angle, and improper torsions. The nonbonded terms describe the electrostatic and van der Waals interactions between atoms that are separated by at least 3 bonds or between atoms in different

molecules.[301] The expression describing the potential energy of a molecular system can be formulated as eq.3 [297]:

$$U(r) = \sum_{bonds} \frac{k_l}{2}(l-l_0)^2 + \sum_{angles} \frac{k_b}{2}(\Theta-\Theta_0)^2 + \sum_{dihedrals} \frac{V_n}{2}(1+\cos(n\chi-\alpha)) + \sum_{improper} \frac{k_\psi}{2}(\psi-\psi_0)^2 + \sum_{\substack{non\text{-}bonded \\ pairs\ (i,j)}} \frac{q_i q_j}{4\pi\varepsilon_0 r_{ij}} + \sum_{\substack{non\text{-}bonded \\ pairs\ (i,j)}} 4\varepsilon_{ij}\left[\left(\frac{\sigma_{ij}}{r_{ij}}\right)^{12} - \left(\frac{\sigma_{ij}}{r_{ij}}\right)^{6}\right] \quad \text{(eq. 3)}$$

The first term in eq. 3 (harmonic potential) represents the potential energy of bond length variation. k_l represents the force constant of the bond, l represents the bond length, and l_0 represents the equilibrium bond length. The second term in eq. 3 represents the potential energy of bond angle deviating from an equilibrium angle, Θ_0. k_b represents the force constant of the angle. The third term in eq. 3 represents the dihedral potential energy as a function of rotation about each dihedral angle, X. V_n is related to the height of the energy barrier, n is related to the number of minima in the energy function, and α is the phase factor that determines the position of the energy minima. The last bonded interaction term in eq. 3 represents improper torsion angles. This term is introduced to preserve planarity of groups with flat geometry. In the term, ψ_0 represents the equilibrium angle, and k_ψ represents the force constant.

The last two terms represent nonbonded interactions. The fifth term in eq. 3 represents the potential energy of electrostatic interactions. All atoms have assigned partial charges which remain constant throughout the simulation. In the electrostatic term, r_{ij} represents the distance between atoms i and j which respectively have charges q_i and q_j. ε_0 is a physical constant which describes the dielectric permittivity of vacuum. The sixth and final term describes the van der Waals component of the potential. This term is also known as the Lennard-Jones 12-6 potential and contains an attractive (powered by 6) and a repulsive term (powered by 12). Here, ε_{ij} is the energy minimum of the interactions between i and j, and σ_{ij} is the distance at which the potential energy is zero.

8.2.2 *NPT* ensemble

Experiments are often conducted at constant temperature and pressure. It is therefore desirable to perform MD simulations with constant number of atoms (*N*) in an isothermal (*T*)-isobaric (*P*) environment (*NPT* ensemble). Using Desmond for MD simulations, the temperature is by default kept constant with a Nosé-Hoover thermostat.[310] This thermostat maintains the temperature constant by introducing an additional term to the equation of motion, which simulates a fictional heat bath mass from which temperature (energy) can be exchanged.[305] The pressure is by default held constant by the Martyna–Tobias–Klein barostat.[311] This method keeps the pressure constant by allowing the volume of the simulation box to change.

8.2.3 Boundary conditions

An MD simulation is set up in a simulation box with a confined size. To avoid interactions of the molecules with the boundaries of the box, periodic boundary conditions are applied. With periodic boundary conditions, the simulation box is replicated infinitely in all directions forming a lattice. The molecules in each box will move in exactly the same way, hence when a molecule leaves one box an identical molecule will enter through the opposite face of the box.

8.3 Experimental procedures

In the following, procedures to build initial structures of the catalytic domains of the *human* TPH isoforms are presented. The procedures on how the to build the MD simulation systems are also described.

8.3.1 Model structures

Proper initial models are needed for MD simulations. Preliminary work was conducted on a homology model of c*h*TPH2 which was build using the crystal structure of c*h*TPH1 (PDB entry: 1MLW) as template. However, in October 2014 a crystal structure of ct*h*TPH2 was uploaded to the PDB (PDB entry: 4V06), which made the homology model redundant. Instead, the crystal structure is used in the analysis of TPH2. In the following, the preparation of the input structures of c*h*TPH1 and c*h*TPH2 are presented.

8.3.1.1 MD input structure of c*h*TPH1 and system setup

In the experiments, an NΔ99/CΔ31-*h*TPH1 variant was used (c*h*TPH1). This variant is purified as a fusion protein with MBP which is cleaved during the purification leaving two residues in the N-terminus of c*h*TPH1 (chapter 2). These residues are a glycine and a proline from the protease recognition site. A c*h*TPH1 sequence including Gly and Pro was therefore used for preparation of the input structure.

As described in chapter 7, there are seven structures of *human* cTPH1 in the PDB. Of these structures, 1MLW (PDB entry) was chosen, as it has well resolved resolution in the loop of interest and compared to some of the other c*h*TPH1 structures, 1MLW does not include a bulky inhibitor which perturbs the structure.

The sequence used in the experiments was aligned using Clustal Omega with the primary structure of 1MLW, Figure 8.1. The sequence alignment in Figure 8.1 shows that the sequence is not fully covered by the structure of 1MLW, especially in the C-terminus. Furthermore, two residues do not match, as 1MLW has serine in position 104 and arginine in position 179, which are threonine and glutamine in the c*h*TPH1 sequence, respectively.

The missing C-terminal part is covered by the crystal structure of ct*h*TPH2 (PDB entry: 4V06). Therefore, a prime energy based homology model was build based on the templates 1MLW and 4V06 (chain A), Figure 8.1. Met102 and Glu103 were built on 4V06, Thr104 to Ile393 were built on 1MLW, and Lys394 to Asp413 were built on 4V06. The missing residues Gly98 to Gly101 in the N-terminus were modeled by prime (energy based). Iron was included from 1MLW.

In the graphical interface of Maestro, iron was reduced from +3 to +2, and the model was renumbered starting from Gly98. Resolved water molecules from 1MLW were retained (including the three water molecules coordinating to iron) by aligning the structures and superimposing the water molecules into the model structure. In the following, superimposing refers to aligning the structures, deleting everything other than e.g. the water molecules (or ligand), and then merging the files. This way the position of the water molecules (or ligand) have been adopted. The model was further prepared by using the Protein Preparation Wizard (PPW) software in the Maestro suite.[312] PPW was used to add hydrogen atoms and assign bond orders. Overlapping water molecules were deleted (six molecules). Refinement of the structure was performed by iterative restrained minimization (OPLS3, 0.3 Å) and PropKa optimization [313] at pH 8.0. No change in protonation state was observed as a result of the optimization (net charge of zero).

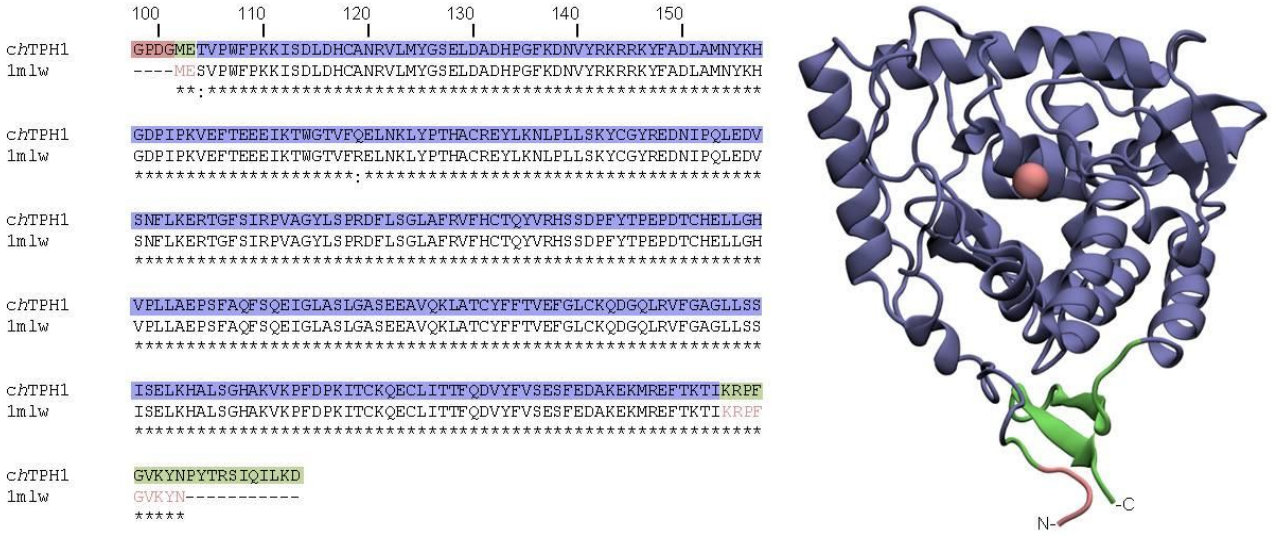

Figure 8.1. Homology model of c*h*TPH1. Left: Alignment of the sequence of c*h*TPH1 (used in experiments) and 1MLW. Highlighted sequence represents parts of the sequence modeled by prime (pink), build with 1MLW as template (blue), and build with 4V06 as template (green). Pink letters represent parts of the 1MLW sequence which have no structure (insufficient density). Right: Cartoon illustration of the c*h*TPH1 homology model with same color code as in the alignment.

To setup the system for simulation, the model was placed in an orthorhombic box with boundaries exceeding 10 Å in each direction from the protein using System Builder workflow in Desmond [314]. For the experiments, c*h*TPH1 was prepared with 100 mM $(NH_4)_2SO_4$. To mimic these conditions salt was also added to the simulations. NaCl was chosen as $(NH_4)_2SO_4$ is not parameterized. The concentration of NaCl to achieve the same ionic strength was calculated using eq. 4 [315]:

$$I = \frac{1}{2}\sum_{i=1}^{n} c_i z_i^2 \qquad \text{(eq. 4)}$$

The same ionic strength is obtained by adding a concentration of 300 mM NaCl. 0.3 M NaCl (61 Na^+ and 61 Cl^-) was added to the simulation box together with 10593 TIP3P (TIP3P water model [316]) water molecules.

8.3.1.2 MD input structure of chTPH2 and system setup

In the experiments, an NΔ145/CΔ31-*h*TPH2 variant was used (c*h*TPH2). For the same reason as for c*h*TPH1, the sequence of c*h*TPH2 includes Gly and Pro in the N-terminus. As described in chapter 7, only one structure of TPH2 (PDB entry: 4V06) resides in the PDB. The sequence used in the experiments was aligned using Clustal Omega with the primary structure of 4V06, Figure 8.2. The sequence alignment in Figure 8.2 shows that the sequence is covered by the crystal structure. However, the first six residues in the N-terminus of the crystal structure do not match the sequence. These residues are probably part of a purification His-tag with a tobacco etch virus protease cleavage site, as the sequence "MHHHHHHSSGVDLGTENLYFQ↓SM" is often found in crystal structures utilizing this purification strategy.[317-319]

To obtain a model structure with an N-terminus that matches the sequence used in the experiments, a homology model was build based on the template 4V06 (chain A), Figure 8.2. Chain A was chosen over chain B because it has well resolved side chains of all residues in the active site loop. The missing residues in the N-terminus were modeled by prime (energy based). Iron was included from 4V06.

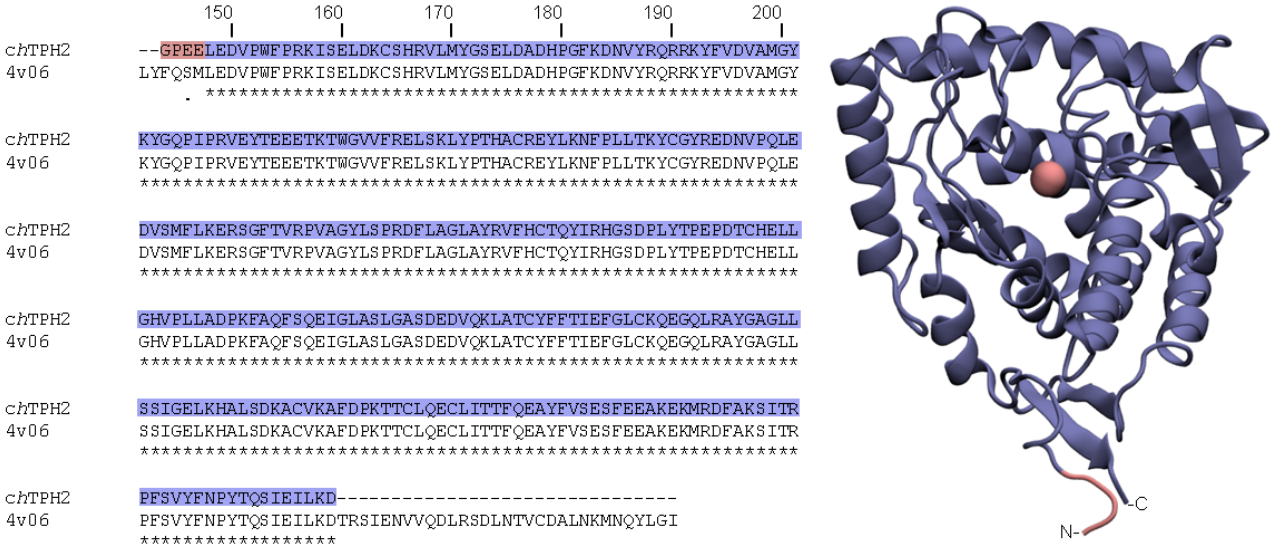

Figure 8.2. Homology model of c*h*TPH2. Left: Alignment of the sequence of c*h*TPH2 (used in experiments) and 4V06. Highlighted sequence represents parts of sequence modeled by prime (pink) and was built with 4V06 as template (blue). Right: Cartoon illustration of the c*h*TPH2 homology model with same color code as in the alignment.

In the graphical interface of Maestro, iron was reduced from +3 to +2 and the model was renumbered starting from Gly144. Resolved water molecules from 4V06 were retained by aligning the structures and superimposing the water molecules into the model structure. In c*h*TPH1 (1MLW), three water molecules were found to coordinate iron. The position of these water molecules were transferred to the model structure of c*h*TPH2 by superimposition. PPW was used to add hydrogen atoms and assign bond orders. Refinement of the structure was performed by iterative restrained minimization (OPLS3, 0.3 Å) and PropKa optimization at pH 7.0. No change in protonation state was observed as a result of the optimization (net charge of -6).

To setup the system for simulation, the model was placed in a orthorhombic box with boundaries exceeding 10 Å in each direction from the protein. 10176 TIP3P water molecules and 0.3 M NaCl (plus six sodium ions to neutralize the system) were added to the simulation box.

MD simulations and RMSD verification

After the system setups, 100 ns simulations were conducted with the c*h*TPH1 and c*h*TPH2 models as input structures. The MD simulations were performed with the Desmond package using the OPLS3 force-field [320] and periodic boundary conditions in all three Cartesian coordinates. Particle-mesh Ewald method [321] was applied to calculate long-range electrostatic interactions. Short-range electrostatic interactions and van der Waals were smoothly truncated at 9 Å. The simulations were run with *NPT* ensemble with constant temperature of 300 K maintained with Nosé–Hoover thermostat [310], and constant pressure maintained at 1.01325 bar with the Martyna–Tobias–Klein barostat method [311]. RESPA integrator [322], with a 2.0-fs time step was utilized to solve the equations of motion for bonded and short-range interactions. The RESPA integrator default setting for nonbonded interactions beyond the 0.9-nm cutoff was 6.0 fs time step. Before every 100 ns production simulation run, the model structure was relaxed using a default relaxation protocol in Desmond. Configurations and energies were saved at 5 ps intervals.

The simulations were analyzed for convergences based on RMSD calculations.[323] Figure 8.3 shows that RMSD-plots of c*h*TPH1 (A) and c*h*TPH2 (B) seem to converge to a stable value after relatively short time (~10 ns). This suggests that the protein has reached a state of equilibrium.

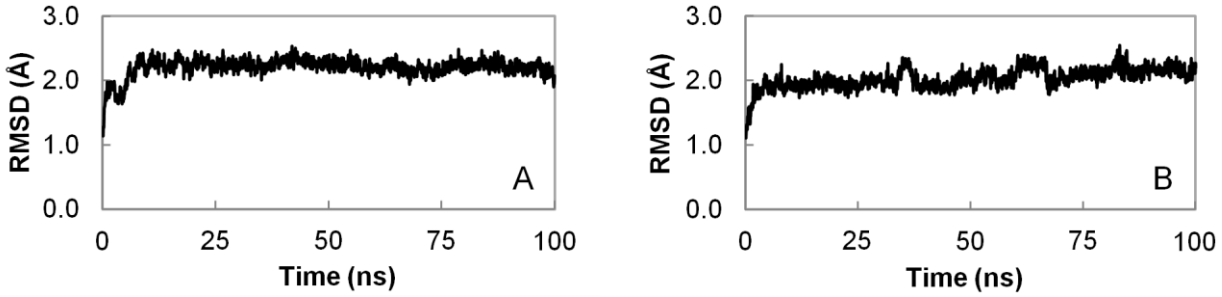

Figure 8.3. RMSD plots from 100 ns simulations of c*h*TPH1 (A) and c*h*TPH2 (B). RMSD in each 10th frame is calculated for all heavy atoms in the protein with the first frame as the reference structure.

To examine the structural and dynamical influence of substrate and co-substrate binding, tryptophan and BH_4 were introduced into the binding pockets of c*h*TPH1. Substrate tryptophan was introduced into the binding pocket by superimposition from *chicken* cTPH1 (PDB entry: 3E2T) which has tryptophan bound. Substrate tryptophan was prepared by charging the amino group to +1 and the carboxyl group to -1 and adding hydrogen atoms using the Protein Preparation Wizard. The binding pose of BH_4 was obtained from the crystal structure of *human* cTPH1 (PDB entry: 1MLW) which has BH_2 bound. BH_2 was superimposed into the model structure and changed to BH_4 by creating the appropriate double bonds. Protein Preparation Wizard was used to assign bond orders and add hydrogen atoms. A series of 100 ns simulations were conducted on c*h*TPH1•Trp, c*h*TPH1•BH_4, and c*h*TPH1•Trp•BH_4, Figure 8.4. RMSD-plots extracted from all simulations in Figure 8.4 were found to converge within the 100 ns simulations (Appendix I).

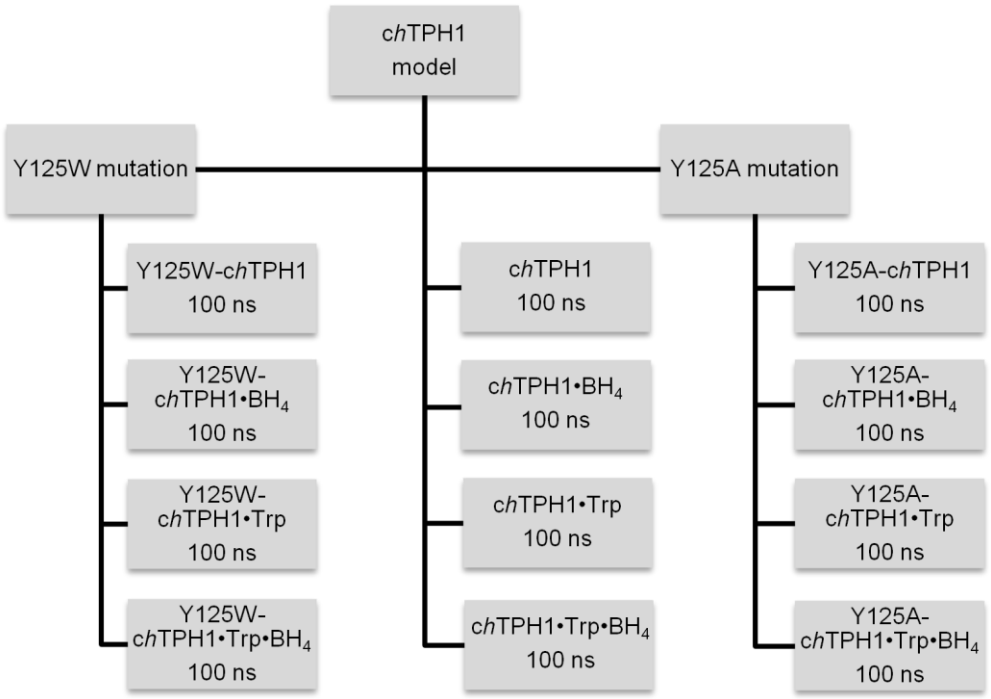

Figure 8.4. Diagram visualizing the conducted MD simulations on the c*h*TPH1 variants with or without substrates.

Mutations of Tyr125 in the active site loop to alanine or tryptophan were performed utilizing Residue Scanning in the BioLuminate suite.[324] Simulations of the mutant variants were also conducted according to Figure 8.4. The exact same simulations conducted for the c*h*TPH1 variants, were also conducted for c*h*TPH2 and mutant variants (Y171A-c*h*TPH2 and Y171W-c*h*TPH2). RMSD-plots extracted from all these simulations were found to converge within the 100 ns simulations (Appendix I).

8.4 Mutation stability prediction

In chapter 7, it was found that a tyrosine residue in the center of the active site loop is orientated differently in the TPH isoforms. A mutational study was made to investigate if this residue had any effect on the properties of the isoforms. To identify amino acids that would not destabilize the structure of the TPH isoforms, the software I-Mutant3.0, Prediction of Protein Mutant Stability Changes (PoPMuSiC), and Residue Scanning were used. In all three software, the model structures of the TPH isoforms were given as input.

I-Mutant3.0 [325] and PoPMuSiC [326] calculate protein stability changes (ΔΔG values) upon single-site mutations. The software is based on machine learning and has been trained on a large database of thermodynamic data of mutated proteins. In the calculations, e.g. spatial environment and relative solvent accessible area of the residue that undergoes mutation are considered.[327,328]

Residue Scanning [324] calculates the change in stability (ΔΔG) upon mutation from a thermodynamic cycle in which the difference in free energy is calculated between the folded state and the unfolded state of the protein. In the calculation, the unfolded protein is represented as a tripeptide, Gly-X-Gly, where X is the residue that is mutated. The energy is calculated with the Prime energy function using an implicit solvation model.[329]

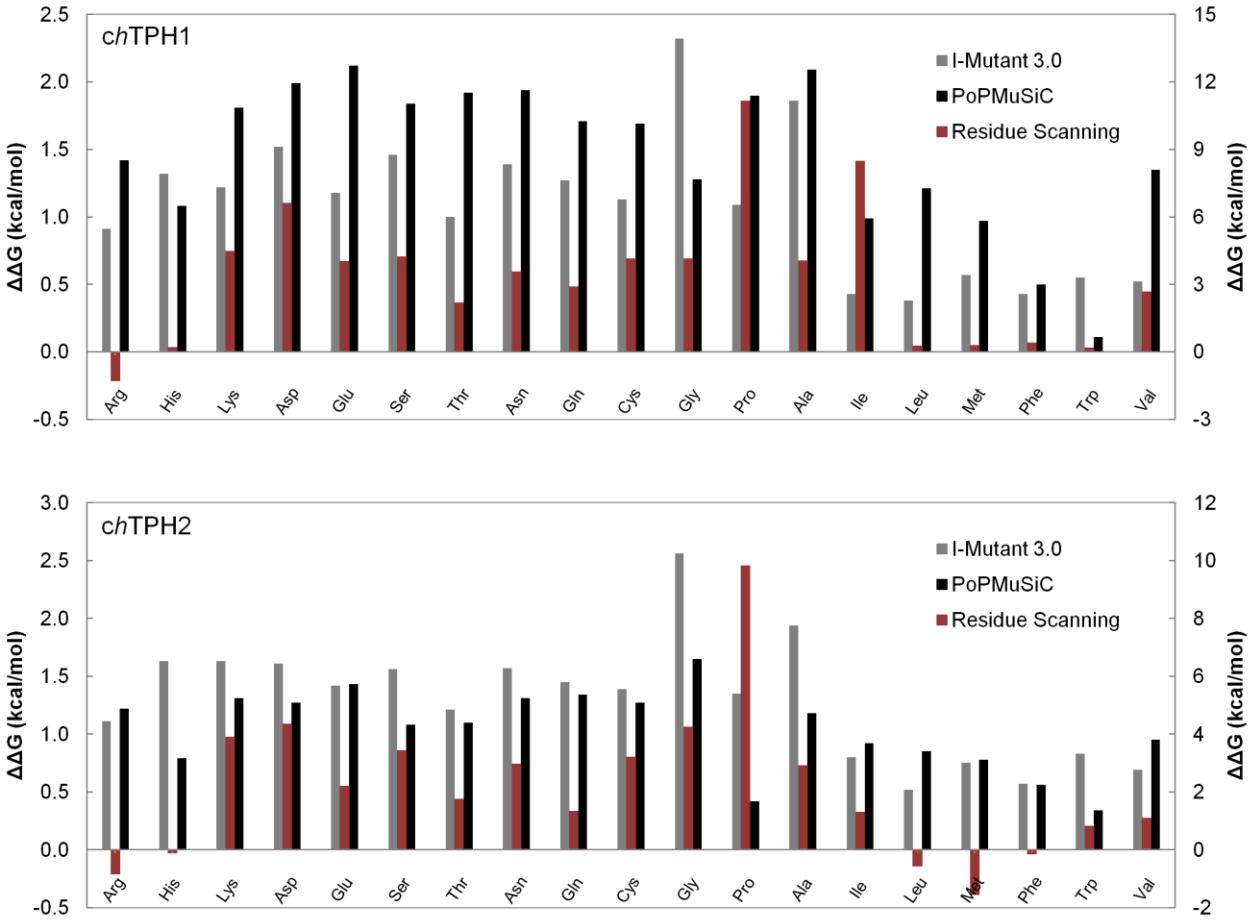

Figure 8.5. Change in Gibbs free energy of single point mutation of Tyr125 in c*h*TPH1 (top) or Tyr171 in c*h*TPH2 (bottom). I-Mutant3.0 and PoPMuSiC use the primary vertical axis (left) while Residue Scanning uses the secondary vertical axis (right).

According to the results of the three stability prediction tools in Figure 8.5, almost every amino acid will result in reduced stability of the TPH isoforms. Leucine and tryptophan were chosen as all three software only

predict small destabilizing effects upon mutation to these amino acids in both TPH isoforms. Furthermore, they were chosen as tryptophan is more bulky and leucine is less bulky than tyrosine, respectively. As a safety precaution, Tyr125 was also mutated to alanine, in case the other mutations resulted in insoluble TPH variants.

8.5 MD trajectory analysis

In the following, efforts to illuminate the observed substrate inhibition mechanism on a molecular level are described. The conducted MD simulations (Figure 8.4) were used to study the influence of substrate binding in the active site of the TPH isoforms. Furthermore, the importance of the tyrosine residue in the center of the active site loop was investigated by the point mutations performed based on the analysis in Figure 8.5.

As described in chapter 7, the Y125L-c*h*TPH1 and Y125A-c*h*TPH1 variants displayed identical kinetics, but the latter resulted in significantly greater purification yield (chapter 2). For these reasons only Y125A-c*h*TPH1 was characterized *in silico*.

8.5.1 Active site blockage

In chapter 6, it was described how substrate tryptophan causes inhibition of c*h*TPH1 at elevated concentrations (~50 µM). The underlying molecular mechanism was investigated by comparing the simulations trajectories of c*h*TPH1 without substrates and c*h*TPH1 with bound tryptophan (c*h*TPH1•Trp). Here, it was observed that in the simulation of c*h*TPH1•Trp, the entrance to the BH_4 binding pocket was blocked by Tyr235, Figure 8.6.

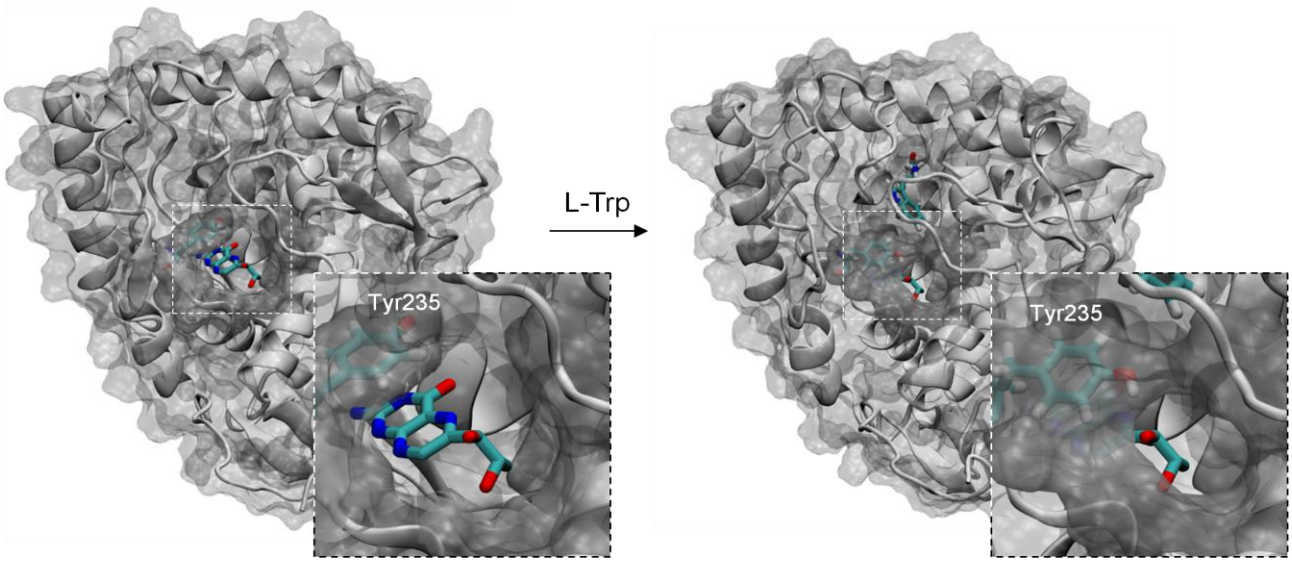

Figure 8.6. Substrate Trp induced blocking of the BH_4 binding pocket. BH_2, shown in cyan licorice, is not included in the simulations but have been superimposed into the structures (from PDB entry: 1MLW) to illustrate its binding pose. Left: snapshot extracted from MD simulation of c*h*TPH1 without substrates. Right: snapshot extracted from MD simulation of c*h*TPH1 with bound substrate Trp. The snapshots represent the average position of Tyr235 based on the distance measurements over the 100 ns simulations.

As described in chapter 7, Tyr235 constitutes part of the BH_4 binding pocket. The crystal structure of c*h*TPH1 with bound BH_2 (PDB entry: 1MLW), shows that Tyr235 interacts with BH_2 through π-stacking interactions, Figure 8.7. In Figure 8.7, it can be seen that Tyr235 is in direct contact with the active site loop through Tyr125. This residue might therefore have an influence on the orientation of Tyr235. This is further investigated in the following sections.

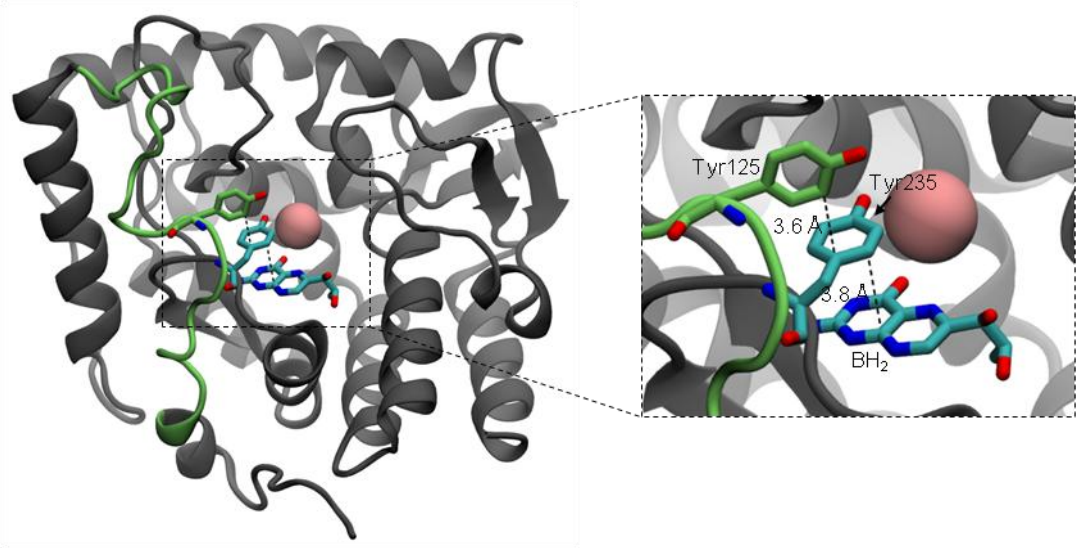

Figure 8.7. The position and orientation of Tyr125, Tyr235, and BH_2 in the crystal structure of c*h*TPH1 (PDB entry: 1MLW). The active site loop is colored green and dashed lines represent distances.

8.5.2 The orientation of Tyr235

The initial model used as input structure for the MD simulations was build on the crystal structure of c*h*TPH1 which has BH_2 bound (PDB entry: 1MLW). The presence of BH_2 in the structure might have an influence on the orientation of Tyr235 as they are in direct contact, Figure 8.7. It was therefore investigated whether the orientation of Tyr235 changes during a 100 ns MD simulation in the absence of BH_4 in the active site.

This was analyzed by calculating the average RMSD of Tyr235 (all heavy atoms) between every 10th frame in the trajectory and the crystal structure 1MLW. In the calculation, the model structure was aligned to 1MLW in all frames. The same calculation was made with the crystal structure of *chicken* cTPH1 (Trp bound, PDB entry: 3E2T) as the reference structure. In the absence of tryptophan, an average $RMSD_{Tyr235}$ of 1.1 ± 0.3 Å was obtained with 1MLW as the reference structure and 3.6 ± 0.2 Å with 3E2T as the reference structure. This is illustrated in Figure 8.8 (left), and this means that Tyr235 maintained the orientation observed in the crystal structure throughout the simulation.

Figure 8.6 illustrates that Tyr235 changes orientation in the simulation of c*h*TPH1•Trp compared to that of c*h*TPH1 without Trp. The $RMSD_{Tyr235}$ was similarly calculated for the simulation of c*h*TPH1•Trp. Here, an average $RMSD_{Tyr235}$ of 3.0 ± 0.6 Å was obtained with 1MLW as the reference structure and 1.8 ± 0.6 Å with 3E2T as the reference structure. This means that Tyr235 has changed orientation upon substrate binding. This tryptophan induced change in orientation of Tyr235 is clearly visualized in Figure 8.8. The resulting movements of Tyr235 observed in MD simulations of c*h*TPH1 and c*h*TPH1•Trp correlate very well with the structural information obtained from the crystal structures.

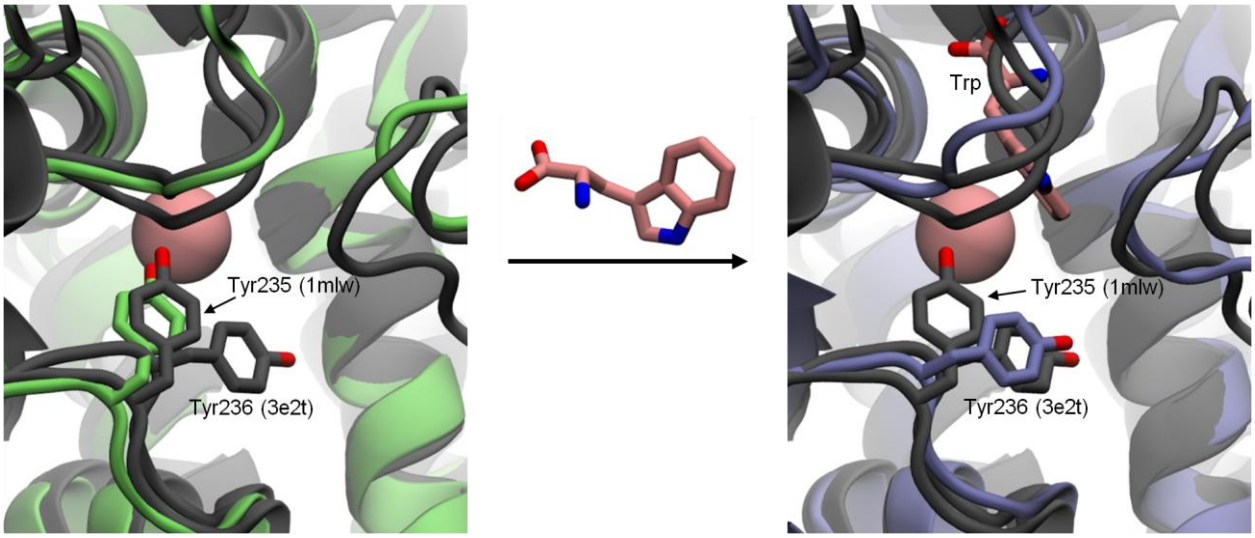

Figure 8.8. Tyr235 movement upon substrate tryptophan binding. Left: Snapshot illustrating the average position (based on $RMSD_{Tyr235}$) of Tyr235 in the simulation of c*h*TPH1 (green). Right: Snapshot illustrating the average position (based on $RMSD_{Tyr235}$) of Tyr235 in the simulation of c*h*TPH1•Trp (blue). Gray structures represent the crystal structures of c*h*TPH1 (PDB entry: 1MLW) and *chicken* cTPH1 (PDB entry: 3E2T). Substrate tryptophan is shown in pink.

When the simulation trajectories of c*h*TPH1 and c*h*TPH1•Trp were compared, it was found that substrate tryptophan pulls the loop comprising Ile366 to Thr368 towards the active site, Figure 8.9. This in turn results in formation of hydrogen bonding interaction with Tyr125 in the active site loop (Leu123-Asp138) lining the opposite site of the BH_4 binding pocket. As Tyr125 interacts with Tyr235 through π-stacking, these residues move consecutively, resulting in blocking of the BH_4 binding pocket.

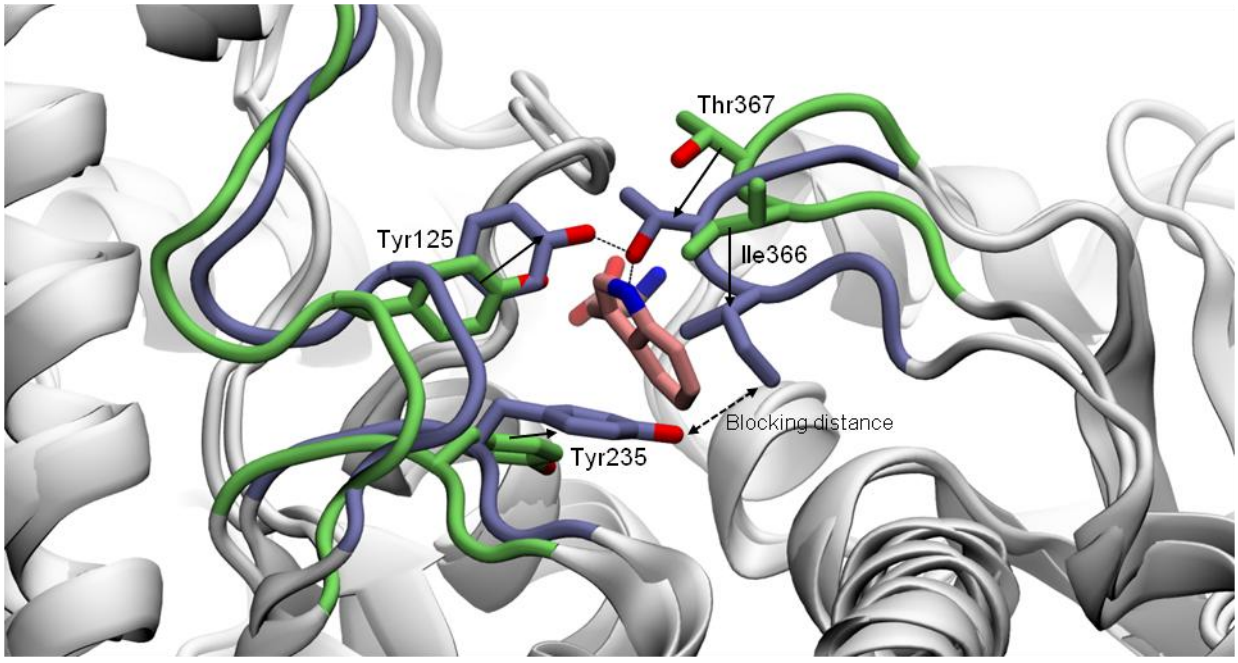

Figure 8.9. Residue movements upon substrate tryptophan binding in c*h*TPH1. Snapshots from MD simulations of c*h*TPH1 (green) and c*h*TPH1•Trp (blue). Substrate tryptophan is shown in pink and is from the simulation of c*h*TPH1•Trp. The snapshots were chosen based on average $RMSD_{Tyr235}$ calculations. Arrows represent movements caused by tryptophan and dashed lines represent hydrogen bonding distance (both distances are 2.8 Å). The double headed arrow represents the distance measured to quantify the blocking effect.

The interactions observed in Figure 8.9 were analyzed throughout the simulation trajectory of c*h*TPH1•Trp by measuring the distances between the involved residues, Figure 8.10. Figure 8.10 A (closed circles) shows that initially the distance between substrate tryptophan and Thr367 in the loop over the active site is relatively large (~5 Å). As the hydrogen bonding interaction is formed, the loop is pulled towards tryptophan and the distance is reduced to ~2 Å. It takes around 5 ns to fully establish this interaction. To verify that the loop is pulled down and not just tryptophan being pulled towards the loop, the distance between tryptophan and iron (anchor point assumed not to move) was measured, Figure 8.10 B. This distance is not changed significantly which confirms that the loop moves towards the active site. Such a movement of the loop is also observed in the crystal structures of c*h*PAH and *chicken* cTPH upon substrate/substrate analogue binding.[330,331] Following the established interaction between tryptophan and Thr367, formation of hydrogen bonding interactions between Thr367 and Tyr125 are formed, Figure 8.10 A (open circles). Hydrogen bonding distance (< 3 Å) between these residues is observed in 62 % (after 5 ns) of the frames. In the simulation of c*h*TPH1 without tryptophan, hydrogen bonding distance is observed in 0 % (average distance of 5 Å) of the frames. The movement of Tyr125 ultimately causes Tyr235 to move closer to Ile366 (Figure 8.10 C) which is positioned at the opposite side of the BH_4 binding pocket resulting in blocking of the binding site. This is further discussed in the following section.

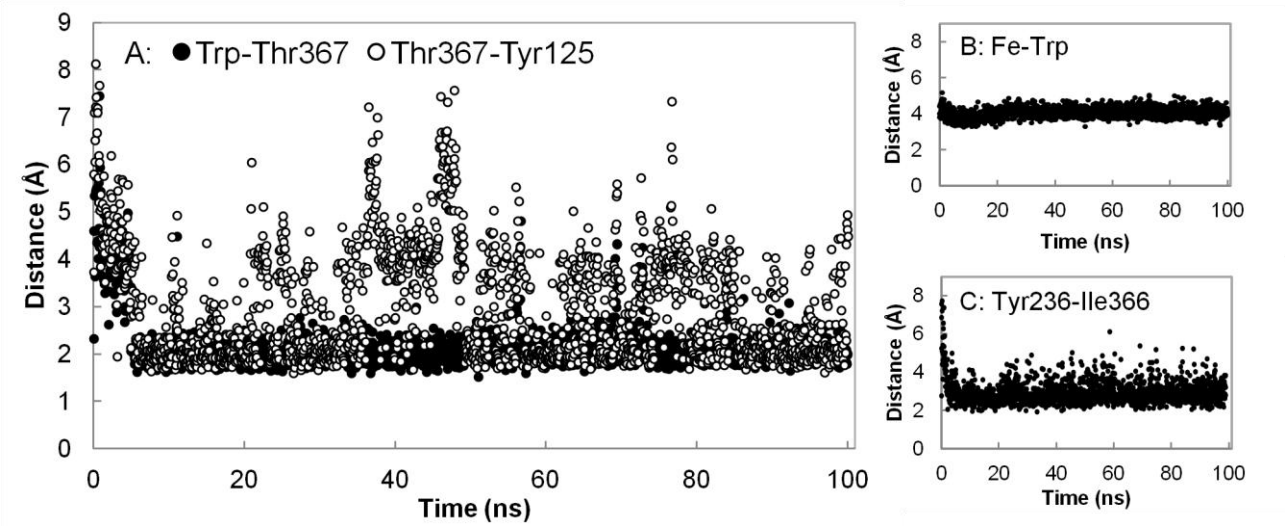

Figure 8.10. Measured distances between the residues involved in the BH_4 binding site blocking mechanism (Figure 8.9) extracted from the MD simulation trajectory of c*h*TPH1•Trp.

8.5.3 Influence of Tyr125 on active site blockage

Results from the MD simulations suggest that tryptophan binding in the active site pocket induces a change in the orientation of Tyr235, which results in blockage of the BH_4 binding pocket. This blocking mechanism might explain the substrate tryptophan inhibition observed in chapter 6. In chapter 7, it was found that mutation of Tyr125 in c*h*TPH1 to alanine or tryptophan resulted in increased inhibition constants (K_i) (retardation of the inhibition).

The structural origin of the changes in K_i was investigated by analyzing the blocking mechanism in the TPH variants. To quantify the blocking effect induced by tryptophan, the shortest distance from Tyr235 to the loop (residue 363 to 370) lining the opposite site of the BH_4 binding pocket was measured, Figure 8.9. In all the simulations the shortest distance observed was to Ile366. Only distances to this residue will therefore be presented.

The simulation results of c*h*TPH1 show that tryptophan induces a reduction in the average distance from 6.8 Å to 2.93 Å (Table 8.1). This reduced distance causes the blocking of the active site visualized in Figure 8.6.

In Y125A-c*h*TPH1, tryptophan only induces a reduction in the average distance to 3.4 Å, while the average distance observed in Y125W-c*h*TPH1 with tryptophan bound is 5.1 Å. These observations indicate that the BH_4 binding pocket of Y125A-c*h*TPH1 and especially Y125W-c*h*TPH1 are not blocked to the same extent as observed in c*h*TPH1 upon tryptophan binding.

In c*h*TPH2, the average distance is 8.1 ± 0.6 Å between Tyr281 (corresponding to Tyr235 in c*h*TPH1) and the loop lining the opposite site of the BH_4 binding pocket. This distance is larger than the one observed in c*h*TPH1, Table 8.1. In c*h*TPH1, Tyr125 π-stacks onto Tyr235 forming a T-shaped interaction (Figure 8.7), which presumably causes restricted movement of Tyr235. In c*h*TPH2, Tyr281 does not interact with Tyr171 (corresponding to Tyr125 in c*h*TPH1) because this residue is orientated away from the active site, as discussed in chapter 7. The movement of Tyr281 is hence less restrained in c*h*TPH2 compared to Tyr235 in c*h*TPH1.

In the presence of substrate tryptophan, the distance in c*h*TPH2 is reduced to 5.7 Å, which is significantly larger than the observed distance of 2.9 Å in c*h*TPH1. Hence, tryptophan binding in c*h*TPH2 results in a more open structure which can presumably still accommodate binding of BH_4. The same is true for Y171A-c*h*TPH1, in which tryptophan only induces a reduction in the average distance to 5.7 Å, and Y171W-c*h*TPH1 where the distance is increased to 9.7 Å.

Table 8.1. Average distances measured between Tyr235 (c*h*TPH1 variants) or Tyr281 (c*h*TPH2 variants) and Ile366 (c*h*TPH1 variants) or Ile412 (c*h*TPH2 variants) extracted from MD simulations of the TPH variants with or without substrate tryptophan in the active site. Standard errors of means are based on the blocking method [332] based on five 20 ns fragments. Right panel illustrates the correlation between the measured distances and K_i-values (from chapter 7).

	Distance (Å)	
Variant	**Empty**	**Trp**
c*h*TPH1	6.8 ± 0.3	2.93 ± 0.02
Y125A-c*h*TPH1	4.6 ± 0.3	3.4 ± 0.1
Y125W-c*h*TPH1	4.7 ± 0.3	5.1 ± 0.3
c*h*TPH2	8.1 ± 0.6	5.7 ± 0.3
Y171A-c*h*TPH2	6.4 ± 0.2	5.7 ± 0.8
Y171W-c*h*TPH2	5.8 ± 0.8	9.7 ± 0.2

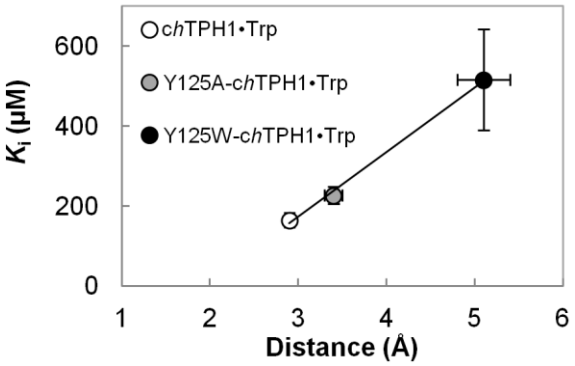

The interpretation of the measured distances correlates well with the kinetic data presented in chapter 7, insert in Table 8.1. If tryptophan binding results in a short distance, which is interpret as low accessibility to the BH_4 binding site, strong substrate inhibition (low K_i) is observed. Upon Trp binding, the distance in Y125A-c*h*TPH1 is reduced to a value slightly greater than the one observed in c*h*TPH1, which results in a small increase in K_i. The effect is more pronounced in Y125W-c*h*TPH1, where tryptophan binding reduces the distance to a value only slightly lower than the one observed in c*h*TPH2. This results in a retardation of the substrate inhibition mechanism. In the c*h*TPH2 variants, tryptophan binding results in large distances that presumably reflect conformations of the c*h*TPH2 variants, which can still accommodate binding of BH_4. The c*h*TPH2 variants are therefore not subjected to substrate inhibition.

Figure 8.9 illustrates that the Tyr235 blocking mechanism upon tryptophan binding is mediated by Tyr125. The distance analysis summarized in Table 8.1, shows that Tyr235 in Y125A-c*h*TPH1 and especially Y125W-c*h*TPH1 do not block the active site to the same extend as in c*h*TPH1. This is probably due to the missing hydrogen bonding interaction between position Tyr125 and Thr367. A more thorough analysis of the trajectories of all the TPH variants are, however, required to fully illuminate the complex interplay between

substrate tryptophan, Thr367, Tyr125, and Tyr235, which results in blocking of the BH_4 binding pocket and ultimately lowers the enzymatic activity.

8.6 Discussion

In chapter 6, it was demonstrated that c*h*TPH1 is subjected to competitive substrate inhibition. The inhibition by tryptophan was found to be competitive towards BH_4, as increased BH_4 concentrations increased the apparent substrate inhibition constant. In chapter 7, it was found that substrate inhibition only applies to TPH isoform 1. It was proposed that this originates from the different orientations of Tyr125 (c*h*TPH1) and Tyr171 (c*h*TPH2) in the active site loops of the isoforms. To further support this hypothesis and to understand the underlying mechanism on a molecular level, the active site loop was analyzed *in silico*.

Mutation stability prediction tools were utilized to predict which amino acids Tyr125/Tyr171 could be mutated to, without destabilizing the proteins. Here, it was found that mutations to leucine or tryptophan should not compromise the stability significantly. Purification results (chapter 2), however, revealed that Y125L-c*h*TPH1 resulted in low purification yields. In contrast, Y125A-c*h*TPH1 resulted in similar purification yields. Thermostability measurements (DSF, chapter 3) revealed that mutation of Tyr125/Tyr171 to alanine or tryptophan did not cause changes in the transition temperature of the TPH variants. According to the prediction tools, mutation to alanine should cause decreased stability. The predicted stabilities do therefore not correlate well with the experimental observations.

To analyze the substrate inhibition mechanism on a molecular level, models of c*h*TPH1 and c*h*TPH2 and their mutant variants were built, and MD simulations of all the variants were conducted. From the MD simulation trajectories, it is observed that tryptophan binding in c*h*TPH1 caused a blocking of the BH_4 binding pocket. The tryptophan-induced blocking mechanism occurs through a hydrogen bonding network including Thr367, Tyr125, and Tyr235. Residue movements are propagated from the tryptophan binding pocket to Tyr235, which moves to a position that presumably prevents BH_4 binding. The residues in the network have previously been found to have important functions or reside in important loops. The loop containing Thr367 in c*h*TPH1 is known to participate in substrate binding and is part of the closing mechanism discussed in chapter 7.[330,331] The residue corresponding to Tyr125 in PAH (Phe184) and TH (Tyr138) has also been found to be important for proper enzymatic function. In TH, Phe184 has been found to be important for substrate binding and catalysis, as a F184A mutation resulted in a 20-fold decrease in V_{max} and a 4-fold decrease in $K_{m,Tyr}$.[333] In PAH, Tyr138 has similarly been found to be important for enzymatic efficiency.[334] The last residue in the network, Tyr235, has also been demonstrated to play a significant role. A mutagenesis study by Jiang *et al.*[335] has shown that Tyr235 is crucial for the substrate inhibition mechanism of *h*TPH1, as mutation of this residue to alanine or leucine resulted in elimination of substrate inhibition.

The blocking mechanism observed in the MD simulations compliments the kinetic model in which a dead-end complex is formed when tryptophan binds before BH_4. Collectively, the kinetic and MD results imply that the competitive substrate inhibition, which occurs at elevated tryptophan concentration, is caused by binding of tryptophan as the first substrate which results in blocking of the BH_4 binding pocket and therefore prevents BH_4 from binding. This substrate inhibition mechanism is further supported by the correlation between the Tyr235-Ile366 distances and the measured K_i-values. By combining results from the kinetic study with the results obtained from the MD simulations, the loop is conclusively found to have an important contribution to the inhibition mechanism of c*h*TPH1.

Unfortunately, due to time constraints not all MD simulation trajectories have been included in the exploration of the substrate inhibition mechanism. How the mutations hamper the blocking mechanism, therefore remain unresolved.

8.7 Conclusion

Steady-state kinetic measurements revealed that c*h*TPH1 is substrate inhibited and that mutation of Tyr125 results in retardation of the inhibition mechanism. The MD simulation results presented in this chapter, demonstrate that the inhibition mechanism occurs through a tryptophan induced blocking of the BH_4 binding pocket. Tyr125 is an important residue in the inhibition mechanism, as it mediates residue movements from the tryptophan binding pocket to the BH_4 binding pocket. This mechanism only applies to isoform 1, as the corresponding tyrosine residue in c*h*TPH2 is orientated away from the active site.

8.8 References

[295] França, T. C., 2015, Homology modeling: an important tool for the drug discovery, *J. Biomol. Struct. Dyn. 33(8)*, 1780-1793.

[296] Rost, B., 1999, Twilight zone of protein sequence alignments, *Protein Eng. 12(2)*, 85-94.

[297] Zvelebil, M. and Baum, J. O., 2008, Understanding Bioinformatics, Garland Science Taylor and Francis Group LLC, New York, USA.

[298] Cavasotto, C. N. and Phatak, S. S., 2009, Homology modeling in drug discovery: current trends and applications, *Drug Discov. Today 14(13-14)*, 676-683.

[299] Altschul, S. F., Gish, W., Miller, W., Myers, E. W., and Lipman, D. J., 1990, Basic local alignment search tool, *J. Mol. Biol. 215*, 403-410.

[300] Sievers, F., Wilm, A., Dineen, D. G., Gibson, T. J., Karplus, K., Li, W., Lopez, R., McWilliam, H., Remmert, M., Söding, J., Thompson, J. D., and Higgins, D., 2011, Fast, scalable generation of high-quality protein multiple sequence alignments using Clustal Omega, *Mol. Syst. Biol. 7*, 539.

[301] Hug, S., 2013, Chapter 6 - Classical Molecular Dynamics in a Nutshell, in Biomolecular Simulations – Methods and Protocols, edited by L. Monticelli, E. Salonen, Humana Press, New York, USA.

[302] Klepeis, J. L., Lindorff-Larsen, K., Dror, R. O., and Shaw, D. E., 2009, Long-timescale molecular dynamics simulations of protein structure and function, *Curr. Opin. Struct. Biol. 19*, 120–127.

[303] Henzler-Wildman, K. A., Lei, M., Thai, V., Kerns, S. J., Karplus, M., and Kern, D., 2007, A hierarchy of timescales in protein dynamics is linked to enzyme catalysis, *Nature 450*, 913-916.

[304] Peters, G. H., 2004, Chapter 6 - Computer Simulations: A Tool for Investigating the Function of Complex Biological Macromolecules, in Enzyme Functionality – Design, Engineering, and Screening, edited by Allan Svendsen, Marcel Dekker, Inc., New York, USA.

[305] Leach, A. R., 2001, Chapter 7 - Molecular Dynamics Simulation Methods, in Molecular Modelling - Principles and Applications 2nd edition. Pearson Education Limited, Essex, England.

[306] Snyman, J. A., 1982, A new and dynamic method for unconstrained minimization, *Appl. Math. Modelling 6*, 449-462.

[307] Swope, W. C., Andersen, H. C., Berens, P. H., and Wilson, K. R., 1982, A computer simulation method for the calculation of equilibrium constants for the formation of physical clusters of molecules: Application to small water clusters, *J. Chem. Phys. 76*, 637-649.

[308] Monticelli, L. and Tieleman, D. P., 2013, Chapter 8 – Force Fields for Classical Molecular Dynamics, in Biomolecular Simulations – Methods and Protocols, edited by L. Monticelli, E. Salonen, Humana Press, New York, USA.

[309] Lorenz, C. and Doltsinis, N. L., 2012, Chapter 7 - Molecular Dynamics Simulation: From “Ab Initio” to “Coarse Grained”", in "Handbook of Computational Chemistry", edited by J. Leszczynski, Springer Science + Business Media B.V., Dordrecht, Netherlands.

[310] Hoover, W. G., 1985, Canonical dynamics: Equilibrium phase-space distributions, *Phys. Rev. A 31(3)*, 1695-1697.

[311] Martyna, G. J., Tobias, D. J., and Klein, M. L., 1994, Constant pressure molecular dynamics algorithms, *J. Chem. Phys. 101*, 4177-4189.

[312] Schrödinger Release 2017-2: Schrödinger Suite 2017-2 Protein Preparation Wizard; Epik, Schrödinger, LLC, New York, NY, 2017; Impact, Schrödinger, LLC, New York, NY, 2017; Prime, Schrödinger, LLC, New York, NY, 2017.

[313] Li, H., Robertson, A. D., and Jensen, J. H., 2005, Very Fast Empirical Prediction and Rationalization of Protein pKa Values, *Proteins 61*, 704-721.

[314] Shivakumar, D., Williams, J., Wu, Y., Damm, W., Shelley, J., and Sherman, W., 2010, Prediction of Absolute Solvation Free Energies using Molecular Dynamics Free Energy Perturbation and the OPLS Force Field, *J. Chem. Theory Comput. 6*, 1509–1519.

[315] Atkins, P. and De Paula, J., 2011, Chapter 5 – Thermodynamics of ion and electron transport, in Physical Chemistry for the life sciences, 2nd ed., W.H. Freeman and Company, New York, USA.

[316] Jorgensen, W. L., Chandrasekhar, J., Madura, J. D., Impey, R. W., and Klein, M. L., 1983, Comparison of Simple Potential Functions for Simulating Liquid Water, *J. Chem. Phys. 79*, 926-935.

[317] Johansson, C., Kavanagh, K. L., Gileadi, O., and Oppermann, U., 2007, Reversible sequestration of active site cysteines in a 2Fe-2S-bridged dimer provides a mechanism for glutaredoxin 2 regulation in human mitochondria, *J. Biol. Chem. 282*, 3077-3082.

[318] Qian, X., Hamid, F. M., El Sahili, A., Darwis, D. A., Wong, Y. H., Bhushan, S., Makeyev, E. V., and Lescar, J., 2016, Functional Evolution in Orthologous Cell-Encoded RNA-Dependent RNA Polymerases, *J. Biol. Chem. 291*, 9295.

[319] Ubhi, D., Kavanagh, K. L., Monzingo, A. F., and Robertus, J. D., 2011, Structure of Candida albicans methionine synthase determined by employing surface residue mutagenesis, *Arch. Biochem. Biophys. 513*, 19-26.

[320] Harder, E., Damm, W., Maple, J., Wu, C., Reboul, M., Xiang, J. Y., Wang, L., Lupyan, D., Dahlgren, M. K., Knight, J. L., Kaus, J. W., Cerutti, D., Krilov, G., Jorgensen, W. L., Abel, R., and Friesner, R. A., 2016, OPLS3: a force field providing broad coverage of drug-like small molecules and proteins, *J. Chem. Theory Comput. 12 (1)*, 281–296.

[321] Essmann, U., Perera, L., Berkowitz, M. L., Darden, T., Lee, H., and Pedersen, L. G., 1995, A smooth particle mesh Ewald method, *J. Chem. Phys.103*, 8577-8593.

[322] Humphreys, D. D., Friesner, R. A., and Berne, B. J., 1994, A Multiple-Time-Step Molecular Dynamics Algorithm for Macromolecules, *J. Phys. Chem. 98 (27)*, 6885–6892.

[323] Cramer, C. J., 2004, Chapter 3 - Simulations of Molecular Ensembles, in Essentials of Computational Chemistry: Theories and Models, 2nd Edition, John Wiley & Sons Ltd, West Sussex, England.

[324] Schrödinger Release 2016-4: BioLuminate, Schrödinger, LLC, New York, NY, USA 2016

[325] I-Mutant3.0 – link from 11.08.17: http://gpcr2.biocomp.unibo.it/cgi/predictors/I-Mutant3.0/I-Mutant3.0.cgi

[326] Prediction of Protein Mutant Stability Changes (PoPMuSiC) – link from 11.08.17: http://babylone.ulb.ac.be/popmusic/

[327] Capriotti, E., Fariselli, P., and Casadio, R., 2005, I-Mutant2.0: predicting stability changes upon mutation from the protein sequence or structure, *Nucleic Acids Res. 33*, 306-310.

[328] Dehouck, Y., Grosfils, A., Folch, B., Gilis, D., Bogaerts, P., and Rooman, M., 2009, Fast and accurate predictions of protein stability changes upon mutations using statistical potentials and neural networks: PoPMuSiC-2.0, *Bioinformatics 25(19)*, 2537-2543.

[329] BioLuminate 1.0 – User Manual, 2012, Schrödinger, LLC, New York, NY, USA

[330] Windahl, M. S., Petersen, C. R., Christensen, H. E. M., and Harris, P., 2008, Crystal structure of tryptophan hydroxylase with bound amino acid substrate, *Biochemistry 47*, 12087-12094.

[331] Andersen, O. A., Stokka, A. J., Flatmark, T., and Hough, E., 2003, 2.0 Å resolution crystal structures of the ternary complexes of human phenylalanine hydroxylase catalytic domain with tetrahydrobiopterin and 3-(2-thienyl)-L-alanine or L-norleucine: substrate specificity and molecular motions related to substrate binding, *J Mol Biol. 31, 333(4)*, 747-57.

[332] Flyvbjerg, H., 1989, Error estimates on averages of correlated data, *J. Chem. Phys. 91(1)*, 461-466.

[333] Daubner, S. C., McGinnis, J. T., Gardner, M., Kroboth, S. L., Morris, A. R., and Fitzpatrick, P. F., 2006, A Flexible Loop in Tyrosine Hydroxylase Controls Coupling of Amino Acid Hydroxylation to Tetrahydropterin Oxidation, *J. Mol. Biol. 359*, 299–307.

[334] Leandro, J., Stokka, A. J., Teigen, K., Andersen, O. A., and Flatmark, T., 2017, Substituting Tyr138 in the active site loop of human phenylalanine hydroxylase affects catalysis and substrate activation, *FEBS Open Bio 7(7)*, 1026-1036.

[335] Jiang, G. C. T., Yohrling, G. J., Schmitt, I. V. J. D., and Vrana, K. E., 2000, Identification of Substrate Orienting and Phosphorylation Sites Within Tryptophan Hydroxylase Using Homology-based Molecular Modeling, *J. Mol. Biol. 302*, 1005-1017.

Overall conclusions

The overall aim of this project was to shed light on the intriguing and important enzyme tryptophan hydroxylase. In the process of doing so, a variety of experimental techniques and computational tools have been utilized. In conjugation, the obtained results have revealed interesting properties of both isoforms of TPH.

The initial goal was to increase the stability of *h*TPH2 variants containing the regulation domain, as such variants are inherently instable and tend to aggregate. This cause low purification yields and hampers characterization. An *h*TPH2 variant with deletion mutations in both terminals, NΔ47-rc*h*TPH2, was produced. This variant was purified as an MBP-fusion protein utilizing a rapid two-step purification procedure with on-column cleavage of MBP. This procedure was demonstrated efficient in purification of a variety of TPH1 and TPH2 variants. Compared to full-length *h*TPH2, the NΔ47-rc*h*TPH2 variant showed improved properties which resulted in around 20-fold increase in purification yield.

Utilizing differential scanning fluorimetry, it was found that phenylalanine stabilized *h*TPH2 variants comprising the regulatory and catalytic domains in a concentration-dependant fashion. Phenylalanine was subsequently demonstrated to cause a ~3-fold decrease in the rate of inactivation. Analytical gel filtration revealed that these variants reside in a monomer-dimer equilibrium which was significantly shifted towards dimer in the presence of phenylalanine. This observation explaines the observed increase in thermostability. With phenylalanine, the purification yields were further increased ~4-fold for NΔ47-rc*h*TPH2 resulting in a total increase of ~80-fold compared to full-length *h*TPH2.

Within the Metalloprotein Chemistry and Engineering Group at DTU, it has been discovered that c*h*TPH1 and c*h*TPH2 display very different kinetic parameters and that only c*h*TPH1 is substrate inhibited. This is puzzling, as the isoforms share high sequence identity and have very similar tertiary structures. Furthermore, results presented in this dissertation demonstrate that the isoforms display the same unfolding temperatures and both reside as mono-disperse monomers.

In this current study, the origin of the different kinetic properties was sought. It was demonstrated that the steady-state mechanism of c*h*TPH1 is a hybrid Ping Pong-ordered mechanism in which the reaction can occur through either a Ping Pong or a sequential mechanism depending on the concentration of tryptophan. In this mechanism, substrate inhibition occurs if tryptophan binds before BH_4, resulting in competitive inhibition. It was found that this inhibition mechanism involves a loop lining the active site. Mutation of Tyr125 in the center of the active site loop of c*h*TPH1 resulted in retardation of the inhibition mechanism. Molecular dynamics simulations revealed that the substrate inhibition mechanism occurs via blocking of the BH_4 binding pocket upon tryptophan binding. Substrate tryptophan binding induces structural changes which propagate through Thr367, Tyr125, and Tyr235 resulting in a lowered accessibility of the BH_4 binding pocket.

The influence of the loop on the inhibition mechanism was confirmed by loop-swap mutations. In agreement with previous results, it was found that c*h*TPH2 is not substrate inhibited. However, mutation of three non-conserved residues in the hinge region of the loop resulted in profound substrate inhibition. Together, these results demonstrate that the different kinetic properties observed for the two TPH isoforms can be traced to the active site loops.

Perspectives and future work

The results in the first chapters demonstrate that the purification yield was increased to quantities sufficient of enzymatic characterization of an *h*TPH2 variant which include the regulatory domain. This enables future studies of the structure and function of the regulatory domain, and even opens up the possibility of crystallization for structure determination. With addition of phenylalanine, even full-length *h*TPH2 can be purified in quantities sufficient for e.g. kinetic studies.

Phenylalanine only had an influence on the thermostability, monomer-dimer equilibrium, and purification yields of *h*TPH2 variants comprising the regulatory domain. The dissociation constant of phenylalanine associated with these changes insinuate that they are induced by binding of phenylalanine in a site other than the active site. This suggests an allosteric site in the regulatory domain, as has been observed in PAH. The existence of such a site has to be confirmed by further experiments.

To support the presence of an allosteric site in the regulatory domain, it should be investigated whether phenylalanine-induced changes in the monomer-dimer equilibrium and transition temperature occur in isolated regulatory domain of *h*TPH2. Alternatively, the dimerizing or stabilizating effects of phenylalanine could be analyzed for rc*h*TPH2 variants in which key residues involved in substrate binding in the catalytic domain are mutated.

The presence of phenylalanine in the purification buffers did not change the purification yield of *h*TPH1 variants comprising the regulatory domain. This suggests that isoform 1 does not posses such an allosteric site. To confirm this hypothesis, DSF and analytical gel filtration experiments should be conducted on the *h*TPH1 variants.

It is a possibility that phenylalanine is not the *in vivo* relevant ligand for the potential allosteric binding site. A more potent ligand could potentially be identified by utilizing DSF with a compound library or using computational docking software. Identification of such a ligand could likely increase the stability of *h*TPH2 and maybe give insight into the complicated regulatory mechanism of TPH *in vivo*. If in fact, the allosteric site is isoform specific and potent ligands for this site can be identified, these ligands might have pharmaceutical applications.

The steady-state kinetic mechanism of c*h*TPH1 was determined in this dissertation by measuring the initial velocities at varied concentrations of tryptophan and BH_4. The obtained mechanism can be further supported by conducting product inhibition experiments. A similar study should be carried out for c*h*TPH2 to deduce its mechanism. This would reveal whether the two highly homologous enzymes follow the same mechanism or c*h*TPH1 follows a more complicated mechanism induced by e.g. the different properties of the active site loops.

The stopped-flow kinetic experiments conducted in Prof. Solomon's group at Stanford University revealed that a relatively long-lived transient intermediate is formed with high yields during catalytic turn-over of c*h*TPH2. These results open up the possibility of isolating and characterizing the so far only theoretical intermediate. Identification of this intermediate is one of the last pieces in the puzzle of the hydroxylation reaction mechanism of the aromatic amino acid hydroxylases.

Appendices

Appendix A

Manuscripts

A.1 Tidemand, K. D., Christensen, H. E. M., Hoeck, N., Harris, P., Boesen, J., and Peters, G. H., 2016, Stabilization of tryptophan hydroxylase 2 by L-phenylalanine-induced dimerization, *FEBS Open Bio 6*, 987-999.

A. 2 Tidemand, K. D., Peters, G. H., Harris, P., Stensgaard, E., and Christensen, H. E. M., 2017, The isoform-specific substrate inhibition mechanism of *human* tryptophan hydroxylase, *submitted*.

FEBS openbio

FEBS PRESS science publishing by scientists

Stabilization of tryptophan hydroxylase 2 by L-phenylalanine-induced dimerization

Kasper D. Tidemand, Hans E. M. Christensen, Niclas Hoeck, Pernille Harris, Jane Boesen and Günther H. Peters

Department of Chemistry, Technical University of Denmark, Kongens Lyngby, Denmark

Keywords
analytical size exclusion chromatography; differential scanning fluorimetry; enzyme characterization; oligomerization; protein purification

Correspondence
H. E. M. Christensen and G. H. Peters, Department of Chemistry, Technical University of Denmark, Kemitorvet 207, DK-2800 Kongens Lyngby, Denmark
E-mails: hemc@kemi.dtu.dk and ghp@kemi.dtu.dk

(Received 23 May 2016, revised 20 June 2016, accepted 29 June 2016)

doi:10.1002/2211-5463.12100

Tryptophan hydroxylase 2 (TPH2) catalyses the initial and rate-limiting step in the biosynthesis of serotonin, which is associated with a variety of disorders such as depression, obsessive compulsive disorder, and schizophrenia. Full-length TPH2 is poorly characterized due to low purification quantities caused by its inherent instability. Three truncated variants of human TPH2 (rc*h*TPH2; regulatory and catalytic domain, NΔ47-rc*h*TPH2; truncation of 47 residues in the N terminus of rc*h*TPH2, and c*h*TPH2; catalytic domain) were expressed, purified, and examined for changes in transition temperature, inactivation rate, and oligomeric state. c*h*TPH2 displayed 14- and 11-fold higher half-lives compared to rc*h*TPH2 and NΔ47-rc*h*TPH2, respectively. Differential scanning calorimetry experiments demonstrated that this is caused by premature unfolding of the less stable regulatory domain. By differential scanning fluorimetry, the unfolding transitions of rc*h*TPH2 and NΔ47-rc*h*TPH2 are found to shift from polyphasic to apparent two-state by the addition of L-Trp or L-Phe. Analytical gel filtration revealed that rc*h*TPH2 and NΔ47-rc*h*TPH2 reside in a monomer–dimer equilibrium which is significantly shifted toward dimer in the presence of L-Phe. The dimerizing effect induced by L-Phe is accompanied by a stabilizing effect, which resulted in a threefold increase in half-lives of rc*h*TPH2 and NΔ47-rc*h*TPH2. Addition of L-Phe to the purification buffer significantly increases the purification yields, which will facilitate characterization of *h*TPH2.

Tryptophan hydroxylase (TPH) catalyses the rate-limiting reaction in the biosynthesis of the hormone and neurotransmitter serotonin (5-HT). TPH uses the cofactor Fe^{2+} and the cosubstrates O_2 and tetrahydrobiopterin (BH_4) to generate 5-hydroxytryptophan (5-HTP) by hydroxylation of L-tryptophan (L-Trp). 5-HTP is enzymatically converted to 5-HT by aromatic amino acid decarboxylase [1,2]. TPH exists in two isoforms, where isoform 1 (TPH1) is mainly responsible for catalyzing the rate-limiting step in the biosynthesis of peripheral serotonin, and isoform 2 (TPH2) primarily is associated with the biosynthesis of neuronal serotonin [1]. The regulation of serotonin levels is involved in various physiological and psychiatric disorders such as irritable bowel syndrome, depression, obsessive compulsive disorder, and schizophrenia [3].

Abbreviations
5-HT, 5-hydroxytryptamin (serotonin); 5-HTP, 5-hydroxytryptophan; AAAH, aromatic amino acid hydroxylase; ACT, aspartate kinase, chorismate mutase and TyrA; BH_4, tetrahydrobiopterin; c*h*TPH2, catalytic domain of human tryptophan hydroxylase; DSC, differential scanning calorimetry; DSF, differential scanning fluorimetry; HEPES, 4-(2-hydroxyethyl)-1-piperazineethanesulfonic acid; L-Phe, L-phenylalanine; L-Trp, L-tryptophan; MBP, maltose binding protein; PAH, phenylalanine hydroxylase; rc*h*TPH2, regulatory and catalytic domains of human tryptophan hydroxylase 2; *rn*PAH, *Rattus norvegicus* phenylalanine hydroxylase; SEC, size exclusion chromatography; TH, tyrosine hydroxylase; TPH, tryptophan hydroxylase.

Of these, depression is associated with decreased levels of neuronal serotonin, whereas some gastrointestinal disorders are associated with increased peripheral serotonin levels [4–6]. The serotonergic systems are therefore important targets in treatment of these disorders [7], which makes both TPH isoforms important enzymes to characterize.

Along with phenylalanine hydroxylase (PAH) and tyrosine hydroxylase (TH), TPH forms an enzyme subfamily of iron(II)-containing mono-oxygenases collectively referred to as the aromatic amino acid hydroxylases (AAAHs). Various truncated variants of all three AAAHs have been structurally characterized [8–12]. For *h*TPH, the catalytic cores of both isoforms have been structurally and enzymatically characterized [13–15] due to successful purification strategies [16,17].

All enzymes in the AAAH family form tetramers through dimers of dimers [18]. Each monomeric subunit consists of an N-terminal regulatory domain, a highly conserved catalytic domain, and a C-terminal tetramerization domain [19]. The N-terminal domains of PAH and TH contain a characteristic ACT fold motif [12,20]. From sequence analysis, TPH has also been proposed to contain an ACT domain [21]. Truncations of the regulatory domains have been found not to change the tetrameric assembly of TPH1 or TPH2 [1,22]. In contrast, when the C-terminal tetramerization domain is also removed, monomeric species are observed [1]. Deletions from the C-terminal domain of rabbit TPH1 have been demonstrated to change the macromolecular structure from a tetramer to predominantly monomeric form without compromising catalytic activity [23,24].

The available crystal structures of TPH1 only comprise the catalytic domain, while the crystal structure of TPH2 includes both the catalytic and the tetramerization domains [13,14,25–27]. The lack of structural information of the regulatory domain is partly due to the great instability of full-length TPH [16,28]. In TPH, the regulatory domain, in particular, has been found to cause instability and therefore limiting the quantities purified from *Escherichia coli* expression systems [1,16]. The regulatory domain of TPH2 has an additional 46 residues compared to TPH1, which are partly responsible for the limited purification quantities [29]. The fundamental role of the regulatory domain and the additional residues in the terminus is, however, poorly understood, as characterization is hampered by the limited purification yields. Therefore, structural insight is obtained from the crystal structure of rat phenylalanine hydroxylase (*rn*PAH) (PDB ID: 1PHZ – Clustal Omega: 35% sequence identity in the regulatory domain and 57% total sequence identity) which comprises the catalytic and the regulatory domains. This structure lacks interpretable electron density in the first 18 residues of the N terminus, suggesting that this region is flexible [20]. The flexibility of the N terminus has also been confirmed by an NMR study [30]. By alignment of the sequences of *rn*PAH and *h*TPH2 (Fig. S1), it is found that residues 20 to 47 of *h*TPH2 align with the mobile 18 residues of *rn*PAH, which suggests that these residues of *h*TPH2 are mobile and might cause instability and insolubility. Therefore, an NΔ47-rc*h*TPH2 variant was expressed, purified, and characterized.

The current study sheds light on the influence of the regulatory domain on macromolecular structure and stability of TPH2 by characterizing three truncated variants (sequences shown in Supporting information); c*h*TPH2 (catalytic domain), rc*h*TPH2 (regulatory and catalytic domains), and NΔ47-rc*h*TPH2 (47 residue truncation in the N-terminal domain). The tetramerization domain (residue 460–490) was removed to investigate the role of the regulatory domain when TPH2 was not in a tetramer. As TPH2 is poorly characterized due to low stability, additional efforts were made to identify ligands that could increase the stability, and hence purification yield, of TPH2.

Results and Discussion

Differential scanning fluorimetry

Very little is known about the regulation and structure of TPH as purification of this enzyme results in limited quantities. The presence of the regulatory domain is known to cause low stability and solubility [1]. To overcome this problem, substrates for the AAAH family (L-phenylalanine, L-tryptophan, and L-tyrosine), other ligands known to bind certain ACT domains (L-valine [31] and L-serine [32]), as well as D-phenylalanine, 5-HTP, and 5-HT were assayed for changes in the thermal unfolding of the TPH2 variants. The ligands were screened in a broad concentration range (0.1 μM–10 mM). For c*h*TPH2, an almost ideal two-state unfolding behavior was observed, Fig. 1. All ligands, except 5-HTP and 5-HT, were found to have no significant effect on the unfolding or T_m value of c*h*TPH2, Fig. 1. 5-HTP and 5-HT appear to change the unfolding of c*h*TPH2 from two-state to continuous; hence, no T_m values could be obtained at high ligand concentration.

Containing the regulatory domain, rc*h*TPH2, gave rise to inconsistent and polyphasic unfolding curves from which no T_m values could be obtained (Fig. S2). The ligand screen showed that L-Trp and L-Phe induced

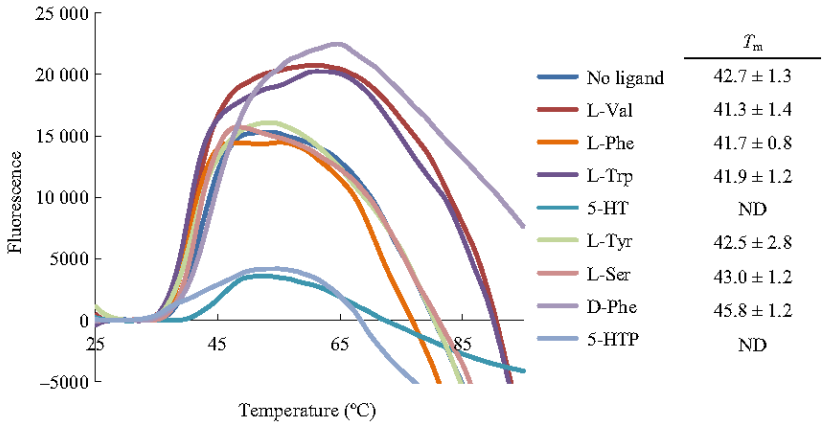

Fig. 1. Baseline corrected differential scanning fluorimetry (DSF) ligand screen on *ch*TPH2 (enzyme concentration of 1 μM). Representative examples of the highest concentration of the ligands in the screen (1.5 mM for tyrosine and 10 mM for all other ligands). To the right T_m values ($n = 3$) of *ch*TPH2 with the respective ligands are listed (ND, Not detectable).

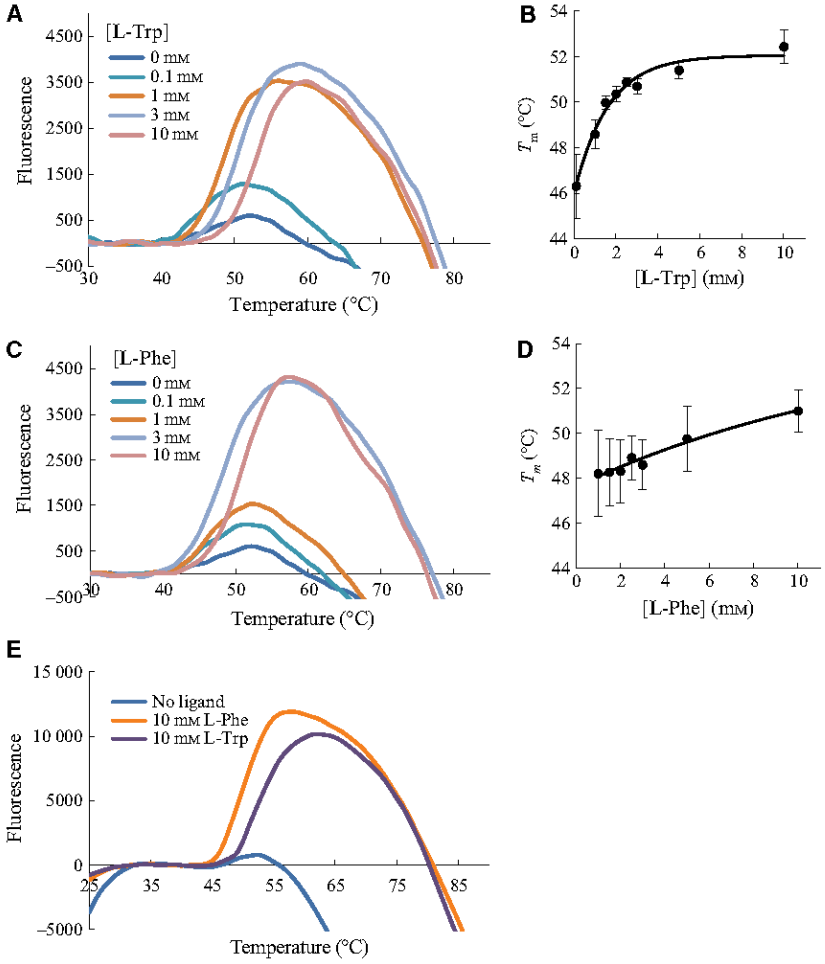

Fig. 2. Representative baseline corrected differential scanning calorimetry curves of rc*h*TPH2 or NΔ47-rc*h*TPH2 (1 μM). (A) DSF curves of rc*h*TPH2 with different L-Trp concentration. (B) T_m values with increasing L-Trp concentration for rc*h*TPH2 with an exponential fit. (C) DSF curves of rc*h*TPH2 with different L-Phe concentration. (D) T_m values with increasing L-Phe concentration for rc*h*TPH2 with an exponential fit. (E) DSF of NΔ47-rc*h*TPH2 curves in the absence of ligand, presence of 10 mM L-Phe, or presence of 10 mM L-Trp.

unfolding transitions with apparent two-state unfolding in a concentration-dependent manner (Fig. 2), which were accompanied by an increase in transition temperatures. The apparent two-state unfolding was gradually acquired with increasing ligand concentration, and robust apparent two-state unfolding was obtained at L-Trp (Fig. 2A) and L-Phe (Fig. 2C) concentrations of 1.0 mM and 3.0 mM, respectively. At 0.1 mM L-Trp, rc*h*TPH2 displayed a transition temperature of 46.3 ± 1.4 °C. This was increased to 52.4 ± 0.7 °C by the addition of 10.0 mM L-Trp. The exponential fit in Fig. 2B shows that saturation has been reached at

10 mM L-Trp. The transition temperature of rc*h*TPH2 was increased from 48.2 ± 1.9 to 51.0 ± 0.9 °C by increasing the L-Phe concentration from 1.0 mM to 10.0 mM (Fig. 2D). Similarly, a study by Gersting *et al.* [33] utilizing differential scanning fluorimetry (DSF) found that 1 mM L-Phe increases the transition temperature of PAH from 47.5 to 50.9 °C. None of the other ligands, including D-Phe, were able to induce this change in unfolding (data not shown). The same stabilizing trend for L-Phe and L-Trp was observed for NΔ47-rc*h*TPH2, Fig. 2E.

As both L-Trp and L-Phe gave rise to increased transition temperatures, a combination of the compounds was analyzed. Figure 3 shows that increasing the concentration of either L-Trp or L-Phe in the presence of the other compound results in increased T_m values, suggesting that L-Trp and L-Phe are able to increase the transition temperature in an additive fashion. The additive effect is supported by the increase in T_m values with increasing L-Phe concentration observed at saturated concentration of L-Trp (10 mM in Fig. 3).

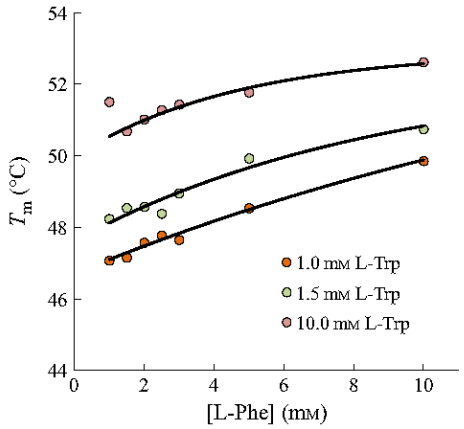

Fig. 3. Transition temperatures ($n = 3$ 4) obtained from DSF experiments of rc*h*TPH2 with the addition of L-Trp and L-Phe. Average standard deviation in each point is 0.8 °C. Curves represent exponential fit of T_m values as a function of [L-Phe] at constant [L-Trp]. Data for the lowest concentration of L-Phe at 10 mM L-Trp were omitted from the fit.

Analytical gel filtration

It has previously been shown in DSF assays that under stabilizing conditions multi-component complexes can change from polyphasic to almost two-state unfolding and that this is indicative of monodispersity and stability [34]. This was investigated in the case of L-Phe and L-Trp as unfolding of rc*h*TPH2 and NΔ47-rc*h*TPH2 was shifted toward two-state with the addition of these compounds. The oligomeric states of the TPH2 variants were analyzed utilizing analytical size exclusion chromatography (SEC). In consensus with the findings of D'Sa *et al.* [22], c*h*TPH2 was found to elute at a volume corresponding to the molecular weight of a monomer (36.2 kDa) [35]. In the loading concentration range of 2 to 60 μM, c*h*TPH2 was found only to reside as a monomer, Fig. 4. Additionally, 3 mM L-Phe did not induce any change in the elution pattern of the monodisperse solution complementing the observations from the DSF experiments.

A study by Mockus *et al.* [23] on rabbit TPH1 has demonstrated that truncation of the C-terminal tetramerization domain resulted in a disruption of the tetrameric assembly. This was also found to be the case for *h*TPH2, as SEC of NΔ47-rc*h*TPH2 yielded two overlapping peaks with elution volumes corresponding to molecular weights of a monomer (47.4 kDa) and a dimer (94.9 kDa) (Fig. 5). The gradual shift of the elution peaks from a monomer to a dimer shows that NΔ47-rc*h*TPH2 is found to be in a concentration-dependent monomer–dimer equilibrium. Within experimental error, the peak widths at half height were constant over the range of TPH

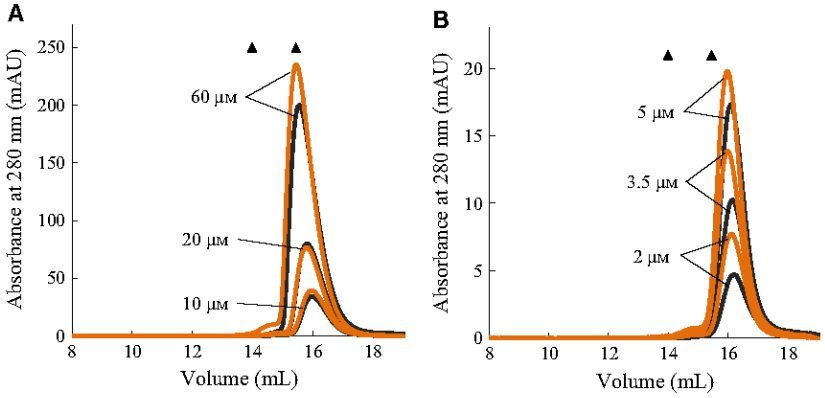

Fig. 4. Size exclusion chromatography of c*h*TPH2 with no ligand (black lines) and with the addition of 3 mM L-phenylalanine (orange lines). The markers (▲) indicate the expected elution volumes of a dimer and a monomer, respectively. Protein loading concentrations are indicated in the chromatograms. (A) High loading concentration range. (B) Low loading concentration range. AU, absorption units.

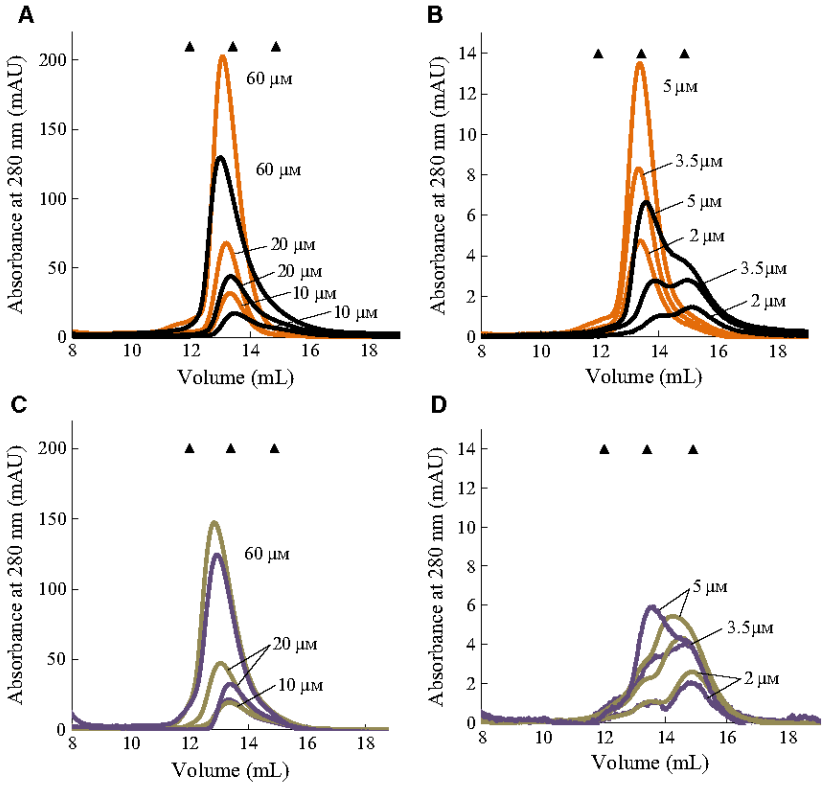

Fig. 5. Size exclusion chromatography of NΔ47-r*ch*TPH2. (A, B) SEC without added L-Phe (black lines) and with 3 mM L-Phe (orange lines). A: High loading concentration range. B: Low loading concentration range. (C, D) SEC with the addition of 3 mM D-Phe (beige lines) or 0.5 mM L-Trp (purple lines). C: High loading concentration range. (D) Low loading concentration range. The markers (▲) indicate the expected elution volume of (from left to right) a tetramer, a dimer, and a monomer, respectively. Protein loading concentrations are indicated in the chromatograms.

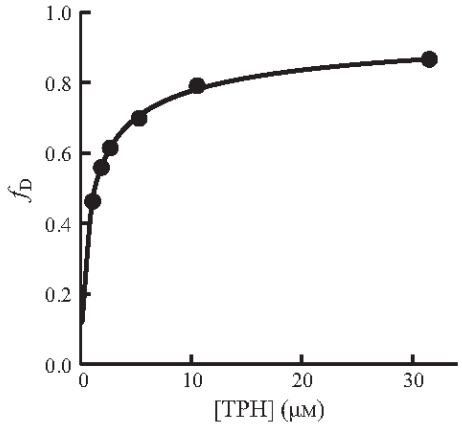

Fig. 6. Fraction of dimer as a function of NΔ47-r*ch*TPH2 concentration (loading concentration divided by dilution factor). The solid line represents the nonlinear regression of the data using equation 11 given in Materials and methods.

concentrations, and the peak heights were also found to be related directly to the concentration of TPH injected. The dilution factor was found to be 1.90 ± 0.13 and constant within the elution range of the TPH variants. From the SEC results, the equilibrium constant, K_d, of the dissociation of a dimer into monomers was calculated (equation (7) in Materials and methods). A K_d value of 1.3 ± 0.1 μM was found based on the six concentrations of NΔ47-r*ch*TPH2 in the absence of L-Phe. This value is lower than the dissociation constant of 46 ± 35 μM determined for the dimerization of the regulatory domain of PAH [36]. A plot of fraction dimer, f_D, as a function of NΔ47-r*ch*TPH2 concentration gave a hyperbolic-like curve as expected for a monomer–dimer equilibrium, Fig. 6.

The difference in oligomeric states of c*h*TPH2 and r*ch*TPH2/NΔ47-r*ch*TPH2 shows that dimerization is caused by the regulatory domain. This finding is supported by a model structure proposed by Jiang *et al.* [37] in which the regulatory domain of one monomer forms intersubunit interactions to an adjacent monomer. The involvement of the regulatory domain in structural assembly is further supported by results from Yohrling *et al.* [38] on rabbit TPH1, where NΔ41 and NΔ90 truncations resulted in monomers indicating that the regulatory domain is involved in the formation of the tetrameric assembly. D'Sa *et al.* [22], however, found that the tetrameric assembly was retained upon truncation of the regulatory domain of human TPH2. Collectively, this might suggest that both the C-terminal tetramerization domain and the N-terminal regulatory domain contribute to the formation of a stable tetramer.

The effect of L-Phe on the monomer–dimer equilibrium was analyzed by performing SEC on

NΔ47-rc*h*TPH2 samples with and without the addition of L-Phe. In Fig. 5, the black curves represent elution of NΔ47-rc*h*TPH2 without the addition of L-Phe, and the orange curves represent the elution of protein when the sample and running buffer contained 3 mM L-Phe. It is evident that L-Phe shifts the equilibrium toward dimer. At a loading concentration of 2 μM NΔ47-rc*h*TPH2, the addition of L-Phe was found to shift the equilibrium from predominately monomer to almost exclusively dimer. The same shift in monomer–dimer equilibrium was observed for rc*h*TPH2 (Fig. 7A). This result correlates well with the observations in the DSF experiments, where the unfolding curves change from polyphasic toward two-state with the addition of L-Phe.

The influence of L-Trp and D-Phe on the monomer–dimer equilibrium was additionally analyzed to investigate the specificity of L-Phe. Figure 5C,D shows the monomer–dimer distribution of NΔ47-rc*h*TPH2 with 0.5 mM L-Trp or 3 mM D-Phe in a protein concentrations range from 2 to 60 μM. From the SEC results in Fig. 5, dimerization K_d values of 1.6 ± 0.7 μM and 1.8 ± 0.9 μM were determined in the presence of L-Trp and D-Phe, respectively. 3 mM D-Phe or 0.5 mM L-Trp does, therefore, not change the monomer–dimer equilibrium constant. At a TPH2 loading concentration of 2 μM, it is evident by comparison of Fig. 5B,D that neither the addition of 0.5 mM L-Trp nor 3 mM D-Phe induced the shift in the monomer–dimer equilibrium toward dimer as observed for L-Phe. L-Trp absorption introduced high background noise and was hence only added to concentrations of 0.5 and 1.0 mM. As a consequence of the background noise, chromatograms of NΔ47-rc*h*TPH2 with loading concentrations below 5 μM could not be obtained at 1.0 mM L-Trp. However, at low protein concentrations (5–20 μM), the monomer–dimer equilibrium does not seem to be influenced by 1.0 mM L-Trp as monomer is present (Fig. 7B), which is not observed in the presence of L-Phe (Fig. 5A,B). The addition of 1 mM L-Trp is compared with 3 mM L-Phe as these concentrations were found in the DSF experiments to change the unfolding from polyphasic to apparent two-state (Fig. 2A,C). The fact that L-Trp did not induce the same shift in equilibrium suggests that the stabilization observed in the DSF experiments occurs through a different mechanism than for L-Phe. Furthermore, L-Phe binding is found to be specific as D-Phe did not induce dimerization. That L-Trp does not induce dimerization in *rch*TPH2 extends recent results obtained by Patel *et al.*, who showed that among the regulatory domains of TH, PAH, and TPH1, only PAH dimerizes in the presence of its natural substrate [39].

Thermal inactivation

To investigate if the dimerizing effect had an impact on TPH2 stability, rates of inactivation at 30 °C in the presence or absence of 3 mM L-Phe were examined. The data were fitted with one-exponential decay curves, and the rate constants, k, were calculated using an exponential function, $E_t = E_0 e^{-kt}$, where E_0 is the initial enzyme activity, and E_t is the activity after time t at 30 °C (Fig. 8). From the decay rate constants, half-lives ($t_{½}$) of the *h*TPH2 variants were calculated using $t_{½} = \ln(2)/k$. At 30 °C and a concentration of 5 μM, rc*h*TPH2, and NΔ47-rc*h*TPH2 displayed $t_{½}$ values of only 15 ± 2 and 18 ± 3 min, respectively. Hence, truncation of the N terminus slightly increased the $t_{½}$ value ($P = 0.18$, T-test). With a $t_{½}$ value of 203 ± 40 min, c*h*TPH2 displayed a 14-fold higher half-life compared to rc*h*TPH2, which is in agreement with the results of Carkaci-Salli *et al.* [1] and confirms that the presence of the regulatory domain causes significant destabilization. With addition of 3 mM L-Phe, $t_{½}$ values of 41 ± 3, 49 ± 5, and 193 ± 29 min were obtained for rc*h*TPH2, NΔ47-rc*h*TPH2, and c*h*TPH2, respectively. Variants containing the regulatory domain displayed nearly 3-fold increase in half-lives whereas c*h*TPH2 was not significantly influenced by L-Phe.

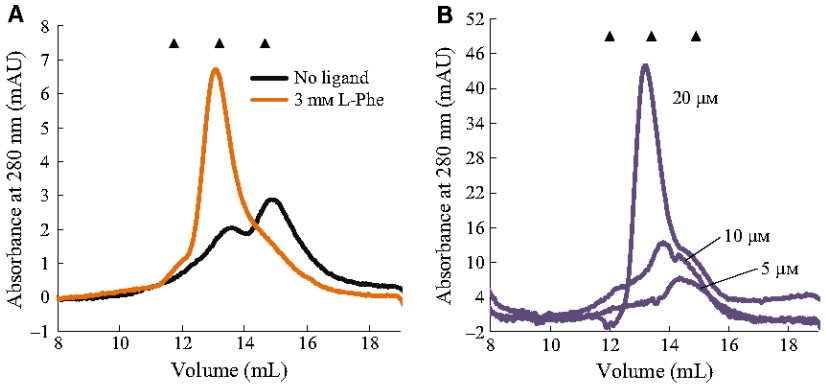

Fig. 7. (A) Size exclusion chromatography of rc*h*TPH2 (loading concentration of 2 μM), with no ligand (black line) and with the addition of 3 mM L-Phe (orange line). (B) Size exclusion chromatography of NΔ47-rc*h*TPH2, with the addition of 1 mM L-Trp. Protein loading concentrations are indicated in the chromatogram. The markers (▲) indicate the expected elution volumes of a tetramer, a dimer, and a monomer, respectively.

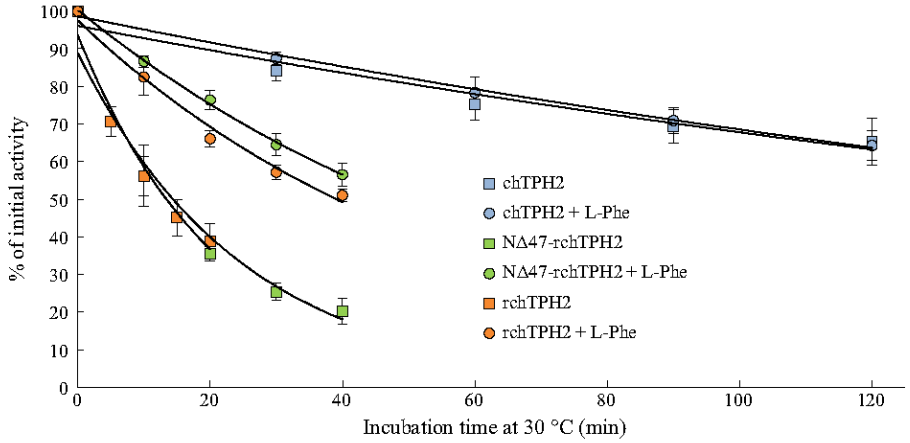

Fig. 8. Heat inactivation of hTPH2 variants. Enzyme samples (5 μM) were incubated at 30 °C, and residual activity in % of initial activity at t_0 was assayed in time intervals. The curves are fit to the mean of three independent measurements performed on each variant. Squares and circles present heat inactivation in the absence or presence of 3 mM L-Phe, respectively.

That the stabilizing effect is exclusively observed for rc*h*TPH2 and NΔ47-rc*h*TPH2 implies that L-Phe is stabilizing through binding to the regulatory domain. Further, as L-Phe induces a stabilizing effect in both rc*h*TPH2 and NΔ47-rc*h*TPH2, binding of L-Phe does not seem to involve the 47 N-terminal residues. L-Phe induced stability and shift in equilibrium toward dimer imply that TPH2 variants containing the regulatory domain are more stable as dimers.

A stabilizing effect of L-Trp has previously been observed by McKinney *et al.* [16] who hypothesized that L-Trp might stabilize through binding in the active site, which might tighten up flexible regions, and hereby protect the active site. The increase in T_m (DSF) upon the addition of L-Phe or L-Trp might, analogously to the hypothesis of McKinney *et al.* [16], occur through binding in the active site which in turn induces a more closed conformation, as it has been seen for binding of tryptophan in chicken TPH [25]. However, a shift in the monomer–dimer equilibrium is only observed for L-Phe, suggesting that the increase in T_m and half-life occur through different mechanisms. Alternatively, L-Phe binds in an allosteric site which stabilizes the regulatory domain through improved interactions with an adjacent monomer. Such an allosteric site in the regulatory domain has been identified in PAH, which has been found to increase PAH activity and stability and induce large conformational changes [20,39–41]. This is consistent with the binding of amino acids to ACT domains which often occurs at domain interfaces and results in conformational changes [42]. This hypothesis is supported by the observed shift in monomer–dimer equilibrium and the additive effect of L-Trp and L-Phe observed in the DSF experiments. Such an allosteric site might have relevance *in vivo* functioning as an allosteric modulating site that stabilizes a dimer in the native tetramer (dimer of dimers). Stabilization of the tetramer is important as disruption of the native tetramer results in decreased enzymatic activity [43].

Differential scanning calorimetry

The transition temperatures, T_m, of the TPH2 variants were measured utilizing differential scanning calorimetry (DSC), to investigate if the low half-life of *rch*TPH2 is caused by premature unfolding of the regulatory domain. The DSC experiments were performed in the presence of L-Phe to observe domain unfolding in a monodisperse solution. All variants displayed irreversible unfolding upon reheating and hence, only T_m values were extracted from the thermograms. Illustrative examples of DSC thermograms of the three variants are presented in Fig. 9.

The unfolding transitions of the three variants seem equivalent, however, by comparison of the thermograms of c*h*TPH2 and NΔ47-rc*h*TPH2 (Fig. 9A,B), it is evident that truncation of the regulatory domain resulted in a reduction in the heat capacity of the low temperature transition (T_m(low)). This suggests that the lowest temperature transitions are partly due to the unfolding of the regulatory domain, as suggested for *h*PAH by Thórólfsson et al. [44]. The remaining transitions, therefore, originate from the unfolding of the more stable catalytic domain, quantified by the transition temperature of the main peak in the thermograms (T_m(high)). Transition temperatures obtained from the thermograms are presented in Table 1.

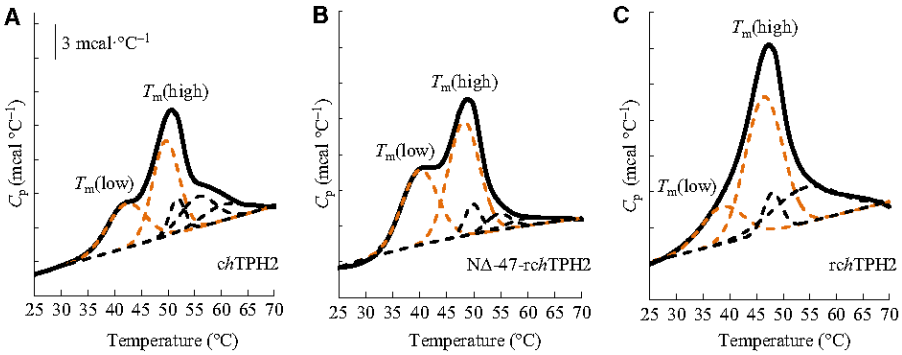

Fig. 9. Examples of DSC thermograms of *ch*TPH2 (A), NΔ47-r*ch*TPH2 (B), and r*ch*TPH2 (C) purified in L-Phe buffer. All variants were analyzed at a concentration of 35 μM. DSC data after baseline subtraction are shown in solid lines and individual peaks from deconvolution as dashed lines. The quantified transitions marked T_m(low) and T_m(high) are highlighted in orange dashed lines.

Table 1. The transition temperature of the investigated *h*TPH2 variants obtained from DSC, where means ± SD of T_m(low) and T_m(high) values (Fig. 9) obtained from three independent experiments are listed. A protein concentration of 35 μM was used in all measurements.

	r*ch*TPH2	NΔ47-r*ch*TPH2	*ch*TPH2
T_m(low), °C	40.1 ± 1.2	39.6 ± 0.5	41.7 ± 0.4
T_m(high), °C	46.8 ± 0.3	47.7 ± 0.5	49.7 ± 0.1

Deletion of the regulatory domain increased the T_m values of the two main transitions by 1.6 and 2.9 °C, respectively. Truncation of the N terminus only induced a slight increase in the T_m(high) value ($P = 0.053$, *T*-test).

The regulatory and catalytic domains of r*ch*TPH2 unfold at 40.1 ± 1.2 °C and 46.8 ± 0.3 °C, respectively. These results are, despite variations in the buffer systems, in the same range as previously reported transition temperatures for AAAHs (47.5–55.5 °C) [33,45,46]. The DSC data relate to the inactivation measurements, as unfolding of the variants containing the regulatory domain is initiated at around 30 °C (Fig. 9C,B), which is the temperature of the inactivation measurements, and around 35 °C for *ch*TPH2 (Fig. 9A). This might explain the significantly higher $t_{½}$ values observed for *ch*TPH2 at 30 °C. Unfolding of r*ch*TPH2 shows a less profound low temperature transition compared to NΔ47-r*ch*TPH2. This might be explained by the mobile N terminus causing a less defined regulatory domain which seems to unfold more continuously initiated at lower temperature than observed for *ch*TPH2. Furthermore, the presence of the regulatory domain causes an earlier unfolding of the catalytic domain; this signifies that attempts to stabilize TPH should occur through the regulatory domain.

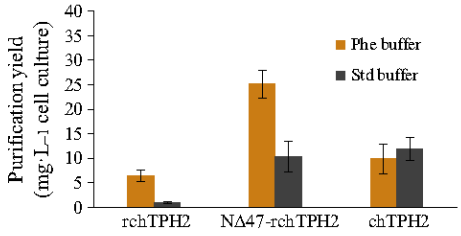

Fig. 10. Purification yields (mg·L^{-1} cell culture, $n = 2$ 6) of the three *h*TPH2 variants (mean ± SD). Orange and dark gray bars state yields obtained from purifications using Phe buffer (20 mM HEPES/NH_4OH, 300 mM $(NH_4)_2SO_4$, pH 7.0, and 3 mM L-Phe) and Std buffer (20 mM HEPES/NH_4OH, 300 mM $(NH_4)_2SO_4$, and pH 7.0), respectively.

Purification yield

Characterization of *h*TPH2 variants containing the regulatory domain has been hampered by the low quantities obtained from *E. coli*, partially due to the poor stability. Figure 10 presents the purification yields obtained for the three variants with and without L-Phe added to the purification buffer. Without L-Phe, very low purification quantities were obtained for r*ch*TPH2 (0.9 ± 0.2 mg·L^{-1}) compared to *ch*TPH2 (12.0 ± 2.4 mg·L^{-1}). The low quantities for r*ch*TPH2 were overcome by truncation of the N terminus which resulted in an 11-fold increase in yield (10.4 ± 3.1 mg·L^{-1}), which was similar to that of *ch*TPH2.

The stabilizing effect of L-Phe was reflected in the purification yields, as they were increased seven- and twofold for r*ch*TPH2 (6.4 ± 1.2 mg·L^{-1}) and NΔ47-r*ch*TPH2 (25.1 ± 2.9 mg·L^{-1}), respectively (Fig. 10). In line with the results observed in the inactivation experiment, no significant change in purification yield was observed for *ch*TPH2 (9.9 ± 3.1 mg·L^{-1}).

Conclusion

The current results demonstrate that L-Trp and L-Phe change the unfolding mechanism of *h*TPH2, but only when the regulatory domain is present. Deletion of the C-terminal tetramerization domain results in a monomer–dimer equilibrium which is shifted to predominately dimer with the addition of L-Phe. In the presence of L-Phe, the dimer displayed significantly increased half-life which in turn resulted in significantly increased purification yields of *h*TPH2 variants containing the regulatory domain. These findings will facilitate future characterization of *h*TPH2.

Materials and methods

Materials

All used chemicals were of analytical grade, and all solutions were prepared using water from an 18.2 MΩ·cm Milli-Q synthesis A10 Q-Gard system which was filtered through a 0.22-μm filter. Protein purification was performed on an ÄKTA purifier 100 from GE Healthcare. Utilized GE Healthcare column variants: HiLoad Superdex 200 26/60 pg, Superdex 200 10/300 GL, and a XK 16/20 column packed with 25 mL Dextrin Sepharose High Performance media. During purifications, all TPH-containing solutions were kept in ice water, except during the chromatographic steps, which were performed at room temperature. Protein solutions were concentrated using an Amicon ultrafiltration cell with an Ultracell PL-3 membrane. Protein concentrations were determined by measuring the absorbance at 280 nm on an ND-1000 NanoDrop Spectrophotometer from Saveen Werner (Limhamn, Sweden).

Cloning and expression

Full-length human TPH2 cDNA optimized for expression in *E. coli* was obtained from GenScript (Piscataway, NJ, USA). All proteins were expressed as maltose binding protein fusion proteins from the pET26 expression vector in *E. coli* BL21 (DE3) (Novagen, Merck Millipore, Darmstadt, Germany) cells. The sequences of the proteins expressed are given in the Supporting information. The recombinant fusion proteins contain a cleavage recognition site for human rhinovirus 3C protease (3CP) [47]. The construct encoding the different protein variants was obtained by PCR. The primers used are listed in Table S1. All DNA sequences were verified by sequencing (Eurofins). Proteins were expressed at 20 °C for 14 h, as previously described [17]. MBP-3CP was cloned and expressed in-house in a similar manner.

Purification

Escherichia coli cells from 650 mL cultures were thawed from −80 °C and resuspended in buffer containing 20 mM HEPES/NH_4OH, 300 mM $(NH_4)_2SO_4$, pH 7.0 (standard buffer, Std buffer) or 20 mM HEPES/NH_4OH, 300 mM $(NH_4)_2SO_4$, pH 7.0, and 3 mM L-Phe (Phe buffer), to a volume of 40 mL. $(NH_4)_2SO_4$ was included in the purification buffer, as it has been found that the purification yield of recombinant catalytic core of rabbit TPH1 was enhanced by the addition of ammonium sulfate [24]. The resuspended cell culture was lysed by sonication for 3 × 30 s using a Satorius Labsonic at 80% amplitude, while kept in ice water. The lysed sample was centrifuged at 4 °C and 18 000 *g* for 20 min. The supernatant was decanted to another tube and centrifuged a second time at 4 °C and 18 000 *g* for 20 min, while the pellet was discarded. The supernatant was collected and filtered through a 0.45-μm filter. A volume of approximately 35 mL filtered supernatant was loaded with a flow rate of 5 mL·min ^{1} onto a Dextrin Sepharose column, which was equilibrated with five column volumes of Std or Phe buffer. Following sample loading, an MBP-3CP solution was prepared by diluting MBP-3CP from stock with Std or Phe buffer to a concentration of 2.2 μM. About 30-mL MBP-3CP solution was loaded onto the column with a flow rate of 5 mL·min ^{1}, and the column was incubated at room temperature for 1 h. Once the flow (5 mL·min ^{1}) was resumed, 10 mL of the protein-containing eluate was collected. The collected solution, containing target protein, was filtered through a 0.45-μm filter prior to loading on a HiLoad Superdex 200 prep grade column, which had been equilibrated with two column volumes of Std or Phe buffer. Std or Phe buffer was used as mobile phase using a flow rate of 2.5 mL·min ^{1}, and UV-detected (280 nm) peaks containing the target protein (verified by SDS/PAGE analysis – Figs S3–S5) were collected. The concentration of the collected protein was determined by UV-Vis absorption at 280 nm utilizing theoretical extinction coefficients obtained from Expasy [48]. The samples were either concentrated by ultrafiltration prior to freezing in liquid nitrogen, or if the concentration of target protein was high enough in the eluate, the ultrafiltration was bypassed, and the protein solution was frozen in liquid nitrogen and stored at −80 °C.

SDS/PAGE

Evaluation of molecular weights and purity were conducted by SDS/PAGE. Proteins were resolved on Mini-PROTEAN TGX gels (7.5%) from Bio-Rad (Hercules, CA, USA) run at 100 V for 75 min with a protein standard from Bio-Rad (no. 161-0304). Gels were stained with Coomassie Blue to visualize the proteins.

Differential scanning fluorimetry

The unfolding of the TPH2 variants was recorded with an Agilent Technologies Stratagene MX3005 P RT-PCR machine (Santa Clara, CA, USA). The ligand screen was

performed with a total volume of 25 μL in 96-well plates (polypropylene plates from Agilent Technologies). Each well was composed of protein at a concentration of 1 μM, SYPRO orange at a concentration of 2× (diluted from SYPRO® 5000× stock from Sigma, St. Louis, MO, USA), and ligand (diluted in purification buffer) in a concentration range of 0.1 μM to 10 mM. Each plate contained control wells with the purification buffer with and without protein and ligand. Scans were carried out using a scan rate of 1 °C·min ^{1}, going from 20 °C to 95 °C. The thermograms were baseline corrected with MXPRO QPCR Software (Agilent Technologies, Santa Clara, CA, USA) and analyzed for transition temperatures with GRAPHPAD PRISM 6 (GraphPad Software, Inc, La Jolla, CA, USA) utilizing a Boltzmann sigmoid fit:

$$y = \mathrm{LL} + \frac{\mathrm{UL} - \mathrm{LL}}{1 + \exp\left(\frac{T_m - x}{a}\right)}$$

where LL and UL are the values of minimum and maximum intensities, respectively, and a denotes the slope of the unfolding curve at T_m [49].

Analytical size exclusion chromatography

Determination of the oligomeric state of the TPH2 variants was performed on a Superdex 200 10/300 GL column. Prior to analysis, the column was equilibrated with two column volumes of the buffer of investigation, and the samples were spiked with concentrated stock solutions of L-Trp, L-Phe, or D-Phe and allowed to equilibrate for 20 min. Samples were injected with a 500 μL loop and analyzed at a flow rate of 0.5 mL·min ^{1}. Calibration curve of molecular weights was obtained from GE Healthcare [35].

The equilibrium constant of the dissociation of a dimer into monomers was based on the scheme below

$$\mathrm{D} \xrightarrow{K_d} \mathrm{M} + \mathrm{M}$$

The equilibrium dissociation constant, K_d, is defined by

$$K_d = \frac{[\mathrm{M}]^2}{[\mathrm{D}]} \quad (1)$$

where [M] and [D] are the molar concentrations of monomer and dimer, respectively. The total protein concentration, $[\mathrm{M}]_{total}$, can be expressed in terms of molar monomer equivalents

$$[\mathrm{M}]_{total} = [\mathrm{M}] + 2[\mathrm{D}] \quad (2)$$

and the concentration of dimer is therefore given by

$$[\mathrm{D}] = \frac{[\mathrm{M}]_{total} - [\mathrm{M}]}{2} \quad (3)$$

Under the assumptions that $\varepsilon_{280,dimer} = 2{\cdot}\varepsilon_{280,monomer}$ and area under the size exclusion curve (SEC) curve (AUC) $\propto$ [M], the molecular concentration of monomer is given by

$$[\mathrm{M}] = \frac{\mathrm{AUC_M}}{\mathrm{AUC_M} + \mathrm{AUC_D}} * [\mathrm{M}]_{total} \quad (4)$$

where $\mathrm{AUC_M}$ and $\mathrm{AUC_D}$ are the area under the curve of the peaks representing the monomer and dimer, respectively, obtained by deconvolution of the chromatograms from the SEC experiments. Substituting [M] in equation (3) by the expression of [M] in equation (4) yields

$$[\mathrm{D}] = \frac{1}{2}\frac{\mathrm{AUC_D}}{\mathrm{AUC_M} + \mathrm{AUC_D}}[\mathrm{M}]_{total} \quad (5)$$

where $\mathrm{AUC_D}/(\mathrm{AUC_M} + \mathrm{AUC_D})$ is the mole fraction of dimer, f_D. Substituting [M] and [D] from equation (4) and (5), respectively, into equation (1) yields

$$K_d = \frac{2{*}\mathrm{AUC_M^2}{*}[\mathrm{M}]_{total}}{\mathrm{AUC_D}{*}(\mathrm{AUC_D} + \mathrm{AUC_M})} \quad (6)$$

The sample concentration loaded in SEC will be diluted during separation. Therefore, when applying equation (6), $[\mathrm{M}]_{total}$ must be divided by the dilution factor, DF, introduced during gel filtration

$$K_d = \frac{2{*}\mathrm{AUC_M^2}\frac{[\mathrm{M}]_{total}}{\mathrm{DF}}}{\mathrm{AUC_D}{*}(\mathrm{AUC_D} + \mathrm{AUC_M})} \quad (7)$$

The dilution factor during elution was measured by the width at half height of the peak divided by the sample load volume [50]. This was performed only on monodisperse solutions. The fraction of dimer, f_D, as a function of $[\mathrm{M}]_{total}$ can be expressed as

$$[\mathrm{D}] = \frac{1}{2}{*}f_D{*}\frac{[\mathrm{M}]_{total}}{\mathrm{DF}} \quad (8)$$

$$[\mathrm{M}] = (1 - f_D){*}\frac{\mathrm{M}_{total}}{\mathrm{DF}} \quad (9)$$

Substituting [M] and [D] from equation (8) and (9), respectively, into equation (1) yields

$$K_d = \frac{\left((1 - f_D){*}\frac{\mathrm{M}_{total}}{\mathrm{DF}}\right)^2}{f_D{*}\frac{1}{2}{*}\frac{\mathrm{M}_{total}}{\mathrm{DF}}} \quad (10)$$

Solving equation (10) for the fraction of dimer, f_D, yields

$$f_D = \frac{\frac{1}{4}\left(4{*}\frac{[\mathrm{M}]_{total}}{\mathrm{DF}} + K_d - 1{*}\sqrt{K_d^2 + 8{*}K_d{*}\frac{[\mathrm{M}]_{total}}{\mathrm{DF}}}\right)}{\frac{[\mathrm{M}]_{total}}{\mathrm{DF}}} \quad (11)$$

Activity assay

The activity measurements were performed using a Varian Cary Eclipse Fluorescence Spectrophotometer. For activity measurements, the *h*TPH2 variants were thawed under running water, filtered, and the concentrations were

determined by UV-Vis absorption at 280 nm. The *h*TPH2 samples were diluted to a protein concentration of 5 μM in the buffer in which it was purified. TPH2 activity was assayed in a reaction mixture (10 × 10 mm QS quartz cuvette from Hellma (Müllheim, Germany) – 2500 μL total volume) containing 50 mM HEPES/NH_4OH, 200 mM $(NH_4)_2SO_4$, pH 7.0, 0.025 g·L^{-1} catalase, 25 μM $(NH_4)_2Fe(II)(SO_4)_2{\cdot}6H_2O$, 7 mM dithiothreitol (DTT), 60 μM L-Trp, and 300 μM BH_4 with stirring at 15 °C [14,51]. The excitation wavelength was 300 nm, and the emission was monitored at 330 nm. The activities were determined by the initial slope (intensity·min^{-1}) of the monitored fluorescence and were quantified using VARIAN SPECTROPHOTOMETER software (Agilent Technologies). Quantification occurred through linear regression on a manually placed interval of minimum 0.04 min of the initial curve. Denaturation was performed by heating the protein in aliquots of 1300 μL to 30 °C in a water bath. The denaturation was stopped by cooling the protein solution in ice water.

Differential scanning calorimetry

Differential scanning calorimetry (DSC) measurements were carried out on a TA Instruments (New Castle, DE, USA) 6300 Nano DSC. Solutions of protein in L-Phe containing buffer were used for sample measurements, and the same buffer as used in the purification of the *h*TPH2 variants were used as references. Prior to sample loading, the protein sample and the reference buffer were degassed at approximately 10 °C using a MicroCal (MicroCal, LLC, Northhampton, MA, USA) USB ThermoVac. Three hundred microliters of protein sample and reference buffer were loaded in the respective cells. A constant pressure of 3 atm was applied, and scans were carried out using a scan rate of 1 °C·min^{-1}, going from 5 °C to 70 °C. Deconvolution of the thermograms was performed with Peakfit v4.12 using Gaussian peak functions.

Acknowledgements

KDT acknowledges financial support via an Academic Excellence Scholarship from the Department of Chemistry, Technical University of Denmark. The authors would like to thank Esben Thormann and Jonas R. Henriksen for providing access to their differential scanning calorimeter, as well as David F. Nielsen and Martin H. Pedersen for technical assistance.

Author contributions

KDT: Wrote the paper, performed experiments, and analyzed the data. HEMC and GHP: Designed experiments, contributed to data analysis and in writing the paper. NH and JB: Performed preliminary experiments. PH: Contributed to writing the paper.

References

1 Carkaci-Salli N, Flanagan JM, Martz MK, Salli U, Walther DJ, Bader M and Vrana KE (2006) Functional domains of human tryptophan hydroxylase 2 (hTPH2). *J Biol Chem* **281**, 28105–28112.

2 Udenfriend S, Clark CT and Titus E (1953) 5-hydroxytryptophan decarboxylase: a new route of metabolism of tryptophan. *J Am Chem Soc* **75**, 501–502.

3 Costagliola C, Parmeggiani F, Semeraro F and Sebastiani A (2008) Selective serotonin reuptake inhibitors: a review of its effects on intraocular pressure. *Curr Neuropharmacol* **6**, 293–310.

4 Liu Q, Yang Q, Sun W, Vogel P, Heydorn W, Yu X, Hu Z, Yu W, Jonas B, Pineda R *et al.* (2008) Discovery and characterization of novel tryptophan hydroxylase inhibitors that selectively inhibit serotonin synthesis in the gastrointestinal tract. *J Pharmacol Exp Ther* **325**, 47–55.

5 Popova NK and Kulikov AV (2010) Targeting tryptophan hydroxylase 2 in affective disorder. *Expert Opin Ther Targets* **14**, 1259–1271.

6 Matthes S, Mosienko V, Bashammakh S, Alenina N and Bader M (2010) Tryptophan hydroxylase as novel target for the treatment of depressive disorders. *Pharmocology* **85**, 95–109.

7 Torrente MP, Gelenberg AJ and Vrana KE (2012) Boosting serotonin in the brain: is it time to revamp the treatment of depression? *J Psychopharmacol* **26**, 629–635.

8 Andersen OA, Flatmark T and Hough E (2001) High resolution crystal structures of the catalytic domain of human phenylalanine hydroxylase in its catalytically active Fe(II) form and binary complex with tetrahydrobiopterin. *J Mol Biol* **314**, 279–291.

9 Erlandsen H, Fusetti F, Martinez A, Hough E, Flatmark T and Stevens RC (1997) Crystal structure of the catalytic domain of human phenylalanine hydroxylase reveals the structural basis for phenylketonuria. *Nat Struct Biol* **4**, 995–1000.

10 Andersen OA, Stokka AJ, Flatmark T and Hough E (2003) 2.0 Å resolution crystal structure of the ternary complex of human phenylalanine hydroxylase with tetrahydrobiopterin and 3-(2-thienyl)-L-alanine, or L-norleucine: substrate specificity and molecular motions related to substrate binding. *J Mol Biol* **333**, 747–757.

11 Goodwill KE, Sabatier C, Marks C, Raag R, Fitzpatrick PF and Stevens RC (1997) Crystal structure of tyrosine hydroxylase at 2.3 A and its implications for inherited neurodegenerative diseases. *Nat Struct Biol* **4**, 578–585.

12 Zhang S, Huang T, Ilangovan U, Hinck AP and Fitzpatrick PF (2014) The solution structure of the regulatory domain of tyrosine hydroxylase. *J Mol Biol* **426**, 1483–1497.
13 Wang L, Erlandsen H, Haavik J, Knappskog PM and Stevens RC (2002) Three-dimensional structure of human tryptophan hydroxylase and its implications for the biosynthesis of the neurotransmitters serotonin and melatonin. *Biochemistry* **41**, 12569–12574.
14 Kopec J, Oberholzer A, Fitzpatrick PF, Newman J, Tallant C, Kiyani W, Shrestha L, Burgess-Brown N, von Delft F, Arrowsmith C *et al.* (2014) Crystal structure of human tryptophan hydroxylase 2 (TPH2), catalytic domain, pdb entry: 4V06.
15 Windahl MS, Boesen J, Karlsen PE and Christensen HEM (2009) Expression, purification and enzymatic characterization of the catalytic domains of human tryptophan hydroxylase isoforms. *Protein J* **28**, 400–406.
16 McKinney J, Knappskog PM, Pereira J, Ekern T, Toska K, Kuitert BB, Levine D, Gronenborn AM, Martinez A and Haavik J (2004) Expression and purification of human tryptophan hydroxylase from *Escherichia coli* and *Pichia pastoris*. *Protein Expr Purif* **33**, 185–194.
17 Nielsen MS, Petersen CR, Munch A, Vendelboe TV, Boesen J, Harris P and Christensen HEM (2008) A simple two step procedure for purification of the catalytic domain of chicken tryptophan hydroxylase 1 in a form suitable for crystallization. *Protein Expr Purif* **57**, 116–126.
18 Liberles JS, Thórólfsson M and Martínez A (2005) Allosteric mechanisms in ACT domain containing enzymes involved in amino acid metabolism. *Amino Acids* **28**, 1–12.
19 Fitzpatrick PF (1999) Tetrahydropterin-dependant amino acid hydroxylases. *Annu Rev Biochem* **68**, 355–381.
20 Kobe B, Jennings IG, House CM, Michell BJ, Goodwill KE, Santarsiero BD, Stevens RC, Cotton RG and Kemp BE (1999) Structural basis of autoregulation of phenylalanine hydroxylase. *Nat Struct Biol* **6**, 442–448.
21 Aravind L and Koonin EV (1999) Gleaning non-trivial structural, functional and evolutionary information about proteins by iterative database searches. *J Mol Biol* **287**, 1023–1040.
22 D'Sa CM, Arthur RE and Kuhn DM (1996) Expression and deletion mutagenesis of tryptophan hydroxylase fusion proteins: delineation of the enzyme catalytic core. *J Neurochem* **67**, 917–926.
23 Mockus SM, Kumer SC and Verana KE (1997) Carboxyl terminal deletion analysis of tryptophan hydroxylase. *Biochim Biophys Acta* **1342**, 132–140.
24 Moran GR, Daubner SC and Fitzpatrick PF (1998) Expression and characterization of the catalytic core of tryptophan hydroxylase. *J Biol Chem* **273**, 12259–12266.
25 Windahl MS, Petersen CR, Christensen HEM and Harris P (2008) Crystal structure of tryptophan hydroxylase with bound amino acid substrate. *Biochemistry* **47**, 12087–12094.
26 Jin H, Cianchetta G, Devasagayaraj A, Gu K, Marinelli B, Samala L, Scott S, Stouch T, Tunoori A, Wang Y *et al.* (2009) Substituted 3-(4-(1,3,5-triazin-2-yl)-phenyl)-2-aminopropanoic acids as novel tryptophan hydroxylase inhibitors. *Bioorg Med Chem Lett* **19**, 5229–5232.
27 Cianchetta G, Stouch T, Yu W, Shi Z, Tari LW, Swanson RV, Hunter MJ, Hoffman ID and Liu Q (2010) Mechanism of inhibition of novel tryptophan hydroxylase inhibitors revealed by co-crystal structures and kinetic analysis. *Curr Chem Genomics* **4**, 19–26.
28 D'Sa CM, Arthur Jr RE, States JC and Kuhn DM (1996) Tryptophan hydroxylase: cloning and expression of the rat brain enzyme in mammalian cells. *J Neurochem* **67**, 900–906.
29 Murphy KL, Zhang X, Gainetdinov RR, Beaulieu JM and Caron MG (2008) A regulatory domain in the N-terminus of tryptophan hydroxylase 2 controls enzyme expression. *J Biol Chem* **283**, 13216–13224.
30 Horne J, Jennings IG, Teh T, Gooley PR and Kobe B (2002) Structural characterization of the N-terminal autoregulatory sequence of phenylalanine hydroxylase. *Protein Sci* **11**, 2041–2047.
31 Chen L, Chen Z, Zheng P, Sun J and Zeng AP (2012) Study and reengineering of the binding sites and allosteric regulation of biosynthetic threonine deaminase by isoleucine and valine in *Escherichia coli*. *Appl Microbiol Biotechnol* **97**, 2939–2949.
32 Schuller DJ, Grant GA and Banaszak LJ (1995) The allosteric ligand site in the V-max-Type cooperative enzyme phosphoglycerate dehydrogenase. *Nat Struct Biol* **2**, 69–76.
33 Gersting SW, Staudigl M, Truger MS, Messing DD, Danecka MK, Sommerhoff CP, Kemter KF and Muntau AC (2010) Activation of phenylalanine hydroxylase induces positive cooperativity towards the natural cofactor. *J Biol Chem* **285**, 30686–30697.
34 Chari A, Haselbach D, Kirves JM, Ohmer J, Paknia E, Fischer N, Ganichkin O, Möller V, Frye JJ, Petzold G *et al.* (2015) ProteoPlex: stability optimization of macromolecular complexes by sparse-matrix screening of chemical space. *Nat Methods* **12**, 859–865.
35 Calibration curve obtained from: GE Healthcare, Gel Filtration Calibration Kit LMW, Gel Filtration Kit HMW, Data File 28-4073-84-AA.
36 Zhang S, Roberts KM and Fitzpatrick PF (2014) Phenylalanine binding is linked to dimerization of the

regulatory domain of phenylalanine hydroxylase. *Biochemistry* **53**, 6625–6627.
37 Jiang GC, Yohrling GJ, Schmitt JD and Vrana KE (2000) Identification of substrate orienting and phosphorylation sites within tryptophan hydroxylase using homology-based molecular modeling. *J Mol Biol* **302**, 1005–1017.
38 Yohrling GJ, Mockus SM and Vrana KE (1999) Identification of amino-terminal sequences contributing to tryptophan hydroxylase tetramer formation. *J Mol Neurosci* **12**, 23–34.
39 Patel D, Kopec D, Fitzpatrick F, McCorvie TJ and Yue WW (2016) Structural basis for ligand-dependent dimerization of phenylalanine hydroxylase regulatory domain. *Sci Rep* **6**, 23748.
40 Jaffe EK, Stith L, Lawrence SH, Andrake M and Dunbrack Jr RL (2013) A new model for allosteric regulation of phenylalanine hydroxylase: implications for disease and therapeutics. *Arch Biochem Biophys* **530**, 73–82.
41 Zhang S, Hinck AP and Fitzpatrick PF (2015) The amino acid specificity for activation of phenylalanine hydroxylase matches the specificity for stabilization of regulatory domain dimers. *Biochemistry* **54**, 5167–5174.
42 Lang EJM, Cross PJ, Mittelstädt G, Jameson GB and Parker EJ (2014) Allosteric ACTion: the varied ACT domains regulating enzymes of amino-acid metabolism. *Curr Opin Struct Biol* **29**, 102–111.
43 Tenner K, Walther D and Bader M (2007) Influence of human tryptophan hydroxylase 2 N- and C-terminus on enzymatic activity and oligomerization. *J Neurochem* **102**, 1887–1894.
44 Thórólfsson M, Ibarra-Molero B, Fojan P, Petersen SB, Sanchez-Ruiz JM and Martínez A (2002) L-phenylalanine binding and domain organization in human phenylalanine hydroxylase: a differential scanning calorimetry study. *Biochemistry* **41**, 7573–7585.
45 Calvo AC, Scherer T, Pey AL, Ying M, Winge I, McKinney J, Haavik J, Thöny B and Martinez A (2010) Effect of pharmacological chaperones on brain tyrosine hydroxylase and tryptophan hydroxylase 2. *J Neurochem* **114**, 853–863.
46 Royo M, Daubner SC and Fitzpatrick PF (2005) Effects of mutations in tyrosine hydroxylase associated with progressive dystonia on the activity and stability of the protein. *Proteins* **58**, 14–21.
47 Walker PA, Leong LEC, Ng PWP, Tan SH, Waller S, Murphy D and Porter AG (1994) Efficient and rapid affinity purification of proteins using recombinant fusion proteases. *Nat Biotechnol* **12**, 601–605.
48 Gasteiger E, Hoogland C, Gattiker A, Duvaud S, Wilkins MR, Appel RD and Bairoch A (2005) *Protein Identification and Analysis Tools on the ExPASy Server. The Proteomics Protocols Handbook*. Humana Press Inc., Totowa, NJ.
49 Niesen FH, Berglund H and Vedadi M (2007) The use of differential scanning fluorimetry to detect ligand interactions that promote protein stability. *Nat Protoc* **2**, 2212–2221.
50 Manning LR, Jenkins WT, Hess JR, Vandegriff K, Winslow RM and Manning JM (1999) Subunit dissociations in natural and recombinant hemoglobins. *Protein Sci* **5**, 775–781.
51 Moran GR and Fitzpatrick PF (1999) A continuous fluorescence assay for tryptophan hydroxylase. *Anal Biochem* **266**, 148–152.

Supporting information

Additional Supporting Information may be found online in the supporting information tab for this article:

Appendix S1. Sequences of *h*TPH2 protein variants.

Table S1. Primers for cloning the recombinant truncated *h*TPH2 protein variants.

Fig. S1. Alignment of the regulatory domains of *h*TPH2 and *m*PAH.

Fig. S2. Representative example of raw data from differential scanning fluorimetry.

Fig. S3. SDS-PAGE results of collected peaks from purification of rc*h*TPH2 using Phe buffer.

Fig. S4. SDS-PAGE results of collected peaks from purification of NΔ47-rc*h*TPH2 using Phe buffer.

Fig. S5. SDS-PAGE results of collected peaks from purification of c*h*TPH2 using Phe buffer.

Supplementary Material

Sequences

Color-code:

XXXX = MBP

XXXX = 3CP

XXXX = Linker

XXXX = 3CP recognition and cleavage site (shown as ↓)

XXXX = Regulatory domain

XXXX = Catalytic domain

MBP-*ch*TPH2:

MKIEEGKLVIWINGDKGYNGLAEVGKKFEKDTGIKVTVEHPDKLEEKFPQVAATGDGPDIIFWAHDRFGGYAQSGLLAEI
TPDKAFQDKLYPFTWDAVRYNGKLIAYPIAVEALSLIYNKDLLPNPPKTWEEIPALDKELKAKGKSALMFNLQEPYFTWP
LIAADGGYAFKYENGKYDIKDVGVDNAGAKAGLTFLVDLIKNKHMNADTDYSIAEAAFNKGETAMTINGPWAWSNIDTSK
VNYGVTVLPTFKGQPSKPFVGVLSAGINAASPNKELAKEFLENYLLTDEGLEAVNKDKPLGAVALKSYEEELAKDPRIAA
TMENAQKGEIMPNIPQMSAFWYAVRTAVINAASGRQTVDEALKDAQTNSSSNNNNNNNNNNLGLEVLFQ↓GPEELEDVPW
FPRKISELDKCSHRVLMYGSELDADHPGFKDNVYRQRRKYFVDVAMGYKYGQPIPRVEYTEEETKTWGVVFRELSKLYPT
HACREYLKNFPLLTKYCGYREDNVPQLEDVSMFLKERSGFTVRPVAGYLSPRDFLAGLAYRVFHCTQYIRHGSDPLYTPE
PDTCHELLGHVPLLADPKFAQFSQEIGLASLGASDEDVQKLATCYFFTIEFGLCKQEGQLRAYGAGLLSSIGELKHALSD
KACVKAFDPKTTCLQECLITTFQEAYFVSESFEEAKEKMRDFAKSITRPFSVYFNPYTQSIEILKD

MBP-NΔ47-rc*h*TPH2:

MKIEEGKLVIWINGDKGYNGLAEVGKKFEKDTGIKVTVEHPDKLEEKFPQVAATGDGPDIIFWAHDRFGGYAQSGLLAEI
TPDKAFQDKLYPFTWDAVRYNGKLIAYPIAVEALSLIYNKDLLPNPPKTWEEIPALDKELKAKGKSALMFNLQEPYFTWP
LIAADGGYAFKYENGKYDIKDVGVDNAGAKAGLTFLVDLIKNKHMNADTDYSIAEAAFNKGETAMTINGPWAWSNIDTSK
VNYGVTVLPTFKGQPSKPFVGVLSAGINAASPNKELAKEFLENYLLTDEGLEAVNKDKPLGAVALKSYEEELAKDPRIAA
TMENAQKGEIMPNIPQMSAFWYAVRTAVINAASGRQTVDEALKDAQTNSSSNNNNNNNNNNLGLEVLFQ↓GPGNKGSSKR
EAATESGKTAVVFSLKNEVGGLVKALRLFQEKRVNMVHIESRKSRRRSSEVEIFVDCECGKTEFNELIQLLKFQTTIVTL
NPPENIWTEEEELEDVPWFPRKISELDKCSHRVLMYGSELDADHPGFKDNVYRQRRKYFVDVAMGYKYGQPIPRVEYTEE
ETKTWGVVFRELSKLYPTHACREYLKNFPLLTKYCGYREDNVPQLEDVSMFLKERSGFTVRPVAGYLSPRDFLAGLAYRV
FHCTQYIRHGSDPLYTPEPDTCHELLGHVPLLADPKFAQFSQEIGLASLGASDEDVQKLATCYFFTIEFGLCKQEGQLRA
YGAGLLSSIGELKHALSDKACVKAFDPKTTCLQECLITTFQEAYFVSESFEEAKEKMRDFAKSITRPFSVYFNPYTQSIE
ILKD

MBP-rc*h*TPH2:

MKIEEGKLVIWINGDKGYNGLAEVGKKFEKDTGIKVTVEHPDKLEEKFPQVAATGDGPDIIFWAHDRFGGYAQSGLLAEI
TPDKAFQDKLYPFTWDAVRYNGKLIAYPIAVEALSLIYNKDLLPNPPKTWEEIPALDKELKAKGKSALMFNLQEPYFTWP
LIAADGGYAFKYENGKYDIKDVGVDNAGAKAGLTFLVDLIKNKHMNADTDYSIAEAAFNKGETAMTINGPWAWSNIDTSK
VNYGVTVLPTFKGQPSKPFVGVLSAGINAASPNKELAKEFLENYLLTDEGLEAVNKDKPLGAVALKSYEEELAKDPRIAA
TMENAQKGEIMPNIPQMSAFWYAVRTAVINAASGRQTVDEALKDAQTNSSSNNNNNNNNNNLGLEVLFQ↓GPQPAMMMFS
SKYWARRGFSLDSAVPEEHQLLGSSTLNKPNSGKNDDKGNKGSSKREAATESGKTAVVFSLKNEVGGLVKALRLFQEKRV
NMVHIESRKSRRRSSEVEIFVDCECGKTEFNELIQLLKFQTTIVTLNPPENIWTEEEELEDVPWFPRKISELDKCSHRVL
MYGSELDADHPGFKDNVYRQRRKYFVDVAMGYKYGQPIPRVEYTEEETKTWGVVFRELSKLYPTHACREYLKNFPLLTKY
CGYREDNVPQLEDVSMFLKERSGFTVRPVAGYLSPRDFLAGLAYRVFHCTQYIRHGSDPLYTPEPDTCHELLGHVPLLAD
PKFAQFSQEIGLASLGASDEDVQKLATCYFFTIEFGLCKQEGQLRAYGAGLLSSIGELKHALSDKACVKAFDPKTTCLQE
CLITTFQEAYFVSESFEEAKEKMRDFAKSITRPFSVYFNPYTQSIEILKD

MBP-3CP:

MKIEEGKLVIWINGDKGYNGLAEVGKKFEKDTGIKVTVEHPDKLEEKFPQVAATGDGPDIIFWAHDRFGGYAQSGLLAEI
TPDKAFQDKLYPFTWDAVRYNGKLIAYPIAVEALSLIYNKDLLPNPPKTWEEIPALDKELKAKGKSALMFNLQEPYFTWP
LIAADGGYAFKYENGKYDIKDVGVDNAGAKAGLTFLVDLIKNKHMNADTDYSIAEAAFNKGETAMTINGPWAWSNIDTSK
VNYGVTVLPTFKGQPSKPFVGVLSAGINAASPNKELAKEFLENYLLTDEGLEAVNKDKPLGAVALKSYEEELAKDPRIAA
TMENAQKGEIMPNIPQMSAFWYAVRTAVINAASGRQTVDEALKDAQTNSSSNNNNNNNNNNLGGIPGPEHEFLNALIRRN
CHIITTDKGEFNLLGIYSNCAVVPTHAEPGDVVDIDGRLVRVLKQQVLTDMNDVDTEVTVLWLDQNEKFRDIRRFIPEHQ
QDWHNIHLATNVTKFPMLNVEVGHTVPYGEINLSGNATCRLYKYDYPTQPGQCGAVLANTGNIIGIHVGGNGRVGYAAAL
LRKYFAEEQ

Table S1. Primers utilized to construct the TPH2 variants.

Variant	Forward Primer	Reverse Primer
MBP-c*h*TPH2	5'- aaaagggcccgaagagctggaagatgtgc – 3'	5'- ttttctcgagttactaatctttcagaatttcaatgctct – 3'
MBP-rc*h*TPH2	5'- aaaagggccccagccggcgat – 3'	5'- ttttctcgagttactaatctttcagaatttcaatgctct – 3'
MBP-NΔ47-rc*h*TPH2	5'- aaaagggcccggcaacaaaggcagc – 3'	5'- ttttctcgagttactaatctttcagaatttcaatgctct – 3'
MBP-3C Protease	5'- aaaacatatgaaaatcgaagaaggtaaactggt – 3'	5'- aaaaggatcccaccgaggttgttgttattgtt – 3'

```
                                                                  18
rnPAH ----------------------MA-AV-----VLE----NGVLSRKLSDFGQETSYIEDNSNQNGAISLIFSLKEEVGALAKVLRL
hTPH2 MQPAMMMFSSKYWARRGFSLDSAVPEEHQLLGSSTLNKPNSGKNDDKGNKGSSKREAATESGKTAVVFSLKNEVGGLVKALRL
                           :  **     :*     *   * * .*.*:: *  .: :.:.*  :::****:***.*.*.***
                                                                  47
rnPAH FEENDINLTHIESRPSRLNKDEYEFFTYLDKRTKPVLGSIIKSLRNDIGATVHELSRDKEKNT--
hTPH2 FQEKRVNMVHIESRKSRRRSSEVEIFVDCECGKTE-FNELIQLLKFQT--TIVTLNPPENIWTEE
      *:*: :*:.***** ** ...* *:*.  :  ..  : .:*: *: :   *:  *.  ::  *
```

Fig. S11. Alignment of the regulatory domains of *h*TPH2 and *rn*PAH using Clustal Omaga (1.2.1). "-" marks a gap in the primary structure. The grey background illustrates the highly mobile part of the N-terminal region, for which no crystal structure is available for *rn*PAH and the presumably equivalently mobile region of *h*TPH2. "*" marks conserved residues, ":" marks conservation of residues with highly similar properties and "." marks conservation of residues with slightly similar properties.

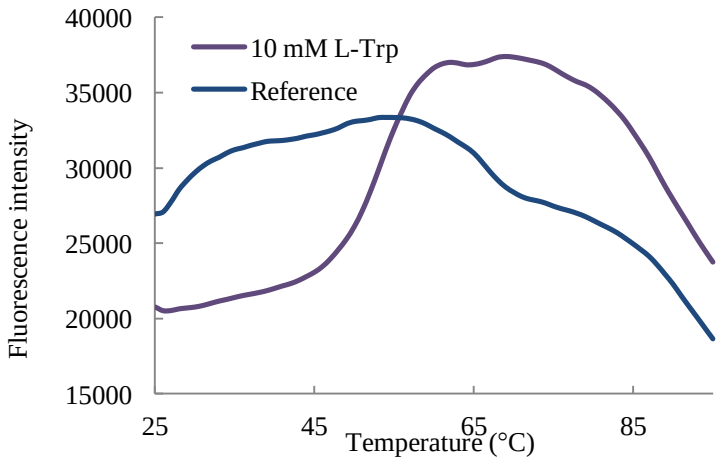

Fig. S12. Representative example of raw data from differential scanning fluorimetry of rc*h*TPH2 (enzyme concentration of 1 µM) with no ligand (blue line, reference) and with addition of 10 mM L-Trp (purple line).

rc*h*TPH2:

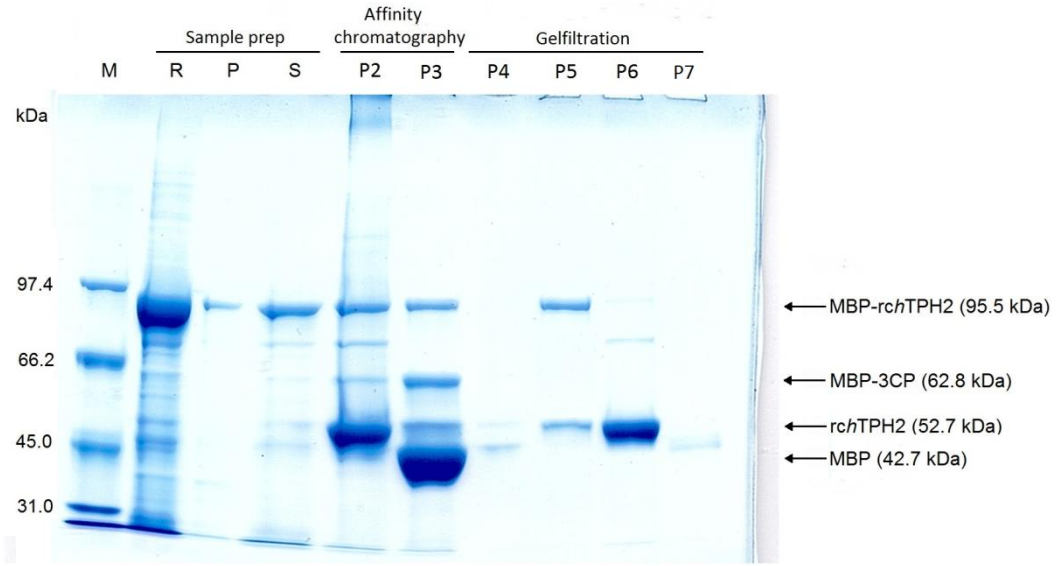

Fig. S13. SDS-PAGE results of collected peaks from purification of rc*h*TPH2 using Phe buffer. M: Molecular weight standard. R: Resuspension of cell culture. P: Resuspended pellet. S: Supernatant. P2: Peak eluting after cleavage with MBP-3CP. P3: Peak from elution of MBP-bound species. P4-P7: Peaks from size exclusion chromatography. P6: Collected fraction of rc*h*TPH2.

NΔ47-rc*h*TPH2:

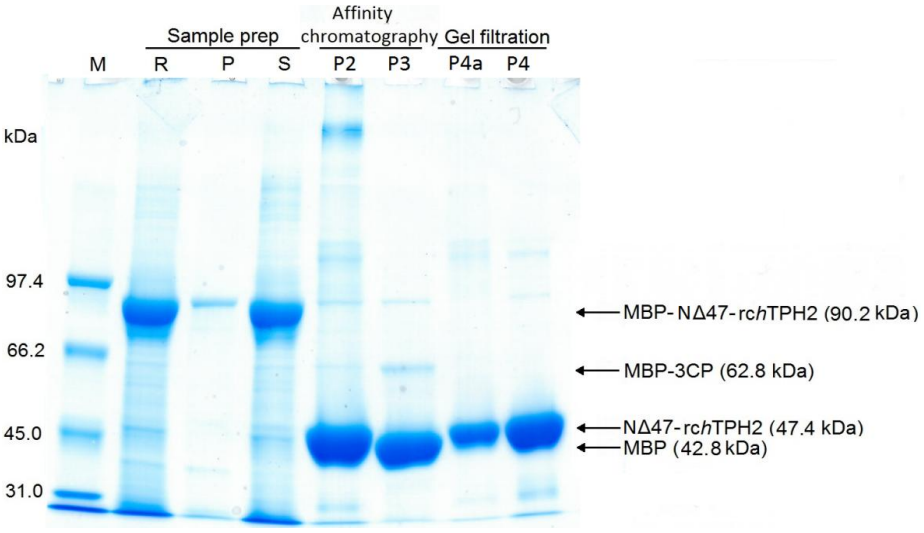

Fig. S14. SDS-PAGE results of collected peaks from purification of NΔ47-rc*h*TPH2 using Phe buffer. M: Molecular weight standard. R: Resuspension of cell culture. P: Resuspended pellet. S: Supernatant. P2: Peak eluting after cleavage with MBP-3CP. P3: Peak from elution of MBP-bound species. P4 and P4a: Peak from size exclusion chromatography. P4: Collected fraction of NΔ47-rc*h*TPH2.

c*h*TPH2:

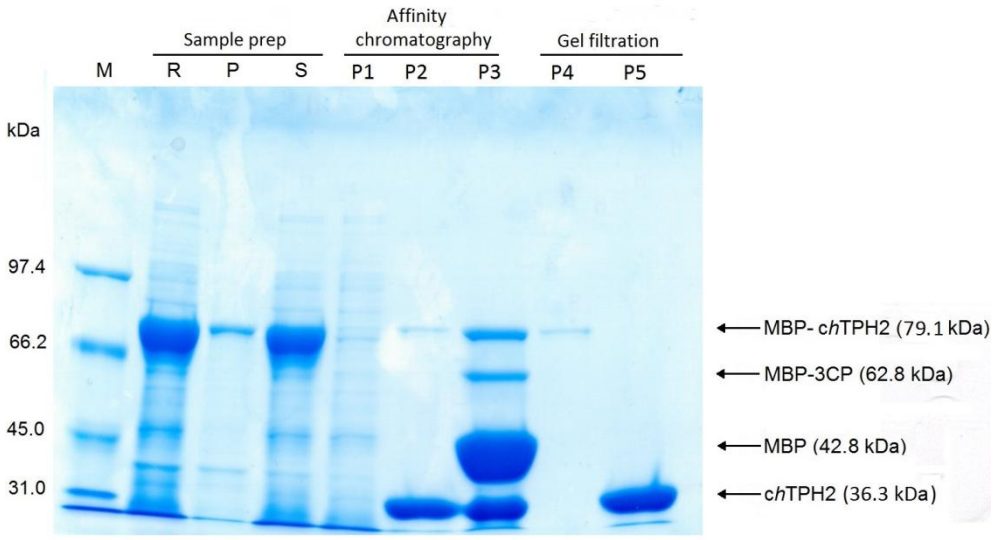

Fig. S15. SDS-PAGE results of collected peaks from purification of c*h*TPH2 using Phe buffer. M: Molecular weight standard. R: Resuspension of cell culture. P: Resuspended pellet. S: Supernatant. P1: Flow-through of unbound species. P2: Peak eluting after cleavage with MBP-3CP. P3: Peak from elution of MBP-bound species. P4 and P5: Peaks from size exclusion chromatography. P5: Collected fraction of c*h*TPH2. The presence of target protein in P3 is indicative of incomplete cleavage of 3CP protease in the on-column purification step.

The isoform-specific substrate inhibition mechanism of *human* tryptophan hydroxylase

Kasper D. Tidemand, Günther H. Peters[a], Pernille Harris, Eva Stensgaard, and Hans E. M. Christensen[b].

Department of Chemistry, Technical University of Denmark, Kemitorvet 207, DK-2800 Kgs. Lyngby, Denmark.
Corresponding authors: ghp@kemi.dtu.dk[a], hemc@kemi.dtu.dk[b].

Abbreviations

3CP, 3C-protease; 5-HT, 5-hydroxytryptamin (serotonin); 5-HTP, 5-hydroxytryptophan; AAAH, aromatic amino acid hydroxylase; BH_4, tetrahydrobiopterin; DSF, differential scanning fluorimetry; DTT, dithiothreitol; HEPES, 4-(2-hydroxyethyl)piperazine-1-ethanesulfonic acid; MBP, maltose binding protein; MD, molecular dynamics; PAH, phenylalanine hydroxylase; RMSD, root mean square deviation; SEC, size exclusion chromatography; TH, tyrosine hydroxylase; Trp, tryptophan; TPH, tryptophan hydroxylase; c*h*TPH, catalytic domain of *human* tryptophan hydroxylase.

Abstract

Tryptophan hydroxylase (TPH) catalyses the initial and rate-limiting step in the biosynthesis of serotonin, which is associated with a variety of disorders such as depression and irritable bowel syndrome. TPH exists in two isoforms; TPH1 and TPH2. TPH1 catalyses the initial step in the synthesis of serotonin in the peripheral tissues, while TPH2 catalyses this step in the brain. In this study, the steady-state kinetic mechanism for the catalytic domain of *human* TPH1 has been determined. Varying substrate tryptophan (Trp) and tetrahydrobiopterin (BH_4) results in a hybrid Ping Pong-ordered mechanism in which the reaction can either occur through a Ping Pong or a sequential mechanism depending on the concentration of tryptophan. The catalytic domain of TPH1 shares a sequence identity of 81 % with TPH2. Despite the high sequence identity, differences in the kinetic parameters of the isoforms have been identified, i.e. only TPH1 displays substrate tryptophan inhibition. This study demonstrates that the difference can be traced to an active site loop which displays different properties in the TPH isoforms. Steady-state kinetic results of the isoforms, and variants with point mutations in a loop lining the active site, show that the kinetic parameters of only TPH1 are significantly changed upon mutations. Mutations in the active site loop of TPH1 result in an increase in the substrate inhibition constant, $K_{i,}$ and therefore turnover rate. Molecular dynamics simulations reveal that this substrate inhibition mechanism occurs through a closure of the co-substrate, BH_4, binding pocket, which is induced by Trp binding.

Introduction

Tryptophan hydroxylase (TPH) catalyses the first and rate-limiting reaction in the biosynthesis of the hormone and neurotransmitter serotonin (5-HT). TPH uses Fe^{2+}, tetrahydrobiopterin (BH_4), and O_2 to generate 5-hydroxytryptophan (5-HTP) by hydroxylation of tryptophan (Trp).[1] 5-HTP is converted to 5-HT by aromatic amino acid decarboxylase [2,3]. Together with phenylalanine hydroxylase (PAH) and tyrosine hydroxylase (TH), TPH is a member of the enzyme subfamily of iron(II)-containing mono-oxygenases which are known as aromatic amino acid hydroxylases (AAAHs). The enzymes in the AAAH family form tetramers, in which each monomeric subunit consists of an N-terminal regulatory domain, a highly conserved catalytic domain, and a C-terminal tetramerization domain. [1,4]
In *human* two isoforms of TPH exist, where isoform 1 (TPH1) mainly is responsible for catalyzing the initial step in the biosynthesis of peripheral serotonin, and isoform 2 (TPH2) is associated with biosynthesis of neuronal serotonin [1]. Dysregulation of serotonin levels is involved in various physiological and psychiatric disorders such as irritable bowel syndrome, depression, obsessive compulsive disorder, and schizophrenia [5]. Decreased levels of neuronal serotonin are associated with neurological disorders, whereas some gastrointestinal disorders are associated with increased peripheral serotonin levels [6-8].

The kinetic mechanism has not unambiguously been determined for the aromatic amino acid hydroxylases. Despite great efforts to dissect the mechanism, ambiguities still exist. Of the AAAHs, PAH and TH have been more thoroughly studied. Steady-state kinetic studies have shown that *bovine* TH follows a Ping Pong mechanism.[9,10] This mechanism is supported by observation that in *rat* TH, where oxidation of BH_4 can occur in the absence of substrate tyrosine at pH 8.2.[11] However, the oxidation occurs at slower rates at pH 7.2 and not at all at pH 6.5.[11,12] In contrast, another steady-state kinetic study on *rat* TH finds an ordered sequential mechanism involving a quaternary complex with all three substrates bound.[12] The presence of a ternary complex which binds O_2 during catalysis in *rat* TH, is supported by a spectroscopic study.[13] Furthermore, a sequential mechanism is supported by single turn-over kinetic studies on PAH from *chromabacterium violaceum* [14,15] and *rat* [16]. Similar results have been obtained for rabbit TPH1.[17]
The substrate binding order in the AAAHs have been established to occur in an ordered fashion where pterin binds followed by substrate amino acid and then O_2. [9,15,16] That pterin binds as the first substrate is consistent with finding in TPH1 where inhibitors display uncompetitive inhibition towards 6-MePH_4, which indicates that pterin binds first.[18] Additionally, the crystal structure of *chicken* TPH (pdb: 3e2t) shows that binding of tryptophan and possibly imidazole results in a closed conformation, which indicates the formation of a dead-end complex.[19]

Despite a sequence identity of 71 %, the two isoforms of TPH display differences in their kinetic properties.[20,21] Some of the differences are accounted for by the N-terminal regulatory domains. TPH2 has an additional 46 residues in the regulatory domain compared to TPH1. This terminal extension has a

great impact on enzymatic activity, and serine 19 in the terminus of TPH2 has been identified as a phosphorylation site.[22] However, even in the absence of the regulatory domains, the isoforms display different kinetic properties.[21] Besides differences in kinetic parameters (K_m and V_{max}-values), TPH1 displays a greater degree of substrate tryptophan inhibition compared to TPH2.[20,21] *Human* TPH1 variants without the regulatory or tetramerization domain exhibit substrate inhibition comparable to full-length TPH1.[23] The underlying molecular mechanism of this inhibition and the differences in the isoforms that govern these observations remains elusive.

Here, we describe results that identify the steady-state kinetic mechanism for the catalytic domain of *human* TPH1. Furthermore, we describe results that identify the structural origin of the competitive substrate inhibition mechanism. The inhibition mechanism of TPH1 is governed by the orientation of Tyr125 which enables the active site loop to participate in the mechanism. Participation of Tyr125 occurs through the adjacent Tyr235 which is found to block the active site access upon substrate tryptophan binding.

Results

Enzymatic mechanism - To explore the kinetic mechanism of TPH1, the initial velocities of the catalytic domain of *human* TPH1 (c*h*TPH1) was determined at various tryptophan and BH_4 concentrations. The concentrations of the substrates were varied in a concentration matrix of 14 tryptophan concentrations and six BH_4 concentrations. The O_2 concentration was 500 µM in all measurements and apparent kinetic parameters were hence derived. This data are presented in Figure 16. For clarity, only the lowest seven concentrations of tryptophan are shown in Figure 16B. For all concentration see supporting information Figure S1.

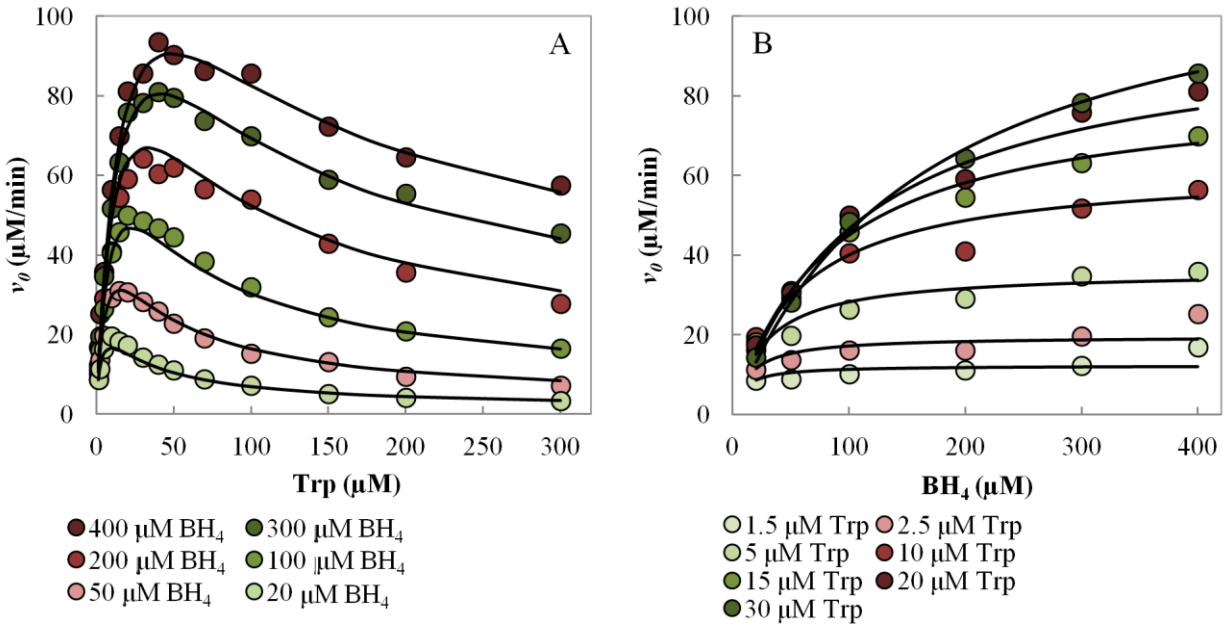

Figure 16. Global fits to initial velocity measurements for c*h*TPH1. The oxygen concentration was 500 µM in all measurements. (A) Initial velocities versus Trp concentration at fixed concentration of BH_4. (B) Initial velocities versus BH_4 concentration at fixed concentration of Trp. The plots are fitted with eq. 3 (Hybrid Ping Pong-ordered EB mechanism).

Figure 16A shows that the data deviate from the classical hyperbolic curve. The data can be fitted very well with the Michaelis-Menten equation with a substrate inhibition term (eq. 2 in experimental procedures – Figure S2), which describes linear substrate inhibition resulting from a dead-end complex formation between substrate and a non-productive enzyme form.[24] When the data in Figure 16A are replotted as v_0 versus [BH_4], the plots in Figure 16B are obtained. The data follow a classic hyperbolic shape, and the Michaelis-Menten equation (eq. 1 in experimental procedures) fits well to the data (Figure S3).

By fitting eq. 2 to the data for each fixed BH_4 concentration, an apparent tryptophan substrate inhibition constants, K_i, can be determined. The secondary plot in Figure 17 shows that c*h*TPH1 displays BH_4 concentration-dependent substrate inhibition. For instance, at low fixed concentrations of BH_4 (20 µM), c*h*TPH1 has an apparent K_i of 24 µM, while at high BH_4 concentration (400 µM) the apparent K_i is increased to 206 µM.

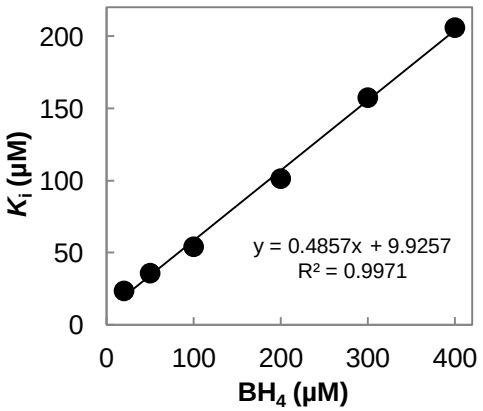

Figure 17. Secondary plot of apparent K_i-values obtained at different BH_4 concentrations. Values obtained by fitting the v_0 vs. Trp concentration data at fixed BH_4 concentrations presented in Figure 16A with eq. 2

To evaluate which mechanism the kinetic data represents, global fitting was conducted. The datasets were fitted to the velocity equations describing a *i)* Ping Pong mechanism with a dead-end EB complex formation, *ii)* sequential mechanism with a dead-end EB complex formation, *iii)* sequential mechanism with dead-end EA_2 complex formation, and *iv)* hybrid Ping Pong-ordered mechanism with dead-end EB complex formation (hybrid EB).[25]

The hybrid Ping Pong-ordered mechanism in Figure 6.10 was included in the analysis because both Ping Pong and sequential mechanisms have been observed in steady-state kinetic studies of the AAAHs.[9,10,12] In the hybrid model [26,27], the reaction can either occur through a Ping Pong or a sequential mechanism depending on the concentration of tryptophan. Substrate inhibition is caused by competitive formation of a dead-end EB (TPH•Trp) complex formed when tryptophan binds before BH_4. Such hybrid mechanisms have also been observed in e.g. pyruvate carboxylase, glutathione reductase, hypoxanthine phosphoribosyltransferase, and glutathione S-transferase A.[28-31]

Table 2. Kinetic parameters derived from global fits. Parameters are derived by fitting the data with a Ping Pong mechanism with dead-end EB and a hybrid Ping Pong-ordered mechanism with dead-end EB formation (Hybrid EB – eq. 3) to all the data. The model error is given by the sum of squared residuals. *: F-test, p<0.01.

Mechanism	V_{max} µM min^{-1}	V_2 min^{-1}	$K_{m,Trp}$ µM	$K_{m,BH4}$ µM	K_i µM	K_3	K_4 µM^{-1}	Error
Ping Pong EB	213	-	23	181	51	-	-	551
Hybrid EB	210	0.3	24	135	52	2.8	0	445*

In the global fit, the sequential mechanisms (*ii* and *iii*) resulted in identical fits, as K_A was reduced to zero resulting in a reduction of the equations to that of a Ping Pong mechanism (*i*). For this reason identical kinetic parameters were obtained for the three mechanisms, and the sequential mechanisms were discarded. Based on this analysis of the conventional non-branched mechanisms, a Ping Pong mechanism fit the total dataset best. The hybrid EB model, however, results in an improved global fit ($p < 0.01$) compared to that of a Ping Pong mechanism, Table 2. Fitting this model to the data results in a redundancy of K_4.

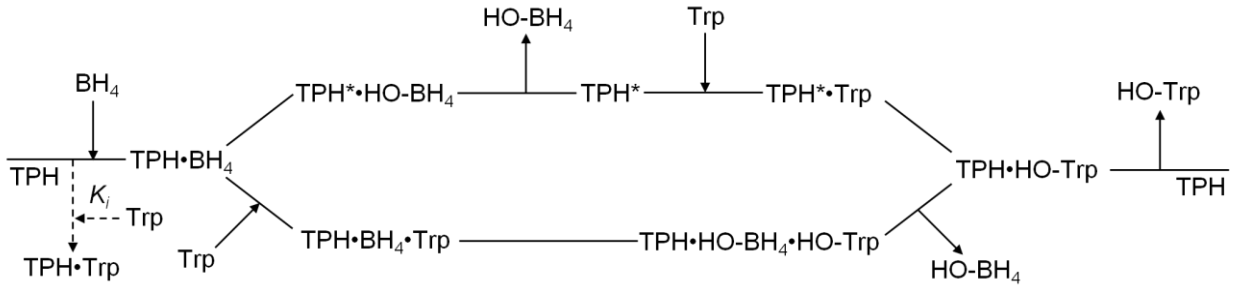

Figure 18. Basic scheme for a branching mechanism of c*h*TPH1. The scheme corresponds to a hybrid Ping Pong-ordered mechanism with dead-end TPH•Trp complex (EB). TPH* indicates a TPH that has undergone an irreversible change (e.g. formation of Fe^{IV}=O). Upper path represents a Ping Pong mechanism, and the lower path represents a sequential mechanism.

In the proposed hybrid mechanism in Figure 6.10, the order of pterin and substrate binding is in agreement with the majority of studies conducted on the AAAHs.[9-11,15-17] Substrate inhibition occurs through competitive inhibition by tryptophan versus BH_4. This yields a BH_4 concentration-dependent substrate tryptophan inhibition constant which has similarly been observed for TH [10]. A hybrid Ping Pong-ordered model in which tryptophan binds before BH_4 also resulted in an improved global fit ($p < 0.01$) compared to that of a Ping Pong EB mechanism. This model was, however, discarded because of the accumulated experimental data, that evidently find that BH_4 binds as the first substrate.[9-11,15-17] Biphasic data was obtained by Oka *et al.*[10] who therefore analyzed the data separately for velocity data obtained at respectively higher or lower than 0.2 mM BH_4. Such data might be explained by a hybrid Ping Pong-ordered model, which follows different mechanisms depending on substrate concentration.

According to this proposed hybrid model, the reaction will occur through a sequential mechanism at high tryptophan concentrations. This correlates well with the fact that several of the AAAH studies which obtain a

sequential mechanism were conducted with relatively high substrate concentrations (typically >0.5 mM range).[13,14,16,17]

Sequential and structural analysis of isoform differences – The *human* TPH isoforms display significantly different kinetic parameters, and only TPH1 is subjected to substrate inhibition.[21] In this study, it was investigated how inhibition only apply to c*h*TPH1. The isoforms of TPH have a sequence identity of 81 % in the catalytic domain, which is reflected in their similar tertiary structures. The crystal structures of the catalytic domains of *human* TPH1 (c*h*TPH1 - pdb: 1MLW [32]) and *human* TPH2 (c*h*TPH2 - pdb: 4V06) display a root mean square deviation of the C_α-atoms ($RMSD_{C\alpha}$) of 1.1 Å. The TPH structures have BH_2 and imidazole bound in the pterin binding pocket, respectively. Crystal structures of the homologous phenylalanine hydroxylase have shown that binding of BH_2 or BH_4 do not cause structural changes.[33,34] The two TPH structures are therefore comparable.

It was found that the 19 % non-conserved residues are randomly distributed mainly on the surface of the protein. Within 10 Å of the active site iron, only 2 out of 37 residues are not conserved, and these residues are distant from the binding pockets of the substrate and co-substrate (Supporting information, Figure S4).

As the non-conserved residues are not clustered in one area and are not close to the substrate or co-substrate binding sites, differences in the crystal structures determined by $RMSD_{C\alpha}$ were analyzed. The alignment, with color-coded $RMSD_{C\alpha}$-values, in Figure 19 shows that a stretch of sequence, corresponding to a loop over the active site, displays relatively high $RMSD_{C\alpha}$-values compared to the rest of the structure despite a high sequence homology. The loops span residues 117-137 of TPH1 and 163-183 of TPH2 and are shown in Figure 20. Especially tyrosine 125/171 in the center of the loop displays a relatively high $RMSD_{C\alpha}$-value (5.2 Å).

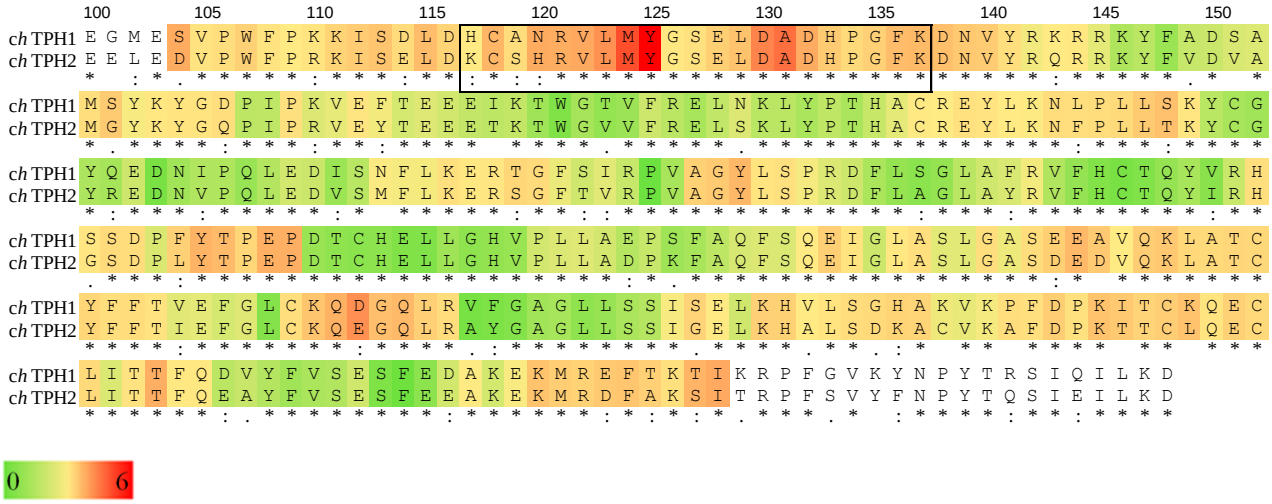

Figure 19. Sequence alignment of the catalytic domains of TPH1 and TPH2 (Clustal Omega 1.2.3 - * = identical, : = very similar, . = similar). The color scale (green is low and red is high) in the alignment shows the RMSD of the C_α-atoms calculated between c*h*TPH1 (pdb: 1MLW) and c*h*TPH2 (pdb: 4V06). The black box indicates the sequence of the active site loop. The numbering of the sequence is based on TPH1.

The corresponding loop in PAH has been found to reside in either an open or closed conformation depending on the active site occupancy. A closed conformation has only been observed in the presence of both a pterin and a substrate analogue.[35,36] However, a structure of PAH with only a substrate/substrate analogue has not been determined, and it is therefore unknown whether the loop closure occurs solely upon binding of substrate or a combination of substrate and co-substrate. Compared to the closed structures of PAH, both isoforms of *human* TPH exist in open conformations. For TPH, a closed conformation has been observed in a crystal structure of *chicken* TPH1 with bound substrate Trp and imidazole (pdb: 3E2T).[19]

From Figure 20, it is noticed that the side chain of the tyrosine residue is oriented towards the active site in TPH1 but is pointing away from the active site in TPH2. The structures of the loops and the orientation of the tyrosine residues in the crystal structures are assessed by electron density in the loops. The $2F_o$-F_c electron density maps of the crystal structures show that the structures of the loops in both isoforms are well resolved (Supporting information Figure S5 and S6).

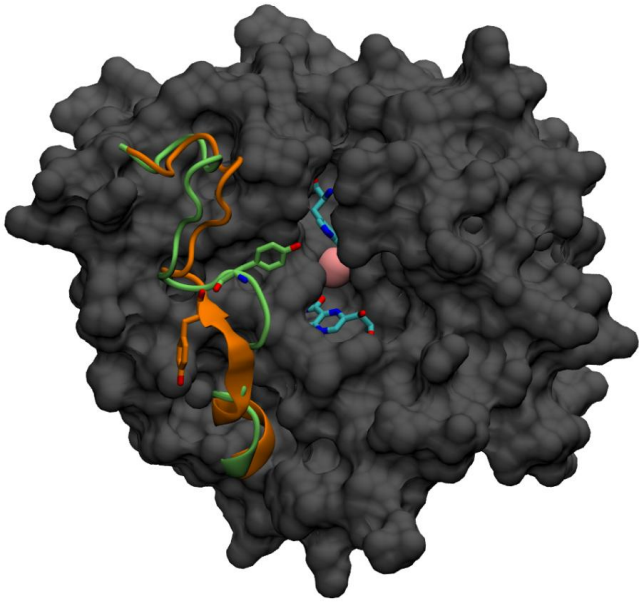

Figure 20. Crystal structure of c*h*TPH1 (pdb: 1MLW – open conformation) with gray surface. The active site loop of c*h*TPH1 is shown in green with tyrosine 125 displayed as sticks and the loop of c*h*TPH2 (superimposed from pdb: 4V06 – open conformation) is shown in orange with tyrosine 171 displayed as sticks. For illustration, Trp (superimposed from pdb: 3E2T) and BH_2 have been placed in their respective binding pockets. Trp and BH_2 are shown as cyan sticks and iron is shown as sphere.

The effect of Tyr125/171 point mutations on TPH kinetics - In order to probe the importance of the loop in TPH, Tyr125 in c*h*TPH1 and Tyr171 in c*h*TPH2 were mutated to the smaller amino acid alanine or the more bulky amino acid tryptophan and characterized for changes. As the oligomeric state and the transition temperatures of the isoform mutant variants were not changed (Supporting information, Figure S7, Table S1, and Table S2), the kinetic parameters can be directly compared. Apparent kinetic parameters are determined given that saturated concentrations of the non-varied substrate could not be obtained due to substrate inhibition.

In agreement with Windahl *et al.* [21], c*h*TPH1 displays substrate inhibition, with a substrate inhibition constant of 165 ± 18 µM, while c*h*TPH2 does not display substrate inhibition (Table 3, Figure 21 panel A and C open circles). Additionally, c*h*TPH1 displays a 10-fold higher $K_{m,BH4}$ compared to c*h*TPH2.

The kinetic analysis shows that mutation of the tyrosine residue in the loop results in great changes in the kinetic parameters of c*h*TPH1 (Table 3 and Figure 21). Mutation to alanine results in a small reduction of $K_{m,BH4}$, while mutation to tryptophan results in a 5-fold reduction. A change in $K_{m,Trp}$ is only observed for Y125W-c*h*TPH1. Notably, the mutations result in a significant increase in the substrate inhibition constant, K_i. Mutation to alanine increases the K_i-value slightly, while mutation to tryptophan results in a greater than 3-fold increase. The decreased substrate inhibition is clearly visualized in Figure 21 panel A.

Beside the reduced $K_{m,BH4}$ and increased K_i-values, $k_{cat,Trp}$ is also found to change with the mutations. Similar to the other kinetic parameters, $k_{cat,Trp}$ is slightly increased with mutation to alanine and increased 3-fold by mutation to tryptophan.

Table 3. Kinetic parameters of c*h*TPH1 and c*h*TPH2 variants derived from data presented in Figure 21. Parameters are given with standard deviations of at least three independent experiments from at least two purification batches. *: $p < 0.05$, **: $p < 0.01$.

	Tryptophan			**BH_4**	
Variant	k_{cat} (µM min^{-1})	K_i (µM)	K_m (µM)	K_m (µM)	k_{cat} (µM min^{-1})
c*h*TPH1	**108 ± 10**	**165 ± 18**	12.7 ± 1.4	**285 ± 15**	145 ± 17
Y125A-c*h*TPH1	**164 ± 10****	**227 ± 21***	12.6 ± 0.5	**188 ± 19****	192 ± 13*
Y125W-c*h*TPH1	**315 ± 55****	**544 ± 126****	36.7 ± 4.6**	**57 ± 5****	203 ± 9*
Loop-swap-c*h*TPH1	178 ± 12**	189 ± 27	13.9 ± 2.7	240 ± 42	191 ± 18*
c*h*TPH2	258 ± 20	-	13.1 ± 1.3	26.7 ± 0.9	239 ± 12
Y171A-c*h*TPH2	220 ± 9	-	12.1 ± 1.3	31.1 ± 6.0	201 ± 27
Y171W-c*h*TPH2	315 ± 34	-	21.7 ± 1.5**	19.2 ± 3.4	274 ± 16
Loop-swap-c*h*TPH2	212 ± 4	497 ± 54	14.0 ± 0.7	37.6 ± 8.1	145 ± 8**

For c*h*TPH2, mutation from tyrosine to alanine or tryptophan results in no significant changes in the kinetic parameters, apart from a change in the $K_{m,Trp}$. These observations correlate well with the different orientations of the tyrosine residue seen in the two crystal structures. In c*h*TPH1, the tyrosine residue is in vicinity of the active site and influences the kinetics of the enzyme, while in c*h*TPH2, the tyrosine residue point away from the active site which results in a less pronounced effect on the kinetics.

Loop-swap mutations of non-conserved residues - Of the 21 residues located in the loop, only three residues are not conserved between the isoforms (Figure 19). To examine whether these residues contribute to the different orientations of the tyrosine residue, the three non-conserved residues in c*h*TPH1 were mutated to the corresponding residues of the sequence of c*h*TPH2 and *vice versa*. In c*h*TPH1, His117, Ala119, and Asn120 were mutated to Lys, Ser, and His, respectively (referred to as loop-swap-c*h*TPH1), while the

opposite mutations were performed in position 163, 165, and 166 of c*h*TPH2 (referred to as loop-swap-c*h*TPH2).

The kinetic results of the loop-swap mutations are presented in Figure 21, and the kinetic parameters are summarized in Table 3. In c*h*TPH1, the loop-swap mutations result in only modest changes in the kinetic parameters. Although statistically insignificant, the kinetic parameters change in the same fashion as observed for the Tyr125 mutations; $K_{m,BH4}$ decreases, K_i increases, and $k_{cat,Trp}$ increases.

In c*h*TPH2, the loop-swap mutations similarly only introduce modest changes to the kinetic parameters. However, the loop-swap mutations in c*h*TPH2 result in introduction of substrate tryptophan inhibition with a K_i-value of 497 ± 54 µM (Figure 21, panel C black circles). In c*h*TPH1, K_i and $K_{m,BH4}$ seem to be inversely related. This correlates with the observations in loop-swap-c*h*TPH2 where $K_{m,BH4}$ is increased with the introduced substrate inhibition.

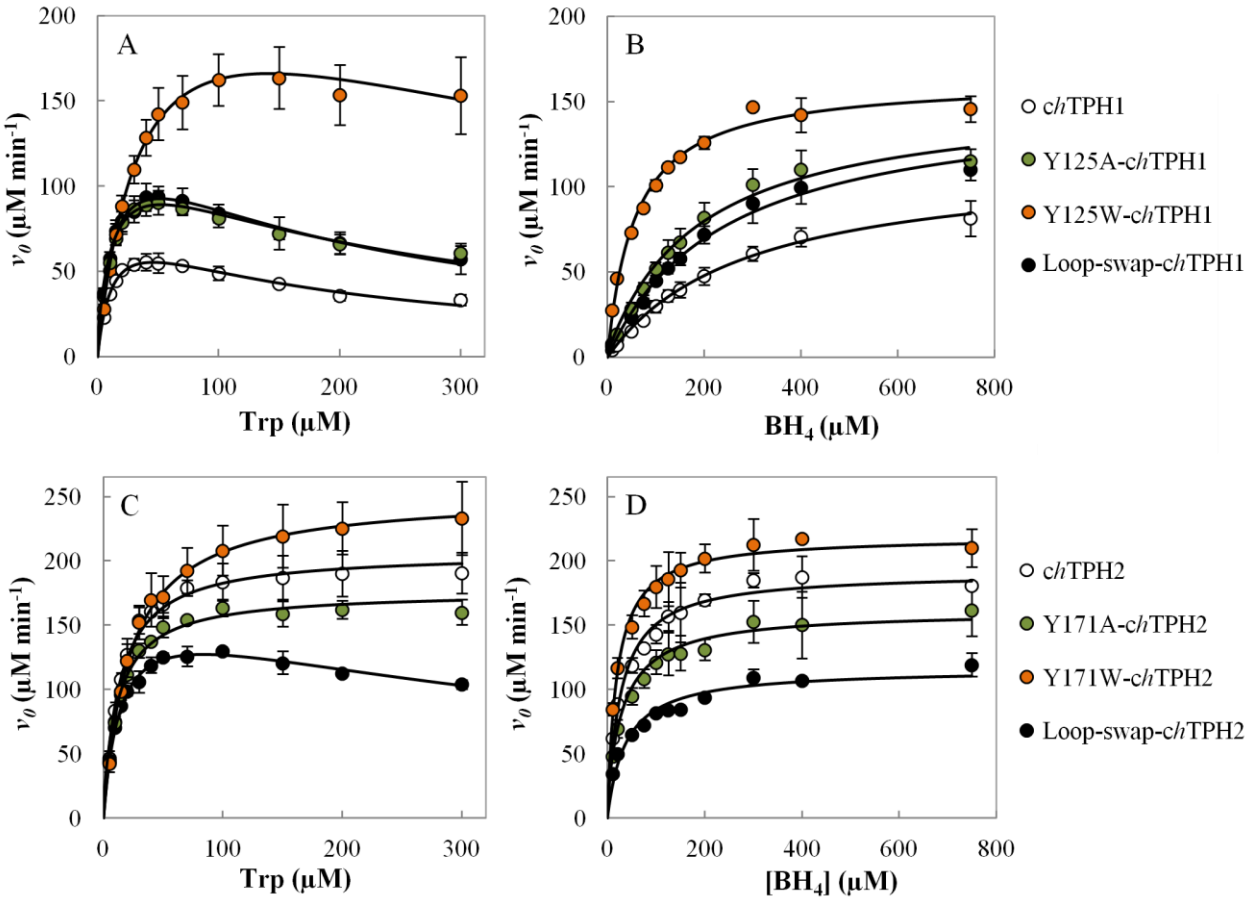

Figure 21. The initial rates of the c*h*TPH1 variants (panel A and B) and of the c*h*TPH2 variants (panel C and D) as a function of Trp or BH_4 concentration. The oxygen concentration was 500 µM in all measurements. Each measurement is reported as an average with standard deviation of at least three independent experiments from at least two purification batches. The TPH concentration was 0.8 µM in all measurements.

The conservation of the loops was analyzed (logo plot [37] in Supporting information Figure S8) with sequences of TPH1 and TPH2 from 61 and 63 vertebrate species, respectively. It was found that His117,

Ala119 and Asn120 of TPH1 are 13, 100, and 97 % conserved, respectively. In TPH2, Lys163, Ser165, and His166 are conserved 75, 100, and 33 %, respectively. Of the residues in TPH1, Ala119 and Asn120 show a high degree of conservation, while for TPH2, Ser165 is highly conserved. This implies that these residues are important for proper loop orientation and function.

Molecular Dynamics (MD) Simulations - MD simulations were employed to investigate the underlying mechanism that governs the observed substrate inhibition in TPH1. 100 ns MD simulations of c*h*TPH1 with and without substrate Trp were conducted. From comparison of the trajectories, it is observed that in the presence of Trp, the entrance to the BH_4 binding pocket becomes blocked, Figure 22. The blocking of the entrance is caused mainly by Tyr235. Tyr235 is in direct contact with the active site loop through Tyr125, which is under investigation, Figure 23A.[32]

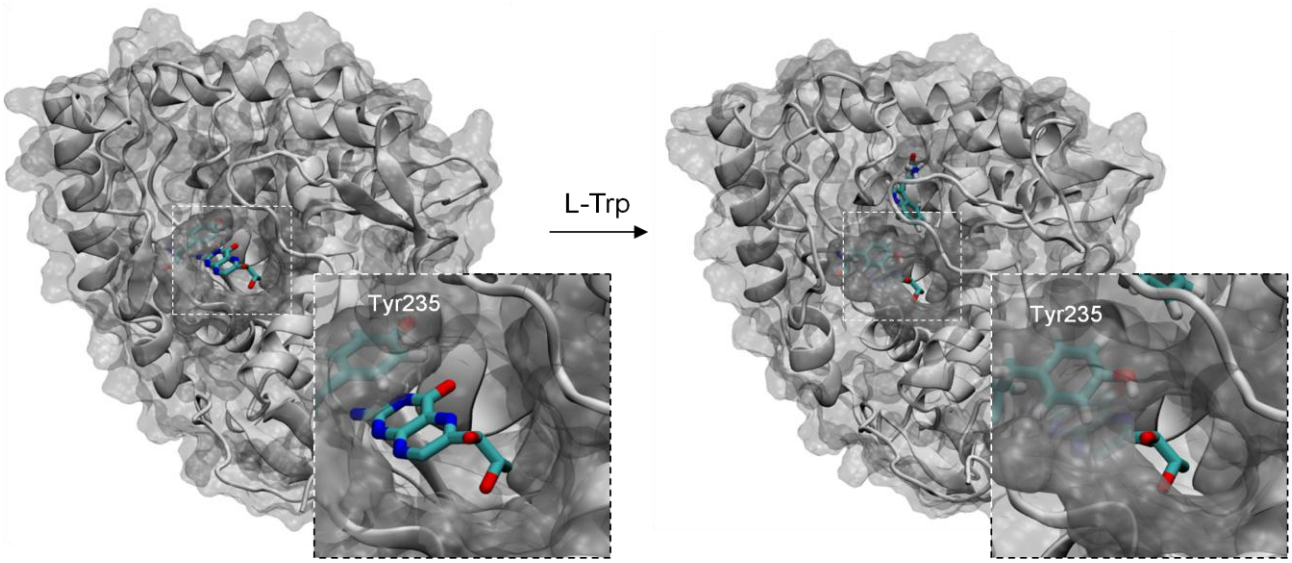

Figure 22. Substrate Trp induced closure of the BH_4 binding pocket. BH_2, shown in cyan licorice, is not included in the simulations but have been superimposed into the structures (from pdb: 1MLW) to illustrate its binding pose. Left: snapshot extracted from MD simulation of c*h*TPH1 without substrates. Right: snapshot extracted from MD simulation of c*h*TPH1 with bound substrate Trp. The snapshots represent the average position of Tyr235 based on the distance measurements over the 100 ns simulations

Throughout the simulation of c*h*TPH1, Tyr235 resides in a position very similar to the one observed in the crystal structure (average $RMSD_{Tyr235}$ of 1.1 Å compared to 1MLW and 3.6 Å compared to 3E2T), Figure 23B. In the simulation of c*h*TPH1 with Trp in the active site, Tyr235 moves to the position which blocks the BH_4 entrance. This new position of Tyr235 is very similar to the one observed for the equivalent Tyr236 in the crystal structure of *chicken* TPH1 [19] which has Trp bound (average $RMSD_{Tyr235}$ of 1.8 Å from 3E2T and 3.0 Å from 1MLW), Figure 23. The movement of Tyr235 observed in the simulation of c*h*TPH1 correlates very well with the structural information obtained from the crystal structures. The importance of Tyr235 for the inhibition mechanism of TPH1 is supported by a mutational study, in which it was found that substrate inhibition was removed upon mutation of Tyr235 to alanine or leucine.[38]

In c*h*TPH1, Tyr235 constitutes part of the BH_4 binding pocket and is in direct contact with the pterin.[32] Tyr125 which is under investigation in this study, π-stacks onto Tyr235 forming a T-shaped interaction.[32] It is therefore reasonable to believe that mutation of Tyr125 has an influence on the orientation of Tyr235 and thereby explain the influence on the kinetic parameters, especially the substrate inhibition.

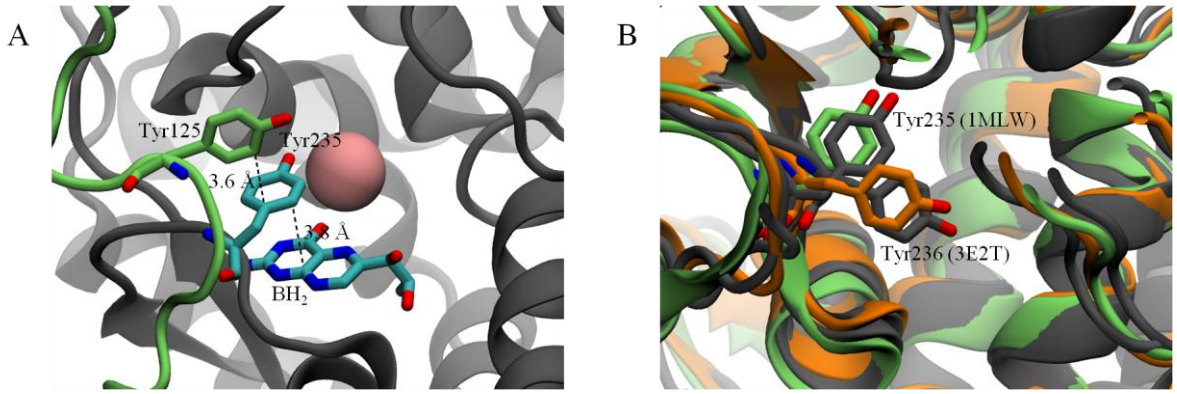

Figure 23. (A) The position and orientation of Tyr125, Tyr235, and BH_2 in the crystal structure of c*h*TPH1 (pdb: 1MLW). The active site loop is colored green and dotted lines represent distances. (B) Superposition of the crystal structure of *human* TPH1 (pdb: 1MLW), *chicken* TPH1 (pdb: 3E2T), snapshot from MD simulation of c*h*TPH1 without substrate (green Tyr235), and snapshot from MD simulation of c*h*TPH1 with bound Trp (orange Tyr235). The snapshots represent the average position of the tyrosine residues based on the distance measurements over the 100 ns simulations.

Discussion

The data presented here shed light on the kinetic mechanism of TPH1 and on the different kinetic properties which are displayed by the TPH isoforms. The kinetic mechanism of TPH has not previously been determined and both Ping Pong and sequential mechanisms have been observed in steady-state kinetic studies of the AAAHs.[9-11] In this study, a hybrid Ping Pong-ordered mechanism in which the reaction can either occur through a Ping Pong or a sequential mechanism depending on the concentration of tryptophan is observed. The substrate binding order is BH_4 followed by tryptophan and substrate inhibition occurs through competitive inhibition of tryptophan versus BH_4. This order of substrate binding is in agreement with the majority of studies conducted on the AAAHs. [9-12,15-17] This model might explain the contradicting results obtained for the AAAHs because very different substrate concentrations are used in these studies.

In this study, wild-type c*h*TPH1 and c*h*TPH2 displayed identical $K_{m,Trp}$-values but a 10-fold difference in $K_{m,BH4}$-values. Furthermore, a ~2-fold greater $k_{cat,Trp}$ was observed for c*h*TPH2 compared to c*h*TPH1 and only c*h*TPH1 displayed substrate inhibition. These kinetic parameters correlate well with previous observation.[21,39] TPH2 has similarly been reported not to be subject of substrate inhibition [1,22,40] but has also been found to display inhibition, however, with relatively high inhibition constants (418 - 970 µM) [20,41]. Substrate inhibition is an important regulatory mechanism observed in a variety of enzymes.[42] Amino acid substrate inhibition has been observed in both full-length *human* TPH1 and *rat* TH.[43,44] Deletion mutagenesis has shown that substrate inhibition is retained to upon deletion of either the regulatory

or tetramerization domain of TPH and TH.[23,44] This suggests that the observed substrate inhibition in full-length TPH and TH only involves the catalytic domain, which implies that the results obtained in this study can be applied to the full-length enzyme.

The sequential and structural analyses of the two isoforms revealed that the biggest difference between the crystal structures is the tyrosine residue in the active site loop. Mutation of this residue resulted in significant changes in the kinetic parameters of only c*h*TPH1. This implies that this residue has a functional importance in TPH1. The importance of this loop and in particular this residue is supported by findings in PAH and TH where the corresponding residues Tyr138 and Phe184 have been found to be important for proper enzymatic function.[45,46]

Crystal structures of TPH and PAH have clearly revealed the presence of an open and a closed conformation. For PAH, closed conformations have only been observed when both a pterin and a substrate analogue are bound.[35,36] A closed conformation has also been observed for *chicken* TPH1 with bound tryptophan and imidazole.[19] Imidazole is bound in the BH_4 binding pocket, which might mimic binding of co-substrate. However, a structure of TPH or PAH with only a substrate/substrate analogue has not been determined, and it is therefore unknown whether the loop closure occurs solely upon binding of substrate or a combination of substrate and co-substrate. The role of the loop closing mechanism is poorly understood. For PAH, it has been suggested that the closing mechanism might protect the co-substrate to enable a high degree of coupling efficiency.[45] Similarly, the loop in TH has been proposed to exclude water from the active site to avoid reaction of the water with the hydroxylating intermediate before hydroxylation of substrate can occur.[34,46,47] A similar functional importance of the loop in TPH is supported by the very high sequence conservation among vertebrate species observed for both TPH isoforms.

From the MD simulations, it is observed that Trp binding in c*h*TPH1 results in a blocking of the BH_4 binding pocket. The Trp-induced blocking mechanism occurs through Tyr235 which moves from a BH_4 binding position to a position in the opening of the BH_4 binding pocket. This observation compliments the kinetic model in which a dead-end complex is formed when Trp binds before BH_4. The influence of Tyr235 on the substrate inhibition mechanism is also supported by the results of Jiang *et al.* where mutations of Tyr235 to alanine or leucine were found to remove substrate inhibition.[38]. Tyr235 is in direct contact with the active site loop through Tyr125.[32] The mutations of Tyr125 will therefore most likely have an influence on the orientation of Tyr235, and thereby explain the influence on the kinetic parameters, especially the substrate inhibition. These results strongly suggest that the inhibition mechanism, which is only observed for c*h*TPH1, can be traced to the loop lining the active site. The induced substrate inhibition observed in loop-swap-c*h*TPH2 suggests that the three mutations change the orientation of the loop to an orientation approaching the one observed in c*h*TPH1.

Besides c*h*TPH1, substrate inhibition is also observed in TH. For TH, substrate inhibition is observed at tyrosine concentrations higher than 50 µM [48]. The tyrosine concentration in the brain has been found to vary as much as a factor of two. [49] Substrate inhibition of TH has been proposed to explain the lack of L-DOPA concentration fluctuations as a consequence of increase Tyr concentration upon food intake.[42] Trp concentrations are around 60 µM in the blood [50] which is close to the Trp concentration at which the maximum velocity of TPH1 is achieved in this study. This suggests that substrate inhibition could play a role in the TPH1 regulation *in vivo*. It is possible that a corresponding mechanism observed for TH is ensuring that the production of 5-HT does not rise to high levels in the peripheral tissues, which is associated with several diseases.[51] The concentration of tryptophan in the brain is in the range of 25-35 µM [52] which is close to the observed $K_{m,Trp}$ of c*h*TPH2. The velocities of 5-HTP production and in turn serotonin production are, therefore, very sensitive to changes in brain Trp concentration.[52,53] This might explain the lack of substrate inhibition observed in TPH2, as rapid responses are desirable in the brain. It could be speculated that different regulatory mechanisms of the two isoforms have evolved to accommodate the diverse need for serotonin biosynthesis in different tissues.

Experimental Procedures

Materials. All used chemicals were of analytical grade, and all solutions were prepared using water from an 18.2 MΩ·cm Milli-Q synthesis A10 Q-Gard system which was filtered through a 0.22 µm filter. Protein purification was performed on an ÄKTA purifier 100 from GE Healthcare. Utilized GE Healthcare column are: HiLoad Superdex 200 26/60 pg, Superdex 200 10/300 GL, and a XK 16/20 column packed with 25 mL Dextrin Sepharose High Performance media. During purifications, all TPH containing solutions were kept in ice water, except during the chromatographic steps, which were performed at room temperature. Protein solutions were concentrated using an Amicon ultrafiltration cell with an Ultracell PL-3 membrane. Protein concentrations were determined by measuring the absorbance at 280 nm on an ND-1000 NanoDrop Spectrophotometer from Saveen Werner.

Cloning and Expression. Full-length *human* TPH2 cDNA optimized for expression in *E. coli* was obtained from GenScript. The construct encoding the different protein variants was obtained by PCR. All DNA sequences were verified by sequencing (Eurofins). All proteins were expressed as maltose binding protein fusion proteins from the pET26 expression vector in *E. coli* BL21(DE3) (Novagen) cells. All TPH1 and TPH2 variants were expressed as NΔ99/CΔ31 and NΔ145/CΔ31, respectively, lacking the N-terminal regulatory domain and the C-terminal tetramerization domain. The sequences of the proteins expressed are given in Supporting information. The recombinant fusion proteins contain a cleavage recognition site for *human* rhinovirus 3C protease (3CP) [54]. Proteins were expressed at 20°C for 14 h as previously described [55]. MBP-3CP was cloned, expressed, and purified in-house.

Purification. The purification procedure comprises an affinity chromatography step utilizing a column packed with dextrin sepharose and a size exclusion step using a HiLoad Superdex 200 prep grade column, as previously described [56]. All variants were cleaved from the MBP fusion protein utilizing an on-column cleavage procedure with MBP-3CP during the first purification step. *Human* TPH1 variants were purified in buffer containing 20 mM TRIS/H_2SO_4, 100 mM $(NH_4)_2SO_4$, pH 8.0 and *human* TPH2 variants in 20 mM HEPES/NH_4OH, 100 mM $(NH_4)_2SO_4$, pH 7.0.

Activity Assay. The activity assay was performed as described by Moran et al. [57] and Nielsen et al.[55], and the sample preparation was conducted as previously described [56]. The activity measurements were performed using a Varian Cary Eclipse Fluorescence Spectrophotometer. For activity measurements, the TPH variants were thawed under running water, filtered, and the concentrations were determined by UV-Vis absorption at 280 nm. The TPH samples were diluted with the buffer in which they were purified. TPH activity was assayed in a reaction mixture (10x10 mm QS quartz cuvette from Hellma - 2500 µL total volume) containing 50 mM HEPES/NH_4OH, 200 mM $(NH_4)_2SO_4$, pH 7.0, 0.025 g/L catalase, 25 µM $(NH_4)_2Fe(II)(SO_4)_2{\cdot}6H_2O$, 7 mM dithiothreitol (DTT) with stirring at 15 °C. The standard substrate concentrations were 70 µM L-Trp, 300 µM BH_4, and 500 µM O_2. The O_2 concentration was achieved by equilibrating the solution with a mixture of O_2 and N_2. Excitation and emission wavelengths were 300 and 330 nm, respectively. Initial velocity was determined from linear regression through the first 0.04 min after BH_4 addition. Apparent kinetic parameters were calculated by curve fitting using non-linear least-squares approach. When only one substrate was varied, the initial velocity data were fitted using eq. 1 or eq. 2 in case of substrate inhibition. When two substrates were varied, the initial velocity data were fitted using eq. 3.[26,27,29]

$$v_i = \frac{V_{max}[S]}{K_m + [S]} \quad (1)$$

$$v_i = \frac{V_{max}[S]}{K_m + [S] + \frac{[S]^2}{K_i}} \quad (2)$$

$$v_i = \frac{V_{max}[A][B] + V_2[A][B]^2}{K_{m,A}[B]\left(1 + \frac{[B]}{K_i}\right) + K_{m,B}[A] + [A][B] + K_3[B]^2 + K_4[A][B]^2} \quad (3)$$

Kinetic parameters were determined from three independent experiments from at least two different purifications batches for each variant.

Molecular Dynamic Simulations. The x-ray structures of TPH1 (pdb: 1MLW, open loop conformation) and TPH2 (pdb: 4V06, open loop conformation) were used as initial models for MD simulations. The crystal structure of *human* TPH1 lacks interpretable electron density in the C-terminus (residue 394 to 413).

Homology modeling was utilized to build the terminus with 4V06 as template. The position and orientation of substrate Trp were obtained from the crystal structure of *chicken* TPH (pdb: 3E2T [19]) and superimposed into the structures of *human* TPH isoforms.

In the Schrödinger suite, mutations were performed by Residue Scanning in the BioLuminate suite.[58] The proteins were prepared for simulation with the default parameters of the Protein Preparation Workflow in Maestro [59]. Protonation states at pH 8.0 were assigned with the PropKa module [60]. The system was built by adding 0.3 M NaCl and water molecules (TIP3P model [61]) in an orthorhombic box exceeding 10 Å in each direction from the protein using System Builder workflow in Desmond [62]. The MD simulations were performed with the Desmond package using the OPLS3 force-field [63], and periodic boundary conditions in all three Cartesian coordinates were applied. Particle-mesh Ewald method [64] was applied to calculate long-range electrostatic interactions. Short-range electrostatic and van der Waals interactions were smoothly truncated at 9 Å. The simulations were run with constant number of atoms, with constant temperature of 300 K maintained with Nosé–Hoover thermostats [65], and constant pressure maintained at 1.01325 bar with the Martyna–Tobias–Klein barostat method [66]. RESPA integrator [67], with a 2.0-fs time step was utilized to solve the equations of motion for bonded and short-range interactions. The RESPA integrator default setting for nonbonded interactions beyond the 0.9-nm cutoff was 6.0-fs time step. Before every 100-ns production simulation run, a relaxation with the default parameters in Desmond was performed. Configurations and energies were saved at 5-ps intervals. Convergences of the MD simulations were based on RMSD calculations.

Acknowledgements

KDT acknowledges financial support via an Academic Excellence Scholarship from the Department of Chemistry, Technical University at Denmark. The authors would like to thank David F. Nielsen and Martin H. Pedersen for technical assistance.

Author Contributions

KDT: Wrote the paper, performed experiments and analyzed the data.

GHP: Designed experiments, contributed to data analysis and in writing the paper.

PH: Contributed in discussing the results and writing the paper.

ES: Performed preliminary experiments.

HEMC: Designed experiments, contributed to data analysis and in writing the paper.

Supporting information

Sequences of *h*TPH2 protein variants and MBP-3CP. Steady-state kinetic results (Figure S1-S3). Structural analysis of TPH isoform sequence conservation (Figure S4). TPH1 and TPH2 loop densities (Figure S5 and S6). Experimental procedure and results obtained from analytical gel filtration of the TPH variants (Figure

S7 and Table S1). Experimental procedure and results obtained from differential scanning fluorimetry measurements conducted on TPH variants (Table S2). Logo conservation plots of the active site loops of the TPH isoforms (Figure S8).

References

[1] Carkaci-Salli, N., Flanagan, J. M., Martz, M. K., Salli, U., Walther, D.J., Bader, M., and Vrana, K. E. (2006) Functional Domains of Human Tryptophan Hydroxylase 2 (hTPH2), *J. Biol. Chem. 281*, 28105-28112.

[2] Fitzpatrick, P.F. (1999) Tetrahydropterin-dependant amino acid hydroxylases, *Annu. Rev. Biochem. 68*, 355–381.

[3] Udenfriend, S., Clark, C. T., and Titus, E. (1953) 5-Hydroxytryptophan Decarboxylase: A New Route of Metabolism of Tryptophan, *J. Am. Chem. Soc. 75*, 501–502.

[4] Liberles, J. S., Thórólfsson, M., and Martínez, A. (2005) Allosteric mechanisms in ACT domain containing enzymes involved in amino acid metabolism, *Amino Acids 28*, 1–12.

[5] Costagliola, C., Parmeggiani, F., Semeraro, F. and Sebastiani, A. (2008) Selective Serotonin Reuptake Inhibitors: A Review of its Effects on Intraocular Pressure, *Curr. Neuropharmacol. 6*, 293-310.

[6] Liu, Q., Yang, Q., Sun, W., Vogel, P., Heydorn, W., Yu, X., Hu, Z., Yu, W., Jonas, B., Pineda, R., Calderon-Gay, V., Germann, M., O'Neill, E., Brommage, R., Cullinan, E., Platt, K., Wilson, A., Powell, D., Sands, A., Zambrowicz, B. and Shi, Z. (2008) Discovery and Characterization of Novel Tryptophan Hydroxylase Inhibitors That Selectively Inhibit Serotonin Synthesis in the Gastrointestinal Tract, J. Pharmacol. *Exp. Ther. 325*, 47-55.

[7] Popova, N. K. and Kulikov, A.V. (2010) Targeting tryptophan hydroxylase 2 in affective disorder, Expert Opin. Ther. *Targets 14*, 1259-1271.

[8] Matthes, S., Mosienko, V., Bashammakh, S., Alenina, N. and Bader, M. (2010) Tryptophan hydroxylase as novel target for the treatment of depressive disorders, *Pharmocology 85*, 95-109.

[9] Ikeda, M., Fahien, L. A., and Udenfriend, S. (1966) A Kinetic Study of Bovine Adrenal Tyrosine Hydroxylase, *J. Biol. Chem. 241*, 4452-4456.

[10] Oka, K., Kato, T., Sugimoto, T., Matsuura, S., and Nagatsu, T. (1981) Kinetic properties of tyrosine hydroxylase with natural tetrahydrobiopterin as cofactor, *Biochim. Biophys. Acta 661*, 45-53.

[11] Dix, T. A., Kuhn, D. M., Benkovic, S. J. (1987) Mechanism of Oxygen Activation by Tyrosine Hydroxylase, *Biochemistry 26*, 3354-3361.

[12] Fitzpatrick, P. F. (1991) Steady-State Kinetic Mechanism of Rat Tyrosine Hydroxylase, *Biochemistry 30*, 3658-3662.

[13] Chow, M. S., Eser, B. E., Wilson, S. A., Hodgson, K. O., Hedman, B., Fitzpatrick, P. F. and Solomon, E. I. (2009) Spectroscopy and Kinetics of Wild-type and Mutant Tyrosine Hydroxylase: Mechanistic Insight into O2 Activation, *J. Am. Chem. Soc. 131*, 7685-7698.

[14] Subedi, B. S. and Fitzpatrick, P. F. (2016) Kinetic Mechanism and intrinsic Rate Constant for the Reaction of a Bacterial Phenylalanine Hydroxylase, *Biochemistry 55*, 6848-6857.

[15] Volner, A., Zoidakis, J., Abu-Omar, M. M. (2003) Order of substrate binding in bacterial phenyalanine hydroxylase and its mechanistic implication for pterin-dependent oxygenases, *J. Biol. Inorg. Chem. 8*, 121-128.

[16] Roberts, K. M., Pavon, J. A., and Fitzpatrick, P. F. (2013) Kinetic mechanism of phenylalanine hydroxylase: intrinsic binding and rate constants from single-turnover experiments. *Biochemistry 52*, 1062−1073.

[17] Pavon, J. A., Eser, B., Huynh, M. T., and Fitzpatrick, P. F. (2010) Single Turnover Kinetics of Tryptophan Hydroxylase: Evidence for a New Intermediate in the Reaction of the Aromatic Amino Acid Hydroxylases, *Biochemistry 49*, 7563-7563.

[18] Cianchetta, G., Stouch, T., Yu, W., Shi, Z., Tari, L. W., Swanson, R. V., Hunter, M. J., Hoffman, I. D., and Liu, Q. (2010) Mechanism of Inhibition of Novel Tryptophan Hydroxylase Inhibitors Revealed by Co-crystal Structures and Kinetic Analysis, *Curr. Chem. Genomics 4*, 19-26.

[19] Windahl, M. S., Petersen, C. R., Christensen, H. E. M., and Harris, P. (2008) Crystal structure of tryptophan hydroxylase with bound amino acid substrate, *Biochemistry 47(46)*, 12087-12094.

[20] McKinney, J., Knappskog, P. M., and Haavik, J. (2005) Different properties of the central and peripheral forms of human tryptophan hydroxylase, *J. Neurochem. 92*, 311-320.

[21] Windahl, M. S., Boesen, J., Karlsen, P. E., and Christensen, H. E. M. (2009) Expression, Purification and Enzymatic Characterization of the Catalytic Domains of Human Tryptophan Hydroxylase Isoforms, *Protein J. 28*, 400–406.

[22] Winge, I., McKinney, J. A., Ying, M., D'Santos, C. S., Kleppe, R., Knappskog, P. M. and Haavik, J. (2008) Activation and stabilization of human tryptophan hydroxylase 2 by phosphorylation and 14-3-3 binding, *Biochem. J. 410*, 195–204.

[23] Yang, X.-J., and Kaufman, S. (1994) High-level expression and deletion mutagenesis of human tryptophan hydroxylase, *Proc. Natl. Acad. Sci. 91*, 6659-6663.

[24] Leskovac, V. (2003) Comprehensive enzyme kinetics, Kluwer Academic/Plenum Press, New York.

[25] Segel, I. H., (1975) Enzyme kinetics - Behavior and analysis of rapid equilibrium and steady-state enzyme systems. John Wiley and Son, Inc., New York.

[26] Mannervik, B. (1973) A Branching Mechanism of Glutathione Reductase, *Biochem. Biophys. Res. Commun. 51(4)*, 1151-1158.

[27] Mannervik, B. (1975) Nonlinear Regression Methods In Design of Experiments and Mathematical Modelling. Applications to the analysis of the Steady-State Kinetics of Glutathione Reductase, *BioSystems 7*, 101-119.

[28] Krenitsky, T. A., Papaioannou, R. (1969) Human Hypoxanthine Phosphoribosyltransferase, *J. Biol. Chem. 244(5)*, 1271-1277.

[29] Montero, S., de Arriaga, D., Busto, F., and Soler, J. (1990) A study of the Kinetic Mechanism followed by Glutathione Reductase from Mycelium of Phycomyces Blakesleeanus, *Arch. Biochem. Biophys. 278(1)*, 52-59.

[30] McClure, W. R., Lardy, H. A., and Kneifel, H. P. (1971) Rat Liver Pyruvate Carboxylase, *J. Biol. Chem. 246(11)*, 3569-3578.

[31] Pabst, M. J., Habig, W. H., and Jakoby, W. B. (1974) Glutathione S-transferase, *J. Biol. Chem. 249(22)*, 7140-7150.

[32] Wang, L., Erlandsen, H., Haavik, J., Knappskog, P. M. and Stevens, R.C. (2002) Three-dimensional structure of human tryptophan hydroxylase and its implications for the biosynthesis of the neurotransmitters serotonin and melatonin, *Biochemistry 41(42)*, 12569-12574.

[33] Erlandsen, H., Bjørgo, E., Flatmark, T., Stevens, R. C. (2000) Crystal structure and site-specific mutagenesis of pterin-bound human phenylalanine hydroxylase, *Biochemistry 39(9)*, 2208-2217.

[34] Andersen, O. A., Flatmark, T., and Hough, E. (2001) High resolution crystal structures of the catalytic domain of human phenylalanine hydroxylase in its catalytically active Fe(II) form and binary complex with tetrahydrobiopterin, *J. Mol. Biol. 314*, 279-291.

[35] Andersen, O. A., Flatmark, T., and Hough, E. (2002) Crystal structure of the ternary complex of the catalytic domain of human phenylalanine hydroxylase with tetrahydrobiopterin and 3-(2-thienyl)-L-alanine, and its implications for the mechanism of catalysis and substrate activation, *J. Mol. Biol. 320(5)*, 1095-1108.

[36] Andersen, O. A., Stokka, A. J., Flatmark, T., and Hough, E. (2003) 2.0 Å resolution crystal structures of the ternary complexes of human phenylalanine hydroxylase catalytic domain with tetrahydrobiopterin and 3-(2-thienyl)-L-alanine or L-norleucine: substrate specificity and molecular motions related to substrate binding, *J. Mol. Biol. 333(4)*, 747-757.

[37] Crooks, G.E., Hon, G., Chandonia, J. M., Brenner, S.E. (2004) WebLogo: A sequence logo generator, *Genome Research 14*, 1188-1190.

[38] Jiang, G. C. T., Yohrling, G. J., Schmitt, I. V. J. D., and Vrana, K. E. (2000) Identification of Substrate Orienting and Phosphorylation Sites Within Tryptophan Hydroxylase Using Homology-based Molecular Modeling, *J. Mol. Biol. 302*, 1005-1017.

[39] Moran, G. R., Daubner, S.C., and Fitzpatrick, P. F. (1998) Expression and Characterization of the Catalytic Core of Tryptophan Hydroxylase, *J. Biol. Chem. 273*, 12259-12266.

[40] Cichon, S., Winge, I., Mattheisen, M., Georgi, A., Karpushova, A., Freudenberg, J., Freudenberg-Hua, Y., Babadjanova, G., Van Den Bogaert, A., Abramova, L. I., Kapiletti, S., Knappskog, P. M., McKinney, J., Maier, W., Jamra, R. A., Schulze, T. G., Schumacher, J., Propping, P., Rietschel, M., Haavik, J., and Nöthen, M. M. (2008) Brain-specific tryptophan hydroxylase 2 (TPH2): a functional Pro206Ser substitution and variation in the 5'-region are associated with bipolar affective disorder, *Hum. Mol. Genet. 17(1)*, 87-97.

[41] Winge, I., McKinney, J. A., Knappskog, P. M., and Haavik, J. (2007) Characterization of wild-type and mutant forms of human tryptophan hydroxylase 2, *J. Neurochem. 100*, 1648–1657.

[42] Reed, M. C., Lieb, A., and Nijhout, H. F. (2010) The biological significance of substrate inhibition: A mechanism with diverse functions, *Bioessays 32*, 422–429.

[43] McKinney, J., Knappskog, P. M., Pereira, J., Ekern, T., Toska, K., Kuitert, B. B., Levine, D., Gronenborn, A. M., Martinez, A., and Haavik, J. (2004) Expression and purification of human tryptophan hydroxylase from Escherichia coli and Pichia pastoris, *Protein Expr. Purif. 33*, 185–194.

[44] Ribeiro, P., Wang, Y., Citron, B. A., and Kaufman, S. (1993) Deletion Mutagenesis of Rat PC12 Tyrosine Hydroxylase Regulatory and Catalytic Domains. *J. Molec. Neurosci. 4(2)*, 125-139.

[45] Leandro, J., Stokka, A. J., Teigen, K., Andersen, O. A., Flatmark, T. (2017) Substituting Tyr138 in the active site loop of human phenylalanine hydroxylase affects catalysis and substrate activation, *FEBS Open Bio 7(7)*, 1026-1036.

[46] Daubner, S. C., McGinnis, J. T., Gardner, M., Kroboth, S. L., Morris, A. R., and Fitzpatrick, P. F. (2006) A Flexible Loop in Tyrosine Hydroxylase Controls Coupling of Amino Acid Hydroxylation to Tetrahydropterin Oxidation, *J. Mol. Biol. 359*, 299–307.

[47] Frantom, P. A. and Fitzpatrick, P. F. (2003) Uncoupled forms of tyrosine hydroxylase unmask kinetic isotope effects on chemical steps, *J. Am. Chem. Soc. 125(52)*, 16190-16191.

[48] Quinsey, N. S., Luong, A. Q., and Dickson, P. W. (1998) Mutational Analysis of Substrate Inhibition in Tyrosine Hydroxylase, *J. Neurochem. 71(5)*, 2132-2138.

[49] Fernstrom, J. D. and Faller, D. V. (1978) Neutral amino acids in the brain: changes in response to food ingestion, *J. Neurochem. 30*, 1531-1538.

[50] Breum, L., Rasmussen, M. H., Hilsted, J., and Fernstrom, J. D. (2003) Twenty-four–hour plasma tryptophan concentrations and ratios are below normal in obese subjects and are not normalized by substantial weight reduction, *Am. J. Clin. Nutr. 77*, 1112–1118.

[51] Amireault, P., Sibon, D., and Coté, F. (2013) Life without Peripheral Serotonin: Insights from Tryptophan Hydroxylase 1 Knockout Mice Reveal the Existence of Paracrine/Autocrine Serotonergic Networks, *Chem. Neurosci. 4*, 64−71.

[52] Fernstrom, J. and Fernstrom, M. (1995) Brain tryptophan concentrations and serotonin synthesis remain responsive to food consumption after the ingestion of sequential meals, *Am. J. Clin. Nutr. 61*, 312–319.

[53] Knott, P. J. and Curzon, G. (1972) Free Tryptophan in Plasma and Brain Tryptophan Metabolism, *Nature 239*, 452-453.

[54] Walker, P. A., Leong, L. E. C., Ng, P. W. P., Tan, S. H., Waller, S., Murphy, D., and Porter, A. G. (1994) Efficient and Rapid Affinity Purification of Proteins Using Recombinant Fusion Proteases, *Nat. Biotechnol. 12*, 601 – 605.

[55] Nielsen, M. S., Petersen, C. R., Munch, A., Vendelboe, T. V., Boesen, J., Harris, P., and Christensen, H. E. M. (2008) A simple two step procedure for purification of the catalytic domain of chicken tryptophan hydroxylase 1 in a form suitable for crystallization, *Protein Expr. Purif. 57*, 116–126.

[56] Tidemand, K. D., Christensen, H. E. M., Hoeck, N., Harris, P., Boesen, J., and Peters, G. H. (2016) Stabilization of tryptophan hydroxylase 2 by L-phenylalanine-induced dimerization, *FEBS Open Bio 6*, 987–999.

[57] Moran, G. R. and Fitzpatrick, P. F. (1999) A Continuous Fluorescence Assay for Tryptophan Hydroxylase, *Anal. Biochem. 266*, 148-152.

[58] Schrödinger Release 2016-4: BioLuminate, Schrödinger, LLC, New York, NY, 2016

[59] Schrödinger Suite 2016-4 Protein Preparation Wizard; Epik, Schrödinger, LLC, New York, NY, 2016; Impact, Schrödinger, LLC, New York, NY, 2016; Prime, Schrödinger, LLC, New York, NY, 2016.

[60] Li, H., Robertson, A. D., and Jensen, J. H. (2005) Very Fast Empirical Prediction and Rationalization of Protein pKa Values, *Proteins 61*, 704-721.

[61] Jorgensen, W. L., Chandrasekhar, J., Madura, J. D., Impey, R. W., and Klein, M. L. (1983) Comparison of Simple Potential Functions for Simulating Liquid Water, *J. Chem. Phys. 79*, 926-935.

[62] Shivakumar, D., Williams, J., Wu, Y., Damm, W., Shelley, J., and Sherman, W. (2010) Prediction of Absolute Solvation Free Energies using Molecular Dynamics Free Energy Perturbation and the OPLS Force Field, *J. Chem. Theory Comput. 6*, 1509–1519.

[63] Harder, E., Damm, W., Maple, J., Wu, C., Reboul, M., Xiang, J. Y., Wang, L., Lupyan, D., Dahlgren, M. K.., Knight, J. L., Kaus, J. W., Cerutti, D., Krilov, G., Jorgensen, W. L., Abel, R., and Friesner, R. A. (2015) OPLS3: a force field providing broad coverage of drug-like small molecules and proteins, *J. Chem. Theory Comput.*, DOI: 10.1021/acs.jctc.5b00864.

[64] Essmann, U., Perera, L., Berkowitz, M. L., Darden, T., Lee, H., and Pedersen, L. G. (1995) A smooth particle mesh Ewald method, *J. Chem. Phys.103*, 8577-8593.

[65] Hoover, W. G. (1985) Canonical dynamics: Equilibrium phase-space distributions, *Phys. Rev. A 31(3)*, 1695-1697.

[66] Martyna, G. J., Tobias, D. J., and Klein, M. L. (1994) Constant pressure molecular dynamics algorithms, *J. Chem. Phys. 101*, 4177-4189.

[67] Humphreys, D. D., Friesner, R. A., and Berne, B. J. (1994) A Multiple-Time-Step Molecular Dynamics Algorithm for Macromolecules, *J. Phys. Chem. 98 (27)*, 6885–6892.

Supporting information

Sequences of TPH variants and MBP-3CP

Color-code:

XXXX = MBP
XXXX = 3CP
XXXX = Linker
XXXX = 3CP recognition and cleavage site (shown as ↓)
XXXX = Catalytic domain

MBP-*ch*TPH2:

MKIEEGKLVIWINGDKGYNGLAEVGKKFEKDTGIKVTVEHPDKLEEKFPQVAATGDGPDIIFWAHDRFGGYAQSGLLAEI
TPDKAFQDKLYPFTWDAVRYNGKLIAYPIAVEALSLIYNKDLLPNPPKTWEEIPALDKELKAKGKSALMFNLQEPYFTWP
LIAADGGYAFKYENGKYDIKDVGVDNAGAKAGLTFLVDLIKNKHMNADTDYSIAEAAFNKGETAMTINGPWAWSNIDTSK
VNYGVTVLPTFKGQPSKPFVGVLSAGINAASPNKELAKEFLENYLLTDEGLEAVNKDKPLGAVALKSYEEELAKDPRIAA
TMENAQKGEIMPNIPQMSAFWYAVRTAVINAASGRQTVDEALKDAQTNSSSNNNNNNNNNNLGLEVLFQ↓GPEELEDVPW
FPRKISELDKCSHRVLMYGSELDADHPGFKDNVYRQRRKYFVDVAMGYKYGQPIPRVEYTEEETKTWGVVFRELSKLYPT
HACREYLKNFPLLTKYCGYREDNVPQLEDVSMFLKERSGFTVRPVAGYLSPRDFLAGLAYRVFHCTQYIRHGSDPLYTPE
PDTCHELLGHVPLLADPKFAQFSQEIGLASLGASDEDVQKLATCYFFTIEFGLCKQEGQLRAYGAGLLSSIGELKHALSD
KACVKAFDPKTTCLQECLITTFQEAYFVSESFEEAKEKMRDFAKSITRPFSVYFNPYTQSIEILKD

MBP-Y171A-*ch*TPH2:

MKIEEGKLVIWINGDKGYNGLAEVGKKFEKDTGIKVTVEHPDKLEEKFPQVAATGDGPDIIFWAHDRFGGYAQSGLLAEI
TPDKAFQDKLYPFTWDAVRYNGKLIAYPIAVEALSLIYNKDLLPNPPKTWEEIPALDKELKAKGKSALMFNLQEPYFTWP
LIAADGGYAFKYENGKYDIKDVGVDNAGAKAGLTFLVDLIKNKHMNADTDYSIAEAAFNKGETAMTINGPWAWSNIDTSK
VNYGVTVLPTFKGQPSKPFVGVLSAGINAASPNKELAKEFLENYLLTDEGLEAVNKDKPLGAVALKSYEEELAKDPRIAA
TMENAQKGEIMPNIPQMSAFWYAVRTAVINAASGRQTVDEALKDAQTNSSSNNNNNNNNNNLGLEVLFQ↓GPEELEDVPW
FPRKISELDKCSHRVLMAGSELDADHPGFKDNVYRQRRKYFVDVAMGYKYGQPIPRVEYTEEETKTWGVVFRELSKLYPT
HACREYLKNFPLLTKYCGYREDNVPQLEDVSMFLKERSGFTVRPVAGYLSPRDFLAGLAYRVFHCTQYIRHGSDPLYTPE
PDTCHELLGHVPLLADPKFAQFSQEIGLASLGASDEDVQKLATCYFFTIEFGLCKQEGQLRAYGAGLLSSIGELKHALSD
KACVKAFDPKTTCLQECLITTFQEAYFVSESFEEAKEKMRDFAKSITRPFSVYFNPYTQSIEILKD

MBP-Y171W-*ch*TPH2:

MKIEEGKLVIWINGDKGYNGLAEVGKKFEKDTGIKVTVEHPDKLEEKFPQVAATGDGPDIIFWAHDRFGGYAQSGLLAEI
TPDKAFQDKLYPFTWDAVRYNGKLIAYPIAVEALSLIYNKDLLPNPPKTWEEIPALDKELKAKGKSALMFNLQEPYFTWP
LIAADGGYAFKYENGKYDIKDVGVDNAGAKAGLTFLVDLIKNKHMNADTDYSIAEAAFNKGETAMTINGPWAWSNIDTSK
VNYGVTVLPTFKGQPSKPFVGVLSAGINAASPNKELAKEFLENYLLTDEGLEAVNKDKPLGAVALKSYEEELAKDPRIAA
TMENAQKGEIMPNIPQMSAFWYAVRTAVINAASGRQTVDEALKDAQTNSSSNNNNNNNNNNLGLEVLFQ↓GPEELEDVPW
FPRKISELDKCSHRVLMWGSELDADHPGFKDNVYRQRRKYFVDVAMGYKYGQPIPRVEYTEEETKTWGVVFRELSKLYPT
HACREYLKNFPLLTKYCGYREDNVPQLEDVSMFLKERSGFTVRPVAGYLSPRDFLAGLAYRVFHCTQYIRHGSDPLYTPE
PDTCHELLGHVPLLADPKFAQFSQEIGLASLGASDEDVQKLATCYFFTIEFGLCKQEGQLRAYGAGLLSSIGELKHALSD
KACVKAFDPKTTCLQECLITTFQEAYFVSESFEEAKEKMRDFAKSITRPFSVYFNPYTQSIEILKD

MBP-loop-swap-c*h*TPH2:

MKIEEGKLVIWINGDKGYNGLAEVGKKFEKDTGIKVTVEHPDKLEEKFPQVAATGDGPDIIFWAHDRFGGYAQSGLLAEI
TPDKAFQDKLYPFTWDAVRYNGKLIAYPIAVEALSLIYNKDLLPNPPKTWEEIPALDKELKAKGKSALMFNLQEPYFTWP
LIAADGGYAFKYENGKYDIKDVGVDNAGAKAGLTFLVDLIKNKHMNADTDYSIAEAAFNKGETAMTINGPWAWSNIDTSK
VNYGVTVLPTFKGQPSKPFVGVLSAGINAASPNKELAKEFLENYLLTDEGLEAVNKDKPLGAVALKSYEEELAKDPRIAA
TMENAQKGEIMPNIPQMSAFWYAVRTAVINAASGRQTVDEALKDAQTNSSSNNNNNNNNNNLGLEVLFQ↓GPEELEDVPW
FPRKISELDHCANRVLMYGSELDADHPGFKDNVYRQRRKYFVDVAMGYKYGQPIPRVEYTEEETKTWGVVFRELSKLYPT
HACREYLKNFPLLTKYCGYREDNVPQLEDVSMFLKERSGFTVRPVAGYLSPRDFLAGLAYRVFHCTQYIRHGSDPLYTPE
PDTCHELLGHVPLLADPKFAQFSQEIGLASLGASDEDVQKLATCYFFTIEFGLCKQEGQLRAYGAGLLSSIGELKHALSD
KACVKAFDPKTTCLQECLITTFQEAYFVSESFEEAKEKMRDFAKSITRPFSVYFNPYTQSIEILKD

MBP-c*h*TPH1:

MKIEEGKLVIWINGDKGYNGLAEVGKKFEKDTGIKVTVEHPDKLEEKFPQVAATGDGPDIIFWAHDRFGGYAQSGLLAEI
TPDKAFQDKLYPFTWDAVRYNGKLIAYPIAVEALSLIYNKDLLPNPPKTWEEIPALDKELKAKGKSALMFNLQEPYFTWP
LIAADGGYAFKYENGKYDIKDVGVDNAGAKAGLTFLVDLIKNKHMNADTDYSIAEAAFNKGETAMTINGPWAWSNIDTSK
VNYGVTVLPTFKGQPSKPFVGVLSAGINAASPNKELAKEFLENYLLTDEGLEAVNKDKPLGAVALKSYEEELAKDPRIAA
TMENAQKGEIMPNIPQMSAFWYAVRTAVINAASGRQTVDEALKDAQTNSSSNNNNNNNNNNLGLEVLFQ↓GPDGMETVPW
FPKKISDLDHCANRVLMYGSELDADHPGFKDNVYRKRRKYFADLAMNYKHGDPIPKVEFTEEEIKTWGTVFQELNKLYPT
HACREYLKNLPLLSKYCGYREDNIPQLEDVSNFLKERTGFSIRPVAGYLSPRDFLSGLAFRVFHCTQYVRHSSDPFYTPE
PDTCHELLGHVPLLAEPSFAQFSQEIGLASLGASEEAVQKLATCYFFTVEFGLCKQDGQLRVFGAGLLSSISELKHALSG
HAKVKPFDPKITCKQECLITTFQDVYFVSESFEDAKEKMREFTKTIKRPFGVKYNPYTRSIQILKD

MBP-Y125A-c*h*TPH1:

MKIEEGKLVIWINGDKGYNGLAEVGKKFEKDTGIKVTVEHPDKLEEKFPQVAATGDGPDIIFWAHDRFGGYAQSGLLAEI
TPDKAFQDKLYPFTWDAVRYNGKLIAYPIAVEALSLIYNKDLLPNPPKTWEEIPALDKELKAKGKSALMFNLQEPYFTWP
LIAADGGYAFKYENGKYDIKDVGVDNAGAKAGLTFLVDLIKNKHMNADTDYSIAEAAFNKGETAMTINGPWAWSNIDTSK
VNYGVTVLPTFKGQPSKPFVGVLSAGINAASPNKELAKEFLENYLLTDEGLEAVNKDKPLGAVALKSYEEELAKDPRIAA
TMENAQKGEIMPNIPQMSAFWYAVRTAVINAASGRQTVDEALKDAQTNSSSNNNNNNNNNNLGLEVLFQ↓GPDGMETVPW
FPKKISDLDHCANRVLMAGSELDADHPGFKDNVYRKRRKYFADLAMNYKHGDPIPKVEFTEEEIKTWGTVFQELNKLYPT
HACREYLKNLPLLSKYCGYREDNIPQLEDVSNFLKERTGFSIRPVAGYLSPRDFLSGLAFRVFHCTQYVRHSSDPFYTPE
PDTCHELLGHVPLLAEPSFAQFSQEIGLASLGASEEAVQKLATCYFFTVEFGLCKQDGQLRVFGAGLLSSISELKHALSG
HAKVKPFDPKITCKQECLITTFQDVYFVSESFEDAKEKMREFTKTIKRPFGVKYNPYTRSIQILKD

MBP-Y125W-c*h*TPH1:

MKIEEGKLVIWINGDKGYNGLAEVGKKFEKDTGIKVTVEHPDKLEEKFPQVAATGDGPDIIFWAHDRFGGYAQSGLLAEI
TPDKAFQDKLYPFTWDAVRYNGKLIAYPIAVEALSLIYNKDLLPNPPKTWEEIPALDKELKAKGKSALMFNLQEPYFTWP
LIAADGGYAFKYENGKYDIKDVGVDNAGAKAGLTFLVDLIKNKHMNADTDYSIAEAAFNKGETAMTINGPWAWSNIDTSK
VNYGVTVLPTFKGQPSKPFVGVLSAGINAASPNKELAKEFLENYLLTDEGLEAVNKDKPLGAVALKSYEEELAKDPRIAA
TMENAQKGEIMPNIPQMSAFWYAVRTAVINAASGRQTVDEALKDAQTNSSSNNNNNNNNNNLGLEVLFQ↓GPDGMETVPW
FPKKISDLDHCANRVLMWGSELDADHPGFKDNVYRKRRKYFADLAMNYKHGDPIPKVEFTEEEIKTWGTVFQELNKLYPT
HACREYLKNLPLLSKYCGYREDNIPQLEDVSNFLKERTGFSIRPVAGYLSPRDFLSGLAFRVFHCTQYVRHSSDPFYTPE
PDTCHELLGHVPLLAEPSFAQFSQEIGLASLGASEEAVQKLATCYFFTVEFGLCKQDGQLRVFGAGLLSSISELKHALSG
HAKVKPFDPKITCKQECLITTFQDVYFVSESFEDAKEKMREFTKTIKRPFGVKYNPYTRSIQILKD

MBP-loop-swap-c*h*TPH1:

MKIEEGKLVIWINGDKGYNGLAEVGKKFEKDTGIKVTVEHPDKLEEKFPQVAATGDGPDIIFWAHDRFGGYAQSGLLAEI
TPDKAFQDKLYPFTWDAVRYNGKLIAYPIAVEALSLIYNKDLLPNPPKTWEEIPALDKELKAKGKSALMFNLQEPYFTWP
LIAADGGYAFKYENGKYDIKDVGVDNAGAKAGLTFLVDLIKNKHMNADTDYSIAEAAFNKGETAMTINGPWAWSNIDTSK
VNYGVTVLPTFKGQPSKPFVGVLSAGINAASPNKELAKEFLENYLLTDEGLEAVNKDKPLGAVALKSYEEELAKDPRIAA
TMENAQKGEIMPNIPQMSAFWYAVRTAVINAASGRQTVDEALKDAQTNSSSNNNNNNNNNNLGLEVLFQ↓GPDGMETVPW
FPKKISDLDKCSHRVLMYGSELDADHPGFKDNVYRKRRKYFADLAMNYKHGDPIPKVEFTEEEIKTWGTVFQELNKLYPT
HACREYLKNLPLLSKYCGYREDNIPQLEDVSNFLKERTGFSIRPVAGYLSPRDFLSGLAFRVFHCTQYVRHSSDPFYTPE
PDTCHELLGHVPLLAEPSFAQFSQEIGLASLGASEEAVQKLATCYFFTVEFGLCKQDGQLRVFGAGLLSSISELKHALSG
HAKVKPFDPKITCKQECLITTFQDVYFVSESFEDAKEKMREFTKTIKRPFGVKYNPYTRSIQILKD

MBP-3CP:

MKIEEGKLVIWINGDKGYNGLAEVGKKFEKDTGIKVTVEHPDKLEEKFPQVAATGDGPDIIFWAHDRFGGYAQSGLLAEI
TPDKAFQDKLYPFTWDAVRYNGKLIAYPIAVEALSLIYNKDLLPNPPKTWEEIPALDKELKAKGKSALMFNLQEPYFTWP
LIAADGGYAFKYENGKYDIKDVGVDNAGAKAGLTFLVDLIKNKHMNADTDYSIAEAAFNKGETAMTINGPWAWSNIDTSK
VNYGVTVLPTFKGQPSKPFVGVLSAGINAASPNKELAKEFLENYLLTDEGLEAVNKDKPLGAVALKSYEEELAKDPRIAA
TMENAQKGEIMPNIPQMSAFWYAVRTAVINAASGRQTVDEALKDAQTNSSSNNNNNNNNNNLGGIPGPEHEFLNALIRRN
CHIITTDKGEFNLLGIYSNCAVVPTHAEPGDVVDIDGRLVRVLKQQVLTDMNDVDTEVTVLWLDQNEKFRDIRRFIPEHQ
QDWHNIHLATNVTKFPMLNVEVGHTVPYGEINLSGNATCRLYKYDYPTQPGQCGAVLANTGNIIGIHVGGNGRVGYAAAL
LRKYFAEEQ

Steady-state kinetics

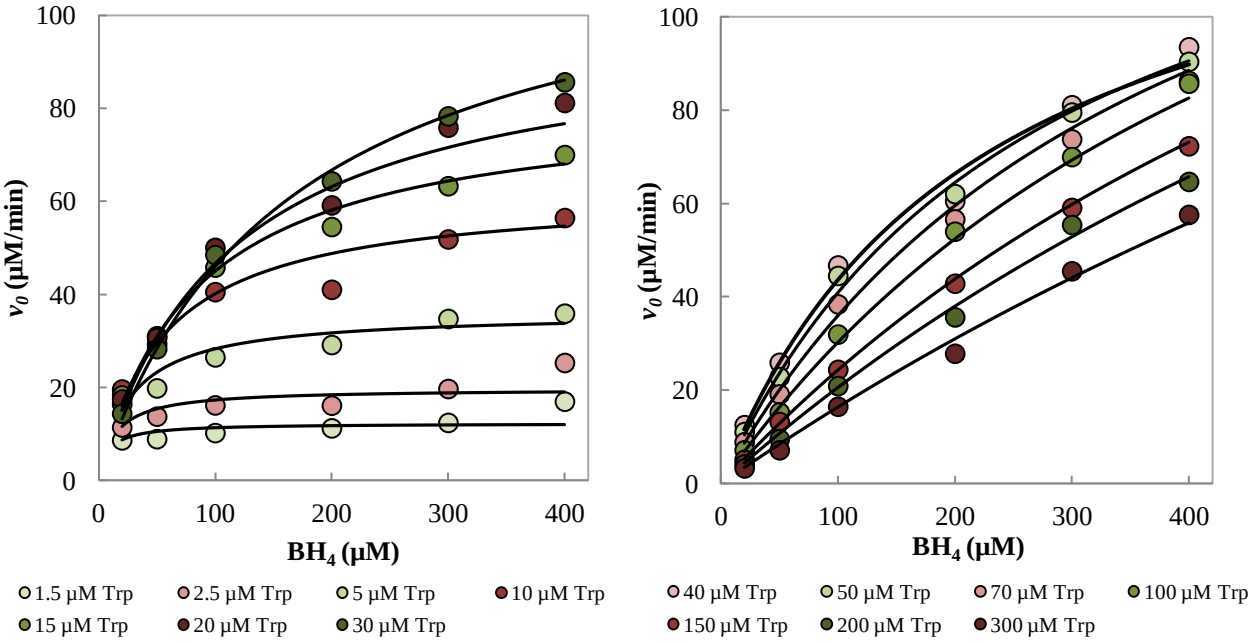

Figure S24. Initial velocity of *ch*TPH1 against BH_4 concentration at fixed concentrations of tryptophan. The oxygen concentration was 500 µM in all measurements. The plots are fitted with the a hybrid Ping Pong-ordered mechanism (eq. 3, experimental procedure).

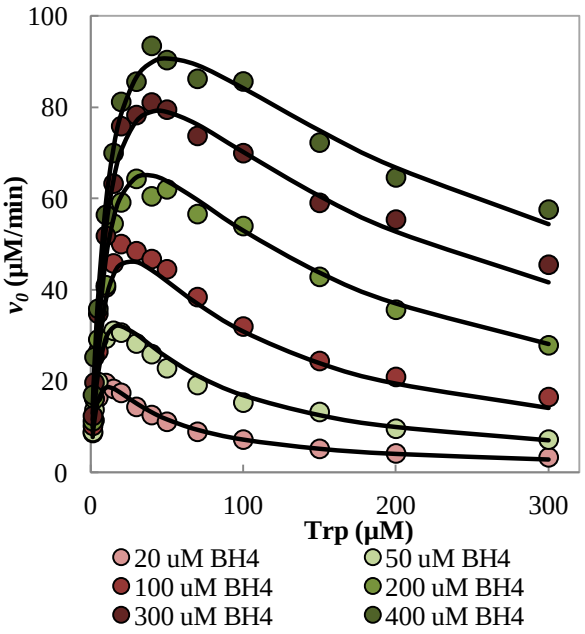

Figure S25. Initial velocity of *ch*TPH1 against Trp concentration at fixed concentrations of BH_4. The oxygen concentration was 500 µM in all measurements. The plots are fitted with the Michaelis-Menten equation with substrate inhibition (eq. 2, experimental procedure).

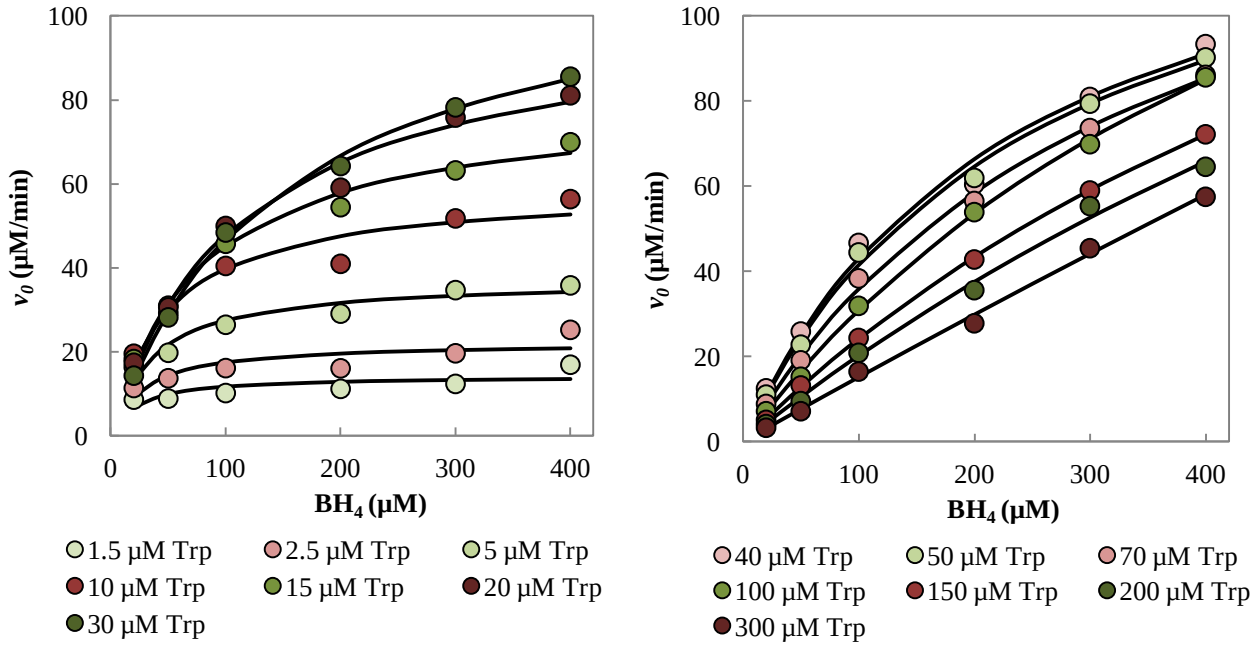

Figure S26. Initial velocity of *ch*TPH1 against BH_4 concentration at fixed concentrations of tryptophan. The oxygen concentration was 500 µM in all measurements. The plots are fitted with the Michaelis-Menten equation (eq. 1, experimental procedure).

Structural analysis of isoform sequence differences

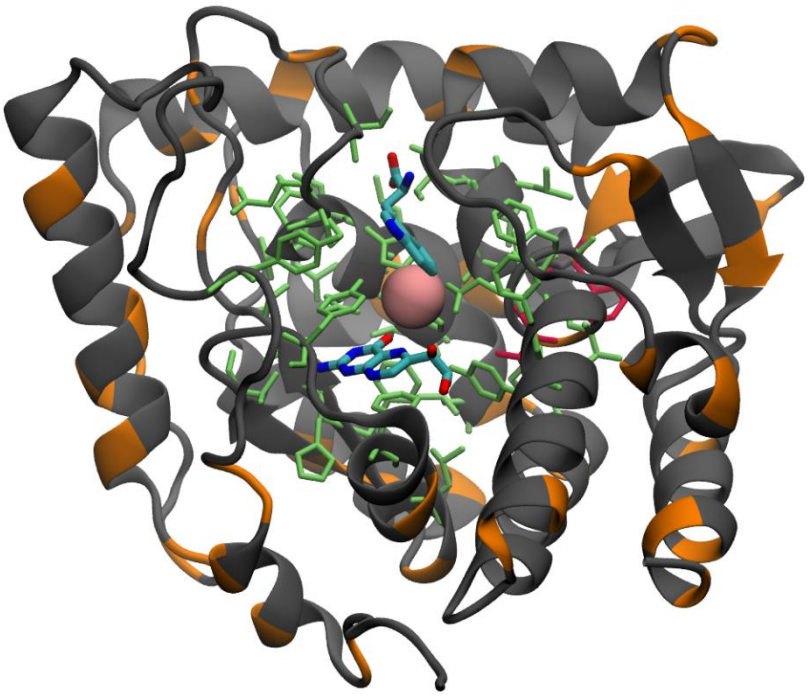

Figure S27. Crystal structure of human c*h*TPH1 with BH_2 and iron (pdb: 1MLW) and Trp (superimposed from chicken TPH1, pdb: 3E2T). Orange secondary structure indicates the position of non-conserved residues and gray indicates conserved residue positions between the isoforms. Residues in red (Val316 and Phe330) or green are non-conserved or conserved residues within 10 Å of active site iron, respectively.

Active site loop density

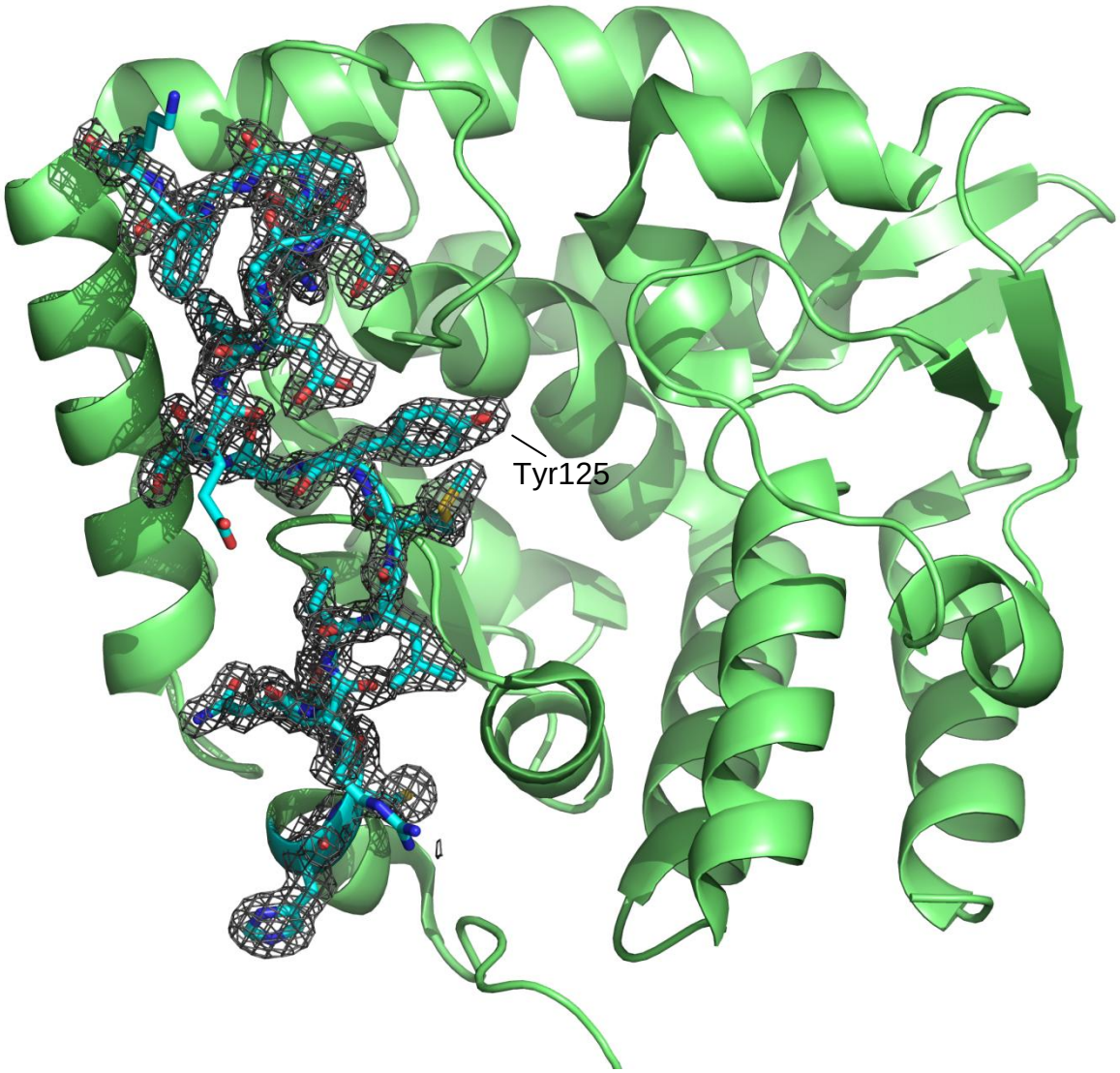

Figure S28. Crystal structure of TPH1 (pdb: 1MLW) with $2F_o$-F_c density map on the loop comprising residue 117 to 137. The mesh map of the loop is contoured at 1.0 σ and within 1.6 Å of the selected atoms.

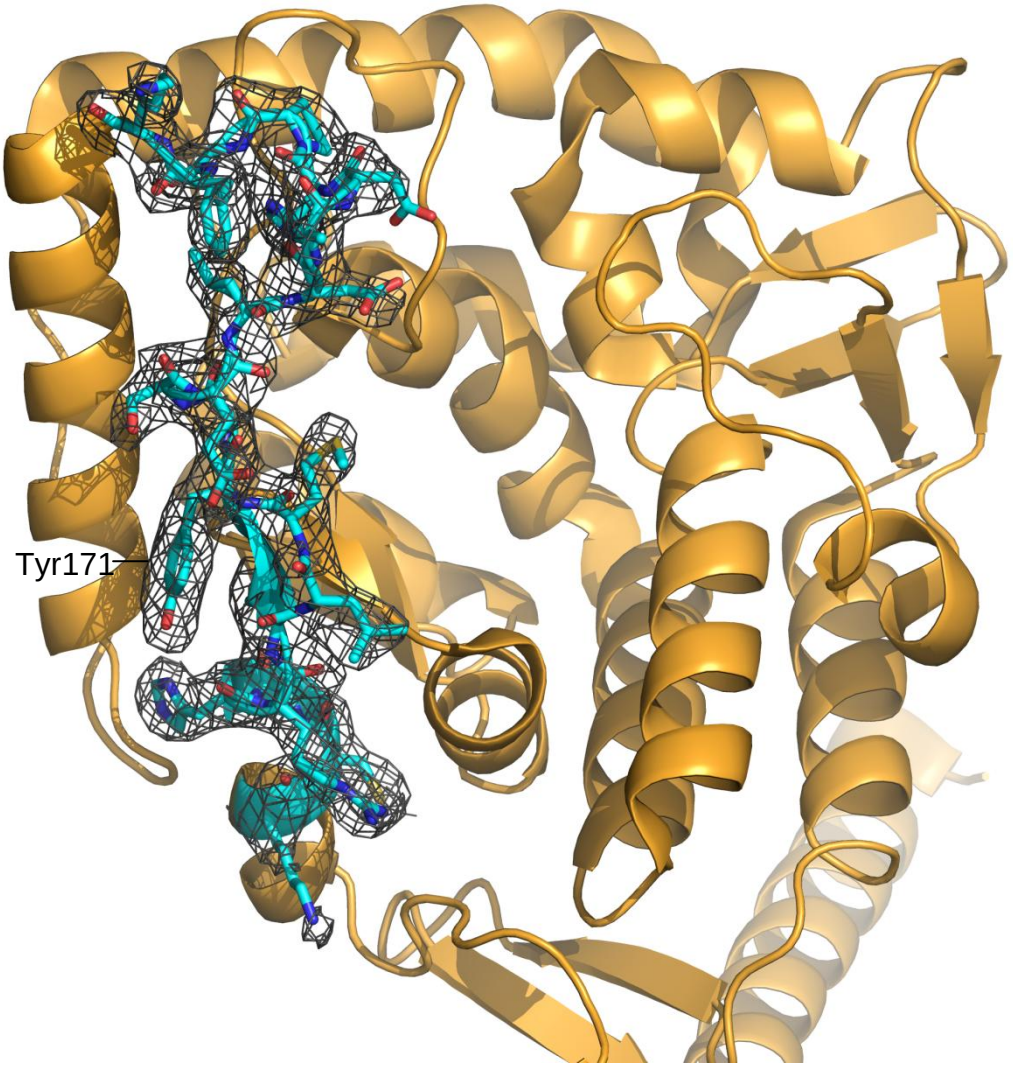

Figure S29. Crystal structure of TPH2 (pdb: 4V06, chain A) with $2F_o$-F_c density map on the loop comprising residue 163 to 183. The mesh map of the loop is contoured at 1.0 σ and within 1.6 Å of the selected atoms.

Analytical gel filtration

Expermental procedure - Determination of the oligomeric state of the TPH variants was performed on a Superdex 200 10/300 GL column. Samples were injected with a 500 µL loop and analyzed at a flow rate of 0.5 mL/min.

Results – The oligomeric states of the eight TPH variants were determined using size exclusion chromatography. The chromatograms display that all TPH variants of the two isoforms are monodisperse (Figure S7). The c*h*TPH1 variants elute at volumes from 15.505 ± 0.004 to 15.64 ± 0.05 mL while the c*h*TPH2 variants elute from 15.70 ± 0.05 to 15.78 ± 0.03 mL (Table S1). These results show that all the TPH variants reside as monomers [1] and that no significant changes within each variant occur as a consequence of mutation. Despite the slightly higher molecular weights of the c*h*TPH2 variants (36274 to 36362 Da) compared to c*h*TPH1 counterparts (36128 to 36250 Da), they elute at a slightly greater elution volume, which indicate that the c*h*TPH2 variants are more compact.

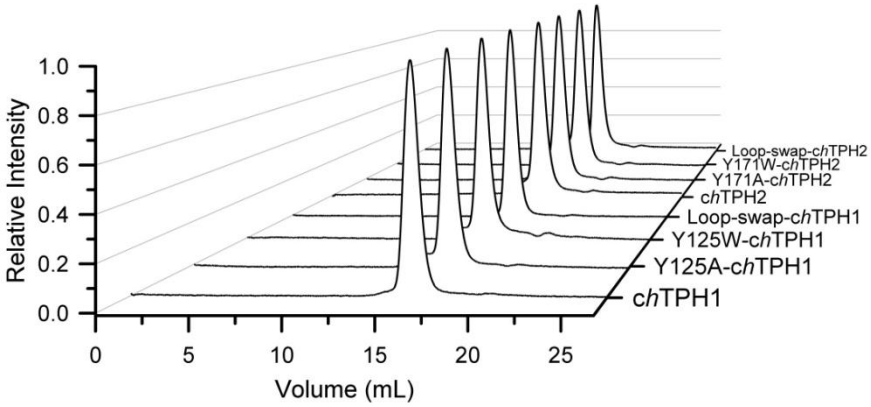

Figure S30. Normalized size exclusion chromatography results of the c*h*TPH variants.

Table S4. Elution volumes (mL) at maximum intensity with standard deviations (n=3).

Variant	Volume ± SD (mL)
c*h*TPH1	15.64 ± 0.05
Y125A-c*h*TPH1	15.505 ± 0.004
Y125W-c*h*TPH1	15.60 ± 0.04
Loop-swap-c*h*TPH1	15.53 ± 0.03
c*h*TPH2	15.72 ± 0.06
Y171A-c*h*TPH2	15.70 ± 0.05
Y171W-c*h*TPH2	15.74 ± 0.05
Loop-swap-c*h*TPH2	15.78 ± 0.03

[1] Tidemand, K. D., Christensen, H. E. M., Hoeck, N., Harris, P., Boesen, J., and Peters, G. H. (2016) Stabilization of tryptophan hydroxylase 2 by L-phenylalanine-induced dimerization, *FEBS Open Bio* 6, 987–999.

Differential scanning fluorimetry

Experimental procedure - The unfolding of the TPH variants was recorded with an Agilent Technologies Stratagene MX3005 P RT-PCR machine. Each measurement was performed with total volume of 25 µL in 96-well plates (polypropylene plates from Agilent Technologies). Each well was composed of protein at a concentration of 2 µM and SYPRO orange at a concentration of 4X (diluted from SYPRO® 5000X stock from Sigma). Scans were carried out using a scan-rate of 1 °C/min, going from 20 °C to 95 °C. The thermograms were baseline corrected with MxPro QPCR Software and analyzed for transition temperatures with GraphPad Prism 6 utilizing a Boltzmann sigmoid fit:

$$y = LL + \frac{UL - LL}{1 + \exp\left(\frac{T_m - x}{a}\right)}$$

where LL and UL are the values of minimum and maximum intensities, respectively, and a denotes the slope of the curve at T_m.[2]

Results – The thermal stability of the TPH variants was determined utilizing differential scanning fluorimetry (DSF). The results are summarized in Table S2. The transition temperature of c*h*TPH1 is determined to 41.4 ± 0.2 ºC. Mutations of Tyr125 to alanine or tryptophan or the three loop-swap mutations did not induce a significant change in the transition temperature. The transition temperature of c*h*TPH2 is determined to 42.1 ± 0.3 ºC which corresponds well with previous results.[1] As it was the case of c*h*TPH1, the substitution of tyrosine to alanine or tryptophan in position 171 or the three loop-swap mutations did not significantly change the transition temperature of the TPH2 variants. Overall, the mutations do not result in major changes in the thermal stability of the TPH variants.

Table S5. Transition temperatures (T_m) obtained from differential scanning fluorimetry experiments (n=4-6).

Variant	T_m ± SD (ºC)
c*h*TPH1	41.4 ± 0.2
Y125A-c*h*TPH1	40.1 ± 0.2
Y125W-c*h*TPH1	43.3 ± 0.1
Loop-swap-c*h*TPH1	42.1 ± 0.2
c*h*TPH2	42.1 ± 0.3
Y171A-c*h*TPH2	40.5 ± 0.3
Y171W-c*h*TPH2	41.3 ± 0.5
Loop-swap-c*h*TPH2	42.4 ± 0.1

[1] Tidemand, K. D., Christensen, H. E. M., Hoeck, N., Harris, P., Boesen, J., and Peters, G. H. (2016) Stabilization of tryptophan hydroxylase 2 by L-phenylalanine-induced dimerization, *FEBS Open Bio* 6, 987–999.
[2] Niesen, F.H., Berglund, H., and Vedadi, M. (2007) The use of differential scanning fluorimetry to detect ligand interactions that promote protein stability, *Nat. Protoc. 2*, 2212–2221.

Sequence conservation in the active site loop

Figure S31. Logo plots of the loops lining the active sites of TPH1 (top) and TPH2 (bottom). Sequences of TPH1 were obtained from an NCBI protein search: (tryptophan 5 hydroxylase 1) AND "vertebrates" accessed 04.21.2017. Sequences of TPH1 were obtained from an NCBI protein search: (tryptophan 5 hydroxylase 2) AND "vertebrates" accessed 04.21.2017. The overall height of a column indicates the sequence conservation at a given position, and the height of a symbol within the column indicates the relative frequency of that amino acid in that position.

Appendix B

TPH sequences

Color-code:

XXXX = MBP

XXXX = 3CP

XXXX = Linker

XXXX = 3CP recognition and cleavage site (shown as ↓)

XXXX = Regulatory domain

XXXX = Catalytic domain

XXXX = Tetramerization domain

MBP-c*h*TPH1:

MKIEEGKLVIWINGDKGYNGLAEVGKKFEKDTGIKVTVEHPDKLEEKFPQVAATGDGPDIIFWAHDRFGGYAQSGLLAEI
TPDKAFQDKLYPFTWDAVRYNGKLIAYPIAVEALSLIYNKDLLPNPPKTWEEIPALDKELKAKGKSALMFNLQEPYFTWP
LIAADGGYAFKYENGKYDIKDVGVDNAGAKAGLTFLVDLIKNKHMNADTDYSIAEAAFNKGETAMTINGPWAWSNIDTSK
VNYGVTVLPTFKGQPSKPFVGVLSAGINAASPNKELAKEFLENYLLTDEGLEAVNKDKPLGAVALKSYEEELAKDPRIAA
TMENAQKGEIMPNIPQMSAFWYAVRTAVINAASGRQTVDEALKDAQTNSSSNNNNNNNNNNLGLEVLFQ↓GPDGMETVPW
FPKKISDLDHCANRVLMYGSELDADHPGFKDNVYRKRRKYFADLAMNYKHGDPIPKVEFTEEEIKTWGTVFQELNKLYPT
HACREYLKNLPLLSKYCGYREDNIPQLEDVSNFLKERTGFSIRPVAGYLSPRDFLSGLAFRVFHCTQYVRHSSDPFYTPE
PDTCHELLGHVPLLAEPSFAQFSQEIGLASLGASEEAVQKLATCYFFTVEFGLCKQDGQLRVFGAGLLSSISELKHALSG
HAKVKPFDPKITCKQECLITTFQDVYFVSESFEDAKEKMREFTKTIKRPFGVKYNPYTRSIQILKD

MBP-Y125A-c*h*TPH1:

MKIEEGKLVIWINGDKGYNGLAEVGKKFEKDTGIKVTVEHPDKLEEKFPQVAATGDGPDIIFWAHDRFGGYAQSGLLAEI
TPDKAFQDKLYPFTWDAVRYNGKLIAYPIAVEALSLIYNKDLLPNPPKTWEEIPALDKELKAKGKSALMFNLQEPYFTWP
LIAADGGYAFKYENGKYDIKDVGVDNAGAKAGLTFLVDLIKNKHMNADTDYSIAEAAFNKGETAMTINGPWAWSNIDTSK
VNYGVTVLPTFKGQPSKPFVGVLSAGINAASPNKELAKEFLENYLLTDEGLEAVNKDKPLGAVALKSYEEELAKDPRIAA
TMENAQKGEIMPNIPQMSAFWYAVRTAVINAASGRQTVDEALKDAQTNSSSNNNNNNNNNNLGLEVLFQ↓GPDGMETVPW
FPKKISDLDHCANRVLMAGSELDADHPGFKDNVYRKRRKYFADLAMNYKHGDPIPKVEFTEEEIKTWGTVFQELNKLYPT
HACREYLKNLPLLSKYCGYREDNIPQLEDVSNFLKERTGFSIRPVAGYLSPRDFLSGLAFRVFHCTQYVRHSSDPFYTPE
PDTCHELLGHVPLLAEPSFAQFSQEIGLASLGASEEAVQKLATCYFFTVEFGLCKQDGQLRVFGAGLLSSISELKHALSG
HAKVKPFDPKITCKQECLITTFQDVYFVSESFEDAKEKMREFTKTIKRPFGVKYNPYTRSIQILKD

MBP-Y125L-c*h*TPH1:

MKIEEGKLVIWINGDKGYNGLAEVGKKFEKDTGIKVTVEHPDKLEEKFPQVAATGDGPDIIFWAHDRFGGYAQSGLLAEI
TPDKAFQDKLYPFTWDAVRYNGKLIAYPIAVEALSLIYNKDLLPNPPKTWEEIPALDKELKAKGKSALMFNLQEPYFTWP
LIAADGGYAFKYENGKYDIKDVGVDNAGAKAGLTFLVDLIKNKHMNADTDYSIAEAAFNKGETAMTINGPWAWSNIDTSK
VNYGVTVLPTFKGQPSKPFVGVLSAGINAASPNKELAKEFLENYLLTDEGLEAVNKDKPLGAVALKSYEEELAKDPRIAA
TMENAQKGEIMPNIPQMSAFWYAVRTAVINAASGRQTVDEALKDAQTNSSSNNNNNNNNNNLGLEVLFQ↓GPDGMETVPW
FPKKISDLDHCANRVLMLGSELDADHPGFKDNVYRKRRKYFADLAMNYKHGDPIPKVEFTEEEIKTWGTVFQELNKLYPT
HACREYLKNLPLLSKYCGYREDNIPQLEDVSNFLKERTGFSIRPVAGYLSPRDFLSGLAFRVFHCTQYVRHSSDPFYTPE
PDTCHELLGHVPLLAEPSFAQFSQEIGLASLGASEEAVQKLATCYFFTVEFGLCKQDGQLRVFGAGLLSSISELKHALSG
HAKVKPFDPKITCKQECLITTFQDVYFVSESFEDAKEKMREFTKTIKRPFGVKYNPYTRSIQILKD

MBP-Y125W-c*h*TPH1:

MKIEEGKLVIWINGDKGYNGLAEVGKKFEKDTGIKVTVEHPDKLEEKFPQVAATGDGPDIIFWAHDRFGGYAQSGLLAEI
TPDKAFQDKLYPFTWDAVRYNGKLIAYPIAVEALSLIYNKDLLPNPPKTWEEIPALDKELKAKGKSALMFNLQEPYFTWP
LIAADGGYAFKYENGKYDIKDVGVDNAGAKAGLTFLVDLIKNKHMNADTDYSIAEAAFNKGETAMTINGPWAWSNIDTSK
VNYGVTVLPTFKGQPSKPFVGVLSAGINAASPNKELAKEFLENYLLTDEGLEAVNKDKPLGAVALKSYEEELAKDPRIAA
TMENAQKGEIMPNIPQMSAFWYAVRTAVINAASGRQTVDEALKDAQTNSSSNNNNNNNNNNLGLEVLFQ↓GPDGMETVPW
FPKKISDLDHCANRVLMWGSELDADHPGFKDNVYRKRRKYFADLAMNYKHGDPIPKVEFTEEEIKTWGTVFQELNKLYPT
HACREYLKNLPLLSKYCGYREDNIPQLEDVSNFLKERTGFSIRPVAGYLSPRDFLSGLAFRVFHCTQYVRHSSDPFYTPE
PDTCHELLGHVPLLAEPSFAQFSQEIGLASLGASEEAVQKLATCYFFTVEFGLCKQDGQLRVFGAGLLSSISELKHALSG
HAKVKPFDPKITCKQECLITTFQDVYFVSESFEDAKEKMREFTKTIKRPFGVKYNPYTRSIQILKD

MBP-loop-swap-c*h*TPH1:

MKIEEGKLVIWINGDKGYNGLAEVGKKFEKDTGIKVTVEHPDKLEEKFPQVAATGDGPDIIFWAHDRFGGYAQSGLLAEI
TPDKAFQDKLYPFTWDAVRYNGKLIAYPIAVEALSLIYNKDLLPNPPKTWEEIPALDKELKAKGKSALMFNLQEPYFTWP
LIAADGGYAFKYENGKYDIKDVGVDNAGAKAGLTFLVDLIKNKHMNADTDYSIAEAAFNKGETAMTINGPWAWSNIDTSK
VNYGVTVLPTFKGQPSKPFVGVLSAGINAASPNKELAKEFLENYLLTDEGLEAVNKDKPLGAVALKSYEEELAKDPRIAA
TMENAQKGEIMPNIPQMSAFWYAVRTAVINAASGRQTVDEALKDAQTNSSSNNNNNNNNNNLGLEVLFQ↓GPDGMETVPW
FPKKISDLDKCSHRVLMYGSELDADHPGFKDNVYRKRRKYFADLAMNYKHGDPIPKVEFTEEEIKTWGTVFQELNKLYPT
HACREYLKNLPLLSKYCGYREDNIPQLEDVSNFLKERTGFSIRPVAGYLSPRDFLSGLAFRVFHCTQYVRHSSDPFYTPE
PDTCHELLGHVPLLAEPSFAQFSQEIGLASLGASEEAVQKLATCYFFTVEFGLCKQDGQLRVFGAGLLSSISELKHALSG
HAKVKPFDPKITCKQECLITTFQDVYFVSESFEDAKEKMREFTKTIKRPFGVKYNPYTRSIQILKD

MBP-rc*h*TPH1

MKIEEGKLVIWINGDKGYNGLAEVGKKFEKDTGIKVTVEHPDKLEEKFPQVAATGDGPDIIFWAHDRFGGYAQSGLLAEI
TPDKAFQDKLYPFTWDAVRYNGKLIAYPIAVEALSLIYNKDLLPNPPKTWEEIPALDKELKAKGKSALMFNLQEPYFTWP
LIAADGGYAFKYENGKYDIKDVGVDNAGAKAGLTFLVDLIKNKHMNADTDYSIAEAAFNKGETAMTINGPWAWSNIDTSK
VNYGVTVLPTFKGQPSKPFVGVLSAGINAASPNKELAKEFLENYLLTDEGLEAVNKDKPLGAVALKSYEEELAKDPRIAA
TMENAQKGEIMPNIPQMSAFWYAVRTAVINAASGRQTVDEALKDAQTNSSSNNNNNNNNNNLGLEVLFQ↓GPIEDNKENK
DHSLERGRASLIFSLKNEVGGLIKALKIFQEKHVNLLHIESRKSKRRNSEFEIFVDCDINREQLNDIFHLLKSHTNVLSV
NLPDNFTLKEDGMETVPWFPKKISDLDHCANRVLMYGSELDADHPGFKDNVYRKRRKYFADLAMNYKHGDPIPKVEFTEE
EIKTWGTVFQELNKLYPTHACREYLKNLPLLSKYCGYREDNIPQLEDVSNFLKERTGFSIRPVAGYLSPRDFLSGLAFRV
FHCTQYVRHSSDPFYTPEPDTCHELLGHVPLLAEPSFAQFSQEIGLASLGASEEAVQKLATCYFFTVEFGLCKQDGQLRV
FGAGLLSSISELKHALSGHAKVKPFDPKITCKQECLITTFQDVYFVSESFEDAKEKMREFTKTIKRPFGVKYNPYTRSIQ
ILKD

MBP-*h*TPH1

MKIEEGKLVIWINGDKGYNGLAEVGKKFEKDTGIKVTVEHPDKLEEKFPQVAATGDGPDIIFWAHDRFGGYAQSGLLAEI
TPDKAFQDKLYPFTWDAVRYNGKLIAYPIAVEALSLIYNKDLLPNPPKTWEEIPALDKELKAKGKSALMFNLQEPYFTWP
LIAADGGYAFKYENGKYDIKDVGVDNAGAKAGLTFLVDLIKNKHMNADTDYSIAEAAFNKGETAMTINGPWAWSNIDTSK
VNYGVTVLPTFKGQPSKPFVGVLSAGINAASPNKELAKEFLENYLLTDEGLEAVNKDKPLGAVALKSYEEELAKDPRIAA
TMENAQKGEIMPNIPQMSAFWYAVRTAVINAASGRQTVDEALKDAQTNSSSNNNNNNNNNNLGLEVLFQ↓GPIEDNKENK
DHSLERGRASLIFSLKNEVGGLIKALKIFQEKHVNLLHIESRKSKRRNSEFEIFVDCDINREQLNDIFHLLKSHTNVLSV
NLPDNFTLKEDGMETVPWFPKKISDLDHCANRVLMYGSELDADHPGFKDNVYRKRRKYFADLAMNYKHGDPIPKVEFTEE
EIKTWGTVFQELNKLYPTHACREYLKNLPLLSKYCGYREDNIPQLEDVSNFLKERTGFSIRPVAGYLSPRDFLSGLAFRV
FHCTQYVRHSSDPFYTPEPDTCHELLGHVPLLAEPSFAQFSQEIGLASLGASEEAVQKLATCYFFTVEFGLCKQDGQLRV
FGAGLLSSISELKHALSGHAKVKPFDPKITCKQECLITTFQDVYFVSESFEDAKEKMREFTKTIKRPFGVKYNPYTRSIQ
ILKDTKSITSAMNELQHDLDVVSDALAKVSRKPSI

MBP-c*h*TPH2:

MKIEEGKLVIWINGDKGYNGLAEVGKKFEKDTGIKVTVEHPDKLEEKFPQVAATGDGPDIIFWAHDRFGGYAQSGLLAEI
TPDKAFQDKLYPFTWDAVRYNGKLIAYPIAVEALSLIYNKDLLPNPPKTWEEIPALDKELKAKGKSALMFNLQEPYFTWP
LIAADGGYAFKYENGKYDIKDVGVDNAGAKAGLTFLVDLIKNKHMNADTDYSIAEAAFNKGETAMTINGPWAWSNIDTSK
VNYGVTVLPTFKGQPSKPFVGVLSAGINAASPNKELAKEFLENYLLTDEGLEAVNKDKPLGAVALKSYEEELAKDPRIAA
TMENAQKGEIMPNIPQMSAFWYAVRTAVINAASGRQTVDEALKDAQTNSSSNNNNNNNNNNLGLEVLFQ↓GPEELEDVPW
FPRKISELDKCSHRVLMYGSELDADHPGFKDNVYRQRRKYFVDVAMGYKYGQPIPRVEYTEEETKTWGVVFRELSKLYPT
HACREYLKNFPLLTKYCGYREDNVPQLEDVSMFLKERSGFTVRPVAGYLSPRDFLAGLAYRVFHCTQYIRHGSDPLYTPE
PDTCHELLGHVPLLADPKFAQFSQEIGLASLGASDEDVQKLATCYFFTIEFGLCKQEGQLRAYGAGLLSSIGELKHALSD
KACVKAFDPKTTCLQECLITTFQEAYFVSESFEEAKEKMRDFAKSITRPFSVYFNPYTQSIEILKD

MBP-Y171A-c*h*TPH2:

MKIEEGKLVIWINGDKGYNGLAEVGKKFEKDTGIKVTVEHPDKLEEKFPQVAATGDGPDIIFWAHDRFGGYAQSGLLAEI
TPDKAFQDKLYPFTWDAVRYNGKLIAYPIAVEALSLIYNKDLLPNPPKTWEEIPALDKELKAKGKSALMFNLQEPYFTWP
LIAADGGYAFKYENGKYDIKDVGVDNAGAKAGLTFLVDLIKNKHMNADTDYSIAEAAFNKGETAMTINGPWAWSNIDTSK
VNYGVTVLPTFKGQPSKPFVGVLSAGINAASPNKELAKEFLENYLLTDEGLEAVNKDKPLGAVALKSYEEELAKDPRIAA
TMENAQKGEIMPNIPQMSAFWYAVRTAVINAASGRQTVDEALKDAQTNSSSNNNNNNNNNNLGLEVLFQ↓GPEELEDVPW
FPRKISELDKCSHRVLMAGSELDADHPGFKDNVYRQRRKYFVDVAMGYKYGQPIPRVEYTEEETKTWGVVFRELSKLYPT
HACREYLKNFPLLTKYCGYREDNVPQLEDVSMFLKERSGFTVRPVAGYLSPRDFLAGLAYRVFHCTQYIRHGSDPLYTPE
PDTCHELLGHVPLLADPKFAQFSQEIGLASLGASDEDVQKLATCYFFTIEFGLCKQEGQLRAYGAGLLSSIGELKHALSD
KACVKAFDPKTTCLQECLITTFQEAYFVSESFEEAKEKMRDFAKSITRPFSVYFNPYTQSIEILKD

MBP-Y171W-c*h*TPH2:

MKIEEGKLVIWINGDKGYNGLAEVGKKFEKDTGIKVTVEHPDKLEEKFPQVAATGDGPDIIFWAHDRFGGYAQSGLLAEI
TPDKAFQDKLYPFTWDAVRYNGKLIAYPIAVEALSLIYNKDLLPNPPKTWEEIPALDKELKAKGKSALMFNLQEPYFTWP
LIAADGGYAFKYENGKYDIKDVGVDNAGAKAGLTFLVDLIKNKHMNADTDYSIAEAAFNKGETAMTINGPWAWSNIDTSK
VNYGVTVLPTFKGQPSKPFVGVLSAGINAASPNKELAKEFLENYLLTDEGLEAVNKDKPLGAVALKSYEEELAKDPRIAA
TMENAQKGEIMPNIPQMSAFWYAVRTAVINAASGRQTVDEALKDAQTNSSSNNNNNNNNNNLGLEVLFQ↓GPEELEDVPW
FPRKISELDKCSHRVLMWGSELDADHPGFKDNVYRQRRKYFVDVAMGYKYGQPIPRVEYTEEETKTWGVVFRELSKLYPT
HACREYLKNFPLLTKYCGYREDNVPQLEDVSMFLKERSGFTVRPVAGYLSPRDFLAGLAYRVFHCTQYIRHGSDPLYTPE
PDTCHELLGHVPLLADPKFAQFSQEIGLASLGASDEDVQKLATCYFFTIEFGLCKQEGQLRAYGAGLLSSIGELKHALSD
KACVKAFDPKTTCLQECLITTFQEAYFVSESFEEAKEKMRDFAKSITRPFSVYFNPYTQSIEILKD

MBP-loop-swap-c*h*TPH2:

MKIEEGKLVIWINGDKGYNGLAEVGKKFEKDTGIKVTVEHPDKLEEKFPQVAATGDGPDIIFWAHDRFGGYAQSGLLAEI
TPDKAFQDKLYPFTWDAVRYNGKLIAYPIAVEALSLIYNKDLLPNPPKTWEEIPALDKELKAKGKSALMFNLQEPYFTWP
LIAADGGYAFKYENGKYDIKDVGVDNAGAKAGLTFLVDLIKNKHMNADTDYSIAEAAFNKGETAMTINGPWAWSNIDTSK
VNYGVTVLPTFKGQPSKPFVGVLSAGINAASPNKELAKEFLENYLLTDEGLEAVNKDKPLGAVALKSYEEELAKDPRIAA
TMENAQKGEIMPNIPQMSAFWYAVRTAVINAASGRQTVDEALKDAQTNSSSNNNNNNNNNNLGLEVLFQ↓GPEELEDVPW
FPRKISELDHCANRVLMYGSELDADHPGFKDNVYRQRRKYFVDVAMGYKYGQPIPRVEYTEEETKTWGVVFRELSKLYPT
HACREYLKNFPLLTKYCGYREDNVPQLEDVSMFLKERSGFTVRPVAGYLSPRDFLAGLAYRVFHCTQYIRHGSDPLYTPE
PDTCHELLGHVPLLADPKFAQFSQEIGLASLGASDEDVQKLATCYFFTIEFGLCKQEGQLRAYGAGLLSSIGELKHALSD
KACVKAFDPKTTCLQECLITTFQEAYFVSESFEEAKEKMRDFAKSITRPFSVYFNPYTQSIEILKD

MBP-NΔ47-rc*h*TPH2:

MKIEEGKLVIWINGDKGYNGLAEVGKKFEKDTGIKVTVEHPDKLEEKFPQVAATGDGPDIIFWAHDRFGGYAQSGLLAEI
TPDKAFQDKLYPFTWDAVRYNGKLIAYPIAVEALSLIYNKDLLPNPPKTWEEIPALDKELKAKGKSALMFNLQEPYFTWP
LIAADGGYAFKYENGKYDIKDVGVDNAGAKAGLTFLVDLIKNKHMNADTDYSIAEAAFNKGETAMTINGPWAWSNIDTSK
VNYGVTVLPTFKGQPSKPFVGVLSAGINAASPNKELAKEFLENYLLTDEGLEAVNKDKPLGAVALKSYEEELAKDPRIAA
TMENAQKGEIMPNIPQMSAFWYAVRTAVINAASGRQTVDEALKDAQTNSSSNNNNNNNNNNLGLEVLFQ↓GPGNKGSSKR
EAATESGKTAVVFSLKNEVGGLVKALRLFQEKRVNMVHIESRKSRRRSSEVEIFVDCECGKTEFNELIQLLKFQTTIVTL
NPPENIWTEEEELEDVPWFPRKISELDKCSHRVLMYGSELDADHPGFKDNVYRQRRKYFVDVAMGYKYGQPIPRVEYTEE
ETKTWGVVFRELSKLYPTHACREYLKNFPLLTKYCGYREDNVPQLEDVSMFLKERSGFTVRPVAGYLSPRDFLAGLAYRV
FHCTQYIRHGSDPLYTPEPDTCHELLGHVPLLADPKFAQFSQEIGLASLGASDEDVQKLATCYFFTIEFGLCKQEGQLRA
YGAGLLSSIGELKHALSDKACVKAFDPKTTCLQECLITTFQEAYFVSESFEEAKEKMRDFAKSITRPFSVYFNPYTQSIE
ILKD

MBP-rc*h*TPH2:

MKIEEGKLVIWINGDKGYNGLAEVGKKFEKDTGIKVTVEHPDKLEEKFPQVAATGDGPDIIFWAHDRFGGYAQSGLLAEI
TPDKAFQDKLYPFTWDAVRYNGKLIAYPIAVEALSLIYNKDLLPNPPKTWEEIPALDKELKAKGKSALMFNLQEPYFTWP
LIAADGGYAFKYENGKYDIKDVGVDNAGAKAGLTFLVDLIKNKHMNADTDYSIAEAAFNKGETAMTINGPWAWSNIDTSK
VNYGVTVLPTFKGQPSKPFVGVLSAGINAASPNKELAKEFLENYLLTDEGLEAVNKDKPLGAVALKSYEEELAKDPRIAA
TMENAQKGEIMPNIPQMSAFWYAVRTAVINAASGRQTVDEALKDAQTNSSSNNNNNNNNNNLGLEVLFQ↓GPQPAMMMFS
SKYWARRGFSLDSAVPEEHQLLGSSTLNKPNSGKNDDKGNKGSSKREAATESGKTAVVFSLKNEVGGLVKALRLFQEKRV
NMVHIESRKSRRRSSEVEIFVDCECGKTEFNELIQLLKFQTTIVTLNPPENIWTEEEELEDVPWFPRKISELDKCSHRVL
MYGSELDADHPGFKDNVYRQRRKYFVDVAMGYKYGQPIPRVEYTEEETKTWGVVFRELSKLYPTHACREYLKNFPLLTKY
CGYREDNVPQLEDVSMFLKERSGFTVRPVAGYLSPRDFLAGLAYRVFHCTQYIRHGSDPLYTPEPDTCHELLGHVPLLAD
PKFAQFSQEIGLASLGASDEDVQKLATCYFFTIEFGLCKQEGQLRAYGAGLLSSIGELKHALSDKACVKAFDPKTTCLQE
CLITTFQEAYFVSESFEEAKEKMRDFAKSITRPFSVYFNPYTQSIEILKD

MBP-*h*TPH2

MKIEEGKLVIWINGDKGYNGLAEVGKKFEKDTGIKVTVEHPDKLEEKFPQVAATGDGPDIIFWAHDRFGGYAQSGLLAEI
TPDKAFQDKLYPFTWDAVRYNGKLIAYPIAVEALSLIYNKDLLPNPPKTWEEIPALDKELKAKGKSALMFNLQEPYFTWP
LIAADGGYAFKYENGKYDIKDVGVDNAGAKAGLTFLVDLIKNKHMNADTDYSIAEAAFNKGETAMTINGPWAWSNIDTSK
VNYGVTVLPTFKGQPSKPFVGVLSAGINAASPNKELAKEFLENYLLTDEGLEAVNKDKPLGAVALKSYEEELAKDPRIAA
TMENAQKGEIMPNIPQMSAFWYAVRTAVINAASGRQTVDEALKDAQTNSSSNNNNNNNNNNLGLEVLFQ↓GPQPAMMMFS
SKYWARRGFSLDSAVPEEHQLLGSSTLNKPNSGKNDDKGNKGSSKREAATESGKTAVVFSLKNEVGGLVKALRLFQEKRV
NMVHIESRKSRRRSSEVEIFVDCECGKTEFNELIQLLKFQTTIVTLNPPENIWTEEEELEDVPWFPRKISELDKCSHRVL
MYGSELDADHPGFKDNVYRQRRKYFVDVAMGYKYGQPIPRVEYTEEETKTWGVVFRELSKLYPTHACREYLKNFPLLTKY
CGYREDNVPQLEDVSMFLKERSGFTVRPVAGYLSPRDFLAGLAYRVFHCTQYIRHGSDPLYTPEPDTCHELLGHVPLLAD
PKFAQFSQEIGLASLGASDEDVQKLATCYFFTIEFGLCKQEGQLRAYGAGLLSSIGELKHALSDKACVKAFDPKTTCLQE
CLITTFQEAYFVSESFEEAKEKMRDFAKSITRPFSVYFNPYTQSIEILKDTRSIENVVQDLRSDLNTVCDALNKMNQYLG
I

MBP-3CP:

MKIEEGKLVIWINGDKGYNGLAEVGKKFEKDTGIKVTVEHPDKLEEKFPQVAATGDGPDIIFWAHDRFGGYAQSGLLAEI
TPDKAFQDKLYPFTWDAVRYNGKLIAYPIAVEALSLIYNKDLLPNPPKTWEEIPALDKELKAKGKSALMFNLQEPYFTWP
LIAADGGYAFKYENGKYDIKDVGVDNAGAKAGLTFLVDLIKNKHMNADTDYSIAEAAFNKGETAMTINGPWAWSNIDTSK
VNYGVTVLPTFKGQPSKPFVGVLSAGINAASPNKELAKEFLENYLLTDEGLEAVNKDKPLGAVALKSYEEELAKDPRIAA
TMENAQKGEIMPNIPQMSAFWYAVRTAVINAASGRQTVDEALKDAQTNSSSNNNNNNNNNNLGGIPGPEHEFLNALIRRN
CHIITTDKGEFNLLGIYSNCAVVPTHAEPGDVVDIDGRLVRVLKQQVLTDMNDVDTEVTVLWLDQNEKFRDIRRFIPEHQ
QDWHNIHLATNVTKFPMLNVEVGHTVPYGEINLSGNATCRLYKYDYPTQPGQCGAVLANTGNIIGIHVGGNGRVGYAAAL
LRKYFAEEQ

Appendix C

Purification chromatograms of c*h*TPH variants

In this appendix, the chromatograms are presented for purifications of *h*TPH2, c*h*TPH1, loop-swap-c*h*TPH1, Y125A-c*h*TPH1, Y125L-c*h*TPH1, Y125W-c*h*TPH1, c*h*TPH2, loop-swap-c*h*TPH2, Y171A-c*h*TPH2, and Y171W-c*h*TPH2.

C. 1 Purification of *h*TPH2

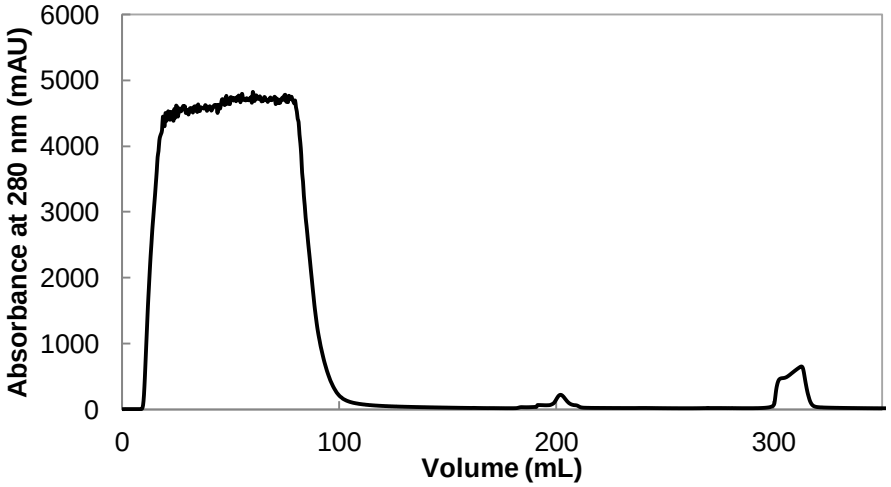

Figure C. 1. Chromatogram from affinity chromatography of c*h*TPH2 using 20 mM HEPES/NH_4OH, 300 mM $(NH_4)_2SO_4$, pH 7.0 as mobile phase on a Dextrin Sepharose 16/12 column.

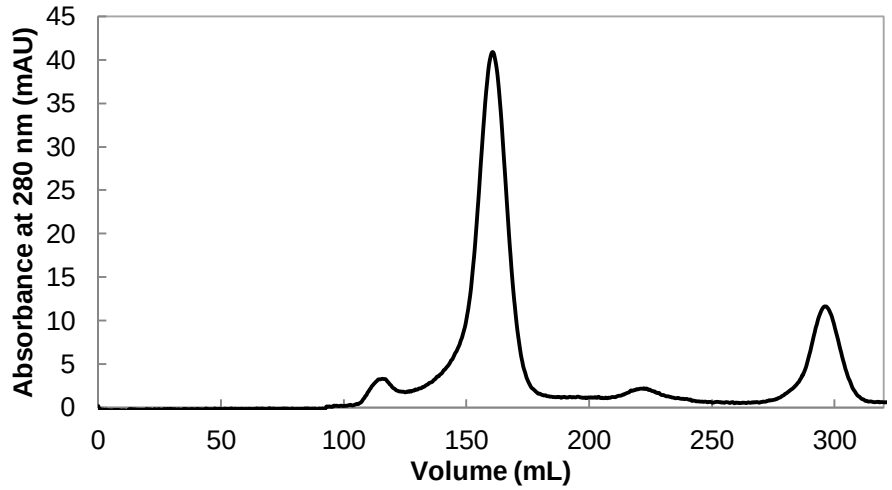

Figure C. 2. Chromatogram from gel filtration on a Hiload 26/600 Superdex 200 column of the collected protein from affinity chromatography in the purification of *h*TPH2 using 20 mM HEPES/NH_4OH, 300 mM $(NH_4)_2SO_4$, pH 7.0.

C. 2 Purification of c*h*TPH1

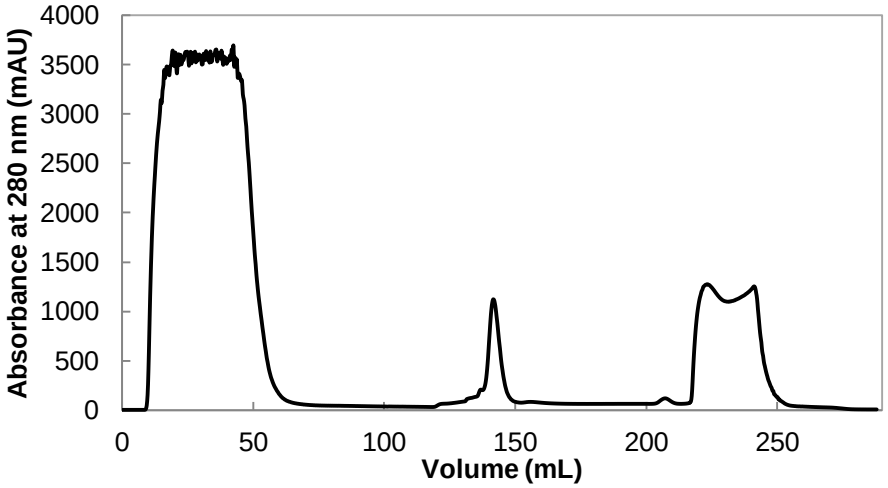

Figure C. 3. Chromatogram from affinity chromatography of c*h*TPH1 using 20 mM TRIS/H_2SO_4, 100 mM $(NH_4)_2SO_4$, pH 8.0 as mobile phase on a Dextrin Sepharose 16/12 column.

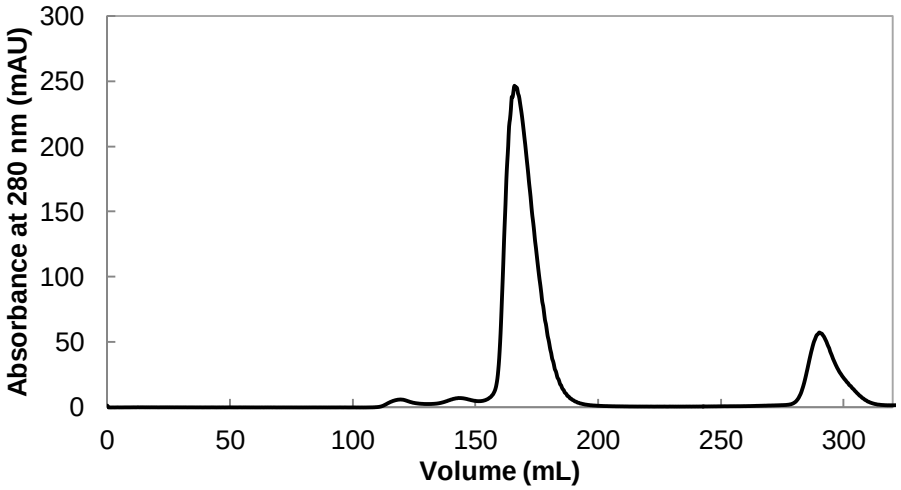

Figure C. 4. Chromatogram from gel filtration on a Hiload 26/600 Superdex 75 column of the collected protein from affinity chromatography in the purification of c*h*TPH1 using 20 mM TRIS/H_2SO_4, 100 mM $(NH_4)_2SO_4$, pH 8.0.

C. 3 Purification of Loop-swap-c*h*TPH1

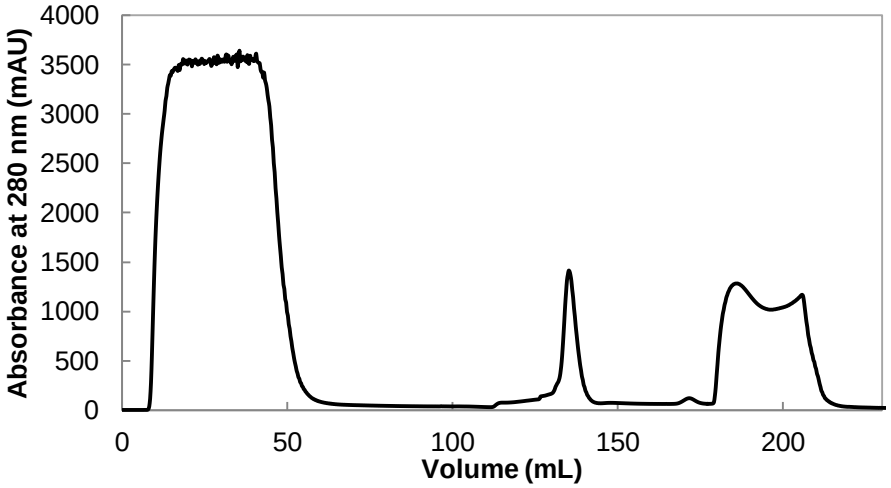

Figure C. 5. Chromatogram from affinity chromatography of loop-swap-c*h*TPH1 using 20 mM TRIS/H_2SO_4, 100 mM $(NH_4)_2SO_4$, pH 8.0 as mobile phase on a Dextrin Sepharose 16/12 column.

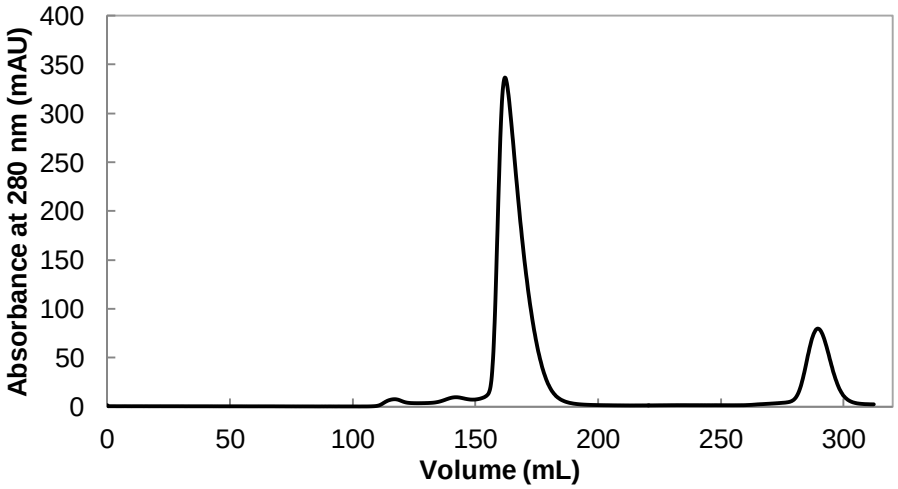

Figure C. 6. Chromatogram from gel filtration on a Hiload 26/600 Superdex 75 column of the collected protein from affinity chromatography in the purification of loop-swap-c*h*TPH1 using 20 mM TRIS/H_2SO_4, 100 mM $(NH_4)_2SO_4$, pH 8.0.

C. 4 Purification of Y125A-c*h*TPH1

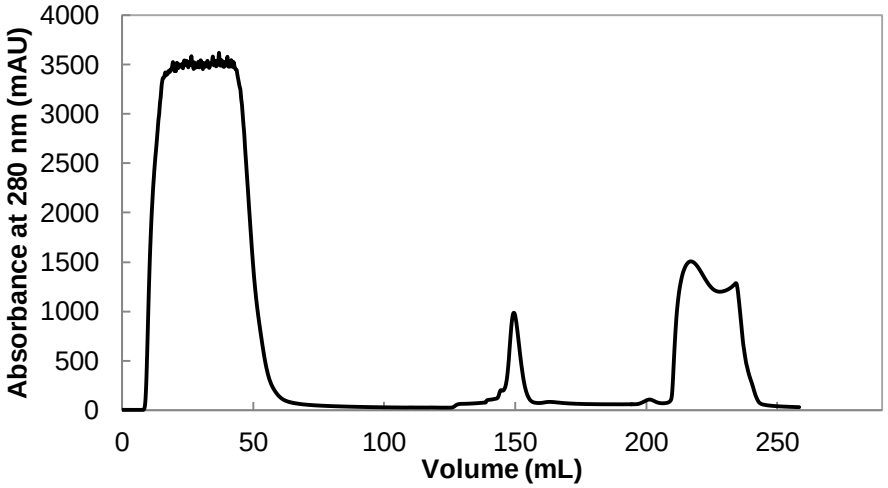

Figure C. 7. Chromatogram from affinity chromatography of Y125A-c*h*TPH1 using 20 mM TRIS/H_2SO_4, 100 mM $(NH_4)_2SO_4$, pH 8.0 as mobile phase on a Dextrin Sepharose 16/12 column.

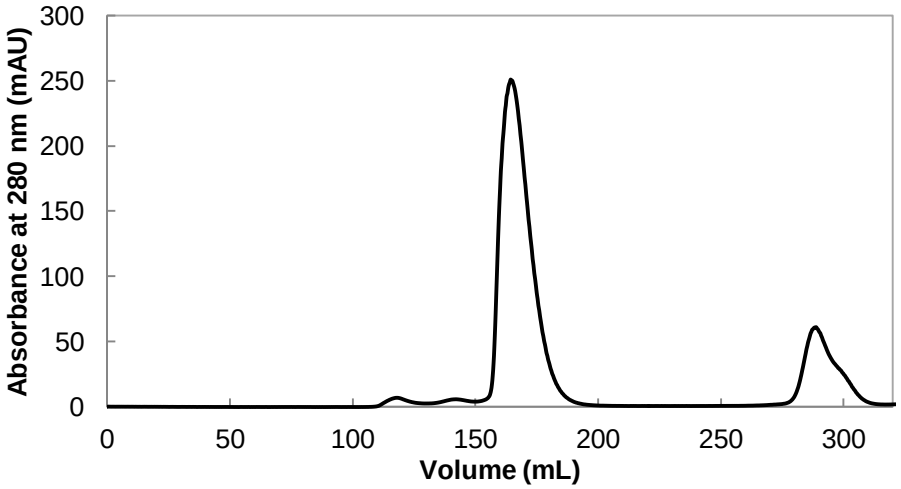

Figure C. 8. Chromatogram from gel filtration on a Hiload 26/600 Superdex 75 column of the collected protein from affinity chromatography in the purification of Y125A-c*h*TPH1 using 20 mM TRIS/H_2SO_4, 100 mM $(NH_4)_2SO_4$, pH 8.0.

C. 5 Purification of Y125L-c*h*TPH1

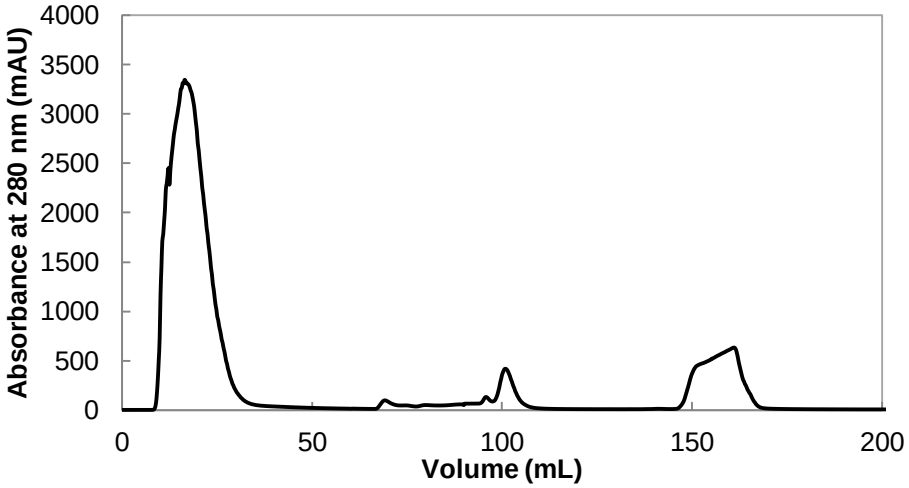

Figure C. 9. Chromatogram from affinity chromatography of Y125L-c*h*TPH1 using 20 mM TRIS/H_2SO_4, 100 mM $(NH_4)_2SO_4$, pH 8.0 as mobile phase on a Dextrin Sepharose 16/12 column.

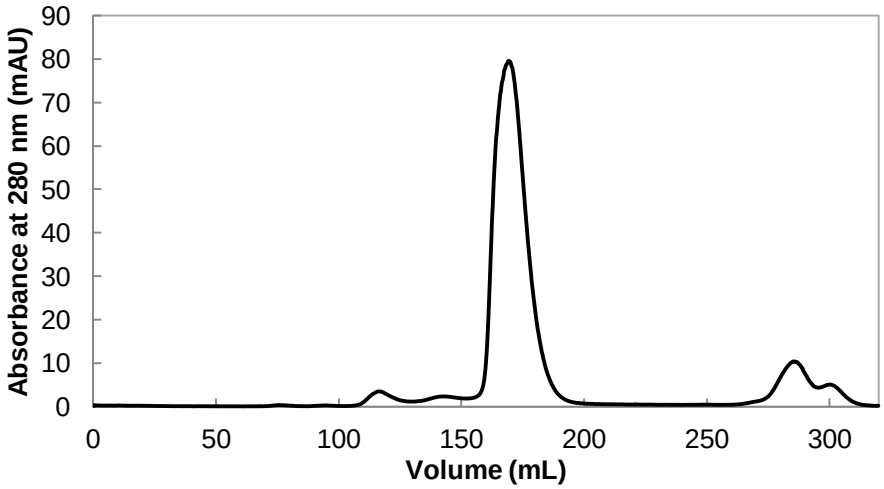

Figure C. 10. Chromatogram from gel filtration on a Hiload 26/600 Superdex 75 column of the collected protein from affinity chromatography in the purification of Y125L-c*h*TPH1 using 20 mM TRIS/H_2SO_4, 100 mM $(NH_4)_2SO_4$, pH 8.0.

C. 6 Purification of Y125W-c*h*TPH

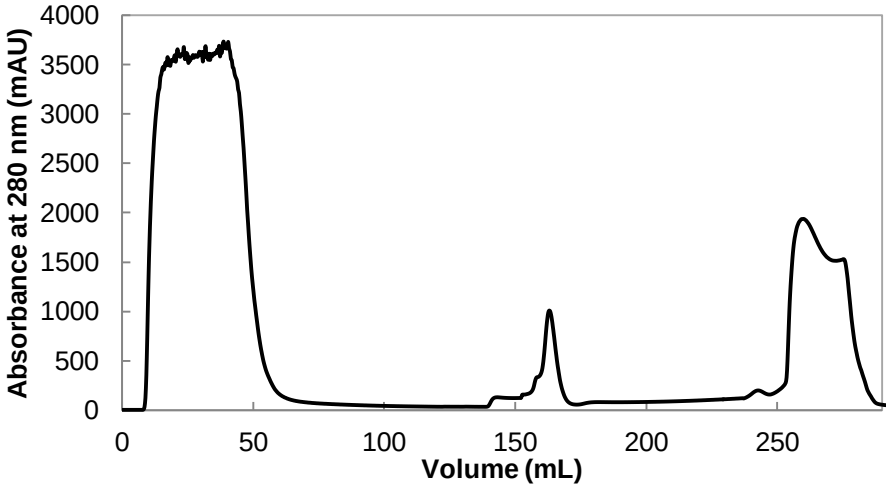

Figure C. 11. Chromatogram from affinity chromatography of Y125W-c*h*TPH1 using 20 mM TRIS/H_2SO_4, 100 mM $(NH_4)_2SO_4$, pH 8.0 as mobile phase on a Dextrin Sepharose 16/12 column.

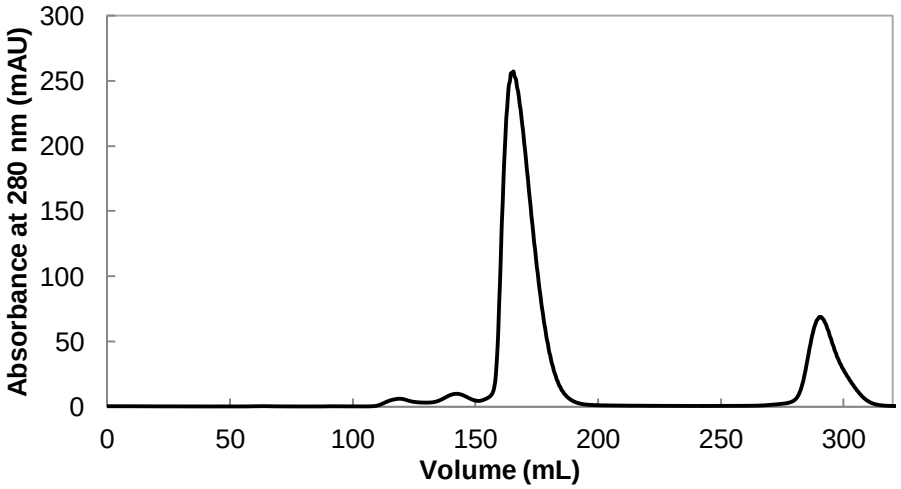

Figure C. 12. Chromatogram from gel filtration on a Hiload 26/600 Superdex 75 column of the collected protein from affinity chromatography in the purification of Y125W-c*h*TPH1 using 20 mM TRIS/H_2SO_4, 100 mM $(NH_4)_2SO_4$, pH 8.0.

C. 7 Purification of c*h*TPH2

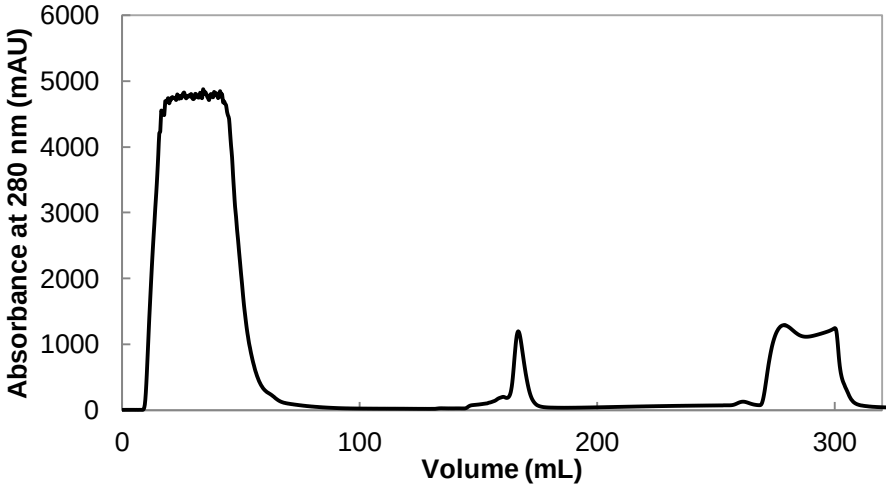

Figure C. 13. Chromatogram from affinity chromatography of c*h*TPH2 using 20 mM HEPES/NH_4OH, 100 mM $(NH_4)_2SO_4$, pH 7.0 as mobile phase on a Dextrin Sepharose 16/12 column.

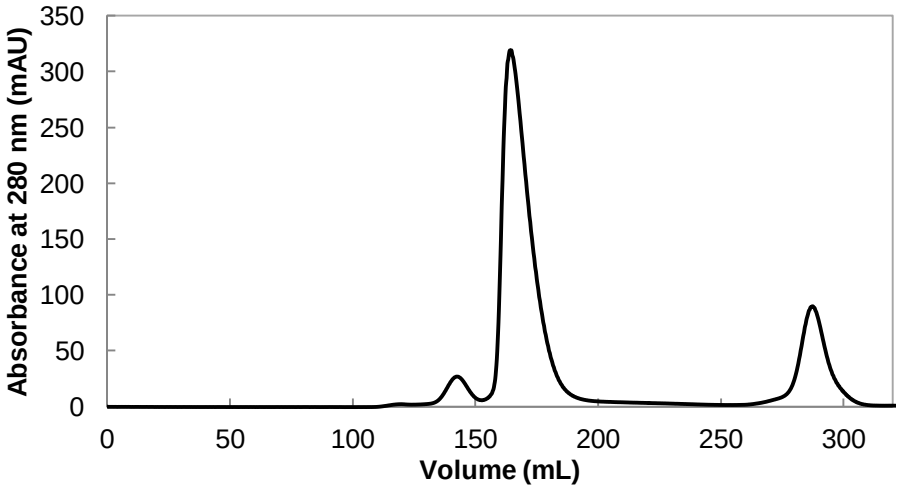

Figure C. 14. Chromatogram from gel filtration on a Hiload 26/600 Superdex 75 column of the collected protein from affinity chromatography in the purification of c*h*TPH2 using 20 mM HEPES/NH_4OH, 100 mM $(NH_4)_2SO_4$, pH 7.0.

C. 8 Purification of Loop-swap-c*h*TPH2

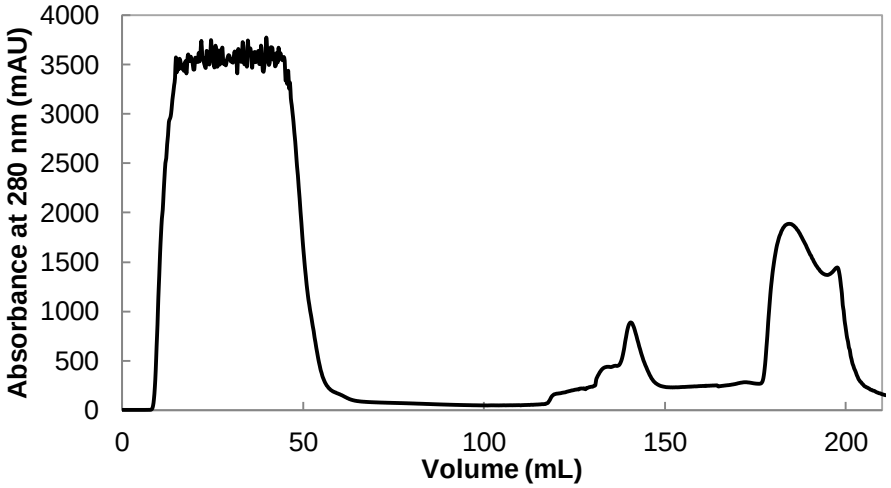

Figure C. 15. Chromatogram from affinity chromatography of loop-swap-c*h*TPH2 using 20 mM HEPES/NH_4OH, 100 mM $(NH_4)_2SO_4$, pH 7.0 as mobile phase on a Dextrin Sepharose 16/12 column.

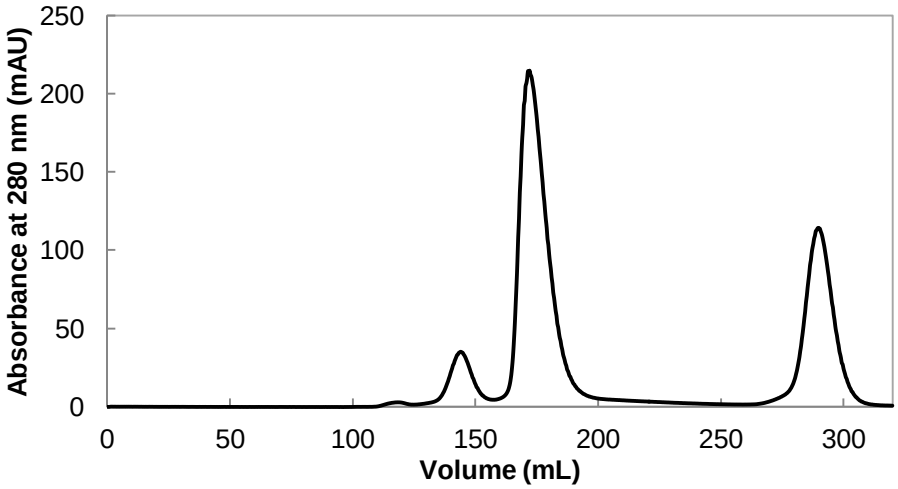

Figure C. 16. Chromatogram from gel filtration on a Hiload 26/600 Superdex 75 column of the collected protein from affinity chromatography in the purification of loop-swap-c*h*TPH2 using 20 mM HEPES/NH_4OH, 100 mM $(NH_4)_2SO_4$, pH 7.0.

C. 9 Purification of Y171A-c*h*TPH2

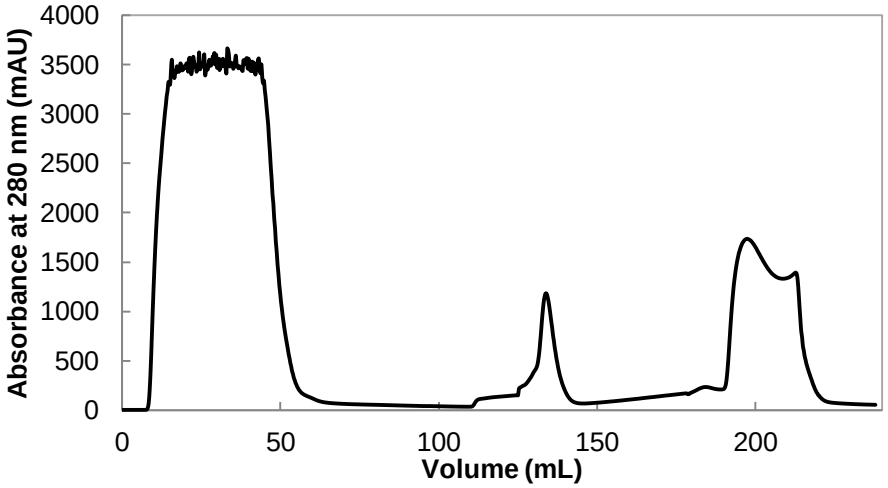

Figure C. 17. Chromatogram from affinity chromatography of Y171A-c*h*TPH2 using 20 mM HEPES/NH_4OH, 100 mM $(NH_4)_2SO_4$, pH 7.0 as mobile phase on a Dextrin Sepharose 16/12 column.

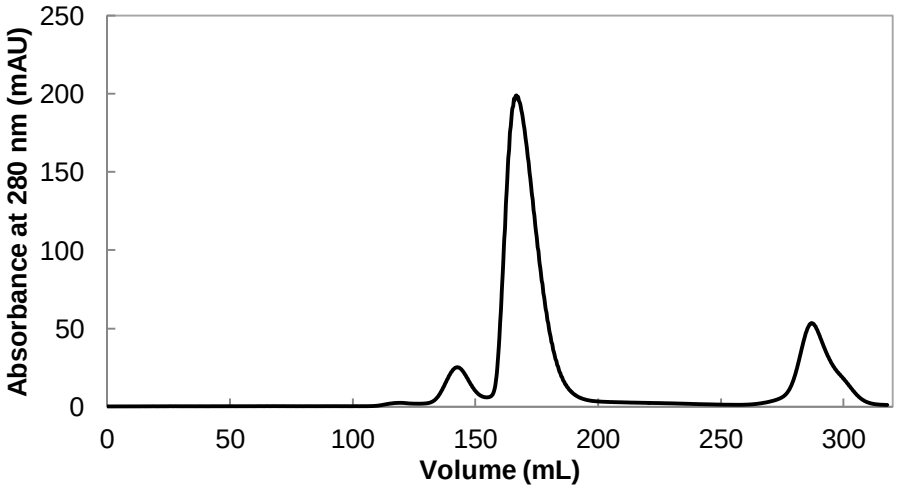

Figure C. 18. Chromatogram from gel filtration on a Hiload 26/600 Superdex 75 column of the collected protein from affinity chromatography in the purification of Y171A-c*h*TPH2 using 20 mM HEPES/NH_4OH, 100 mM $(NH_4)_2SO_4$, pH 7.0.

C. 10 Purification of Y171W-c*h*TPH2

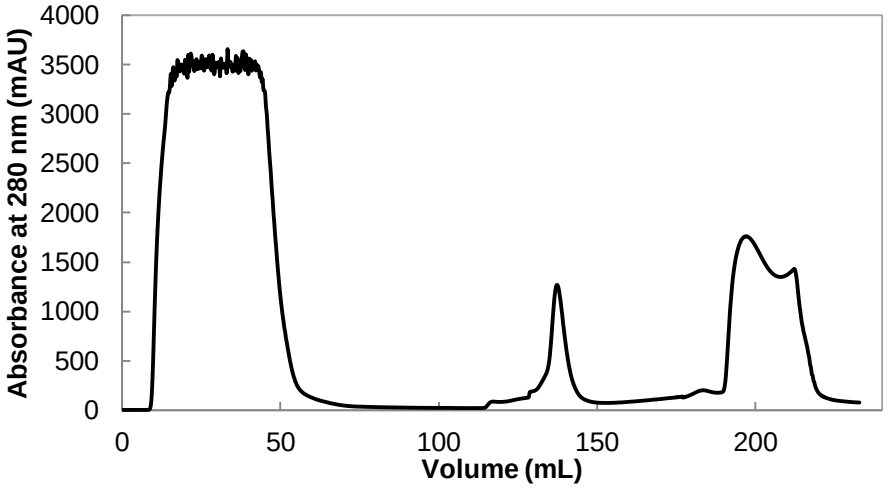

Figure C. 19. Chromatogram from affinity chromatography of Y171W-c*h*TPH2 using 20 mM HEPES/NH_4OH, 100 mM $(NH_4)_2SO_4$, pH 7.0 as mobile phase on a Dextrin Sepharose 16/12 column.

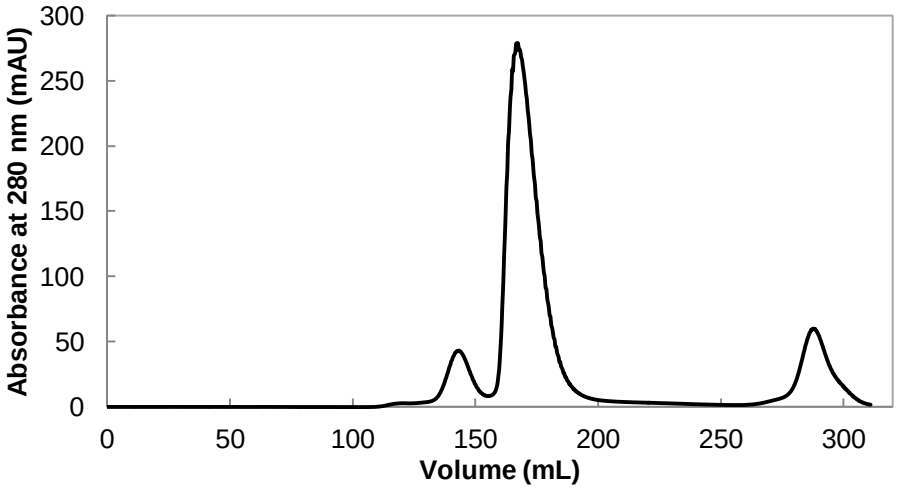

Figure C. 20. Chromatogram from gel filtration on a Hiload 26/600 Superdex 75 column of the collected protein from affinity chromatography in the purification of Y171W-c*h*TPH2 using 20 mM HEPES/NH_4OH, 100 mM $(NH_4)_2SO_4$, pH 7.0.

Appendix D

Purification yields of TPH variants

This appendix presents purification yields obtained for purifications of different TPH variants. All purifications are conducted with the two-step purification procedure presented in chapter 2. In chapter 2, the purification buffer solutions for the individual TPH variants are specified.

Table D. 1. Purification yields (average ± standard deviation of n purifications) obtained for the TPH variants. In the table header, Std and Phe refer to purification in the absence of phenylalanine or presence of 3 mM phenylalanine, respectively.

	Std		Phe	
	Average	**n**	**Average**	**n**
***h*TPH2**	0.4	1	1.9	1
rc*h*TPH2	0.8 ± 0.2	6	4.8 ± 2.2	5
NΔ47-rc*h*TPH2	8.7 ± 4.2	10	32.5 ± 5.5	3
c*h*TPH2	15.8 ± 3.2	7	10.8 ± 3.8	3
Y171A-c*h*TPH2	15.1 ± 1.8	2		
Y171W-c*h*TPH2	12.5 ± 2.3	3		
Loop-swap-c*h*TPH2	9.8 ± 2.3	2		
***h*TPH1**	20.4 ± 3.3	2	16.0	1
rc*h*TPH1	25.5	1	26.4	1
c*h*TPH1	21.8 ± 4.3	4		
Y125A-c*h*TPH1	19.3 ± 4.3	2		
Y125L-c*h*TPH1	5.9	1		
Y125W-c*h*TPH1	21.8 ± 9.0	4		
Loop-swap-c*h*TPH1	22.7 ± 3.1	2		

Appendix E

Differential scanning fluorimetry

E. 1 DSF results obtained for NΔ47-rc*h*TPH2.

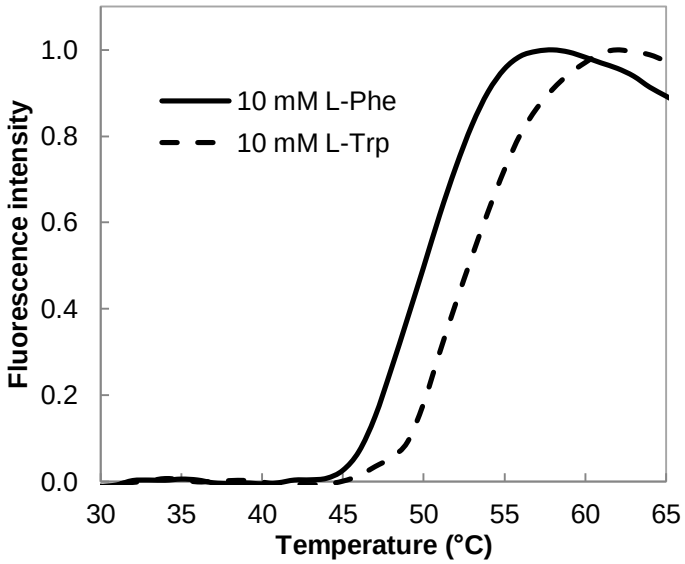

Figure E. 1. Baseline corrected differential scanning fluorimetry of NΔ47-rc*h*TPH2 (enzyme concentration of 1 μM) in absence of ligand, presence of 10 mM L-Phe, or presence of 10 mM L-Trp.

E. 2 DSF results obtained for rc*h*TPH2 illustrated the day-to-day variation.

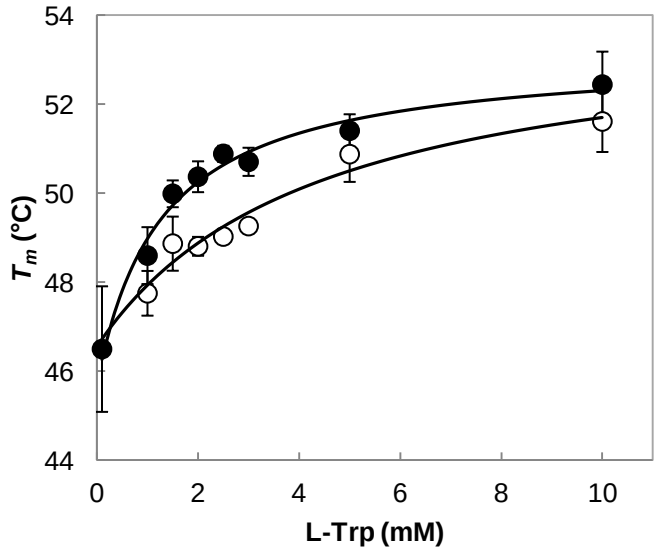

Figure E. 2. DSF results of rc*h*TPH2. Transition temperature as a function of L-Trp concentration obtained from two different days.

Appendix F

Analytical gel filtration

In this appendix, the correlation between maximum UV-absorbance (A_{max}) and protein loading concentration from analytical gel filtrations are presented for c*h*TPH2 and NΔ47-rc*h*TPH2. The exact elution volumes observed for c*h*TPH1, c*h*TPH2, and their mutant variants are also presented.

F. 1 A_{max} versus loading concentration - c*h*TPH2

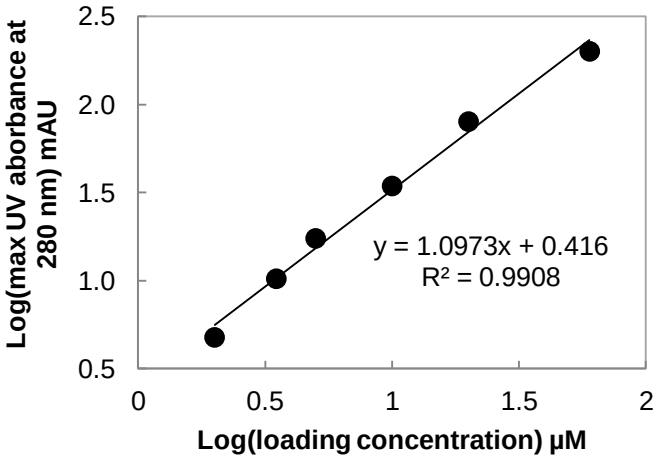

Figure F. 1. Maximum absorbance obtained for c*h*TPH2 at different loading concentrations. The correlation is obtained using a buffer solution containing 20 mM HEPES/NH4OH, 300 mM $(NH_4)_2SO_4$, pH 7.0.

F. 2 A_{max} versus loading concentration - NΔ47-rc*h*TPH2

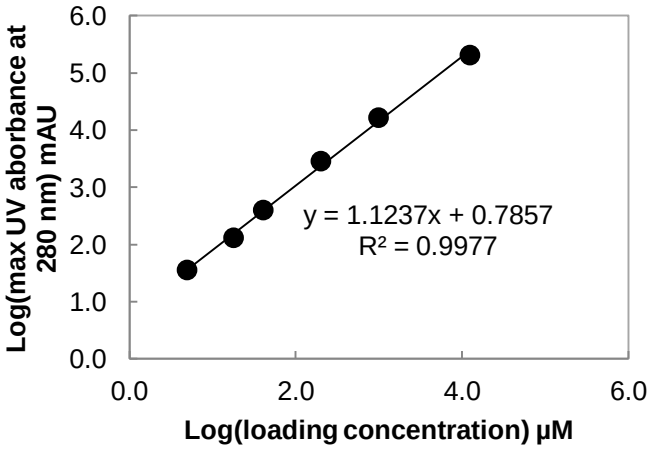

Figure F. 2. Maximum absorbance obtained for NΔ47-rc*h*TPH2 at different loading concentrations. The correlation is obtained using a buffer solution containing 20 mM HEPES/NH4OH, 300 mM $(NH_4)_2SO_4$, 3 mM phenylalanine, pH 7.0.

F. 3 Elution volumes of c*h*TPH variants

Table F. 1. Elution volumes (mL) at maximum intensity with standard deviations (n=3). The elution volumes are obtained from analytical gel filtration on a superdex 200 10/300 GL column.

Variant	Volume ± SD (mL)
c*h*TPH1	15.64 ± 0.05
Y125A-c*h*TPH1	15.505 ± 0.004
Y125W-c*h*TPH1	15.60 ± 0.04
Loop-swap-c*h*TPH1	15.53 ± 0.03
c*h*TPH2	15.72 ± 0.06
Y171A-c*h*TPH2	15.70 ± 0.05
Y171W-c*h*TPH2	15.74 ± 0.05
Loop-swap-c*h*TPH2	15.78 ± 0.03

Appendix G

Steady-state kinetics

In this appendix, standard curves produced for 5-hydroxytryptophan (5-HTP) at different concentrations of BH_4 are presented. The standard curves are produced to convert intensity/min to µM 5-HTP/min. Additional steady-state kinetic results obtained for c*h*TPH1 are also presented.

G. 1 5-HTP standard curve for Varian Cary Eclipse fluorescence spectrophotometer

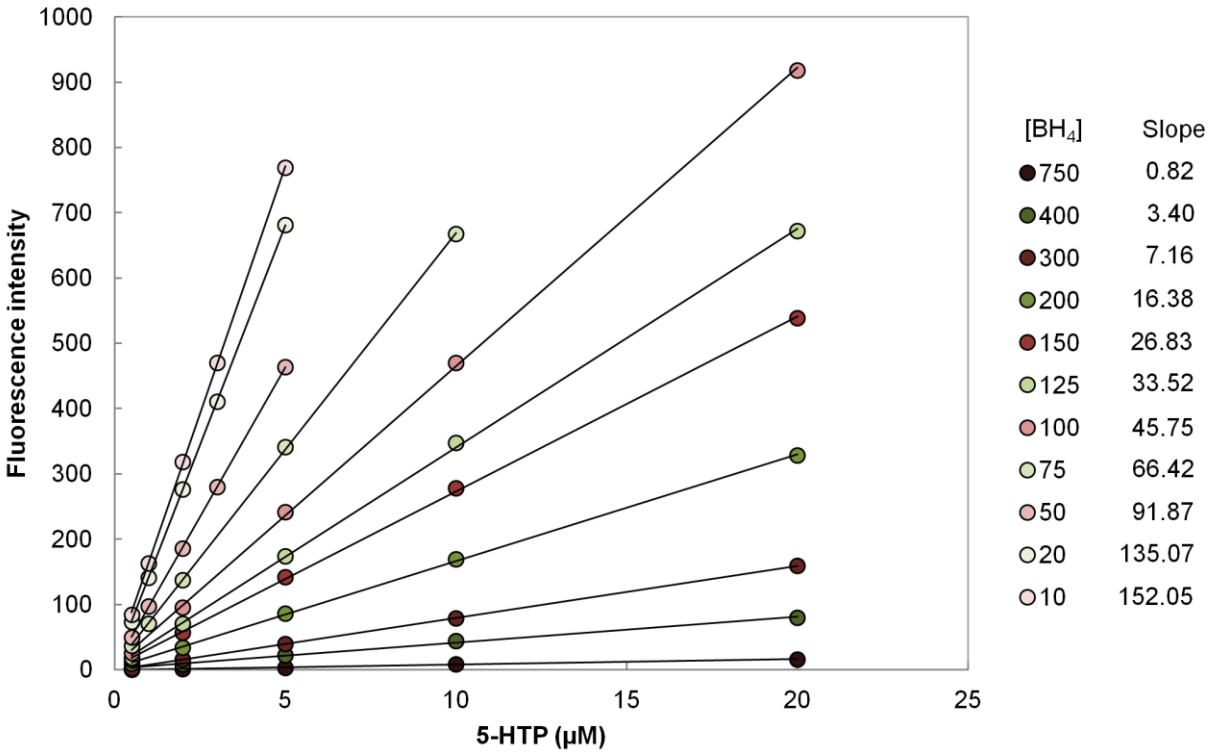

Figure G. 1. Standard curves of 5-HTP at different concentrations of BH_4 (µM). The measurements are conducted with a PMT of 650 V. The insert presents the slopes (intensity/µM 5-HTP) at the different concentrations of BH_4.

G. 2 Initial velocities measured for c*h*TPH1

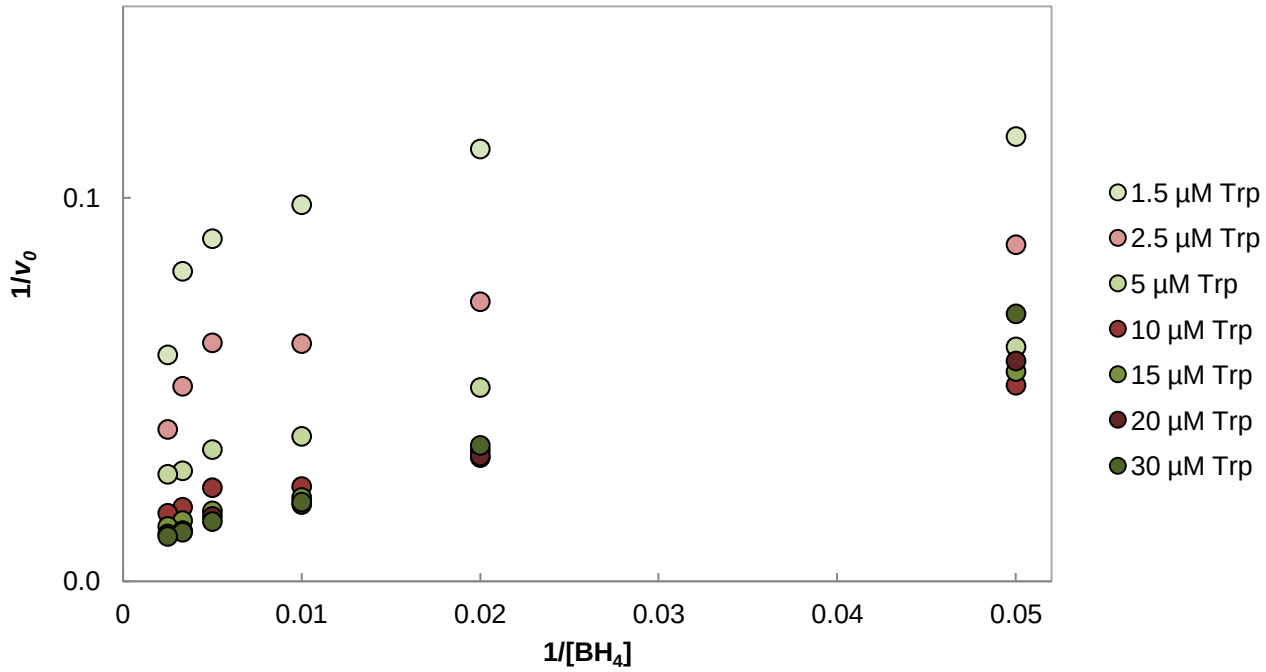

Figure G. 2. Double reciprocal v_0 versus [BH_4] plots of the seven lowest concentrations of tryptophan.

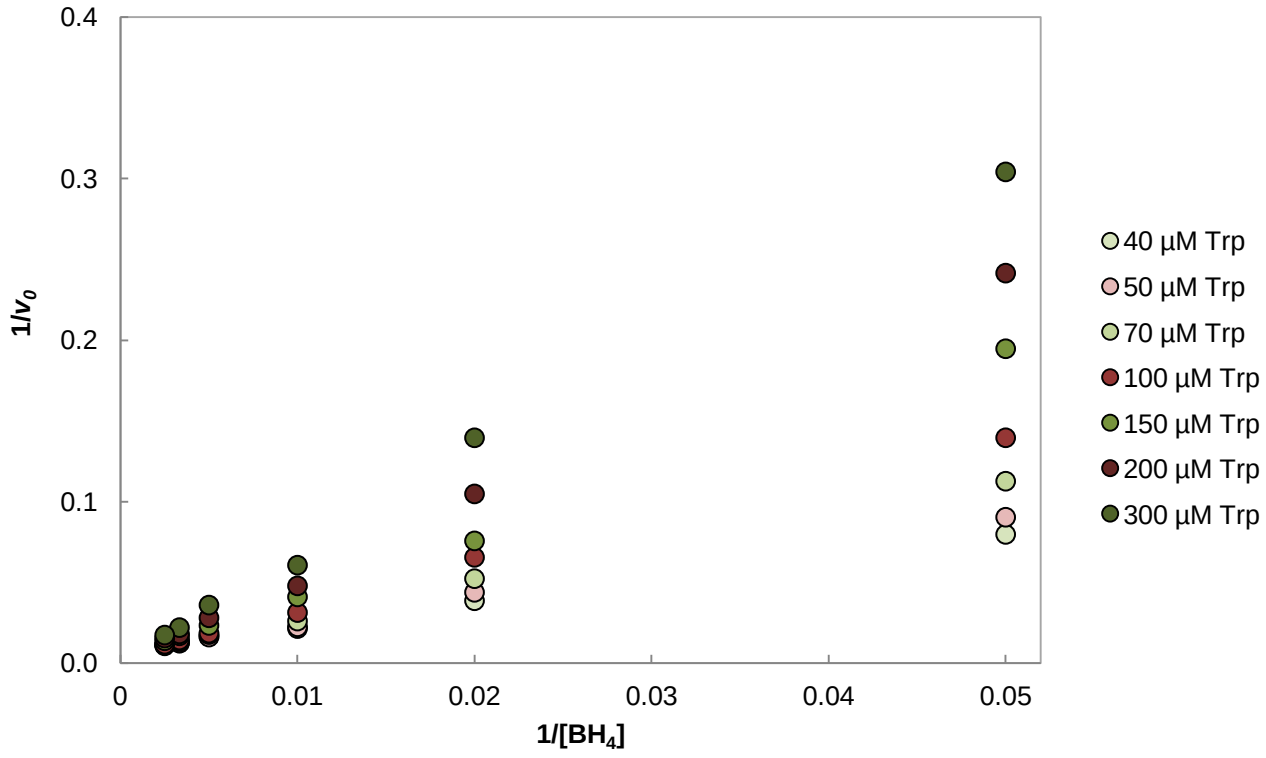

Figure G. 3. Double reciprocal v_0 versus [BH_4] plots of the seven highest concentrations of tryptophan.

G. 3 Apparent kinetic parameters of c*h*TPH1 determined at high and low concentrations of BH_4 – dataset split

Table G. 1. Apparent kinetic parameters for c*h*TPH1 determined from fitting the kinetic data obtained at low BH_4 concentrations (20, 50, and 100 µM) with eq. 1 (chapter 6).

	Trp (uM)													
	1.5	**2.5**	**5**	**10**	**15**	**20**	**30**	**40**	**50**	**70**	**100**	**150**	**200**	**300**
V_{max}	10.2	17.6	30.3	55.9	76.5	106.9	140.6	186.6	349.6	675.4	17650	14066.4	11757.8	9278.6
$K_{m,BH4}$	4.2	11.6	19.5	40.6	68.7	116	191.7	300.9	689	1664.6	55439	56577.9	57151	57660.3
$1/V_{max}$	0.0980	0.0568	0.0330	0.0179	0.0131	0.0094	0.0071	0.0054	0.0029	0.0015	0.0001	0.0001	0.0001	0.0001
1/Trp	0.66667	0.4	0.2	0.1	0.06667	0.05	0.03333	0.025	0.02	0.01429	0.01	0.00667	0.005	0.00333
K_m/V_{max}	0.41176	0.65909	0.64356	0.7263	0.89804	1.08513	1.36344	1.61254	1.97082	2.46461	3.14102	4.0222	4.86069	6.21433

Table G. 2. Apparent kinetic parameters for c*h*TPH1 determined from fitting the kinetic data obtained at low BH_4 concentrations (200, 300, and 400 µM) with eq. 1 (chapter 6).

	Trp (uM)													
	1.5	**2.5**	**5**	**10**	**15**	**20**	**30**	**40**	**50**	**70**	**100**	**150**	**200**	**300**
V_{max}	37.5	62.1	47.4	90.8	97.4	130.1	128.4	203.2	166	180.7	211.1	229.3	270.3	12513.2
$K_{m,BH4}$	520.9	601.9	121.1	237.1	158.9	231.3	197.1	464.2	332.2	437.6	591.9	868.1	1242.9	85583.1
$1/V_{max}$	0.0267	0.0161	0.0211	0.0110	0.0103	0.0077	0.0078	0.0049	0.0060	0.0055	0.0047	0.0044	0.0037	0.0001
1/Trp	0.66667	0.4	0.2	0.1	0.06667	0.05	0.03333	0.025	0.02	0.01429	0.01	0.00667	0.005	0.00333
K_m/V_{max}	13.8907	9.69243	2.55485	2.61123	1.63142	1.77786	1.53505	2.28445	2.0012	2.42169	2.80388	3.78587	4.59822	6.83943

Appendix H

Available crystal structures of phenylalanine hydroxylase

Table H. 1. Crystal structures of phenylalanine hydroxylase from all available species. In the header, substrate and co-substrate refers to presence of a (co-)substrate/(co-)substrate analogue in their respective binding sites. Open/closed refers to an open or closed conformation of the active site loops. AA in/out refers to Phe138 pointing towards active site or away from active site. *: different orientation compared to mammalian variants, **: lack residues 137-139.

PDB entry	Domain(s)	species	Metal	Substrate	Co-substrate	Open/closed	AA in/out
1PAH	c	*Human*	Fe^{3+}	-	-	Open	Out
3PAH	c	*Human*	Fe^{3+}	-	D-adrenaline	Open	Out
4PAH	c	*Human*	Fe^{3+}	-	L-norepinephrine	Open	Out
5PAH	c	*Human*	Fe^{3+}	-	L-dopamine	Open	Out
6PAH	c	*Human*	Fe^{3+}	-	L-DOPA	Open	Out
1PHZ	r/c	*Rat*	Fe^{3+}	-	-	No density	-
2PHM	r/c	*Rat*	Fe^{3+}	-	-	No density	-
2PAH	c/t	*Human*	Fe^{3+}	-	-	No density	-
1DMW	c	*Human*	Fe^{3+}	-	BH_2	Open	Out
1J8T	c	*Human*	Fe^{2+}	-	-	Open	Out
1J8U	c	*Human*	Fe^{2+}	-	BH_4	Open	Out
1LRM	c	*Human*	Fe^{3+}	-	BH_2	Open	Out
1LTU	c	*Cv*	-	-	-	Open*	Out
1LTV	c	*Cv*	Fe^{3+}	-	-	Open*	Out
1LTZ	c	*Cv*	Fe^{3+}	-	BH_2	Open*	Out
1KW0	c	*Human*	Fe^{2+}	3-(2-thienyl)-L-alanine	BH_4	Closed	In
1MMK	c	*Human*	Fe^{2+}	3-(2-thienyl)-L-alanine	BH_4	Closed	In
1MMT	c	*Human*	Fe^{2+}	L-norleucine	BH_4	Closed	In
1TDW	c	*Human*	Fe^{3+}	-	-	Open	Out
1TG2	c	*Human*	Fe^{3+}	-	BH_4	Open	Out
2V27	c	*Cp*	Fe^{3+}	-	-	No density	-
2V28	c	*Cp*	-	-	-	No density	-
4ANP	c	*Human*	Fe^{3+}	-	Compound 1	Open	Out
3TCY	c	*Cv*	Co^{2+}	-	-	Open*	Out
3TK2	c	*Cv*	Co^{2+}	-	-	Open*	Out
3TK4	c	*Cv*	Co^{2+}	-	-	Open*	Out
4ESM	c	*Cv*	Co^{2+}	-	-	Open*	Out
4ETL	c	*Cv*	Co^{2+}	-	-	Open*	Out
4JPX	c	*Cv*	Co^{2+}	-	-	Open*	Out
4JPY	c	*Cv*	Fe^{3+}	-	-	Open*	Out
4BPT	c	*Lp*	-	-	-	Open*	Out
4Q3W	c	*Cv*	Co^{2+}	-	-	Open*	Out
4Q3X	c	*Cv*	Co^{2+}	-	-	Open*	Out
4Q3Y	c	*Cv*	Co^{2+}	-	-	Open*	Out
4Q3Z	c	*Cv*	Co^{2+}	-	-	Open*	Out
5DEN	r/c/t	*Rat*	Fe^{3+}	-	-	No density	-
5EGQ	r/c/t	*Rat*	-	-	-	No density	-
5FGJ	r/c/t	*Rat*	Fe^{3+}	-	-	Open**	-
5JK5	r/c		Fe^{3+}	-	BH_2	Open	In/Not conserved
5JK6	r/c	*Dd*	Fe^{3+}	-	-	Open	In/Not conserved
5JK8	r/c	*Dd*	Fe^{3+}	L-norleucine	BH_2	No density	-

Cv: *Chromobacterium violaceum, Dd*: *Dictyostelium discoideum, Lp*: *Legionella pneumophila*, *Cp*: *Colwellia psychrerythraea*, BH_2: 7,8-dihydrobiopterin, BH_4: 5,6,7,8-tetrahydrobiopterin, Compound 1 (pharmacological chaperone): 5,6-dimethyl-3-(4-methyl-2-pyridinyl)-2-thioxo-2,3-dihydrothieno[2,3-d]pyrimidin-4(1H)-one.

Appendix I

RMSD plots from MD simulations of c*h*TPH variants

This appendix presents RMSD (heavy atoms) plots of the TPH variants calculated from MD simulation trajectories. In the figures, Trp, BH_4, and Trp+BH_4 refer to the presence of tryptophan, BH_4, or both in the binding pockets of the catalytic domain.

I. 1 RMSD plots – c*h*TPH1

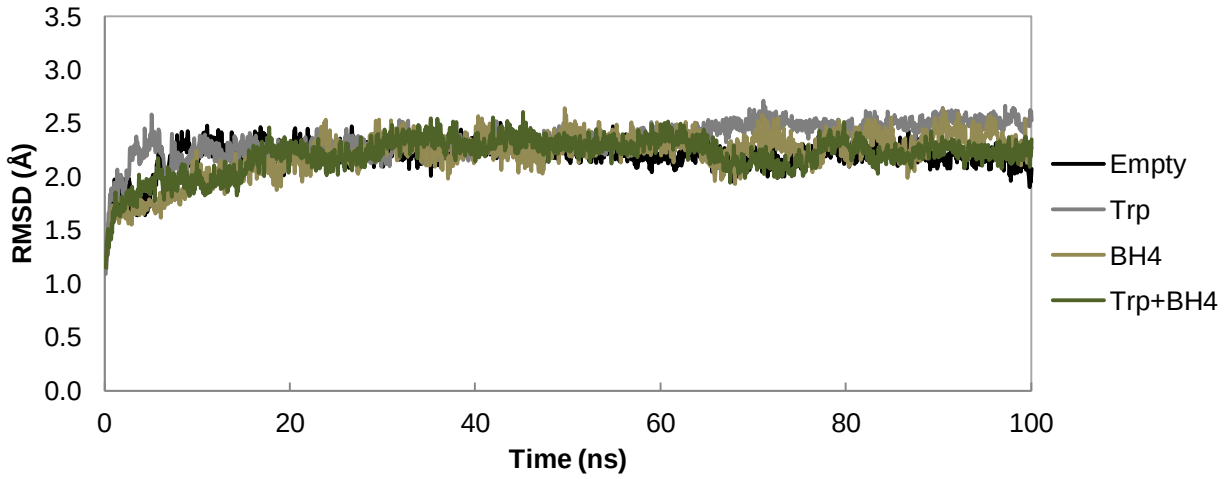

Figure I. 1. RMSD plots from 100 ns simulations of c*h*TPH1 without ligands, with Trp bound, with BH_4 bound, and with both Trp and BH_4 bound. RMSD in each 10th frame is calculated for all heavy atoms in the protein with the first frame as the reference structure.

I. 2 RMSD plots – Y125A-c*h*TPH1

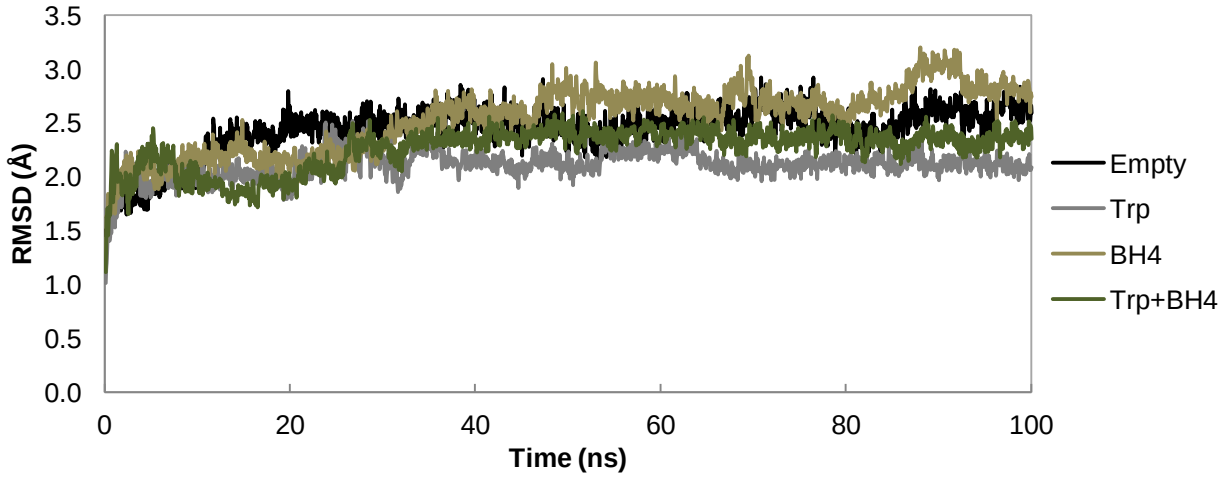

Figure I. 2. RMSD plots from 100 ns simulations of Y125A-c*h*TPH1 without ligands, with Trp bound, with BH_4 bound, and with both Trp and BH_4 bound. RMSD in each 10th frame is calculated for all heavy atoms in the protein with the first frame as the reference structure.

I. 3 RMSD plots – Y125W-c*h*TPH1

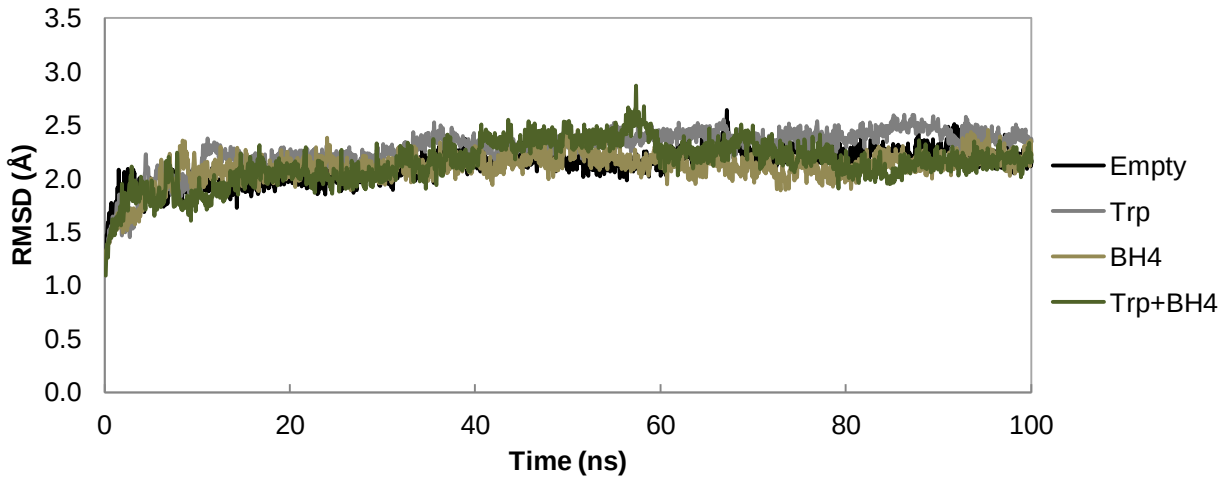

Figure I. 3. RMSD plots from 100 ns simulations of Y125W-c*h*TPH1 without ligands, with Trp bound, with BH_4 bound, and with both Trp and BH_4 bound. RMSD in each 10th frame is calculated for all heavy atoms in the protein with the first frame as the reference structure.

I. 4 RMSD plots –c*h*TPH2

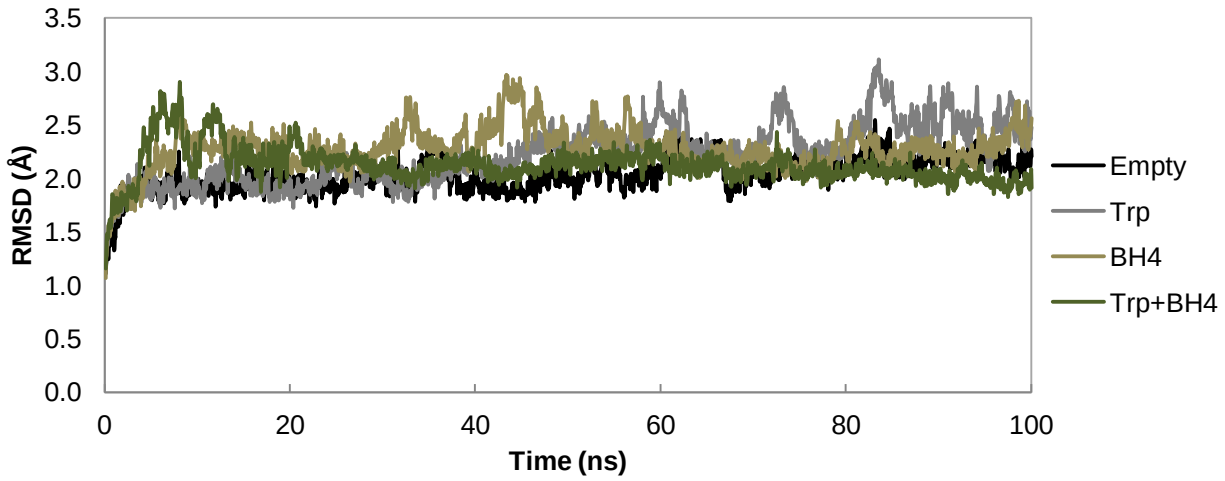

Figure I. 4. RMSD plots from 100 ns simulations of c*h*TPH2 without ligands, with Trp bound, with BH_4 bound, and with both Trp and BH_4 bound. RMSD in each 10th frame is calculated for all heavy atoms in the protein with the first frame as the reference structure.

I. 5 RMSD plots – Y171A-c*h*TPH2

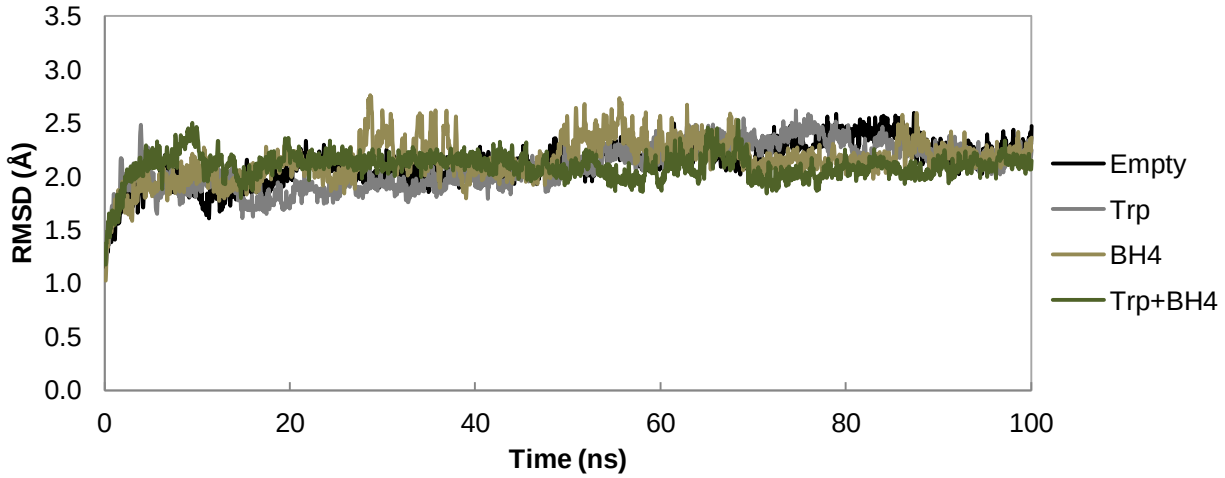

Figure I. 5. RMSD plots from 100 ns simulations of Y171A-c*h*TPH2 without ligands, with Trp bound, with BH_4 bound, and with both Trp and BH_4 bound. RMSD in each 10th frame is calculated for all heavy atoms in the protein with the first frame as the reference structure.

I. 6 RMSD plots – Y171W-c*h*TPH2

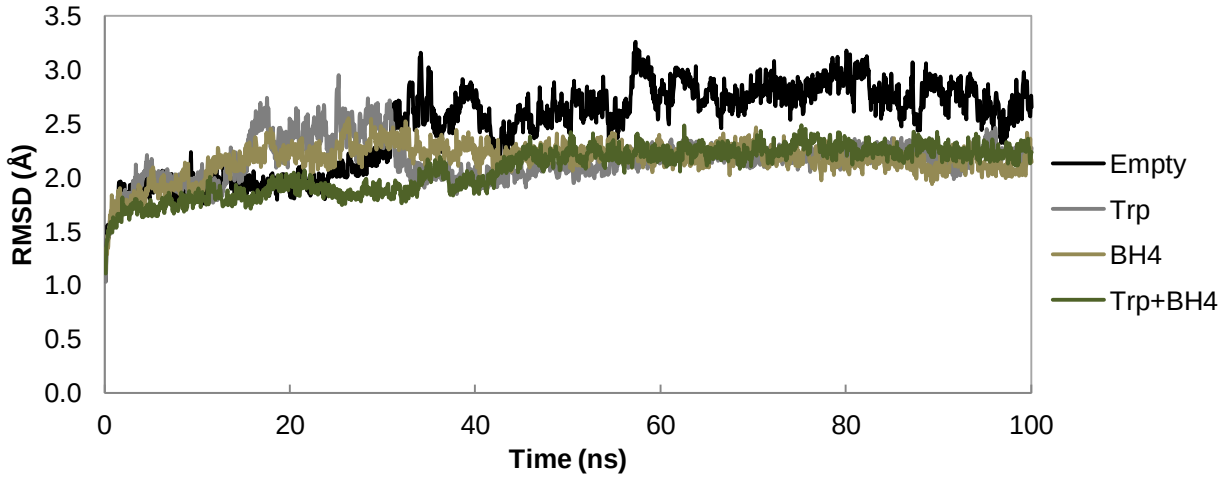

Figure I. 6. RMSD plots from 100 ns simulations of Y171W-c*h*TPH2 without ligands, with Trp bound, with BH_4 bound, and with both Trp and BH_4 bound. RMSD in each 10th frame is calculated for all heavy atoms in the protein with the first frame as the reference structure.